

INFLUENCE OF LOCAL GEOLOGY ON
EARTHQUAKE GROUND MOTION

Thesis by

NIEN CHIEN TSAI

In Partial Fulfillment of the Requirements
For the Degree of
Doctor of Philosophy

California Institute of Technology

Pasadena, California

1969

(Submitted May 28, 1969)

ACKNOWLEDGMENTS

The author wishes to express his sincere appreciation to Professor G. W. Housner for his guidance throughout the investigation and in the preparation of this work. The counsel of Professor P. C. Jennings is also gratefully appreciated.

The author is grateful to the California Institute of Technology and the National Science Foundation for the financial assistance which made this study possible.

ABSTRACT

As a simplified approach for estimating theoretically the influence of local subsoils upon the ground motion during an earthquake, the problem of an idealized layered system subjected to vertically incident plane body waves was studied. Both the technique of steady-state analysis and the technique of transient analysis have been used to analyze the problem.

In the steady-state analysis, a recursion formula has been derived for obtaining the response of a layered system to sinusoidally steady-state input. Several conclusions are drawn concerning the nature of the amplification spectrum of a nonviscous layered system having its layer stiffnesses increasing with depth. Numerical examples are given to demonstrate the effect of layer parameters on the amplification spectrum of a layered system.

In the transient analysis, two modified shear beam models have been established for obtaining approximately the response of a layered system to earthquake-like excitation. The method of continuous modal analysis was adopted for approximate analysis of the models, with energy dissipation in the layers, if any, taken into account. Numerical examples are given to demonstrate the accuracy of the models and the effect of a layered system in modifying the input motion.

Conditions are established, under which the theory is applicable to predict the influence of local subsoils on the ground motion during an earthquake. To demonstrate the applicability of the models to actual cases, three examples of actually recorded earthquake events are examined. It is concluded that significant

modification of the incoming seismic waves, as predicted by the theory, is likely to occur in well defined soft subsoils during an earthquake, provided that certain conditions concerning the nature of the incoming seismic waves are satisfied.

TABLE OF CONTENTS

<u>PART</u>	<u>TITLE</u>	<u>PAGE</u>
I	INTRODUCTION	1
II	STEADY-STATE ANALYSIS OF A LAYERED SYSTEM	11
III	EXACT TRANSIENT ANALYSIS OF A NON- VISCOUS LAYERED SYSTEM	47
IV	MODIFIED SHEAR BEAM MODELS FOR APPROXIMATE TRANSIENT ANAL- YSIS OF A LAYERED SYSTEM	60
V	APPLICATIONS	142
VI	SUMMARY AND CONCLUSIONS	185
	APPENDIX I	189
	APPENDIX II	193
	APPENDIX III	195
	REFERENCES	197

I. INTRODUCTION

Damage to engineering structures during earthquakes is known to depend on the nature of the arriving seismic waves as well as on the properties of the structures. The characteristics of ground shaking that are of major interest to engineers for purposes of design are the intensity, the frequency composition and the total duration. Broadly speaking, such features are functions of the following three factors: the source mechanism, the material properties of the earth media along the various paths through which the seismic waves travel, and the local geological conditions of the site under consideration. The complicated nature of the earthquake source mechanism, the highly irregular structure of the earth's mantle and crust, and the difficulty of making significant measurements make it difficult to elucidate the real influences on the ground motion. For example, the focus of a potentially destructive earthquake is not an ideal point source, but it is a fault plane with dimensions ranging from several miles to several hundred miles. When the accumulation of strain energy around the fault exceeds a certain limit slippage will occur along the fault plane. During the slipping process a portion of the energy is released in the form of elastic waves emitted from the source and a portion is dissipated in generating heat. The elastic waves, after traveling various paths through the earth, will eventually arrive at the site where observations are made of the ground motions. The seismic waves generated at the source are composed of both dilational waves (P-waves) and shear

waves (S-waves). The P- and S-waves are conventionally called body waves. In addition to the body waves there are also surface waves whose energy is concentrated near the surface of the ground. The relative contributions to the total ground motion and the corresponding times of arrival of each type of wave depends on the epicentral distance of the station, the focal depth of the earthquake source, and the reflection and refraction of the waves along their paths. A highly idealized scheme is presented in Fig. 1.1 to show the relative location of the earthquake source O, the recording station S, a typical body wave path OAS, and a typical surface wave path OCS.

It is the primary purpose of this thesis to study the influence of the local geology on the incoming seismic waves. By "local" we refer to that part of the ground media having a total path of approximately one thousand feet and a horizontal dimension of several miles, which are essentially local when compared with the dimensions of the wave paths as well as the thickness of the earth's crust. This is the situation in the circled area around the station S in Fig. 1.1. In some past earthquakes the subsoil conditions were observed to have a pronounced influence on the amplitude of the recorded ground motion and on the total duration. (1,2,3) One way to investigate this influence is to compare the motions simultaneously recorded during the same earthquake at two nearby stations with different subsoil conditions. Some comparisons were made by Gutenberg (2) for very weak motion produced by small magnitude earthquakes recorded at several nearby sites in Pasadena, California. He

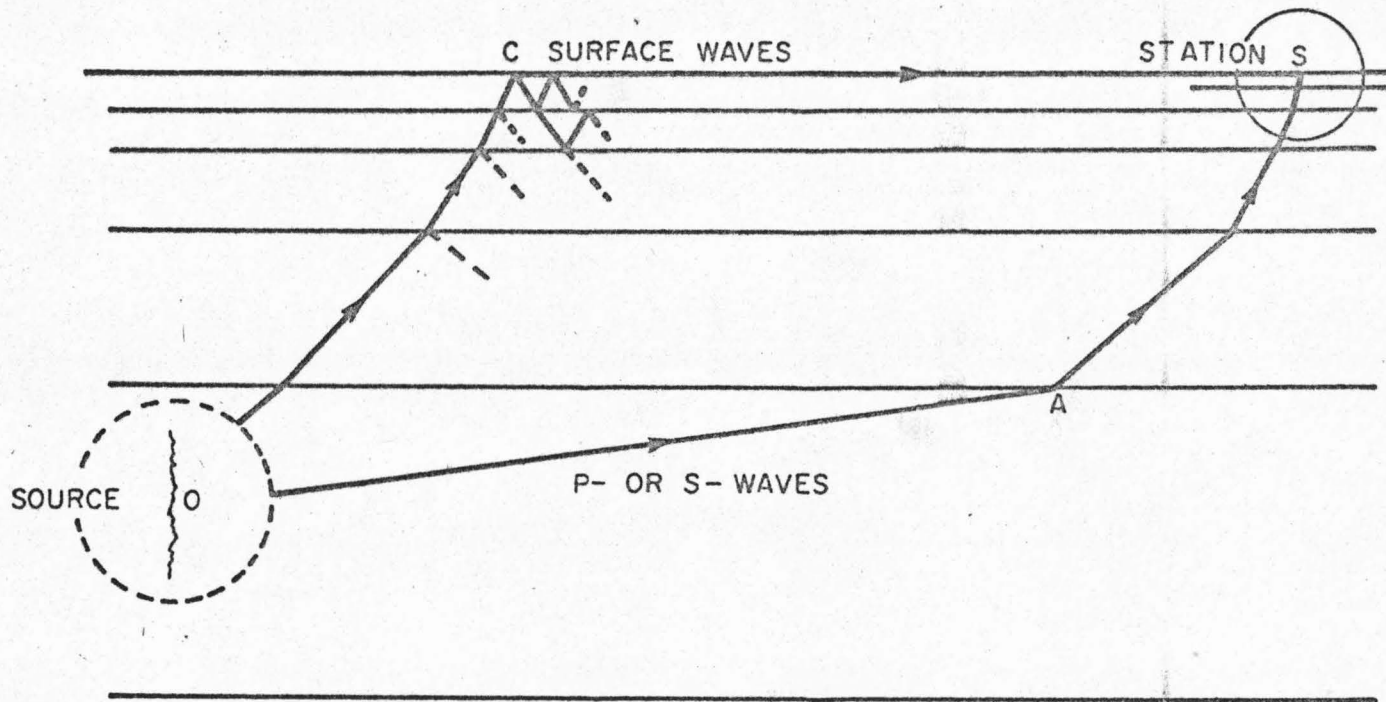


Fig. 1.1. IDEALIZED RELATION AMONG EARTHQUAKE SOURCE,
WAVE PATHS AND OBSERVING STATION

observed that, for waves having periods of 1 to 1.5 seconds, the amplitude of the motion at these sites located on alluvium more than 500 feet deep was about five times larger than that recorded at the Seismological Laboratory of the California Institute of Technology, which is on an outcrop of crystalline rock. Ground shaking with a dominant period has also been reported for strong-motion earthquakes and for microtremors. For strong-motion earthquakes, the best examples are the ground motions recorded in Mexico City, Mexico, which is situated on some unusually soft alluvial deposits approximately 100 feet deep. Zeevaert has observed a dominant period of 2.5 seconds for the earthquake recorded on 28 July 1957⁽⁴⁾ and the earthquakes on 11 May and 19 May 1962.⁽¹⁾ Kanai also observed dominant periods in the ground motions recorded during microtremors in certain areas of Japan, which he believed to be associated with the properties of the ground layers.^(5,6) On the other hand, in addition to such positive evidence, many strong ground motions recorded in the western United States where the subsoils are relatively stiff do not show any appreciable effect of the subsoil. It is also known that structures built on softer ground do not necessarily receive more severe damage than those founded on stiffer ground. Judging the ground effect by simply observing the extent of damage of structures can lead to a conclusion badly in error. Consequently the following question arises: How does the local geology actually affect the incoming seismic waves and under what conditions will it produce effects of engineering significance? To answer this question on a theoretical basis is not a simple matter since there are many

complexities in the incoming seismic waves as well as irregularities and inhomogeneities in the geometric configurations and the material properties of the local subsoil media. Hence, it is necessary to start the theoretical studies with a simple, idealized model and then try to relate the analytical results to the cases actually encountered. A conventional model that has widely been used by geophysicists for the earth's crust consists of many homogeneous, spherically stratified layers. As far as studies of the influence of local subsoils are concerned, the curvature of the layer boundaries need not be taken into account, and a simpler model consisting of linear, homogeneous, horizontally stratified layers overlying a homogeneous half-space can be analyzed. The layer boundaries are ideal planes extending to infinity in both horizontal directions. Also, it is known that wave velocities in the earth usually increase with depth and, therefore, the paths of the waves tend to bend upwards like the path OAS in Fig. 1.1, and this tendency is stronger for greater velocity gradients. By the time the waves reach the bottom of the local subsoil strata the waves will in most cases be incident nearly vertically, depending on the epicentral distance and the focal depth of the earthquake. (7,8) Therefore, as a further simplification the incoming body waves are taken to be vertically incident plane waves and the problem of one-dimensional wave propagation is conceivable.

In 1930, the Japanese seismologists, Sezawa and Kanai, pointed out the possible effects of superficial soil layers on observed ground motions. (9,10,11) Since then, extensive research work has been carried out both theoretically and experimentally to study this

problem. Theoretical studies have been based on the simple layered model described before, and two different approaches, namely, the sinusoidal steady-state analysis and the transient-state analysis, have been used to analyze the model.

The purpose of sinusoidal steady-state analysis is to compare the response of a given layered system subjected to excitation of steady-state sinusoidal waves. Contributions in this area were made by Kanai,^(5,6) Matthiesen, Duke and Leeds,⁽¹²⁾ Herrera and Rosenblueth,⁽¹³⁾ and Haskell,^(14,15) where Haskell has particularly studied the more general problem of a layered system excited by both P- and S-plane waves that are incident obliquely rather than vertically. Kanai has derived the steady-state solution for vertically propagating plane waves in layered systems containing from one to three layers. Matthiesen et al.⁽¹²⁾ derived the solution for the case of a viscous N-layer system, and the results were applied to the sites of 64 strong-motion earthquake stations in southern California. Using the technique of graphical solution developed by Takahasi,⁽¹⁶⁾ Herrera and Rosenblueth⁽¹³⁾ derived the solution for a viscoelastic N-layer system in matrix form. Layered systems with continuously varying properties with each layer have been studied by Onda⁽¹⁷⁾ and Gupta^(18,19) for some simple cases.

Kanai has offered the following general conclusions from the steady-state analysis as follows:

(i) For nonviscous layered systems, a system with one layer only has prominent response at the resonant frequencies, but a multi-layer system has less prominent resonant response.

(ii) During earthquakes, there is a dominant period associated with the ground layers. This period is proportional to the thickness of the layers.

(iii) Due to the deformability of the half-space foundation, there is always a portion of wave energy transmitted from the layered system back into the foundation. Such a dissipative mechanism is called "geometrical dissipation," and this is the reason why there is no infinite resonant response even if the system is non-viscous. (20)

Sinusoidal steady-state analysis is capable of indicating precisely the frequency-selective property of a given layered system. However, steady-state analysis is insufficient for studying the effect of a layered system on earthquake-like excitation and, therefore, transient analysis has to be used.

Earthquake engineers are most interested in the velocity spectrum of the ground acceleration, and two different methods of analysis have been used in studying the effect of a layered system on the output acceleration. The first method is a probabilistic approach, the purpose of which is to establish a formula by statistical techniques to estimate the velocity spectrum of the output motion of a layered system from the given velocity spectrum of the input motion. Theoretical studies have been made by Herrera and Rosenblueth, (13) and the derived results were applied to estimate the velocity spectra for Mexico City with considerable success. (21) However, this approach has rather limited application to actual earthquakes unless further refinement in the theory can be made.

The second method of analysis is a deterministic approach which computes the response of a layered system subjected to arbitrarily given excitation at the base of the system. The velocity spectrum is then computed for the output. An exact method was derived by Baranov and Kunetz⁽²²⁾ to calculate the desired output of a nonviscous layered system from the point of view of wave propagation directly in the time-domain. This method is called the "ray-tracing" scheme, and applies to nonviscous layered systems only. For viscous layered systems, geophysicists use the frequency-domain method. In this method, the Fourier spectrum of the input motion is calculated and then multiplied by the transfer function of the layered system to produce the Fourier spectrum of the output motion. The inverse transformation of the output spectrum is then performed to obtain the time history of the output, and it is at this step that considerable error can be introduced. Earthquake engineers, on the other hand, treat the layered system as a shear beam because of the analogy between the governing differential equations for these two systems. The shear beam is lumped into a discrete mechanical system and a technique of modal analysis or direct numerical integration is applied to analyze the system, as has been done by Whitman⁽²³⁾ and Idriss and Seed.^(24,25) In their analysis, Idriss and Seed⁽²⁴⁾ also considered the more general case of a layered system of which the media are described by a bilinear hysteretic stress-strain law. However, their method of shear beam analogy does not take into account the deformability of the half-space foundation. In this thesis, the shear beam model is modified so as to take

into account the energy lost into the half-space foundation due to the deformability of the foundation.

In Chapter II, an explicit recursion formula is derived for steady-state analysis of a linearly viscoelastic N-layer system. This recursion formula is in a form of greater practical utility than previously derived formulas. Several important conclusions are drawn concerning the characteristics of the steady-state response of a nonviscous layered system having its layer stiffnesses increasing with depth.

Chapter III gives a brief review of the ray-tracing technique. This provides an exact solution for the transient response of a nonviscous layered system.

Chapter IV establishes models which give approximate solutions for the transient response of a viscous layered system. One model is an exact analog of the original layered system if there is no viscosity present. Otherwise, it is approximate. Computation with this model is time-consuming because a system of coupled differential equations must be solved. Another model is developed that greatly reduces the computation time but which gives good results only for response near the surface of a layered system that has a relatively large difference in stiffness between the foundation and the lowest layer. However, this model is sufficiently accurate for most problems of engineering interest.

The last chapter discusses the applicability of the previous theoretical results to problems involving the influence of local geology on real earthquakes. Ground motions recorded during three

earthquakes are presented for purposes of illustration. Finally, conclusions are drawn about the conditions under which appreciable resonance is likely to take place during earthquakes.

II. STEADY-STATE ANALYSIS OF A LAYERED SYSTEM

A. Introduction

The technique of steady-state analysis has long been used by earthquake engineers to study the effect of ground layers on vertically propagating seismic waves. The merit of this approach is that it clearly exhibits the frequency-selective property of a given layered system, namely, how certain frequency components of the incident waves are amplified while the rest are suppressed by the system.

In this chapter, there is derived an explicit recursion formula for finding the steady-state response of an N-layer system subjected to vertically incident, sinusoidal plane body waves. The layered system to be analyzed is composed of linear, isotropic and homogeneous elastic layers the interface of which are parallel planes that extend infinitely in both horizontal directions, and the system is overlying a homogeneous half-space foundation.

Several important assertions are established concerning the nature of the steady-state response of a nonviscous layered system having its layer stiffnesses increasing with depth. For simplicity, analysis is made only for the case of incident S-waves in the analyses that follow. The results derived for incident S-waves can readily be converted to those for the case of incident P-waves by simply replacing the corresponding elastic constant and, if energy dissipation of waves is involved, the corresponding viscosity constants.

A list of the important symbols to be used is given below, and they are defined again when they first appear in the text.

SYMBOLEXPLANATION OR DEFINITION

a_j, b_j	wave amplitudes in the j^{th} layer
A	$\tau/(1+r)$
AMP(ω)	amplification spectrum for the surface response
c_0	S-wave velocity in a nonviscous elastic medium
$c(\omega)$	complex S-wave velocity in a viscous medium
$f_j(\omega, z_j), g_j(\omega, z_j)$	parameters defining the amplitude of response in the j^{th} layer of a viscoelastic layered system
$G_j(\omega)$	$\sqrt{\text{Re}_j^2 + \text{Im}_j^2}$
H_j	thickness of the j^{th} layer
i	$\sqrt{-1}$
I, R	subscripts referring to the imaginary and the real part respectively
Im_j, Re_j	recursive parameters in the recursive formula
j	layer index, as subscript
k	wave number
r	viscosity parameter
s_j	$k_j H_j$
t	time
$u_j(z_j, t)$	response in the j^{th} layer
$y(t + z_N/c_{N+1})$	incident plane S-wave
z_j	space coordinate for the j^{th} layer
$(\alpha_0)_{j-1}$	impedance ratio, equal to $\rho_{j-1}(c_0)_{j-1}/\rho_j(c_0)_j$ in a nonviscous layered system
α_{j-1}	impedance ratio in a viscous layered system, equal to $\rho_{j-1}c(\omega)_{j-1}/\rho_j c(\omega)_j$

<u>SYMBOL</u>	<u>EXPLANATION OR DEFINITION</u>
$\phi_{N+1}(\omega), \psi_j(\omega)$	phase angle
$\sigma(t); \dot{\sigma}(t)$	shearing stress; rate of shearing stress
$\epsilon(t); \dot{\epsilon}(t)$	shearing strain; rate of shearing strain
μ_a, μ_b	spring stiffness parameters of a standard linear model
μ_o	shearing modulus of a nonviscous elastic material
$\mu(\omega)$	complex overall shearing modulus of a viscous material during steady-state deformation
η	viscosity constant
τ	retardation time of the Voigt model, equal to η/μ_o
ρ	density
λ	wave length
ω, Ω	frequency
ω_n	the n^{th} characteristic frequency

B. Steady-State Response of a Linearly Viscoelastic Layered System

In most cases of practical interest the layered system is energy-dissipative. The assumption of perfect elasticity for the layer media is only a special idealization and, therefore, we shall start the analysis by considering a viscous layered system. Several well known linear viscoelastic models are commonly used for theoretical descriptions of the mechanism of energy dissipation in viscous media. The most widely used models are the Maxwell model, the Voigt model and the standard linear model. Each of these is

described by a certain combination of spring and dashpot elements, and is shown in Figs. 2.1(a), 2.1(b), and 2.1(c) respectively.

The Maxwell model consists of a spring element, μ_0 , and a dashpot, η , in series where μ_0 is the shearing modulus and η the viscosity constant. Letting σ be the shearing stress and ϵ the shearing strain, the stress-strain law can then be written

$$\sigma + (\eta/\mu_0)\dot{\sigma} = \eta\dot{\epsilon} \quad (2.1)$$

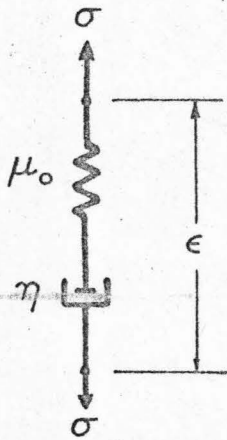
where $\dot{\sigma}$ and $\dot{\epsilon}$ are, respectively, the rate of shearing stress and the rate of shearing strain. In Eq. 2.1 the quantity η/μ_0 has the dimension of time and is called the "relaxation time" of the Maxwell model. This model is suitable for material subjected to excitations of very high frequency and hence has rarely been used by earthquake engineers or geophysicists in their theoretical studies.

The Voigt model, independently proposed by Kelvin in 1875 and Voigt in 1889, consists of a spring element μ_0 and a dashpot η in parallel. The shearing stress σ is proportional to both the strain ϵ and the strain rate $\dot{\epsilon}$, namely,

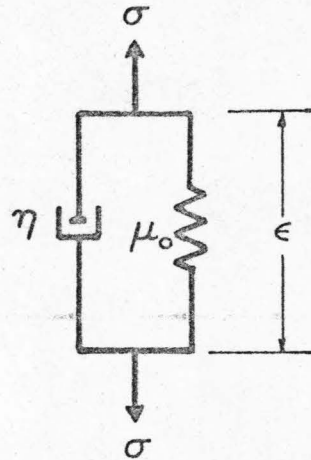
$$\sigma = \mu_0\epsilon + \eta\dot{\epsilon} \quad (2.2)$$

where the quantity η/μ_0 is commonly called the "retardation time," τ , of the Voigt model.

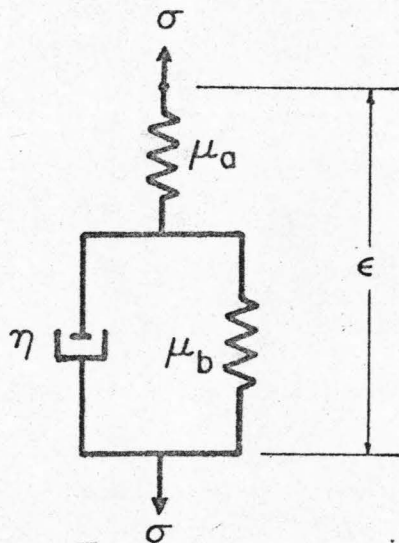
The standard linear model was first proposed by Zener⁽²⁶⁾ in 1948 and later independently by Hillier⁽²⁷⁾ in 1949 in a slightly different form. The one suggested by Hillier is adopted here. The stress-strain law for this model, shown in Fig. 2.1(c), is



(a) MAXWELL MODEL



(b) VOIGT-KELVIN MODEL



(c) STANDARD LINEAR MODEL

Fig. 2.1. THREE COMMONLY USED LINEAR VISCO-ELASTIC MODELS

$$(\mu_a + \mu_b)\sigma + \eta\dot{\sigma} = \mu_a\mu_b\epsilon + \eta\mu_a\dot{\epsilon}$$

or

$$\sigma + \frac{\tau}{1+r}\dot{\sigma} = \mu_o(\epsilon + \tau\dot{\epsilon}) \quad (2.3)$$

where

$$r = \mu_a/\mu_b$$

and

$$\mu_o = \frac{r}{1+r}\mu_b$$

In Eq. 2.3, the quantity $\tau = \eta/\mu_b$ is the retardation time constant of the Voigt element in this model. Observe that Eq. 2.3 includes Eq. 2.2 as a special case for $r = \infty$ and hence Eq. 2.3 can be considered as a general stress-strain law for both the Voigt model and the standard linear model.

For steady-state deformation, assume $\epsilon = e^{i\omega t}$ and $\sigma = \mu(\omega)e^{i\omega t}$, and Eq. 2.3 becomes

$$\sigma = \mu(\omega)\epsilon = \mu_o \left(\frac{1 + i\omega\tau}{1 + i\omega A} \right) \epsilon \quad (2.4)$$

where $A = \frac{1}{1+r}$. Eq. 2.4 indicates that the overall shearing modulus, $\mu(\omega)$, under steady-state deformation is a complex and frequency-dependent quantity which is equal to the real shearing modulus, μ_o , if the material is nonviscous. In Eq. 2.4, A vanishes for a Voigt material and, furthermore, the viscosity parameter τ is identically zero for a nonviscous elastic material.

According to Eq. 2.4, the complex shear wave velocity will

be, by definition ,

$$\begin{aligned} c(\omega) &= \sqrt{\mu(\omega)/\rho} \\ &= c_0 \sqrt{\frac{1 + \omega^2 \tau A}{1 + \omega^2 A^2}} \sqrt{1 + i\omega \frac{\tau - A}{1 + \omega^2 \tau A}} \end{aligned} \quad (2.5)$$

with ρ being the density, and $c_0 = \sqrt{\mu_0/\rho}$ being the shear wave velocity in a nonviscous material. Defining

$$\begin{aligned} e &= \sqrt{\frac{1 + \omega^2 \tau^2}{1 + \omega^2 \tau A}} \\ d &= \sqrt{\frac{1 + \omega^2 \tau A}{1 + \omega^2 A^2}} \\ P &= \sqrt{\frac{e + d}{2e}} \\ Q &= \sqrt{\frac{e - d}{2e}} \end{aligned} \quad (2.6)$$

the complex wave number, k , can be written as

$$k = \omega/c = k_R + ik_I \quad (2.7)$$

where

$$k_R = \frac{\omega P}{c_0 e} \quad \text{and} \quad k_I = \frac{\omega Q}{c_0 e} \quad (2.8)$$

are, respectively, the real and the imaginary part of k .

Consider an N -layer system of which the media are assumed to obey the general stress-strain law, i. e., Eq. 2.4, under steady-

state deformation. The layered system is shown in Fig. 2.2 with the top layer indexed 1 and the half-space $N+1$. A set of N coordinates, z_j , $j = 1, 2, \dots, N$, is also defined as shown. Under steady-state sinusoidal excitation the response of the system is governed by the following one-dimensional wave equations

$$c_j^2(\omega) \frac{\partial^2 u_j(z_j, t)}{\partial z_j^2} = \frac{\partial^2 u_j(z_j, t)}{\partial t^2}, \quad j = 1, 2, \dots, N+1 \quad (2.9)$$

where u_j is the response in the j^{th} layer. Imagine a steady-state source at z_N equal to ∞ , which gives rise to a vertically incident plane S-wave of the form $y(t+z_N/c_{N+1}) = a_{N+1} e^{i(\omega t + k_{N+1} z_N)}$ with a_{N+1} being a known amplitude. The solution of Eq. 2.9 can then be expressed as the sum of an upward traveling wave and a downward traveling one in each layer as

$$u_j(z_j, t) = a_j e^{i(\omega t + k_j z_j)} + b_j e^{i(\omega t - k_j z_j)} \quad (2.10)$$

for $z_j = -H_j$ to $z_j = 0$. The determination of a_j and b_j requires the application of the proper boundary conditions at each of the interfaces of the system. Firstly, at the free surface where $z_1 = -H_1$, the stress-free condition yields

$$\sigma_1(-H_1, t) = \mu_1 \left. \frac{\partial u_1}{\partial z_1} \right|_{z_1 = -H_1} = 0$$

which implies

$$b_1 = a_1 e^{-2is_1} = a_1 e^{-2i(s_R)_1 - 2(s_I)_1} \quad (2.11)$$

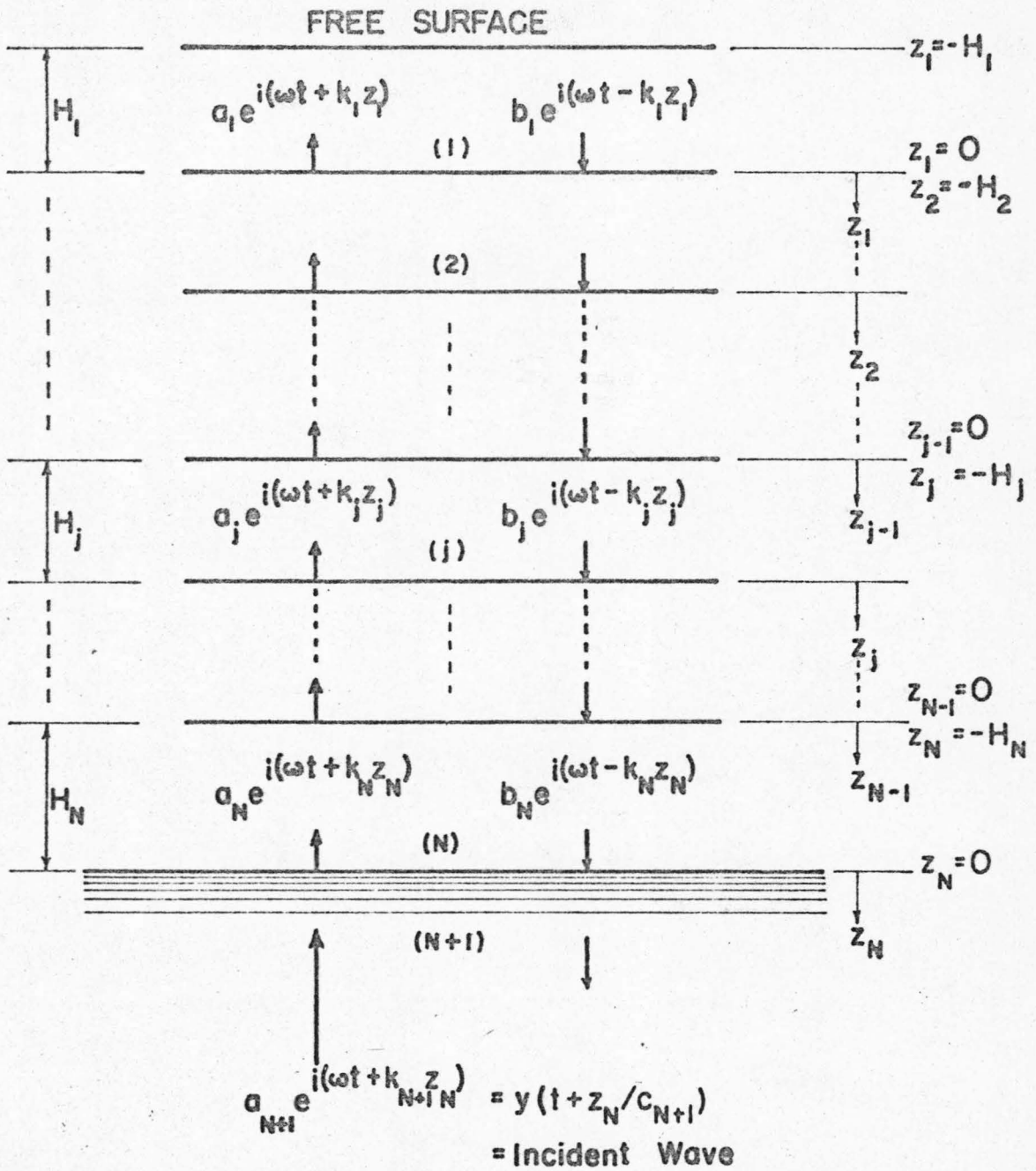


Fig. 2.2. AN N-LAYER SYSTEM UNDER STEADY-STATE EXCITATION

where, for simplification purpose, we have put

$$\begin{aligned} s_j &= k_j H_j = (k_R)_j H_j + i(k_I)_j H_j \\ &= (s_R)_j + i(s_I)_j \end{aligned} \quad (2.12)$$

The boundary conditions at the interface between the $(j-1)^{\text{th}}$ and the j^{th} layer, defined by $z_{j-1} = 0$ and $z_j = -H_j$ for $j = 2, 3, \dots, N$, are

(i) the continuity of the displacements

$$u_{j-1}(0, t) = u_j(-H_j, t)$$

which gives

$$a_{j-1} + b_{j-1} = a_j e^{-is_j} + b_j e^{-is_j} \quad (2.13)$$

and (ii) the continuity of the shearing stresses

$$\sigma_{j-1}(0, t) = \sigma_j(-H_j, t)$$

which yields

$$\alpha_{j-1}(a_{j-1} - b_{j-1}) = a_j e^{-is_j} - b_j e^{is_j} \quad (2.14)$$

In Eq. 2.14, α_{j-1} is the complex acoustic impedance ratio between the media of the $(j-1)^{\text{th}}$ and the j^{th} layer, and is equal to

$\rho_{j-1} c_{j-1} / \rho_j c_j$. Using the notation defined in Eq. 2.6 we can write

$$\begin{aligned} \alpha_{j-1} &= (\alpha_R)_{j-1} + i(\alpha_I)_{j-1} \\ &= (\alpha_o)_{j-1} d_{j-1} [(P_{j-1} P_j + Q_{j-1} Q_j) + i(Q_{j-1} P_j - P_{j-1} Q_j)] / e_j \end{aligned} \quad (2.15)$$

where $(\alpha_o)_{j-1} = \rho_{j-1}(c_o)_{j-1} / \rho_j(c_o)_j$. Define

$$[S]_j = \begin{bmatrix} e^{is_j} & \\ & e^{-is_j} \end{bmatrix} \quad [T]_j = \frac{1}{2} \begin{bmatrix} 1+\alpha_j & 1-\alpha_j \\ 1-\alpha_j & 1+\alpha_j \end{bmatrix} \quad (2.16)$$

Equations 2.13 and 2.14 then give, for $j = 2, \dots, N$,

$$\begin{Bmatrix} a_j \\ b_j \end{Bmatrix} = [S]_j [T]_{j-1} \begin{Bmatrix} a_{j-1} \\ b_{j-1} \end{Bmatrix} \quad (2.17)$$

and, for $j = N+1$,

$$\begin{Bmatrix} a_{N+1} \\ b_{N+1} \end{Bmatrix} = [T]_N \begin{Bmatrix} a_N \\ b_N \end{Bmatrix} \quad (2.18)$$

By using repeatedly the recursive relation, Eq. 2.17, a_j and b_j can be expressed in terms of a_1 and b_1 , where b_1 is related to a_1 by Eq. 2.11. Hence, for $j = 2, \dots, N$,

$$\begin{Bmatrix} a_j \\ b_j \end{Bmatrix} = a_1 e^{-is_1} ([S]_j [T]_{j-1}) \dots ([S]_2 [T]_1) [S]_1 \begin{Bmatrix} 1 \\ 1 \end{Bmatrix}$$

For convenience in doing analysis, the last equation can be written as

$$\begin{Bmatrix} a_j \\ b_j \end{Bmatrix} = a_1 e^{-is_1} [S]_j \begin{Bmatrix} (\text{Re}_j + \text{Re}'_j) + i(\text{Im}_j + \text{Im}'_j) \\ (\text{Re}_j - \text{Re}'_j) - i(\text{Im}_j - \text{Im}'_j) \end{Bmatrix} \quad (2.19)$$

where it can be shown by induction that Re_j , Re'_j , Im_j , and Im'_j are given by the following recursion formula

$$\begin{aligned}
 \text{Re}_j &= p_{j-1} \cosh(s_I)_{j-1} - p'_{j-1} \sinh(s_I)_{j-1} \\
 \text{Re}'_j &= (\alpha_R)_{j-1} [p_{j-1} \sinh(s_I)_{j-1} - p'_{j-1} \cosh(s_I)_{j-1}] \\
 &\quad + (\alpha_I)_{j-1} [q_{j-1} \cosh(s_I)_{j-1} - q'_{j-1} \sinh(s_I)_{j-1}] \quad (2.20)
 \end{aligned}$$

$$\begin{aligned}
 \text{Im}_j &= (\alpha_R)_{j-1} [q_{j-1} \cosh(s_I)_{j-1} - q'_{j-1} \sinh(s_I)_{j-1}] \\
 &\quad - (\alpha_I)_{j-1} [p_{j-1} \sinh(s_I)_{j-1} - p'_{j-1} \cosh(s_I)_{j-1}] \\
 \text{Im}'_j &= -q_{j-1} \sinh(s_I)_{j-1} + q'_{j-1} \cosh(s_I)_{j-1}
 \end{aligned}$$

for $j = 2, 3, \dots, N+1$, in which

$$\begin{aligned}
 p_{j-1} &= \text{Re}_{j-1} \cos(s_R)_{j-1} - \text{Im}_{j-1} \sin(s_R)_{j-1} \\
 p'_{j-1} &= \text{Re}'_{j-1} \cos(s_R)_{j-1} - \text{Im}'_{j-1} \sin(s_R)_{j-1} \quad (2.21) \\
 q_{j-1} &= \text{Im}_{j-1} \cos(s_R)_{j-1} + \text{Re}_{j-1} \sin(s_R)_{j-1} \\
 q'_{j-1} &= \text{Im}'_{j-1} \cos(s_R)_{j-1} + \text{Re}'_{j-1} \sin(s_R)_{j-1}
 \end{aligned}$$

and, for $j = 1$, $\text{Re}_1 = 1$, $\text{Re}'_1 = \text{Im}_1 = \text{Im}'_1 = 0$

Substituting Eq. 2.19 for $j = N$ into Eq. 2.18 gives a_1 in terms of the known amplitude a_{N+1} .

$$a_1 = \frac{a_{N+1} e^{is_1}}{(\text{Re}_{N+1} + \text{Re}'_{N+1}) + i(\text{Im}_{N+1} + \text{Im}'_{N+1})} \quad (2.22)$$

Hence, Eq. 2.19 gives a_j and b_j in terms of a_{N+1} as

$$\begin{aligned} \begin{Bmatrix} a_j \\ b_j \end{Bmatrix} &= \frac{a_{N+1}}{(\text{Re}_{N+1} + \text{Re}'_{N+1}) + i(\text{Im}_{N+1} + \text{Im}'_{N+1})} \begin{bmatrix} e^{is_j} \\ e^{-is_j} \end{bmatrix} \\ &\cdot \begin{Bmatrix} (\text{Re}_j + \text{Re}'_j) + i(\text{Im}_j + \text{Im}'_j) \\ (\text{Re}_j - \text{Re}'_j) - i(\text{Im}_j - \text{Im}'_j) \end{Bmatrix} \end{aligned} \quad (2.23)$$

and the response at the surface of the layered system will be

$$u_1(-H_1, t) = \frac{2a_{N+1}}{\sqrt{(\text{Re}_{N+1} + \text{Re}'_{N+1})^2 + (\text{Im}_{N+1} + \text{Im}'_{N+1})^2}} e^{i(\omega t - \phi_{N+1})} \quad (2.24)$$

with

$$\phi_{N+1}(\omega) = \tan^{-1} \left(\frac{\text{Im}_{N+1} + \text{Im}'_{N+1}}{\text{Re}_{N+1} + \text{Re}'_{N+1}} \right) \quad (2.25)$$

being the phase angle of u_1 with respect to the incident wave when arriving at the base.

Define the following ratio

$$\begin{aligned} \text{AMP}(\omega) &= \frac{|u_1(-H_1, t)|}{|2y(t)|} = \frac{|u_1(-H_1, t)|}{|2a_{2N+1}|} \\ &= \frac{1}{\sqrt{(\text{Re}_{N+1} + \text{Re}'_{N+1})^2 + (\text{Im}_{N+1} + \text{Im}'_{N+1})^2}} \end{aligned} \quad (2.26)$$

where $y(t)$ is the wave form of the incident wave, $y(t+z_N c_{N+1})$, when it arrives at the base where $z_N = 0$. The plots of $\text{AMP}(\omega)$ and $\phi_{N+1}(\omega)$ as functions of the frequency ω are called respectively

the amplification spectrum and the phase spectrum for the surface response with respect to $2y(t)$. Observe that the double amplitude, $2a_{N+1}$, has been used in the definition of $AMP(\omega)$ because $2a_{N+1}$, according to Eq. 2.24, would be the amplitude of the surface motion of the foundation if there were no superficial layers.

By defining the following parameters

$$\begin{aligned} (h_1)_j &= [\text{Re}_j^2 + \text{Re}_j'^2 + \text{Im}_j^2 + \text{Im}_j'^2 + 2(\text{Re}_j \text{Re}_j' + \text{Im}_j \text{Im}_j')]^{\frac{1}{2}} \\ (h_2)_j &= [\text{Re}_j^2 + \text{Re}_j'^2 + \text{Im}_j^2 + \text{Im}_j'^2 - 2(\text{Re}_j \text{Re}_j' + \text{Im}_j \text{Im}_j')]^{\frac{1}{2}} \\ (D_1)_j &= [(h_1)_j + (h_2)_j] / 2 \\ (D_2)_j &= [(h_1)_j - (h_2)_j] / 2 \\ (w_1)_j &= \tan^{-1} \frac{\text{Im}_j + \text{Im}_j'}{\text{Re}_j - \text{Re}_j'} \\ (w_2)_j &= \tan^{-1} \frac{\text{Im}_j - \text{Im}_j'}{\text{Re}_j - \text{Re}_j'} \end{aligned} \quad (2.27)$$

$$\theta_j = [(w_1)_j + (w_2)_j] / 2$$

$$\begin{aligned} f_j(\omega, z_j) &= \cos[\theta_j + (k_R)_j (z_j + H_j)] \{ (D_1)_j \cosh[(k_I)_j (z_j + H_j)] \\ &\quad + (D_2)_j \sinh[(k_I)_j (z_j + H_j)] \} \end{aligned}$$

$$\begin{aligned} g_j(\omega, z_j) &= \sin[\theta_j + (k_R)_j (z_j + H_j)] \{ (D_2)_j \cosh[(k_I)_j (z_j + H_j)] \\ &\quad + (D_1)_j \sinh[(k_I)_j (z_j + H_j)] \} \end{aligned}$$

and

$$\psi_j(\omega, z_j) = \phi_{N+1} - [(w_1)_j - (w_2)_j] / 2 + \tan^{-1}(g_j/f_j)$$

the response in the j^{th} layer can be written explicitly as

$$\text{Re}[u_j(z_j, t)] = 2a_{N+1} \text{AMP}(\omega) \sqrt{f_j^2 + g_j^2} \cos(\omega t - \psi_j) \quad (2.28)$$

where $\text{Re}[\]$ stands for the real part of the quantity inside the bracket.

The foregoing results were derived for layered systems of which the media are described by the Voigt or the standard linear model. If the layer media are Maxwell solids, corresponding results can easily be derived by following the same procedure.

C. Steady-State Response of a Nonviscous Elastic Layered System

For a nonviscous elastic layer system, the parameters τ and A that are associated with the material damping will both vanish from Eq. 2.4. As a consequence, all terms that carry the subscript "I" in previously derived equations will vanish. This in turn leads to

$$\text{Re}_j^I = \text{Im}_j^I = 0 \quad , \quad j = 1, 2, \dots, N$$

in Eqs. 2.20 and 2.21. Also, it can easily be shown that

$$c_j = (c_o)_j$$

$$\mu_j = (\mu_o)_j$$

and

$$\alpha_j = (\alpha_o)_j$$

from Eqs. 2.4, 2.5 and 2.15 respectively. The final results for a nonviscous elastic layered system are given below.

(i) Starting with

$$\text{Re}_1 = 1 \quad \text{and} \quad \text{Im}_1 = 0 \quad (2.29)$$

the recursion formula is reduced to

$$\begin{aligned} \text{Re}_j &= \text{Re}_{j-1} \cos s_{j-1} - \text{Im}_{j-1} \sin s_{j-1} \\ \text{Im}_j &= \alpha_{j-1} (\text{Re}_{j-1} \sin s_{j-1} + \text{Im}_{j-1} \cos s_{j-1}) \end{aligned} \quad (2.30)$$

for $j = 2, 3, \dots, N+1$.

(ii) The amplification spectrum becomes

$$\text{AMP}(\omega) = \frac{1}{\sqrt{\text{Re}_{N+1}^2 + \text{Im}_{N+1}^2}} \quad (2.31)$$

and the phase spectrum

$$\phi_{N+1}(\omega) = \tan^{-1} \frac{\text{Im}_{N+1}}{\text{Re}_{N+1}} \quad (2.32)$$

(iii) The response in the j^{th} layer is

$$\text{Re}[u_j(z_j, t)] = 2a_{N+1} \text{AMP}(\omega) G_j(\omega) \cos[k_j(z_j + H_j) + \phi_j] \cos(\omega t - \phi_{N+1}) \quad (2.33)$$

where it is defined that

$$G_j(\omega) = \sqrt{\text{Re}_j^2 + \text{Im}_j^2} \quad (2.34)$$

and

$$\phi_j(\omega) = \tan^{-1} \frac{\text{Im}_j}{\text{Re}_j}$$

Eq. 2.33 indicates that standing waves can exist in a nonviscous elastic layered system under steady-state excitation.

The characteristic frequency of a nonviscous elastic N-layer system is to be defined. Let ω_n satisfy the following equation

$$\operatorname{Re}_{N+1}(\omega_n) = 0, \quad n = 1, 2, \dots \quad (2.35)$$

We then have

$$\begin{aligned} \operatorname{AMP}(\omega_n) &= \frac{1}{|\operatorname{Im}_{N+1}(\omega_n)|} \\ &= \frac{1}{\alpha_N |\operatorname{Re}_N \sin s_N + \operatorname{Im}_N \cos s_N|_{\omega=\omega_n}} \end{aligned}$$

$\operatorname{AMP}(\omega_n)$ is seen to approach infinity as α_N approaches zero. In the limiting case that $\alpha_N = 0$, the foundation is rigid and the system will have resonant response with infinite amplitude at ω_n . Hence, the roots of Eq. 2.35 are the characteristic frequencies of the layered system, which, in the limiting case that $\alpha_N = 0$, are conveniently called the natural frequencies. Also, Eq. 2.35 indicates that the values of the characteristic frequencies are independent of the property of the half-space foundation.

In most realistic layer problems, the foundation would be more or less deformable, namely, the impedance ratio α_N is different from zero, and the value of $\operatorname{AMP}(\omega_n)$ will always be finite. Physically, this implies that the deformability of the foundation causes the loss of a certain amount of energy through trans-

mission back into the foundation from the layered system. Such an interpretation, first emphasized by Kanai, ⁽⁵⁾ can be referred to as the "geometric dissipation" of wave energy due to the deformability of the foundation.

A layered system with increasing layer stiffnesses, i. e., $0 < \alpha_j \leq 1$ for $j = 1, 2, \dots, N$, is of most practical interest, and several important assertions concerning the nature of the amplification spectrum of such a system can be derived as follows.

Assertion A. The quantities $\text{Re}_j(\omega)$ and $\text{Im}_j(\omega)$ never vanish simultaneously.

The truth of assertion A is obvious by inspection for cases of $j = 1$ and $j = 2$. For the cases of $j \geq 3$, Eq. 2.30 gives

$$\begin{aligned} \text{Re}_j^2 + \text{Im}_j^2 / \alpha_{j-1}^2 &= (\cos s_{j-1} \text{Re}_{j-1} - \sin s_{j-1} \text{Im}_{j-1})^2 \\ &\quad + (\sin s_{j-1} \text{Re}_{j-1} + \cos s_{j-1} \text{Im}_{j-1})^2 \\ &= \text{Re}_{j-1}^2 + \text{Im}_{j-1}^2 \end{aligned} \quad (2.36)$$

Rearranging the right-hand side, Eq. 2.36 becomes

$$\text{Re}_j^2 + \text{Im}_j^2 / \alpha_{j-1}^2 = (1 - \alpha_{j-2}^2) \text{Re}_{j-1}^2 + \alpha_{j-2}^2 (\text{Re}_{j-1}^2 + \text{Im}_{j-1}^2 / \alpha_{j-2}^2)$$

Upon repeated application of the above recursive equation, we finally arrive at

$$\begin{aligned}
& \operatorname{Re}_j^2 + \operatorname{Im}_j^2 / \alpha_{j-1}^2 \\
&= \operatorname{Re}_{j-1}^2 (1 - \alpha_{j-2}^2) + \operatorname{Re}_{j-2}^2 (1 - \alpha_{j-3}^2) \alpha_{j-2}^2 + \dots + \left(\prod_{k=1}^{j-2} \alpha_k^2 \right) (\operatorname{Re}_1^2 + \operatorname{Im}_1^2) \\
&= \prod_{k=1}^{j-2} \alpha_k^2 + \sum_{k=2}^{j-1} \operatorname{Re}_k^2 (1 - \alpha_{k-1}^2) \left(\prod_{i=k}^{j-2} \alpha_i^2 \right) \quad j = 3, 4, \dots, N+1 \quad (2.37)
\end{aligned}$$

by using the fact that $\operatorname{Re}_1^2 + \operatorname{Im}_1^2 = 1$. The right-hand side of Eq. 2.37 is obviously greater than zero always and, therefore, assertion A holds.

Assertion B. The value of the amplification spectrum is always finite and is greater than or equal to 1.

To prove this assertion, add $\operatorname{Im}_j^2 (1 - 1/\alpha_{j-1}^2)$ to both sides of Eq. 2.36, and we have

$$\operatorname{Re}_j^2 + \operatorname{Im}_j^2 = \operatorname{Re}_{j-1}^2 + \operatorname{Im}_{j-1}^2 - \operatorname{Im}_j^2 (1 - \alpha_{j-1}^2) / \alpha_{j-1}^2$$

Applying this recursive relation repeatedly gives

$$\begin{aligned}
\operatorname{Re}_j^2 + \operatorname{Im}_j^2 &= (\operatorname{Re}_1^2 + \operatorname{Im}_1^2) - \operatorname{Im}_2^2 (1 - \alpha_1^2) / \alpha_1^2 - \dots - \operatorname{Im}_j^2 (1 - \alpha_{j-1}^2) / \alpha_{j-1}^2 \\
&= 1 - \sum_{k=1}^{j-1} \operatorname{Im}_{k+1}^2 (1 - \alpha_k^2) / \alpha_k^2 \quad (2.38)
\end{aligned}$$

Since we have made the assumption that $\alpha_k^2 \leq 1$ for $k = 1, 2, \dots, N$, the total sum under the summation sign at the right-hand side of Eq. 2.38 will always be positive. Also it follows from assertion A that the quantity $\operatorname{Re}_j^2 + \operatorname{Im}_j^2$ never vanishes. As a consequence, the following inequality holds.

$$0 < \text{Re}_j^2 + \text{Im}_j^2 \leq 1$$

Substituting $j = N + 1$ into the above equation, it immediately follows from Eq. 2.31 that

$$\infty > \text{AMP}(\omega) \geq 1 \quad (2.39)$$

Hence assertion B is proved.

Assertion C. The amplification factor, $\text{AMP}(\omega_n)$, has an upper bound equal to $1/(\alpha_1 \cdot \alpha_2 \cdot \dots \cdot \alpha_N)$ and a lower bound equal to $1/\alpha_N$.

To obtain these bounds, use will be made of assertion A which, for $j = N + 1$, gives

$$\text{Re}_{N+1}^2 + \text{Im}_{N+1}^2 / \alpha_N^2 = \text{Re}_N^2 + \text{Im}_N^2$$

Since $\text{Re}_{N+1}(\omega_n)$ vanishes from Eq. 2.35, it follows that

$$\text{Im}_{N+1}^2(\omega_n) = \alpha_N^2 [\text{Re}_N^2(\omega_n) + \text{Im}_N^2(\omega_n)]$$

Using Eq. 2.38 for $j = N$, the last equation becomes

$$\text{Im}_{N+1}^2(\omega_n) = \alpha_N^2 \left[1 - \sum_{k=1}^{N-1} \text{Im}_{k+1}^2(\omega_n) (1 - \alpha_k^2) / \alpha_k^2 \right] \quad (2.40)$$

Assertion B then suggests that

$$\text{Im}_{N+1}^2(\omega_n) \leq \alpha_N^2 \quad (2.41)$$

or

$$|\text{Im}_{N+1}(\omega_n)| \leq \alpha_N$$

On the other hand, setting $j = N+1$ in Eq. 2.37 gives

$$\begin{aligned} \operatorname{Im}_{N+1}^2(\omega_n)/\alpha_N^2 &= \sum_{k=1}^{N-1} \alpha_k^2 + \sum_{k=2}^N \operatorname{Re}_k^2(1 - \alpha_{k-1}^2) \left(\prod_{i=k}^{N-1} \alpha_i^2 \right) \\ &\geq \prod_{k=1}^{N-1} \alpha_k^2 \end{aligned} \quad (2.42)$$

or simply

$$|\operatorname{Im}_{N+1}(\omega_n)| \geq \alpha_1 \cdot \alpha_2 \cdot \dots \cdot \alpha_N$$

Eq. 2.41 and the last equation together define the bounds for $\operatorname{AMP}(\omega_n)$ as

$$\frac{1}{\alpha_N} \leq \operatorname{AMP}(\omega_n) \leq \frac{1}{\alpha_1 \cdot \alpha_2 \cdot \dots \cdot \alpha_N}$$

and assertion C is thus established.

Assertion D. $\operatorname{AMP}(\omega_n)$ will assume the minimum value given by assertion C if ω_n satisfies

$$\cos s_N(\omega_n) = \sin s_j(\omega_n) = 0 \quad j = 1, N-1 \quad (2.43)$$

and the maximum value if

$$\cos s_1(\omega_n) = \sin s_j(\omega_n) = 0 \quad j = 2, \dots, N \quad (2.44)$$

For single-layer systems ($N = 1$), $\operatorname{AMP}(\omega_n)$ has a constant value of $1/\alpha_1$ which is both the maximum and the minimum itself.

For $N \geq 2$, Eq. 2.35 gives

$$\operatorname{Re}_{N+1}(\omega_n) = \operatorname{Re}_N(\omega_n) \cos s_N(\omega_n) - \operatorname{Im}_N(\omega_n) \sin s_N(\omega_n) = 0 \quad (2.45)$$

The root, ω_n , in general does not make $\text{AMP}(\omega_n)$ a maximum or a minimum unless some particular conditions are met by the layer parameters.

(i) According to Eq. 2.40,

$$|\text{Im}_{N+1}(\omega_n)| = \alpha_N \left[1 - \sum_{k=1}^{N-1} \text{Im}_{k+1}^2(\omega_n) (1 - \alpha_k^2) / \alpha_k^2 \right]^{\frac{1}{2}} \quad (2.46)$$

From assertion C, a minimum of $\text{AMP}(\omega_n)$ equal to $1/\alpha_N$ will take place only if ω_n satisfies the following condition

$$|\text{Im}_{N+1}(\omega_n)| = \alpha_n$$

The last condition implies that, from Eq. 2.46, the following condition

$$\text{Im}_j(\omega_n) = 0 \quad \text{for } j = 2, 3, \dots, N \quad (2.47)$$

should be fulfilled, which in turn implies that

$$\sin s_j(\omega_n) = 0 \quad \text{for } j = 1, 2, \dots, N-1 \quad (2.48)$$

In addition, letting $j = N$ in Eq. 2.47 and substituting into Eq. 2.45, we have

$$\cos s_N(\omega_n) = 0$$

because, by assertion A, $\text{Re}_N(\omega_n)$ can not vanish. The last equation, together with Eq. 2.48, yields Eq. 2.43—the condition under which the minimum value of $\text{AMP}(\omega_n)$ occurs.

(ii) From Eq. 2.42,

$$|\text{Im}_{N+1}(\omega_n)| = \alpha_N \left[\prod_{j=1}^{N-1} \alpha_j^2 + \sum_{j=2}^N \text{Re}_j^2(\omega_n) (1 - \alpha_{j-1}^2) \left(\prod_{i=j}^{N-1} \alpha_i^2 \right) \right]^{\frac{1}{2}} \quad (2.49)$$

From assertion C, the maximum of $\text{AMP}(\omega_n)$ will occur if ω_n satisfies

$$|\text{Im}_{N+1}(\omega_n)| = \alpha_1 \cdot \alpha_2 \cdot \dots \cdot \alpha_N$$

The last condition can be satisfied only if, in Eq. 2.49,

$$\text{Re}_j(\omega_n) = 0 \quad j = 2, 3, \dots, N \quad (2.50)$$

which in turn implies that, from the recursion formula for Re_j ,

$$\cos s_1(\omega_n) = 0, \text{ and } \sin s_j(\omega_n) = 0 \text{ for } j = 2, 3, \dots, N-1 \quad (2.51)$$

Substituting Eq. 2.50 into Eq. 2.45 for $j = N$ gives the additional condition

$$\sin s_N(\omega_n) = 0$$

The last condition together with Eq. 2.48 constitute the condition, Eq. 2.44, under which the maximum value of $\text{AMP}(\omega_n)$ will occur.

Assertion E. A layer is said to be transparent with respect to a particular frequency Ω if the thickness of the said layer is equal to an integer multiple of the half-wave length.

First of all, by transparent layer we mean that at a particular frequency Ω the amplification spectrum, $\text{AMP}(\Omega)$, is completely independent of the parameters of the said layer. In other words, $\text{AMP}(\Omega)$ can be computed as if this layer is absent.

Let us consider the j^{th} layer. Suppose its thickness to be equal to an integer multiple of the half-wave length at Ω , namely,

$$H_j = \frac{m}{2} \lambda_j(\Omega) \quad m = 1, 2, 3, \dots \quad (2.52)$$

where λ_j is the wave length equal to $2\pi/k_j(\Omega)$. Since Eq. 2.52 implies that

$$s_j(\Omega) = k_j(\Omega)H_j = m\pi$$

we have

$$\sin s_j(\Omega) = 0 \quad \text{and} \quad \cos s_j(\Omega) = (-1)^m$$

Substituting the last equation into the recursion formula for Re_{j+1} gives

$$\begin{aligned} \text{Re}_{j+1}(\Omega) &= (-1)^m \text{Re}_j(\Omega) \\ &= (-1)^m [\text{Re}_{j-1}(\Omega) \cos s_{j-1}(\Omega) - \text{Im}_{j-1}(\Omega) \sin s_{j-1}(\Omega)] \end{aligned}$$

Similarly we can obtain

$$\text{Im}_{j+1}(\Omega) = (-1)^m \frac{\rho_{j-1} c_{j-1}}{\rho_{j+1} c_{j+1}} [\text{Re}_{j-1} \sin s_{j-1} + \text{Im}_{j-1} \cos s_{j-1}]_{\omega=\Omega}$$

Both $\text{Re}_{j+1}(\Omega)$ and $\text{Im}_{j+1}(\Omega)$ are obviously independent of the parameters of the j^{th} layer, which in turn implies that $\text{Re}_{N+1}(\Omega)$ and $\text{Im}_{N+1}(\Omega)$ can be computed as if the j^{th} layer is absent. Hence, assertion E is established.

As already mentioned in the first chapter, from steady-state analysis Kanai has drawn the conclusion that a single-layer system

has prominent resonance at its natural frequencies while, on the other hand, the resonant response of a multi-layer system is less prominent or even indistinguishable. He attributed this behavior of the multi-layer systems to the complicated interference of the waves during reflection and transmission across the layer interfaces. Intuitively, since both of these layered systems are physically similar and differ from each other only in the layer parameters, both would be expected to have resonant responses of comparable prominence. Hence, Kanai's conclusion seems inconsistent. In the following, an interpretation is given to explain the apparent inconsistency.

Theoretically, assertion C indicates that a single-layer system ($N = 1$) has a constant amplification equal to $1/\alpha_1$ at ω_n . The value of α_1 apparently depends on the parameters of the system given and, therefore, needs not be small. Hence, the amplifications at ω_n of a single-layer system need not be prominent. On the other hand, let us consider a multi-layer system that has layer stiffnesses increasing with depth. Assertion C then indicates that, at ω_n , the amplifications are bounded from above by $1/(\alpha_1 \cdot \alpha_2 \cdot \dots \cdot \alpha_N)$ and from below by $1/\alpha_1$. The range defined by these bounds is a measure of the possible variations of $AMP(\omega_n)$. In general, some resonant amplifications may be prominent while the others are suppressed or even indistinguishable. Yet, in spite of these possible variations, all the amplifications, $AMP(\omega_n)$, will be prominent if α_N is sufficiently small.

In short, it can be seen that Kanai's conclusion is not true in

general and is valid only for those layered systems he analyzed. For illustration, a single-layer system and a triple-layer system, arbitrarily chosen, are shown in Figs. 2.3(a) and 2.3(b) respectively. For each system amplification spectra have been computed for three different values of α_N obtained by varying the wave velocity of the foundation. The results are shown in Fig. 2.4(a) for the single-layer system and in Fig. 2.4(b) for the triple-layer system. An inspection of the calculated spectra indicates that α_N has the effect of determining the prominence of the resonant peaks around ω_n . The resonant amplifications for both systems are all prominent if α_N is small, but are greatly suppressed if α_N is large. Therefore, the impedance ratio, α_N , is a measure of the wave energy lost into the foundation due to the deformability of the foundation. Also, it is observed that there is a point between every two consecutive natural frequencies where the value of the amplification spectrum is independent of α_N . Theoretically, such points are located at the "valleys" of the spectrum, corresponding to those frequencies, ω_v , that satisfy the following condition

$$\text{Im}_{N+1}(\omega_v) = 0$$

such that

$$\text{AMP}(\omega_v) = \frac{1}{|\text{Re}_{N+1}(\omega_v)|}$$

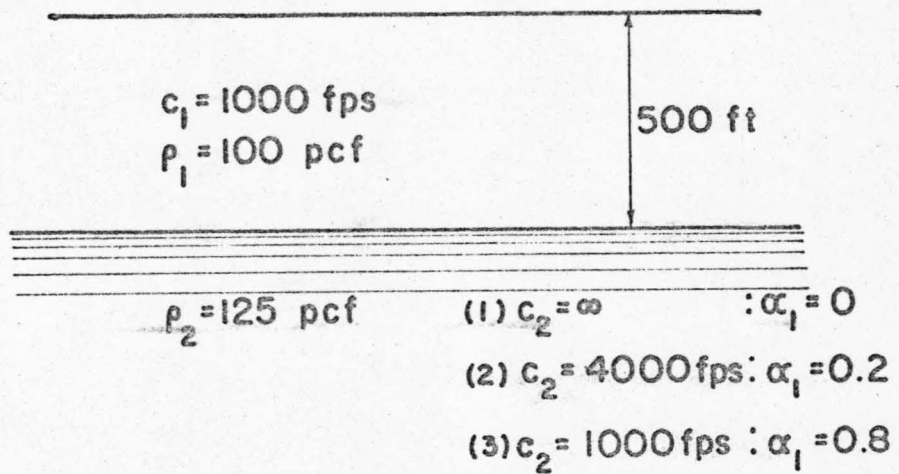


Fig. 2.3(a) THE SINGLE-LAYER SYSTEM (N=1)

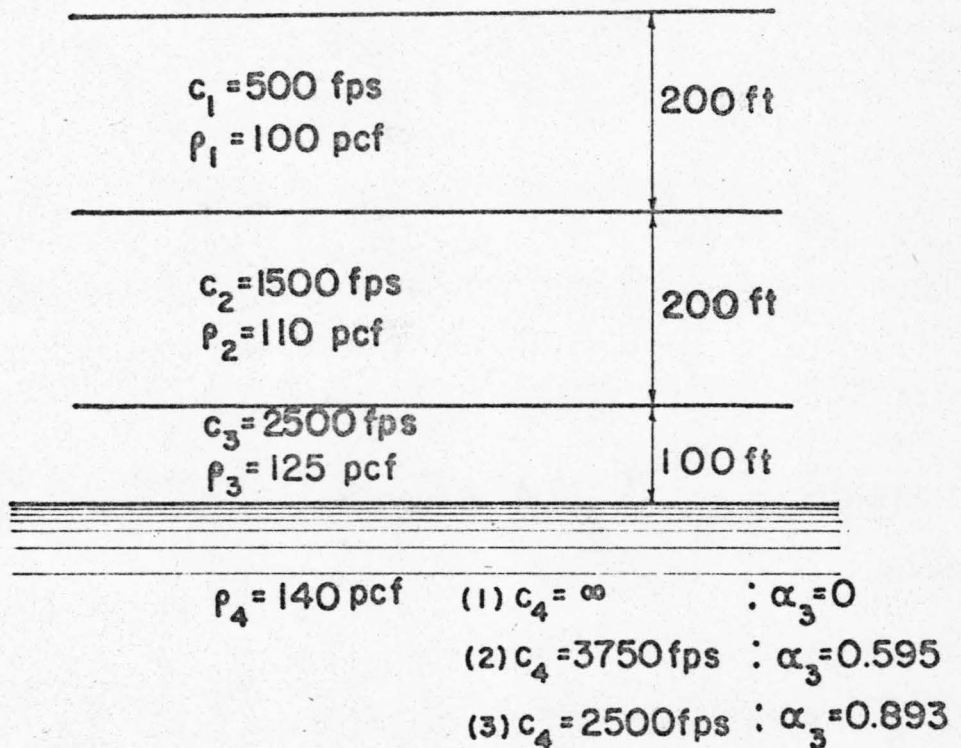
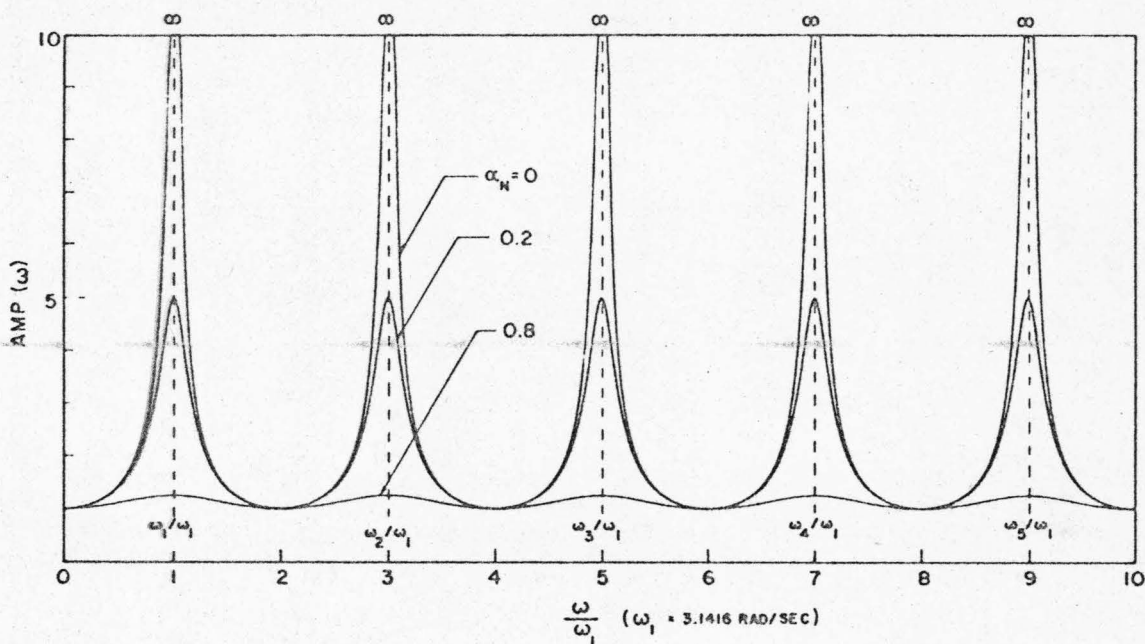


Fig. 2.3(b) THE TRIPLE-LAYER SYSTEM (N=3)

(a) THE SINGLE-LAYER SYSTEM (N=1)



(b) THE TRIPLE-LAYER SYSTEM (N=3)

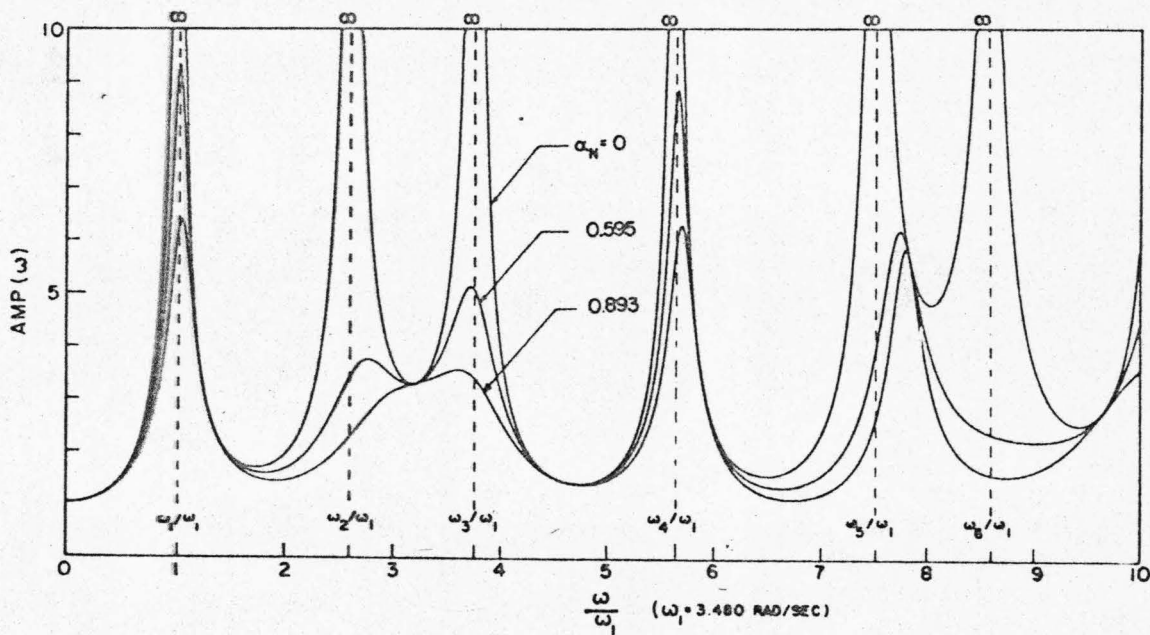


Fig. 2.4. AMPLIFICATION SPECTRA FOR DIFFERENT VALUES OF α_N .

B. NUMERICAL EXAMPLES

Four idealized layered systems were chosen to study the influence of layer parameters, such as the number of layers, layer stiffnesses, viscosities, etc., on the amplification spectrum. The first two systems are double-layered ($N = 2$). The third system is triple-layered ($N = 3$), and the fourth quadruple-layered ($N = 4$). The necessary data for these systems are given in Table 2.1, and were chosen in such a way that the properties of the top layer and those of the foundation are the same for all of the systems. Also, the total thickness of the intermediate layers between the top layer and the foundation is 550 feet for all systems. The effect on the amplification spectrum of a multi-layer system will be studied by varying the number and the properties of the intermediate layers.

As will be shown in Chapter III, the quantity A_1 given in column (8) of Table 2.1 is the amplitude of the surface motion associated with the wave signal that first arrives at the surface due to the incidence of a unit-amplitude impulse at the base. The significance of A_1 is that it measures the amplification of transient input signals after one-way transmission through the layered system. It is interesting to see that the values of A_1 given in Table 2.1 fall into a narrow range from 4.5 to 5.4. Calculations not shown here indicated that, so long as the properties of the top layer and the foundation are fixed, A_1 will essentially be around 5.5 to 5.6 even if the number of intermediate layers is more than three. In other words, increasing the number of intermediate layers would only change A_1 by a

TABLE 2.1. DATA FOR THE IDEALIZED LAYER SYSTEMS

System	(1) Layer No. j	(2) Layer Thickness H_j (ft)	(3) Density ρ_j (pcf)	(4) S-Wave Velocity c_j (ft/sec)	(5) Retardation Time τ_j (sec)	(6) r_j	(7) α_j	(8) A_1
1	1	200	110	1000	0.005	1	0.382	
	2	550	120	2400	0.002	5	0.240	4.67
	BASE		150	8000	0.	100		
2	1	200	110	1000	0.005	1	0.181	
	2	550	135	4500	0.001	20	0.506	4.50
	BASE		150	8000	0.	100		
3	1	200	110	1000	0.005	1	0.382	
	2	200	120	2400	0.002	5	0.474	
	3	350	135	4500	0.001	20	0.506	5.21
	BASE		150	8000	0.	100		
4	1	200	110	1000	0.005	1	0.385	
	2	150	120	2400	0.002	5	0.658	
	3	175	125	3500	0.0015	10	0.720	5.39
	4	225	135	4500	0.001	20	0.506	
	BASE		150	8000	0.	100		

negligible amount.

In order to investigate the effect of material damping, in each system the amplification spectra for three different cases were calculated. These three cases were obtained by considering the layer media as

- (1) nonviscous elastic solids,
- (2) standard linear solids described by the parameters τ_j and r_j which were defined in Eq. 2.3 and are given in column (5) and (6) of Table 2.1,
- (3) Voigt solids described by the same parameters τ_j used in the second case.

The amplification spectra calculated for each layered system are presented in Figs. 2.5(a) to 2.5(d) respectively. Several observations were made of the calculated spectra.

- (a) Except for the first system, the first characteristic frequency, ω_1 , of each system is approximately equal to 6.5 rad/sec.
- (b) The spectra for case (2) always lie between the spectra for case (1) and those for case (3).
- (c) The spectra for the viscous systems are less sensitive than those for the nonviscous systems to the variation of the parameters of the intermediate layers, and they appear very similar to each other. In addition, the spectra for the viscous systems tend to decay with increasing frequency. This is in agreement with theories which show that linear viscoelastic materials always attenuate wave amplitude according to a certain power of wave frequency.

The observations made above lead to the following conclusion.

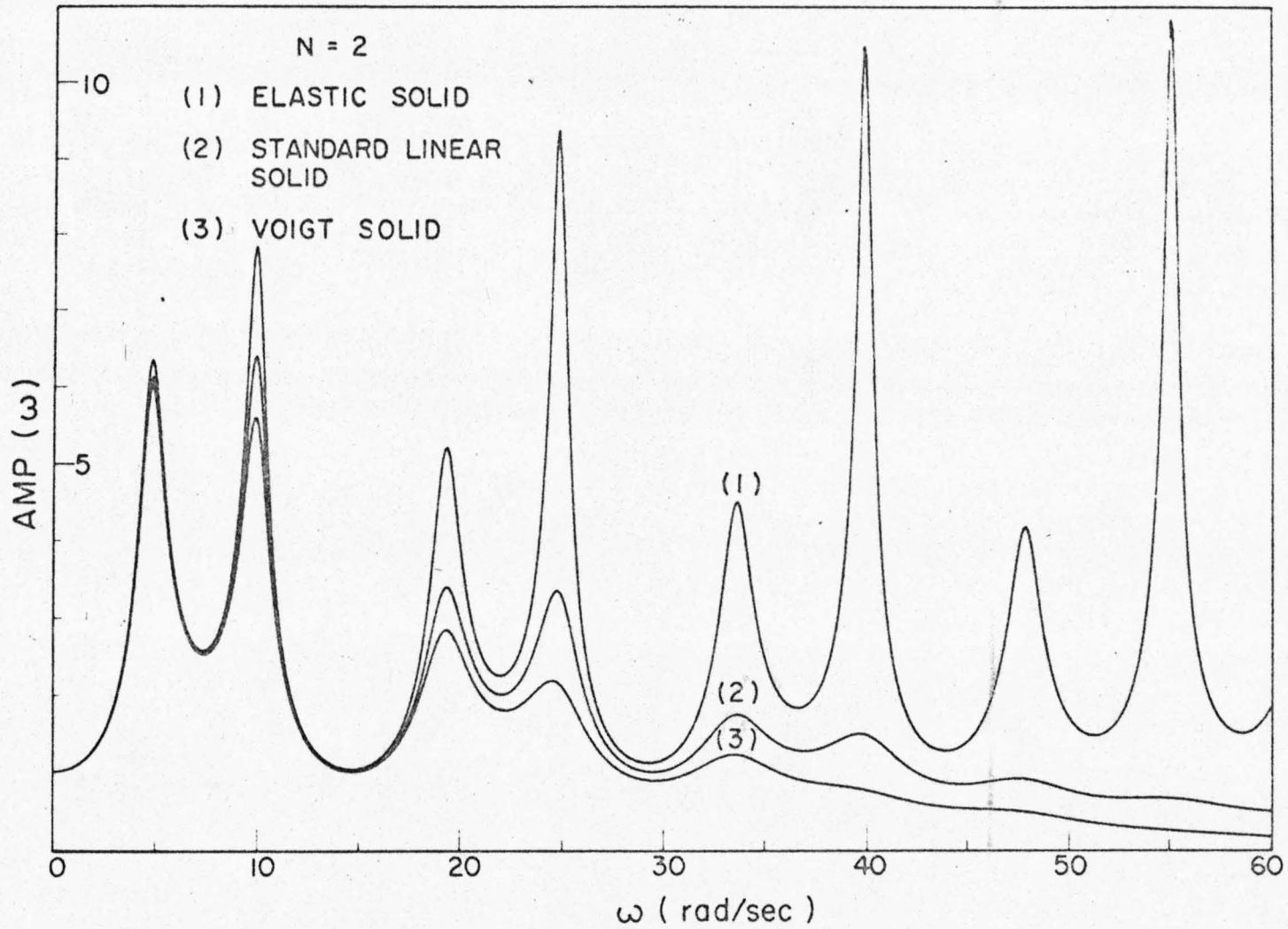


Fig. 2.5(a). AMPLIFICATION SPECTRA

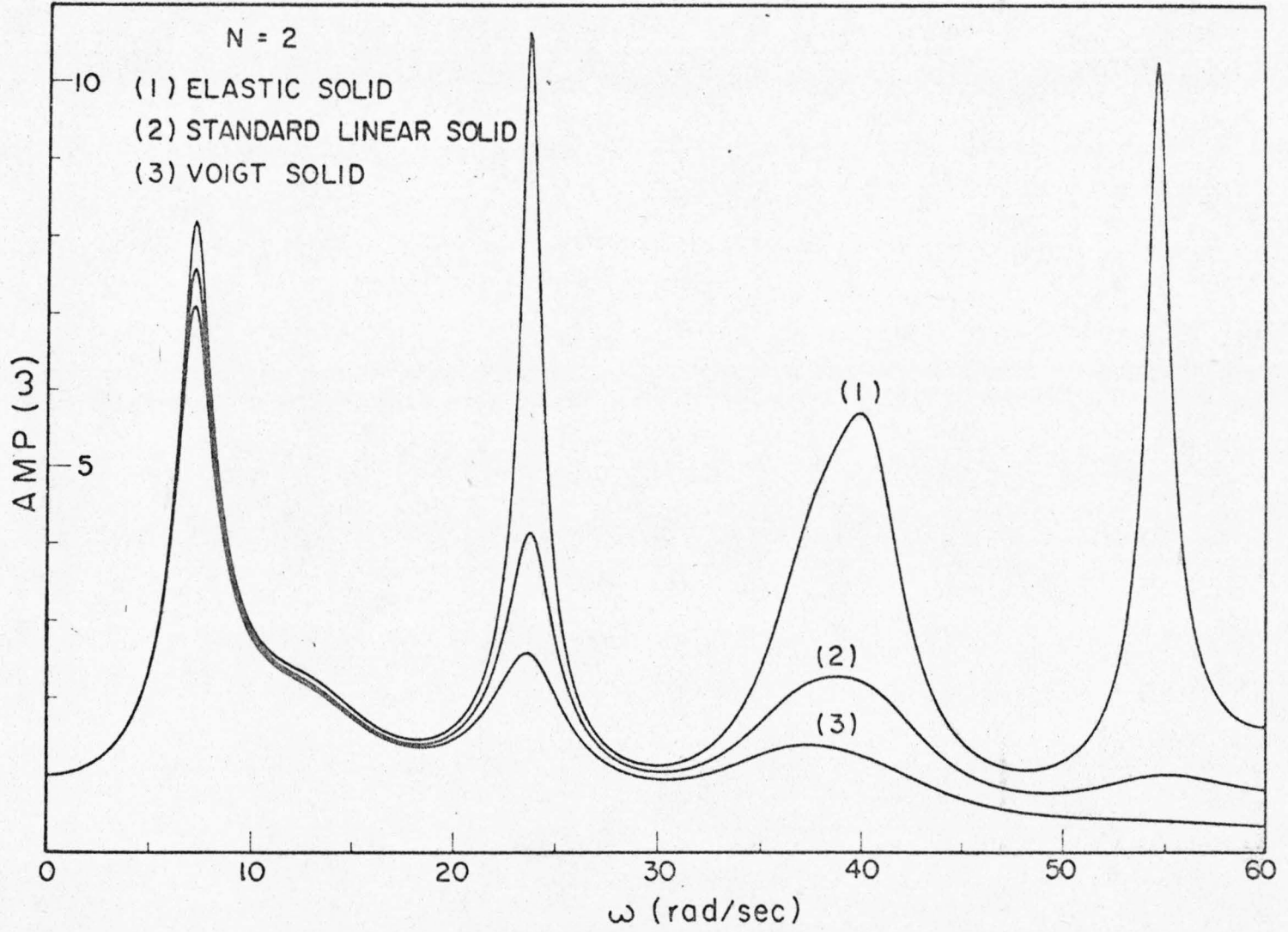


Fig. 2.5(b). AMPLIFICATION SPECTRA

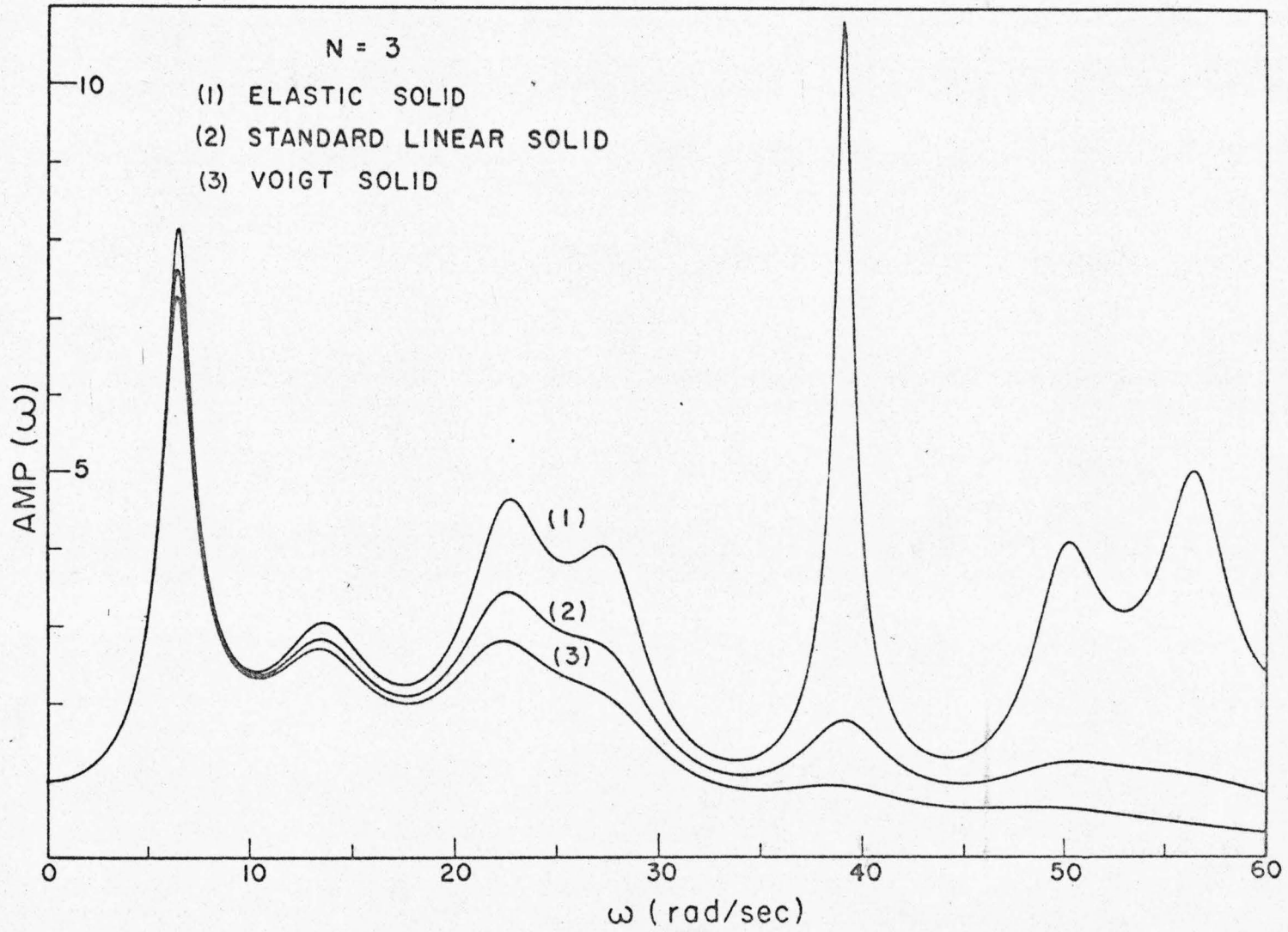


Fig. 2.5(c). AMPLIFICATION SPECTRA

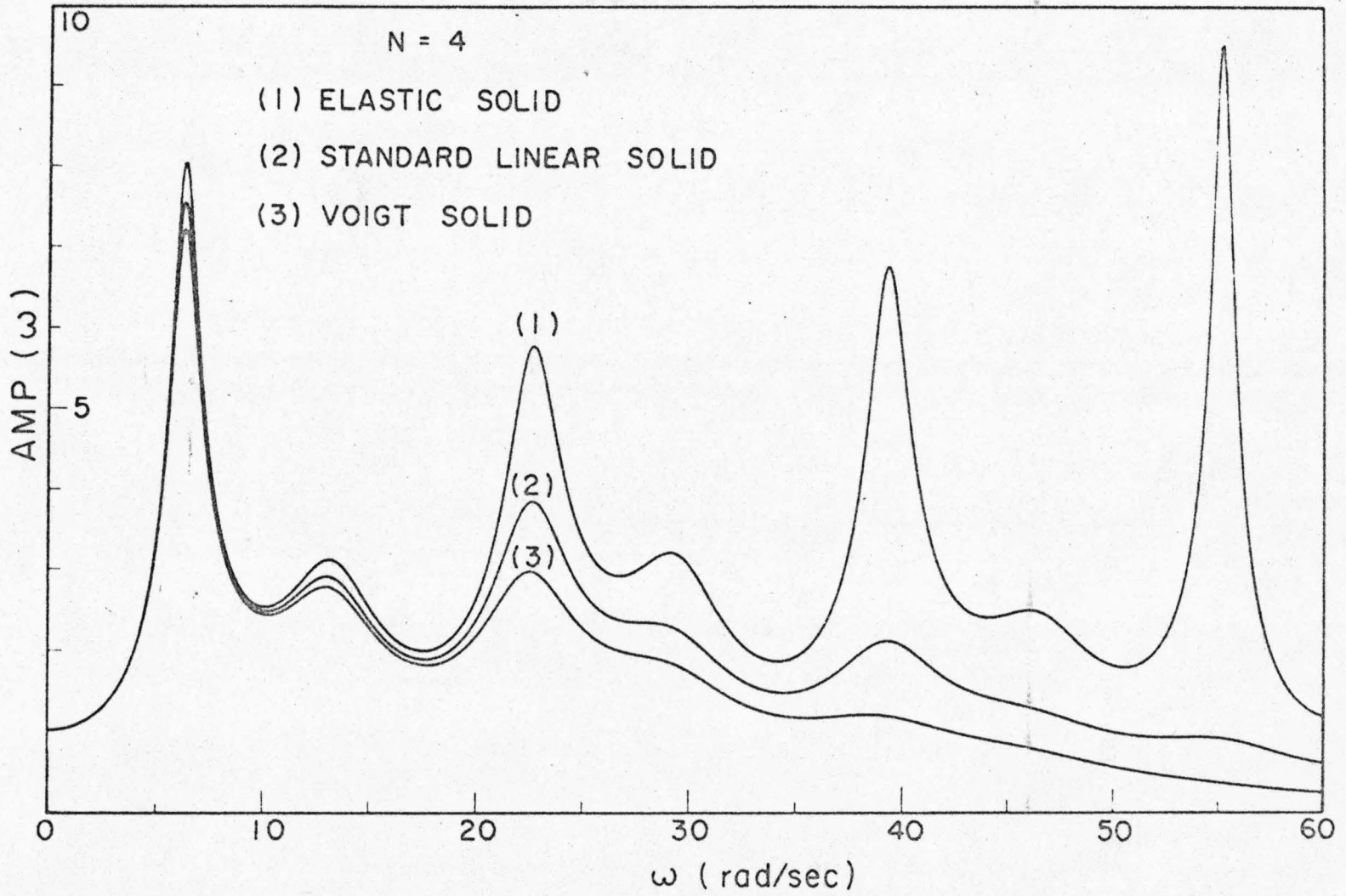


Fig. 2.5(d). AMPLIFICATION SPECTRA

For viscous multi-layer systems having layer stiffnesses increasing with depth, if the properties of the top layer and the foundation are fixed, varying the number and the properties of the intermediate layers will not significantly change the general characteristics of the amplification spectra so long as the total thickness of the intermediate layers remains unchanged. This conclusion may not be valid for nonviscous layered systems because they are more sensitive to the variation of the layer parameters.

III. EXACT TRANSIENT ANALYSIS OF A NONVISCOUS LAYERED SYSTEM

A. Introduction

In this chapter a brief review is given of the techniques for digital computation of the exact response of a nonviscous elastic layered system subjected to transient S-waves normally incident at the base. There are two methods commonly used, namely, the method of Fourier transform and the method of time-domain.

Referring to Fig. 2.2, a transient incident wave, $y(t + z_N/c_{N+1})$, will give rise to an excitation $y(t)$ when arriving at the base where $z_N = 0$. Hereafter, $y(t)$ will be called the input function for a given layered system. Let $h_j(t)$ be the transfer function of the system for the response $u_j(z_j, t)$. Then, $u_j(z_j, t)$ is given theoretically by the following convolutional integral

$$u_j(z_j, t) = \int_0^t 2y(s)h_j(t-s)ds \quad (3.1)$$

Observe that Eq. 3.1 is useful only if $h_j(t)$ is available in an explicit form. For a nonviscous layered system, $h_j(t)$ can be obtained explicitly by the method of time-domain. However, for viscous layered systems, $h_j(t)$ is in general not available in explicit form, and the method of Fourier transform has to be used to compute the response in the frequency-domain. Therefore, the method of Fourier transform is applicable to both viscous and nonviscous systems, and will be reviewed first.

A list of the important symbols to be used in this chapter is given below, and they are defined again when they first appear in the text. Whenever possible, the symbols defined in Chapter II are used.

<u>SYMBOL</u>	<u>EXPLANATION OR DEFINITION</u>
A_j	amplitude of the j^{th} arrival of a wave signal at the surface
ACU	prescribed accuracy for truncating the ray-tracing scheme
c_ℓ	S-wave velocity in ℓ^{th} sublayer
$\delta(t)$	Dirac delta function
$h_j(t)$	transfer function for $u_j(z_j, t)$ in time-domain
$H_j(\omega)$	transfer function for $u_j(z_j, t)$ in frequency-domain
h_ℓ	thickness of ℓ^{th} sublayer
ℓ	layer index for the subdivided layered system
L	total number of sublayers
M	a positive integer number
R_d, R_u	coefficient of downward reflection and coefficient of upward reflection respectively
t_j	arriving time of the j^{th} wave signal at the surface
T_d, T_u	coefficient of downward transmission and coefficient of upward transmission respectively
Δt	h_ℓ/c_ℓ , equal to a constant for $\ell = 1, 2, \dots, L$
ΔT	time interval for the digitized input function $y(t)$
$u_j(z_j, t)$	transient response in the j^{th} layer
$U_j(\omega)$	the Fourier transform of $u_j(z_j, t)$

<u>SYMBOL</u>	<u>EXPLANATION OR DEFINITION</u>
z_ℓ	local coordinate for ℓ^{th} and $\ell+1^{\text{th}}$ sublayers
$y(t)$	input function
$Y(\omega)$	the Fourier transform of $y(t)$

B. The Method of Fourier Transform

By definition, the Fourier transform of the output $u_j(z_j, t)$ is given by

$$U_j(\omega) = \int_{-\infty}^{\infty} u_j(z_j, t) e^{i\omega t} dt \quad (3.2)$$

From the well known formula for the Fourier transform of a convolution integral, Eq. 3.1 is transformed into

$$U_j(\omega) = 2H_j(\omega)Y(\omega) \quad (3.3)$$

in which

$$H_j(\omega) = \int_{-\infty}^{\infty} h_j(t) e^{i\omega t} dt \quad (3.4)$$

and

$$Y(\omega) = \int_{-\infty}^{\infty} y(t) e^{i\omega t} dt \quad (3.5)$$

are, respectively, the Fourier transform of $h_j(t)$ and $y(t)$. Unless $y(t)$ is a special mathematical function, the Fourier transform of $y(t)$ usually cannot be obtained analytically and a digital computer must be used.

According to the definition of $H_j(\omega)$, Eq. 2.33 provides

$$H_j(\omega) = \text{AMP}(\omega) G_j(\omega) e^{-i\phi_{N+1}(\omega)} \quad (3.6)$$

where $\text{AMP}(\omega)$, $G_j(\omega)$ and $\phi_{N+1}(\omega)$ were defined in Eqs. 2.31, 2.34 and 2.32 respectively. Setting $j = 1$ in Eq. 3.6 gives

$$H_1(\omega) = \text{AMP}(\omega) e^{-i\phi_{N+1}(\omega)} \quad (3.7)$$

With the transfer function $H_j(\omega)$ at hand, $U_j(\omega)$ can be calculated according to Eq. 3.3. The inverse Fourier transform is then performed on $U_j(\omega)$ to obtain u_j as

$$u_j(z_j, t) = \frac{1}{2\pi} \int_{-\infty}^{\infty} U_j(\omega) e^{-i\omega t} d\omega \quad (3.8)$$

The inverse transformation usually has to be done by digital computer. However, the digital inversion has a basic difficulty in that severe aliasing errors may be introduced. Briefly speaking, the aliasing errors arise in the following manner. Theoretically, the transfer function $h_j(t)$ has an infinite duration due to multiple reflections of the wave signals inside the layered system. For purpose of practicability, we are usually interested in only that part of the transfer function up to a certain effective time, say, t_{eff} . Note that the transfer function $H_j(\omega)$ at hand is the Fourier transform of the entire history of $h_j(t)$, not that part of $h_j(t)$ occurring prior to t_{eff} . Suppose that it is desired to invert $H_j(\omega)$ numerically at an equal frequency interval $\Delta\omega$, and let $\Delta\tau = 2\pi/\Delta\omega$. Trorey⁽²⁸⁾ has found that a poor inversion would be obtained unless $\Delta\tau$ is sufficiently small so that

$\Delta\tau$ is greater than t_{eff} . Hence, to avoid appreciable inversion errors we must know the value of t_{eff} beforehand in order that a suitable choice of $\Delta\omega$ can be made. But, t_{eff} itself is actually a part of the answer we are seeking and is generally not available in advance. Consequently, there is no way of telling the reliability of the inversion unless, by trial and error, we obtain a value of $\Delta\omega$ that is small enough to cause negligible change in the final answer. Such a procedure is cumbersome, and this is the reason why the method of Fourier transform is little used for finding the exact transient response of a nonviscous layered system.

C. The Method of Time-Domain (The Ray-Tracing Technique)

The method of time-domain enables one to compute explicitly the transfer function $h_j(t)$ for a nonviscous layered system by digital computer. The ray-tracing scheme proposed by Baranov and Kunetz⁽²²⁾ is by far the most efficient method for digital computation of $h_j(t)$. It has the advantage over the method of Fourier transform in that it requires less computing time and the question of aliasing errors does not arise. In addition, the ray-tracing technique can compute $h_j(t)$ of any desired duration.

The principle of the ray-tracing scheme is the subdivision of the original N-layer system into an L-layer system, each sublayer of which has a constant "time thickness" such that the one-way traveling time of a signal through any sublayer is a constant equal to, say Δt . Unless the original N-layer system already satisfies the principle stated above and hence L is equal to N, in general the given system has to be subdivided and L is greater than N. Figure 3.1 shows the subdivided system with

$$\Delta t = h_\ell / c_\ell = \text{constant}, \quad \ell = 1, 2, \dots, L \quad (3.9)$$

where h_ℓ and c_ℓ are respectively the thickness and the S-wave velocity of the ℓ^{th} sublayer.

Now, let the input function at the base be a unit-impulse, i. e., $y(t) = \delta(t)$. If the transfer function, $h_1(t)$, for the surface response is desired, then, by definition $h_1(t)$ can be found by computing the response at the surface of the system to the input function $\delta(t)$. The numerical computations are to be carried out in the z - t plane at the intersecting joints between the following two families of straight lines:

- (1) the straight lines that are parallel to the z -axis and equally spaced at the time interval Δt , and
- (2) the interfaces between any two adjacent sublayers.

Consider a typical intersecting joint, $M(z_M, t_M)$, at a depth z_M and time t_M in the z - t plane. In general, there are two wave signals incident from the neighboring intersections and meeting at M . Referring to Fig. 3.2, let the incident wave signals be b_E and a_F , where b_E propagates downward from the upper intersection $E(z_E, t_M - t)$ and a_F propagates upward from the lower intersection $F(z_F, t_M - t)$. As a consequence, two signals, a_M and b_M are emitted from M due to reflection and transmission of the incident signals across the interface between the ℓ^{th} and $\ell + 1^{\text{th}}$ sublayers where, according to Fig. 3.2, $z_\ell = 0$. Since the governing differential equations for a nonviscous layered system are the one-dimensional wave equations

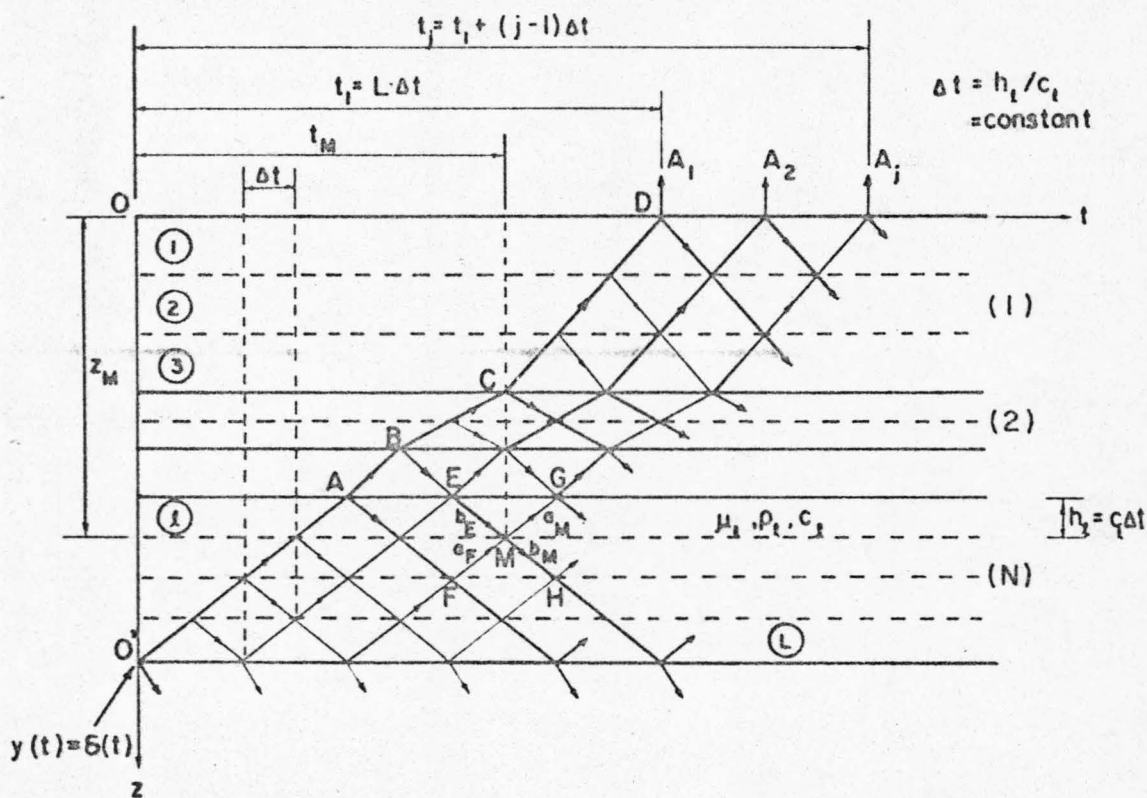


Fig. 3.1 DIAGRAMMATIC SCHEME FOR THE RAY-TRACING TECHNIQUE

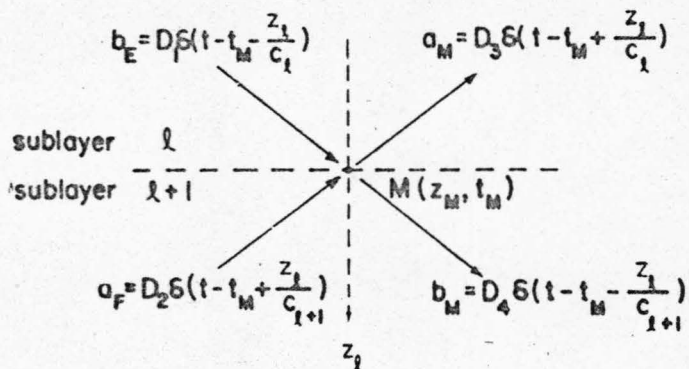


Fig. 3.2 INCIDENT AND EMITTED SIGNALS AT A TYPICAL JOINT M

$$c_l^2 \frac{\partial^2 u_l(z_l, t)}{\partial z_l^2} = \frac{\partial^2 u_l(z_l, t)}{\partial t^2}, \quad \ell = 1, 2, \dots, L \quad (3.10)$$

each of the propagating signals will assume the form of a delta function with a certain amplitude if $\delta(t)$ is the input function. Hence, we can write

$$\begin{aligned} b_E &= D_1 \delta(t - t_M - z_l/c_l) \\ a_F &= D_2 \delta(t - t_M + z_l/c_{l+1}) \\ a_F &= D_3 \delta(t - t_M + z_l/c_l) \end{aligned} \quad (3.11)$$

and

$$b_M = D_4 \delta(t - t_M - z_l/c_{l+1})$$

so that the responses in the ℓ^{th} and $(\ell+1)^{\text{th}}$ sublayers will be, respectively,

$$u_\ell(z_\ell, t) = b_E + a_M$$

and

$$u_{\ell+1}(z_{\ell+1}, t) = a_F + b_M$$

Continuity of the displacements across the interface where $z_\ell = 0$ requires that

$$D_1 + D_3 = D_2 + D_4 \quad (3.12)$$

In addition, continuity of the shearing stresses gives

$$\alpha_\ell (-D_1 + D_3) = D_2 - D_4 \quad (3.13)$$

in which

$$\alpha_\ell = \frac{\rho_\ell c_\ell}{\rho_{\ell+1} c_{\ell+1}}$$

is the impedance ratio between the l^{th} and $l+1^{\text{th}}$ sublayers. Equations 3.12 and 3.13 then give the solutions for D_3 and D_4 as

$$D_3 = (R_u)_l D_1 + (T_u)_l D_2$$

and

(3.14)

$$D_4 = (T_d)_l D_1 + (R_d)_l D_2$$

where

$$(R_u)_l = -\frac{1-\alpha_l}{1+\alpha_l}$$

$$(R_d)_l = \frac{1-\alpha_l}{1+\alpha_l} = -(R_u)_l$$

(3.15)

$$(T_u)_l = \frac{2}{1+\alpha_l} = 1-(R_u)_l$$

and

$$(T_d)_l = \frac{2\alpha_l}{1+\alpha_l} = 1+(R_u)_l$$

are respectively the coefficient of upward reflection, the coefficient of downward reflection, the coefficient of upward transmission, and the coefficient of downward transmission.

With the coefficients of reflection and transmission given by Eq. 3.15 for each of the sublayer interfaces, the ray-tracing scheme can be started from $0'$ where the input signal $\delta(t)$ acts. The numerical scheme is advanced step by step with a step size equal to Δt . At each step the process defined by Eq. 3.14 is operated at every other intersecting joint on the vertical line whose abscissa corresponds to the time of the step under consideration. Proceeding in this manner, the resultant ray paths in the z - t plane will constitute a network as shown in Fig. 3.1, in which the thicker paths are those paths along which signals actually travel.

Because of the propagating nature of waves it is obvious that no disturbance will be felt anywhere inside the region to the left of the path $0'ABCD$. After direct transmission through the layered system, the signal that first arrives at the surface can be represented by $A_1 \delta(t-t_1)$ where

$$A_1 = 2(T_u)_1 (T_u)_2 \cdots (T_u)_L = 2 \prod_{l=1}^L \frac{2}{1+\alpha_l} \quad (3.16)$$

and

$$t_1 = L \cdot \Delta t \quad (3.17)$$

Similarly, the surface response due to the j^{th} subsequent signal arrival at the surface can be denoted by $A_j \delta(t-t_j)$ where

$$t_j = t_1 + 2(j-1)\Delta t \quad (3.18)$$

The entire transfer function, $h_1(t)$, is thus given theoretically by

$$h_1(t) = \frac{1}{2} \sum_{j=1}^{\infty} A_j \delta(t-t_j) \quad (3.19)$$

To compute the entire transfer function will take an infinite amount of time on a digital computer and, therefore, is impractical. Instead, we will compute an effective transfer function that has a duration equal to, say, t_{eff} , if all subsequent signals have died off to such a weak strength that their total contribution to the transfer function is negligible. Since t_{eff} itself is not available beforehand, a different criterion must be used to truncate properly the numerical process as follows.

When the numerical process is operated at each intersecting joint, amplitudes of the emitted signals are checked. An emitted signal is set null if its eventual contribution to $h_1(t)$ is, say, $A_p \delta(t-t_p)$ where A_p satisfies the condition

$$A_p < A_1 \cdot ACU \quad (3.20)$$

In Eq. 3.20, ACU is a given positive number and is considered a measure of the truncating error of the numerical process. The effective transfer function obtained this way is a finite series given by

$$h_1(t) \approx \frac{1}{2} \sum_{j=1}^K A_j \delta(t-t_j) \quad (3.21)$$

and is said to possess an imposed accuracy of ACU because the criterion

$$A_j < A_1 \cdot ACU \text{ for } j \geq K+1$$

is satisfied. Actual calculations have indicated that a value of ACU equal to 0.005 is sufficient in most cases, and the small errors involved are essentially associated with high frequencies only. Substituting the effective transfer function into Eq. 3.1 yields the desired surface response to an arbitrary input function $y(t)$ as

$$u_1(-H_1, t) = \sum_{j=1}^K A_j y(t-t_j) \quad (3.22)$$

D. Discussions

The ray-tracing technique has the advantage over the method of frequency-domain in that the former is much faster and any desired accuracy can be achieved. Yet it has the following drawbacks.

(1) Let the input function $y(t)$ be digitized at a time interval, say, ΔT . To apply Eq. 3.22, an integer-multiple relation between ΔT and $2\Delta t$ will be required. That is, either

$$\Delta T = M(2\Delta t) \quad (M > 1) \quad (3.23)$$

or

$$\Delta T = 2\Delta t/M \quad (M \geq 1) \quad (3.24)$$

has to be satisfied, with M being a positive integer. If the first relation is the case, u_1 will be obtained in a digitized form with the smaller time interval $2\Delta t$. However, if the second relation is the case u_1 will still be digitized in the time interval ΔT . For a given layered system, it is usually necessary to adjust the layer parameters slightly such that either of the previous relations can be satisfied. Such adjustment has to be small to avoid introducing appreciable errors into the computation of the effective transfer function. Moreover, in many cases it is the first relation that has to be fulfilled. In this case, if M is fairly large, analysis using the calculated response, u_1 , as an input will require more computing time than if u_1 is digitized in ΔT .

(2) The ray-tracing technique does not apply to viscous layered systems. Hence, problems involving viscous layered systems will have to be solved by the method of frequency-domain unless a simpler, powerful method is developed.

In summary, both the method of Fourier transform and the ray-tracing technique have some shortcomings, which suggests the need of a better method. The development of such a method is discussed in the next chapter.

IV. MODIFIED SHEAR BEAM MODELS FOR APPROXIMATE TRANSIENT ANALYSIS OF A LAYERED SYSTEM

A. Introduction

The model consisting of a shear beam with a rigid foundation has been used by Whitman⁽²³⁾, Idriss and Seed^(24, 25) for a layered system because of the analogy between the governing differential equations of a shear beam and a layered system. The model is first lumped into a discrete system. Then, by the technique of modal analysis or, if necessary, the technique of direct numerical integration, the discrete model can be analyzed to obtain the approximate transient response of a layered system. The drawback of this model is that the energy loss due to the deformability of the foundation is not taken into account. In this chapter, two modified shear beam models are established which account for the energy lost into the foundation.

The first model consists of a shear beam connected at its base to the input excitation by a suitable viscous dashpot which in effect is a substitute for the half-space foundation. This model is an exact analog of a given layered system which is nonviscous. A technique of continuous modal analysis is used to analyze the model directly. For practical purposes, usually it is sufficient to consider only a finite number of modes of the shear beam. The resultant system of equations to be solved is a set of second order differential equations coupled with a first order differential equation representing the motion of the dashpot. Since viscous damping will have to be included in the model if the given layered system is viscous, an iterative process is proposed for determining the modal dampings directly from the transfer function of the layered system.

The second model is a further approximation of the original layered system, and it is exact if the half-space foundation is rigid. It consists of a viscous shear beam resting on a rigid foundation. The technique of continuous modal analysis is again used to analyze this model. To account approximately for the energy lost into the foundation, a certain amount of viscous damping is introduced in each mode by the iterative scheme used for analyzing the first model. Therefore, there is always some viscous damping in the model. This model gives good results only for computing the response at or near the surface of the layered system that has a considerable difference between the stiffnesses of the foundation and the lowest layer, which does include most cases of practical interest.

Numerical examples are given for computing the transient surface response of a given layered system by both models. Velocity spectra of the output are also computed to study the effect of the layered system.

A list of the symbols to be used in this chapter is given below, and they are defined again when they first appear in the text. Whenever possible, the symbols defined in the previous chapters are used.

<u>SYMBOL</u>	<u>EXPLANATION OR DEFINITION</u>
[A]	normal mode matrix
[B]	diagonalized damping matrix
[C],[C']	damping matrix
C_{eff}	effective damping coefficient
D	viscous damper for the first model, having a damping coefficient equal to $\rho_{N+1} c_{N+1}$

<u>SYMBOL</u>	<u>EXPLANATION OR DEFINITION</u>
$D_r^{(j)}(z_j)$	r^{th} modal participating factor for computing $u_j(z_j, t)$
$(\text{ERR})_r^{(q)}$	q^{th} iterative error when computing β_r
$(F)_r$	$(K_{\text{eff}})_r / \rho_{N+1} c_{N+1}$
$H_j(\omega), \bar{H}_j(\omega)$	respectively the exact and the approximate transfer function for $u_j(z_j, t)$ with respect to $y(t)$
$H_{j,N}(\omega), \bar{H}_{j,N}(\omega)$	respectively the exact and the approximate transfer function for $u_j(z_j, t)$ with respect to $u_N(0, t)$
$[K]$	stiffness matrix
K_{eff}	effective spring stiffness
$\{m\}$	mass vector
m_{eff}	effective mass
$[M]$	mass matrix
q_j	coefficient in the Caughey's series
$(Q)_r$	$(C_{\text{eff}})_r / \rho_{N+1} c_{N+1}$
r	subscript, referring to the modal number
R	number of lumped masses in a lumped representation of the first model
S	total number of modes used in computing the approximate response

SYMBOLEXPLANATION OR DEFINITION

$[U]$	unitary matrix
$\tilde{v}_r(t), v_r(t)$	r^{th} normal coordinate in, respectively, the discrete and the continuous model
$W(t)$	$2y(t)$
$\tilde{x}_r(t), x_r(t)$	r^{th} displacement coordinate in, respectively, the discrete and the continuous model
$y(t)$	input function
$\ Z\ _r^2$	norm of the r^{th} continuous modal shape
$\tilde{\beta}_r, \beta_r$	r^{th} modal fraction of critical damping in, respectively, the discrete and the continuous model
$[\Lambda^2]$	eigenfrequency matrix or diagonalized stiffness matrix
$\tilde{\xi}_r(t), \xi_r(t)$	further transformed normal coordinate in, respectively, the discrete and the continuous model
$\tilde{\omega}_r, \omega_r$	r^{th} natural frequency of the discrete and the continuous model respectively.

B. The First Model for Nonviscous Elastic Layered Systems

As shown in Fig. 4.1, the first model proposed consists of a shear beam connected at its base by a viscous dashpot, D , to the excitation $W(t)$. The shear beam can be thought of as an analog for a unit-area vertical column of the laterally infinite layered system. The dashpot has a damping coefficient equal to $\rho_{N+1} c_{N+1}$. Referring to Fig. 2.2, the incident wave $y(t+z_N/c_{N+1})$ will give rise to

an input $y(t)$ when arriving at the base where $z_N = 0$. The excitation function $W(t)$ is related to $y(t)$ by observing the fact that the motion at the surface of the foundation would be $2y(t)$ if the superficial layers were absent, which suggests that $W(t)$ should be set equal to $2y(t)$. Next, it must be shown that the dashpot D is, in effect, a substitute for the half-space foundation by demonstrating that both the original system and the model have the same coefficient of upward transmission and coefficient of upward reflection at the base where $z_N = 0$.

According to Fig. 4.1 the differential equation governing the motion of the dashpot D is

$$\rho_{N+1} c_{N+1} [\dot{u}_N(0, t) - 2\dot{y}(t)] + \sigma_N(0, t) = 0 \quad (4.1)$$

where $\sigma_N(0, t)$ is the shearing stress across the boundary $z_N = 0$. The response of the N^{th} layer, $u_N(z_N, t)$, to the input $2y(t)$ during the time the transmission across the base interface takes place can be written as

$$u_N(z_N, t) = (T_u')_N y(t + z_N/c_N) \quad (4.2)$$

because $u_N(z_N, t)$ satisfies the following wave equation

$$c_N^2 \frac{\partial^2 u_N}{\partial z_N^2} = \frac{\partial^2 u_N}{\partial t^2}$$

for a nonviscous elastic medium. In Eq. 4.2, $(T_u')_N$ is the coefficient of upward transmission of the model at the base interface. From Eq. 4.2, we can obtain

$$\dot{u}_N(0, t) = (T_u')_N \dot{y}(t)$$

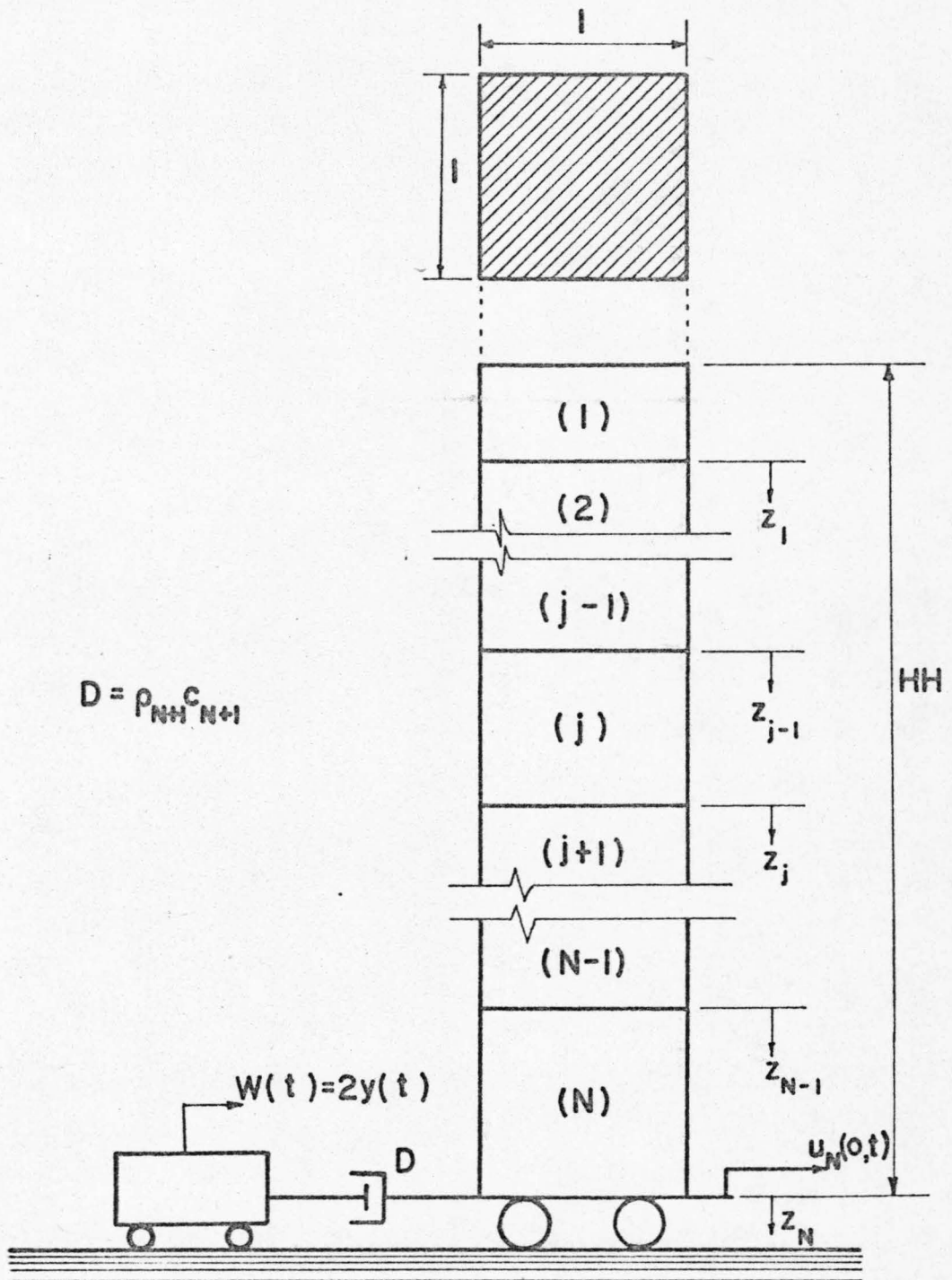


Fig. 4.1 THE FIRST SHEAR BEAM MODEL

and

$$\sigma_N(0, t) = \mu_N \frac{\partial u_N}{\partial z_N} \Big|_{z_N=0} = \rho_N c_N (T_u')_N \dot{y}(t)$$

Substitution of $\dot{u}_N(0, t)$ and $\sigma_N(0, t)$ into Eq. 4.1 gives

$$(T_u')_N = \frac{|u_N(0, t)|}{|y(t)|} = \frac{2}{1 + \alpha_N} \quad (4.3)$$

where α_N is the impedance ratio at $z_N = 0$. Comparing Eq. 4.3 with Eq. 3.15 shows that $(T_u')_N$ is equal to the coefficient of upward transmission, $(T_u)_N$, of the layered system.

To obtain the coefficient of upward reflection of the model, let a signal propagating downward inside the N^{th} layer be $f(t - z_N/c_N)$. Then, the reflected signal can be expressed as $(R_u')_N f(t + z_N/c_N)$, and the total motion in the N^{th} layer will be given by

$$u_N(z_N, t) = f(t - z_N/c_N) + (R_u')_N f(t + z_N/c_N) \quad (4.4)$$

during the time that the downward propagating signal is arriving at the base interface. Equation 4.4 then gives

$$\dot{u}_N(0, t) = [1 + (R_u')_N] \dot{f}(t)$$

and

$$\sigma_N(0, t) = \rho_N c_N [(R_u')_N - 1] \dot{f}(t)$$

Substituting $\dot{u}_N(0, t)$ and $\sigma_N(0, t)$ into Eq. 4.1 and setting $y(t)$ to zero will give

$$(R_u)_N = - \frac{1-\alpha_N}{1+\alpha_N} \quad (4.5)$$

Comparing the last equation with Eq. 3.15 shows again that both the model and the layered system have the same coefficient of upward reflection, $(R_u)_N$. The fact that both systems have the same coefficient of upward transmission and the same coefficient of upward reflection proves that the dashpot D has exactly the same effect as the half-space foundation when the layered system is nonviscous. It can also be shown in the following that the model is an exact analog of a nonviscous elastic layered system by demonstrating that both systems have the same transfer function.

Since the steady-state solution for $u_j(z_j, t)$ is found from Eq. 2.33 to be

$$u_j(z_j, t) = 2a_{N+1} \text{AMP}(\omega) G_j(\omega) \cos[k_j(z_j + H_j) + \phi_j] e^{i(\omega t - \phi_{N+1})} \quad (2.33)$$

for a steady-state incident wave

$$y(t + z_N/c_{N+1}) = a_{N+1} e^{i(\omega t + k_{N+1} z_N)},$$

we have, upon setting $z_N = 0$,

$$u_N(0, t) = 2y(t) \text{AMP}(\omega) \text{Re}_{N+1}(\omega) e^{-i\phi_{N+1}} \quad (4.6)$$

Define $H_{j,N}(\omega)$ as the transfer function of the layered system for the response $u_j(z_j, t)$ with respect to the base response, $u_N(0, t)$. Hence, from Eqs. 2.33 and 4.6,

$$\begin{aligned}
 H_{j,N}(\omega) &= \left| \frac{u_j(z_j, t)}{u_N(0, t)} \right|_{\text{steady-state}} \\
 &= \frac{G_j(\omega)}{\text{Re}_{N+1}(\omega)} \cos[k_j(z_j + H_j) + \phi_j]
 \end{aligned}
 \tag{4.7}$$

Equation 4.7 indicates that, if $u_N(0, t)$ is given, the response $u_j(z_j, t)$ can be computed without knowing the input function $y(t)$ and the properties of the foundation. In fact, it can be shown that the above statement holds for the general case of a linear viscoelastic layered system as well.

As far as the shear beam itself is concerned, the corresponding transfer function between $u_j(z_j, t)$ and $u_N(0, t)$ should be the same as the transfer function $H_{j,N}(\omega)$, and that this is indeed the case will be shown as follows. For steady-state excitation, we can write that

$$\dot{y}(t) = i\omega y(t)$$

and

$$\dot{u}_N(0, t) = i\omega u_N(0, t)$$

Hence, for steady-state excitation, Eq. 4.1 becomes

$$i\omega \rho_{N+1} c_{N+1} [u_N(0, t) - 2y(t)] + \sigma_N(0, t) = 0 \tag{4.8}$$

The steady-state shearing stress, $\sigma_N(0, t)$, is

$$\sigma_N(0, t) = - \frac{\omega \rho_{N+1} c_{N+1} [\sin(k_N H_N) \text{Re}_{N+1} + \cos(k_N H_N) \text{Im}_{N+1}]}{\text{Re}_{N+1}} u_N(0, t)$$

Substituting $\sigma_N(0, t)$ into Eq. 4.8 yields

$$\begin{aligned}
 H_N(\omega) &= \left| \frac{u_N(0, t)}{2y(t)} \right|_{\text{steady-state}} \\
 &= \text{AMP}(\omega) \text{Re}_{N+1}(\omega) e^{-i\phi_{N+1}(\omega)}
 \end{aligned} \tag{4.9}$$

which agrees with Eq. 4.6. Equations 4.7 and 4.9 together prove that the model and the layered system are exactly analogous to each other in that they have the same transfer function

$$H_j(\omega) = H_{j,N}(\omega) H_N(\omega) = \text{AMP}(\omega) G_j(\omega) \cos[k_j(z_j + H_j) + \phi_j] e^{-i\phi_{N+1}} \tag{4.10}$$

In the following section, two methods are presented for the approximate analysis of the foregoing model. The first is the commonly used method of lumped masses, and the second is the method of continuous modal analysis.

(1) The Method of Lumped Masses

A common way of analyzing the model shown in Fig. 4.1 is to subdivide the shear beam into an arbitrary number of elements, each of which is then lumped as a concentrated mass. Thus, a lumped spring-mass system is generated as an approximation of the continuous model. Such a model that has R lumped masses is shown in Fig. 4.2. The various techniques for obtaining the lumped masses and springs can readily be found in the literature and, therefore, will not be discussed here.

According to Fig. 4.2, let $\tilde{u}_N(0, t)$ be the motion at the base and $\tilde{x}_r(t)$ the motion of the r^{th} mass relative to the base. Then, the equations of motion for the lumped system are

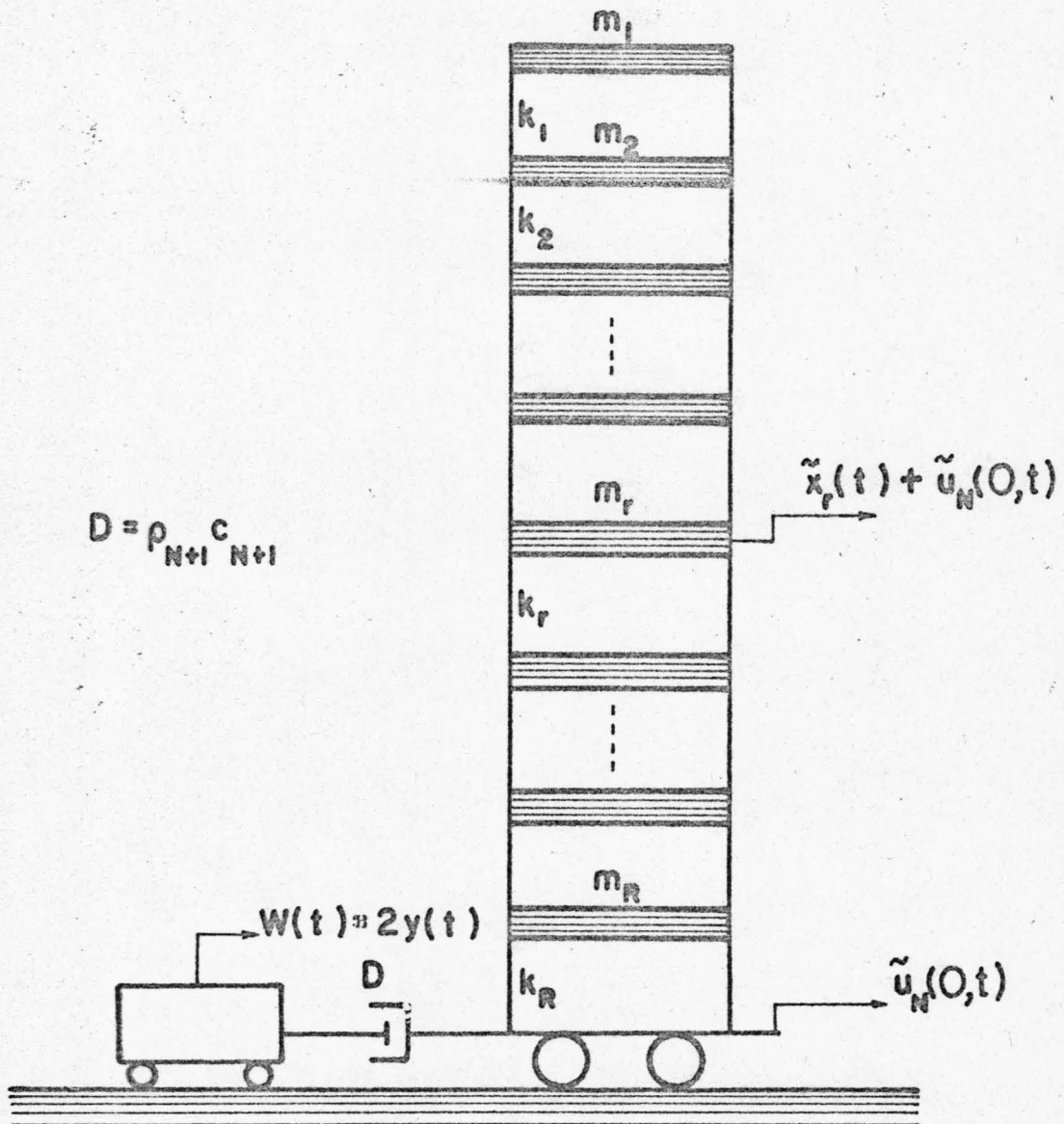


Fig. 4.2 A LUMPED REPRESENTATION OF THE FIRST MODEL FOR A NONVISCIOUS LAYERED SYSTEM

$$[M]\{\ddot{\tilde{x}}(t)\} + [K]\{\tilde{x}(t)\} = -\ddot{\tilde{u}}_N(0, t)\{m\} \quad (4.11)$$

and

$$\rho_{N+1} c_{N+1} [\dot{\tilde{u}}_N(0, t) - 2\dot{y}(t)] - k_R \tilde{x}_R(t) = 0 \quad (4.12)$$

where

$$\{\tilde{x}(t)\} = \begin{Bmatrix} \tilde{x}_1(t) \\ \cdot \\ \cdot \\ \cdot \\ \cdot \\ \tilde{x}_R(t) \end{Bmatrix} = \text{displacement vector,}$$

$[M]$ = mass matrix,

$[K]$ = stiffness matrix,

and

$$\{m\} = \begin{Bmatrix} m_1 \\ \cdot \\ \cdot \\ \cdot \\ m_R \end{Bmatrix}, \text{ mass vector.}$$

Equations 4.11 and 4.12 constitute a coupled system of equations which may be solved by the technique of direct numerical integration on a digital computer. The amount of computing time needed will be proportional to the number R . One way to reduce the computing time is to make an orthogonal transformation of Eq. 4.11 such that a system of R uncoupled modal equations is produced. For most engineering problems it would be sufficiently accurate to consider only the first S modal equations ($S \leq R$) and hence some saving of the computing time can be achieved.

To perform the orthogonal transformation of Eq. 4.11, first introduce the following transformation for $\{\tilde{x}\}$.

$$\{\tilde{x}\} = [M]^{-\frac{1}{2}} \{\tilde{w}\} \quad (4.13)$$

Premultiplied by $[M]^{-\frac{1}{2}}$, Eq. 4.11 becomes

$$\{\ddot{\tilde{w}}\} + [\tilde{K}]\{\tilde{w}\} = -\ddot{u}_N(0, t)[M]^{-\frac{1}{2}}\{m\} \quad (4.14)$$

where $[\tilde{K}] = [M]^{-\frac{1}{2}}[K][M]^{-\frac{1}{2}}$. Next, define the transformation

$$\{\tilde{w}\} = [U]\{\tilde{v}\} \quad (4.15)$$

where $[U]$ is the well known unitary matrix having the following properties

$$[U]^T[U] = [I] = \text{identity matrix,}$$

and

$$[U]^T[\tilde{K}][U] = [\tilde{\Lambda}^2] = \begin{bmatrix} \diagdown & & \\ & \tilde{\omega}^2 & \\ & & \diagup \\ & & & r & \\ & & & & \diagdown \end{bmatrix} \quad (4.16)$$

= eigenfrequency matrix

Upon premultiplication by $[U]^T$, Eq. 4.14 is reduced to an uncoupled system as

$$\{\ddot{\tilde{v}}(t)\} + [\tilde{\Lambda}^2]\{\tilde{v}(t)\} = -\ddot{u}_N(0, t)[U]^T[M]^{-\frac{1}{2}}\{m\} \quad (4.17)$$

where $\{\tilde{v}\}$ is now the vector of normal coordinates. Combining Eqs. 4.13 and 4.15 gives the relation between $\{\tilde{x}\}$ and $\{\tilde{v}\}$ as

$$\{\tilde{x}(t)\} = [A]\{\tilde{v}(t)\} \quad (4.18)$$

where

$$[A] = [M]^{-\frac{1}{2}}[U] \quad (4.19)$$

is the normal mode matrix. From Eqs. 4.16 and 4.19, the matrix $[A]$ has the following properties

$$[A]^T[M][A] = [I], \quad \text{and} \quad [A]^T[K][A] = [\tilde{\Lambda}^2] \quad (4.20)$$

By the definition of $[A]$ given in Eq. 4.19, Eq. 4.17 can be rewritten as

$$\{\ddot{\tilde{v}}(t)\} + [\tilde{\Lambda}^2]\{\tilde{v}(t)\} = -\ddot{\tilde{u}}_N(0,t)[A]^T\{m\}$$

or in terms of modal equations,

$$\ddot{\tilde{v}}_r(t) + \omega_r^2 \tilde{v}_r(t) = -\ddot{\tilde{u}}_N(0,t) \sum_{i=1}^R A_{ir} m_i \quad (4.21)$$

for $r = 1, 2, \dots, R$.

Suppose it is sufficiently accurate to consider only the contributions from the first S modes. Furthermore, define the following transformation

$$\tilde{v}_r(t) = \sum_{i=1}^R A_{ir} m_i \tilde{\xi}_r(t) \quad (4.22)$$

Then, the final system of equations to be solved is

$$\ddot{\tilde{\xi}}_r(t) + \omega_r^2 \tilde{\xi}_r(t) = -\ddot{\tilde{u}}_N(0,t), \quad r = 1, 2, \dots, S$$

and

$$\rho_{N+1} c_{N+1} [\dot{\tilde{u}}_N(0,t) - 2\dot{y}(t)] - k_R \sum_{r=1}^S \tilde{D}_r^{(R)} \tilde{\xi}_r(t) = 0 \quad (4.23)$$

where we have defined

$$\tilde{D}_r^{(j)} = A_{jr} \sum_{i=1}^R A_{ir} m_i \quad (4.24)$$

as the r^{th} modal participating factor for computing $\tilde{x}_j(t)$. Equation 4.23 suggests that it is more convenient to take the given input function as the velocity input, $\dot{y}(t)$, and the corresponding response to be computed is the velocity response, $\dot{\tilde{x}}_j(t)$. From Eqs. 4.18, 4.22 and 4.24, the S-mode approximate solution for $\dot{\tilde{x}}_j(t)$ will be

$$\dot{\tilde{x}}_j(t) \approx \sum_{r=1}^S D_r^{(j)} \dot{\xi}_r(t) \quad (4.25)$$

Equation 4.23 can be solved by the technique of direct numerical integration with a digital computer. The accuracy of the lumped model is proportional to the number of lumped masses, R , and, since this number is limited by practical considerations, it is of interest to develop the following method which analyzes the continuous shear beam directly.

(2) The Method of Continuous Modal Analysis

This method deals with the continuous model directly, and gives closed-form solutions for quantities such as modal participating factors, natural frequencies, etc., in simple formulas. Hence, this method should be more accurate and more economical than the method of lumped masses.

We start with the differential equations for a nonviscous elastic shear beam,

$$c_j^2 \frac{\partial^2 u_j(z_j, t)}{\partial z_j^2} = \frac{\partial^2 u_j(z_j, t)}{\partial t^2}, \quad j = 1, 2, \dots, N \quad (4.26)$$

Let $x_j(z_j, t)$ be the relative motion of the j^{th} layer with respect to the base, namely,

$$u_j(z_j, t) = u_N(0, t) + x_j(z_j, t) \quad (4.27)$$

Equation 4.26 then becomes

$$c_j^2 x_j'' = \ddot{x}_j + \ddot{u}_N(0, t), \quad j = 1, 2, \dots, N \quad (4.28)$$

where the double-prime stands for $\partial^2/\partial z_j^2$ and the double-dot for $\partial^2/\partial t^2$. To solve for x_j in terms of some orthogonal functions we first have to solve the following homogeneous partial differential equation

$$c_j^2 [x_j'']_{\text{homo}} = [\ddot{x}_j]_{\text{homo}} \quad j = 1, 2, \dots, N \quad (4.29)$$

The solution of Eq. 4.29 can be written as

$$[x_j]_{\text{homo}} = a_j e^{i(\omega t + k_j z_j)} + b_j e^{i(\omega t - k_j z_j)} \quad j = 1, 2, \dots, N \quad (4.30)$$

where the parameter ω is to be determined by the boundary conditions. Equation 4.30 is in the same form as that of the steady-state solution for u_j obtained in Chapter II. Also, the boundary conditions for $[x_j]_{\text{homo}}$ are the same as those given in Eqs. 2.11, 2.13 and 2.14 at all the interfaces except the base interface where $z_N = 0$. The boundary condition at $z_N = 0$ is simply

$$[x_N(0, t)]_{\text{homo}} = 0$$

which implies $a_N + b_N = 0$ or

$$\text{Re}_{N+1}(\omega) = 0 \quad (4.31)$$

The roots, say, ω_r , of Eq. 4.31 are the natural frequencies of the shear beam, which are equal to the characteristic frequencies defined in Eq. 2.35. Thus, the exact solution for $[x_j]_{\text{homo}}$ can be written as the sum of the contributions from all the modes. That is,

$$[x_j(z_j, t)]_{\text{homo}} = a \sum_{r=1}^{\infty} (Z_j)_r e^{-i\omega_r t}, \quad j = 1, 2, \dots, N \quad (4.32)$$

where the symbol $()_r$ stands for the function inside the parenthesis evaluated at ω_r , and

a = an arbitrary constant depending on initial conditions,

$$(Z_j)_r = (G_j)_r \cos[(k_j)_r (z_j + H_j) + (\phi_j)_r],$$

$$(G_j)_r = [\text{Re}_j^2(\omega_r) + \text{Im}_j^2(\omega_r)]^{\frac{1}{2}}, \quad (4.33)$$

$$(k_j)_r = \omega_r / c_j,$$

$$(\phi_j)_r = \tan^{-1} \frac{\text{Im}_j(\omega_r)}{\text{Re}_j(\omega_r)}.$$

The function $(Z_j)_r$ represents the mode shape of the r^{th} mode in the j^{th} layer. A proof is given in Appendix I for the orthogonality of the modal shape functions on the interval from $z_1 = -H_1$ to $z_N = 0$ with respect to the weighting function ρ_j . Mathematically, the condition of orthogonality is

$$\sum_{j=1}^N \int_{-H_j}^0 \rho_j (Z_j)_r (Z_j)_q dz_j = 0 \quad \text{if } r \neq q, \quad (\text{A.I. 8})$$

$$= \|Z\|_r^2 \quad \text{if } r = q. \quad (4.34)$$

where $\|Z\|_r^2$ is the norm of the r^{th} modal shape function and was derived in Appendix I as

$$\|Z\|_r^2 = \frac{1}{2} \sum_{j=1}^N (G_j)_r^2 \rho_j H_j \quad (\text{A.I. 9})$$

Now, return to Eq. 4.28 for the solution of x_j . In terms of the orthogonal functions, $(Z_j)_r$, x_j can be expressed in an infinite series as

$$x_j(z_j, t) = \sum_{r=1}^{\infty} (Z_j)_r v_r(t) \quad (4.35)$$

with $v_r(t)$ unknown yet. Substituting Eq. 4.35 into Eq. 4.28 yields

$$\sum_{r=1}^{\infty} (Z_j)_r [\ddot{v}_r(t) + \omega_r^2 v_r(t)] = -\ddot{u}_N(0, t) \quad (4.36)$$

The base motion $\ddot{u}_N(0, t)$ can be expanded in orthogonal space as

$$\ddot{u}_N(0, t) = \ddot{u}_N(0, t) \sum_{r=1}^{\infty} \frac{E_r (Z_j)_r}{\|Z\|_r^2} \quad (4.37)$$

where

$$\begin{aligned}
 E_r &= \sum_{j=1}^N \int_{-H_j}^0 \rho_j \cdot (Z_j)_r dz_j \\
 &= \rho_{N+1} c_{N+1} \text{Im}_{N+1}(\omega_r) / \omega_r
 \end{aligned} \tag{4.38}$$

By orthogonality of the modal shape functions, substituting Eq. 4.37 into Eq. 4.36 gives

$$\ddot{v}_r(t) + \omega_r^2 v_r(t) = - \frac{E_r}{\|Z\|_r^2} \ddot{u}_N(0, t), \quad r = 1, 2, \dots \tag{4.39}$$

Defining the following transformation

$$v_r(t) = \frac{E_r}{\|Z\|_r^2} \xi_r(t) \tag{4.40}$$

Eq. 4.39 becomes

$$\ddot{\xi}_r(t) + \omega_r^2 \xi_r(t) = -\ddot{u}_N(0, t), \quad r = 1, 2, \dots \tag{4.41}$$

Suppose that the contributions from the first S modes only are taken into account for computing x_j . The S -mode approximation for x_j can then be expressed in terms of the transformed normal coordinates, $\xi_r(t)$, as

$$x_j(z_j, t) \approx \sum_{r=1}^S D_r^{(j)} \xi_r(t) \tag{4.42}$$

where $D_r^{(j)}$ is the modal participating factor defined by

$$D_r(j) = \frac{E_r(z_r)}{\|Z\|_r^2} \quad (4.43)$$

To obtain the solution for $\xi_r(t)$ with $y(t)$ as input function, Eq. 4.1 and Eq. 4.41 have to be solved simultaneously. With only the first S modal equations considered, the system of equations to be solved is

$$\text{and } \left\{ \begin{array}{l} \ddot{\xi}_r(t) + \omega_r^2 \xi_r(t) = -\ddot{u}_N(0, t) \quad r = 1, 2, \dots, S \\ \rho_{N+1} c_{N+1} [\dot{u}_N(0, t) - 2\dot{y}(t)] + \sigma_N(0, t) = 0 \end{array} \right. \quad (4.44)$$

in which $\sigma_N(0, t)$ is given by

$$\begin{aligned} \sigma_N(0, t) &= \mu_N \left. \frac{\partial x_N(z_N, t)}{\partial z_N} \right|_{z_N=0} \\ &= -(\rho_{N+1} c_{N+1})^2 \sum_{r=1}^S \frac{\text{Im}_{N+1}(\omega_r)^2 \xi_r(t)}{\|Z\|_r^2} \end{aligned} \quad (4.45)$$

Equation 4.44 can be interpreted as the physical system shown in Fig. 4.3 which consists of S undamped single-degree-freedom oscillators. The r^{th} oscillator has a natural frequency equal to ω_r , and represents the r^{th} transformed normal coordinate, $\xi_r(t)$. This system is thus an S -mode representation of the model. Each of the oscillators can be imagined to have an effective mass, $(m_{\text{eff}})_r$, and a spring stiffness, $(K_{\text{eff}})_r$, such that

$$\dot{u}_j(z_j, t) = \sum_{r=1}^S D_r^{(j)} \dot{\xi}_r(t) + \dot{u}_N(0, t)$$

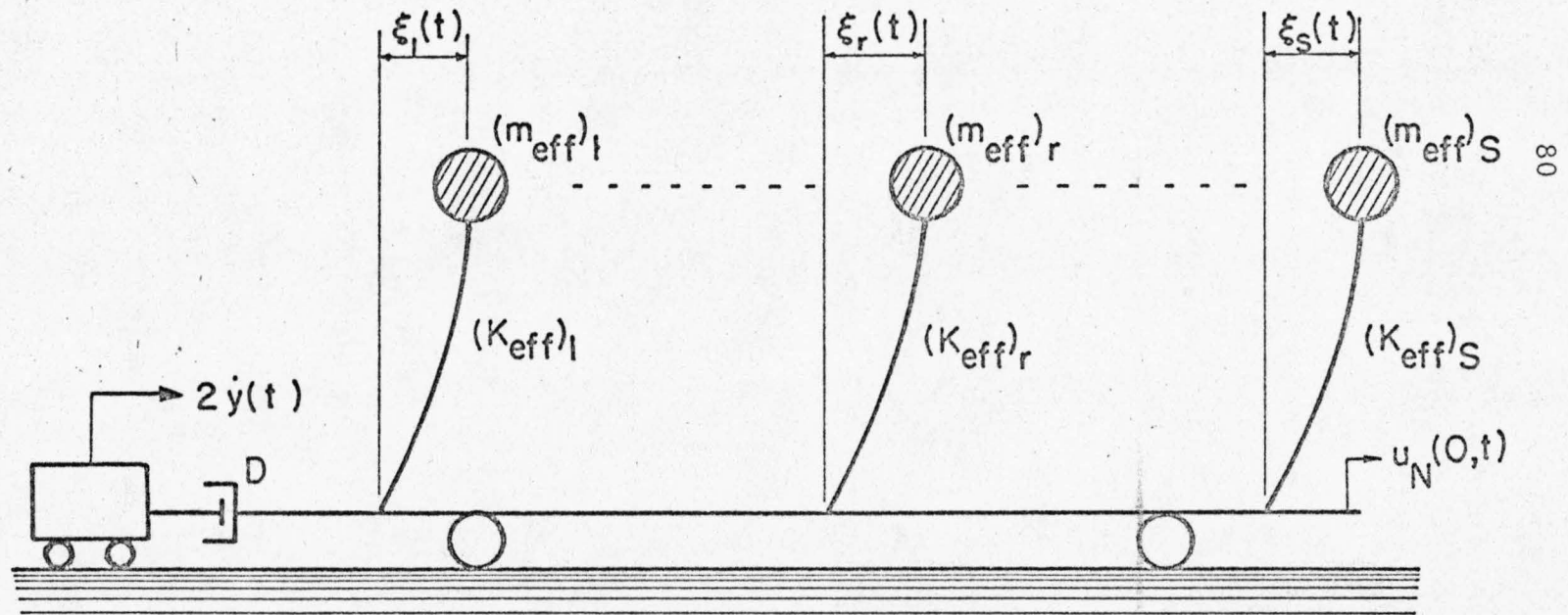


Fig. 4.3 AN S-MODE REPRESENTATION OF THE FIRST MODEL

$$\omega_r = \sqrt{\frac{(K_{\text{eff}})_r}{(m_{\text{eff}})_r}} \quad (4.46)$$

Consequently, $\sigma_N(0, t)$ is given directly by the physical system as

$$\sigma_N(0, t) = - \sum_{r=1}^S (K_{\text{eff}})_r \xi_r(t) \quad (4.47)$$

$$= - \sum_{r=1}^S (m_{\text{eff}})_r \omega_r^2 \xi_r(t)$$

A comparison of Eq. 4.47 with Eq. 4.45 immediately gives

$$(m_{\text{eff}})_r = \frac{E_r^2}{\|Z\|_r^2} \quad (4.48)$$

where E_r was defined in Eq. 4.38.

To solve Eq. 4.44 by a technique of step-by-step numerical integrations on a digital computer, it is necessary to reduce the system to a system of $2S+1$ first order differential equations. The reduction is achieved by defining the following transformation

$$f_r(t) = \xi_r(t) + u_N(0, t) \quad (4.49)$$

Also, define

$$\{\eta(t)\} = \{f_1(t), \dots, f_S(t), \quad u_N(0, t), \dot{f}_1(t), \dots, \dot{f}_S(t)\}, \quad (4.53)$$

$$\{P(t)\} = \{0, \overbrace{\dots\dots\dots}^S, 0, \quad 2\dot{y}(t), \quad 0, \overbrace{\dots\dots\dots}^{\dot{S}}, 0\}, \quad (4.54)$$

and

$$[\Lambda^2]_{S \times S} = \begin{bmatrix} \omega_1^2 & & & \\ & \ddots & & \\ & & \ddots & \\ & & & \omega_S^2 \end{bmatrix} \quad (4.55)$$

With $\dot{y}(t)$ as the given input function, the S-mode solution for the corresponding response, \dot{u}_j , is found from Eqs. 4.27 and 4.42 to be

$$\dot{u}_j(z_j, t) = \sum_{r=1}^S D_r^{(j)} \dot{f}_r(t) + (1 - \sum_{r=1}^S D_r^{(j)}) \dot{u}_N(0, t) \quad (4.56)$$

$$= \sum_{r=1}^S D_r^{(j)} \dot{\xi}_r(t) + \dot{u}_N(0, t) \quad (4.56')$$

So far, the number S is unknown. To determine S we have to compute the S-mode approximate transfer function of the model and compare it with the exact solution in a certain range of frequencies of practical interest. The number S can then be chosen, depending on the desired accuracy of the approximate solution. To derive the approximate transfer function, assume a steady-state excitation $y(t) = e^{i\omega t}$. Accordingly, the steady-state solution for $u_N(0, t)$ can be written as

$$u_N(0, t) = 2\bar{H}_N(\omega) e^{i\omega t} \quad (4.57)$$

which in turn gives the steady-state solution for $f_r(t)$ from Eq. 4.51 as

$$f_r(t) = \frac{u_N(0, t)}{1 - \Omega_r^2} = \frac{2\bar{H}_N(\omega)}{1 - \Omega_r^2} e^{i\omega t} \quad (4.58)$$

where $\Omega_r = \omega/\omega_r$. Substitution of $y(t)$, Eq. 4.57, and Eq. 4.58 into the last equation of Eq. 4.51 yields the S-mode solution for the transfer function $\bar{H}_N(\omega)$ as

$$\bar{H}_N(\omega) = \frac{1}{\sqrt{1 + Y^2(\omega)}} e^{-i\bar{\Psi}_1(\omega)} \quad (4.59)$$

with

$$Y(\omega) = \frac{1}{\omega_r} \sum_{r=1}^S \frac{(F)_r \Omega_r}{1 - \Omega_r^2}$$

and

$$\bar{\Psi}_1(\omega) = \tan^{-1}[Y(\omega)] \quad (4.60)$$

On the other hand, substituting Eqs. 4.57, 4.58 and 4.59 into Eq. 4.56 gives the approximate transfer function, $\bar{H}_j(\omega)$, for the response u_j as

$$\bar{H}_j(\omega) = \left. \frac{u_j(z_j, t)}{2y(t)} \right|_{\text{steady-state}} = \frac{e^{-i\bar{\Psi}_1(\omega)}}{\sqrt{1 + Y^2(\omega)}} \left(1 + \sum_{r=1}^S \frac{D_r^{(j)} \Omega_r^2}{1 - \Omega_r^2} \right) \quad (4.61)$$

(3) Numerical Examples

In the following, numerical examples are given to demonstrate the applicability of the method of continuous modal analysis to a given nonviscous layered system. The nonviscous, idealized quadruple-layer system ($N = 4$) that was used in Chapter II will be considered. The data for this system were given in Table 2.1, and the amplification spectrum was shown in Fig. 2.4(d).

Let $|\bar{H}_j(\omega)|$ stand for the modulus of the transfer function $\bar{H}_j(\omega)$ and be defined as the amplitude transfer function. The approximate transfer functions, $|\bar{H}_1(\omega)|$ and $|\bar{H}_N(\omega)|$, will be computed to compare with the exact solutions of the corresponding functions. First of all, the number S has to be determined. Assume that for engineering problems a range of frequencies from 0 to 60 rad/sec is of most practical interest. Also, let $\omega_1, \omega_2, \dots, \omega_J$ be, among all the natural frequencies of the layered system, the ones that are in the range of frequencies prescribed above. It is found from numerical calculations that, to achieve satisfactory accuracy for the approximate transfer functions, the number S is approximately given by the formula

$$S \approx 2J \quad (4.62)$$

For the layered system under consideration, J is equal to 7 and S is taken to be 13. In Table 4.1 are listed the first 13 natural frequencies calculated by solving Eq. 2.35 numerically. The modal participating factors, $D_r^{(1)}(-H_1)$, and the quantities $(F)_r$ that are associated with $(K_{\text{eff}})_r$ are also given in Table 4.1. Thus the approximate solutions, $|\bar{H}_1(\omega)|$ and $|\bar{H}_N(\omega)|$, can be calculated from Eqs. 4.59 and 4.61 respectively. The results are shown in Figs. 4.4 and 4.5 by the solid curves. In these figures the

Table 4.1 MODAL PARAMETERS OF THE QUADRUPLE-LAYER SYSTEM

MODAL NO.	NATURAL FREQUENCY	MODAL PARTICIPATING FACTOR	
r	ω_r (rad/sec)	$D_r^{(j)}(-H_1)$	$(F)_r^*$
1	6.137	1.645	1.32
2	13.033	-0.951	3.98
3	22.400	0.587	2.32
4	29.638	-0.438	4.00
5	39.241	0.309	1.80
6	46.961	-0.259	5.03
7	55.277	0.168	1.00
8	66.550	-0.161	2.08
9	73.317	0.164	2.31
10	83.600	-0.170	3.75
11	89.504	0.152	3.18
12	100.847	-0.126	2.12
13	107.152	0.123	7.97

* $(F)_r$ is, from Eq. 4.50, equal to $(K_{\text{eff}})_r / \rho_{N+1} c_{N+1}$.

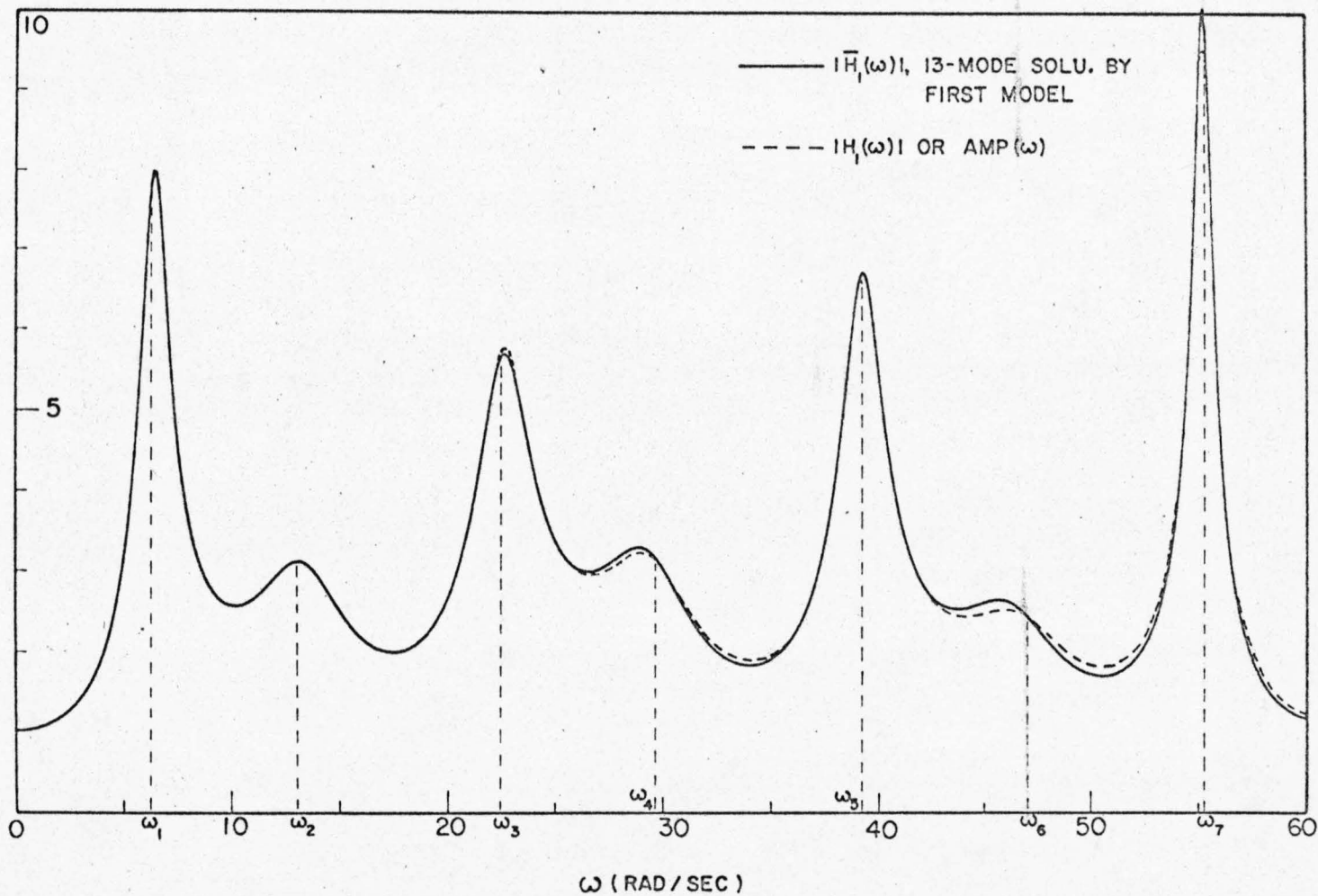


Fig. 4.4 AMPLITUDE TRANSFER FUNCTION OF THE
NONVISCIOUS 4-LAYER SYSTEM

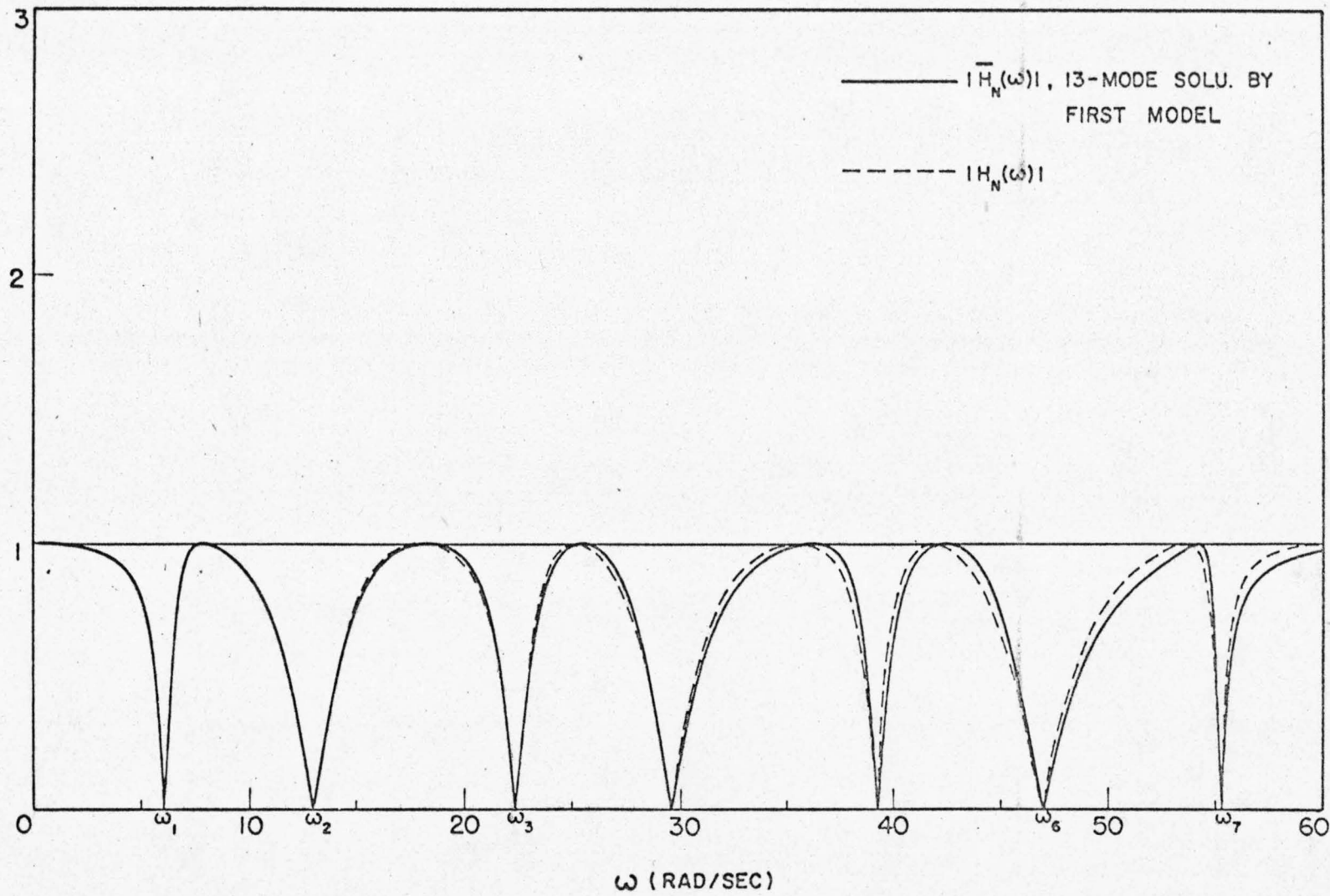


Fig. 4.5 AMPLITUDE TRANSFER FUNCTION OF THE NONVISCIOUS 4-LAYER SYSTEM

corresponding exact solutions, $|H_1(\omega)|$ and $|H_N(\omega)|$, are shown by the dashed curves. A comparison between the approximate and exact solutions indicates that, by considering the contributions from the first 13 modes, excellent accuracy is achieved in the prescribed range of frequencies. Observe that the accuracy of the approximate analysis is proportional to the number S used. On the other hand, for a fixed number S the accuracy is seen to decrease with frequency, being better at lower frequencies.

It is desired to compute the transient response at the surface of the layered system to earthquake-like excitation by both the ray-tracing technique (exact solution) and the method of continuous modal analysis (approximate solution). In order to see the influence of the duration of the input, two input functions of different duration will be used. The first has a duration of 2 seconds and the second has a duration of 10 seconds. Hereafter, they will be referred to as input function (a) and input function (b) respectively. Both input functions were digitized in the time interval of ΔT equal to 0.025 second. Since the first model requires a velocity input, the two input functions will be taken as $(\dot{y})_a$ and $(\dot{y})_b$ respectively for the time being, and are shown in Fig. 4.6.

The exact solution for the corresponding surface response, $\dot{u}_1(-H_1, t)$, was computed by the ray-tracing technique. The given layered system was subdivided into 29 sublayers, i.e., L is equal to 29 in Eqs. 3.16 and 3.17. The constant Δt is, in this case, equal to 0.0125 second. Hence, by assuming the time is zero when the incident wave hits the base, the first signal will arrive at the surface at a time t_1 given by Eq. 3.17

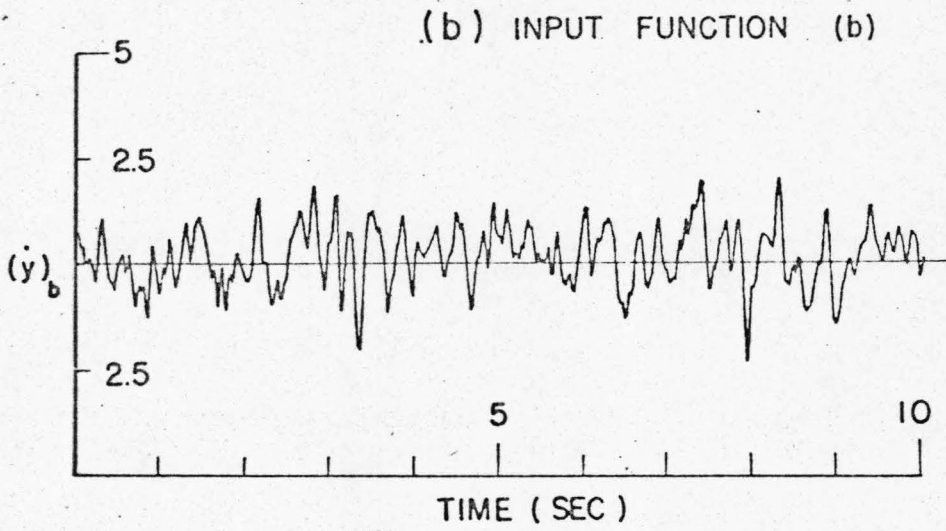
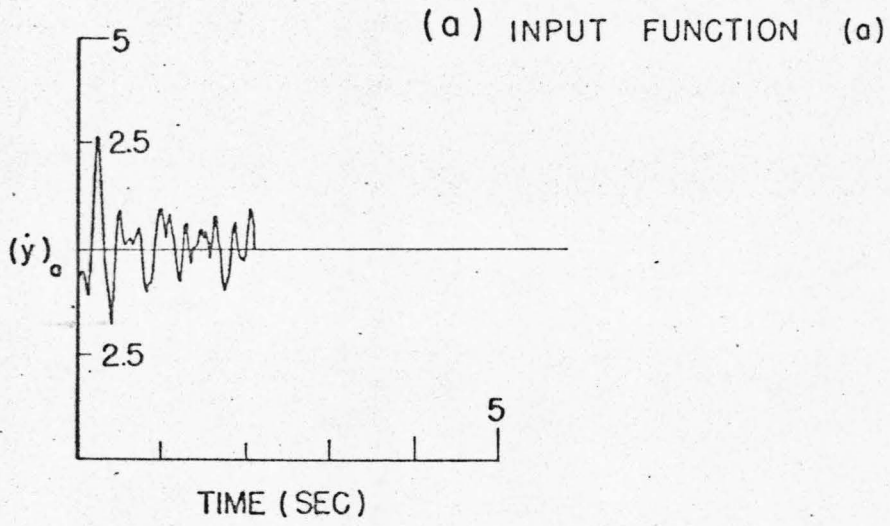


Fig. 4.6 INPUT FUNCTIONS

$$t_1 = L\Delta t = 0.3625 \text{ sec}$$

With $ACU = 0.005$ imposed on Eq. 3.20, the whole numerical scheme stopped at a time instant t_K equal to 4.375 seconds where $K = 119$. The exact solution is then, from Eq. 3.22,

$$\dot{u}_1(-H_1, t) = \sum_{j=1}^{119} A_j \dot{y}(t-t_j) \quad (4.63)$$

where A_1 has been given in Table 2.1 to be 5.39. Since ΔT in this case is equal to $2\Delta t$, the constant M in either Eq. 3.23 or Eq. 3.24 is equal to 1 and, therefore, $\dot{u}_1(-H_1, t)$ is digitized in a time interval of ΔT also. With $(\dot{y})_a$ and $(\dot{y})_b$ as the input functions, the responses computed are shown in Figs. 4.7(a) and 4.8(a) respectively.

To find the approximate solution for $\dot{u}_1(-H_1, t)$, Eq. 4.52 was solved numerically on an IBM 7094 digital computer. Since S is equal to 13, there are 27 first order differential equations contained in Eq. 4.52. The subroutine "DIFSYS" written by the computing center at the California Institute of Technology was adopted to solve Eq. 4.52. This subroutine is based on the method developed by Bulirsch and Stoer⁽²⁹⁾, which is an extrapolation method having advantages over the well known Runge-Kutta method and the method of Adams, Moulton and Bashforth in that it provides more accurate results but needs fewer operations. For instance, at the same level of accuracy this method executes twice faster than the Runge-Kutta method of the third order. With $(\dot{y})_a$ and $(\dot{y})_b$ as the input functions, the approximate solutions computed for $\dot{u}_1(-H_1, t)$ are shown in Figs. 4.7(b) and 4.8(b) respectively to compare with the corresponding exact solutions. The excellent agreement between

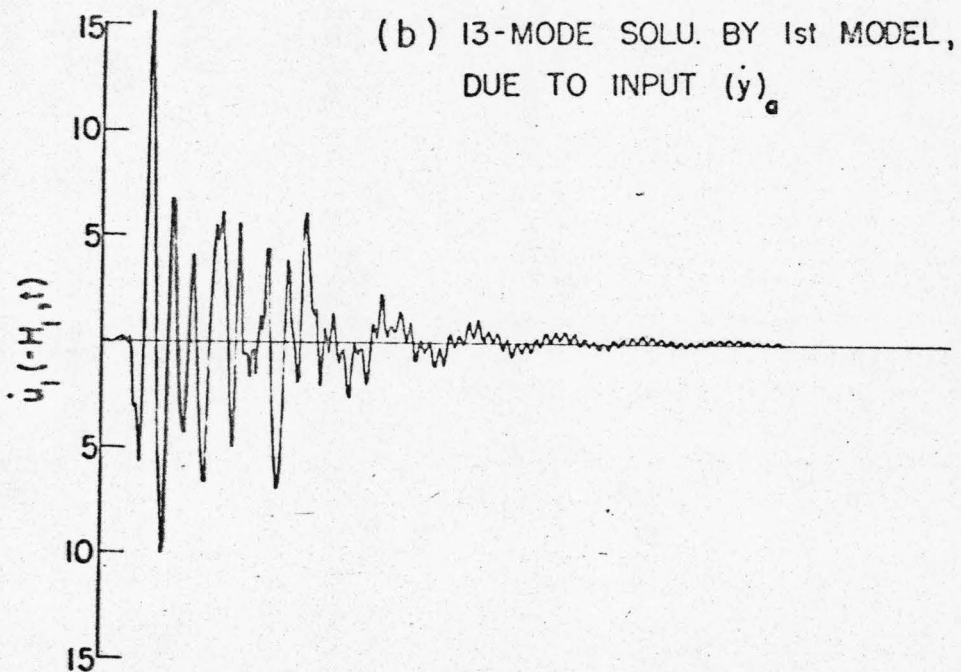
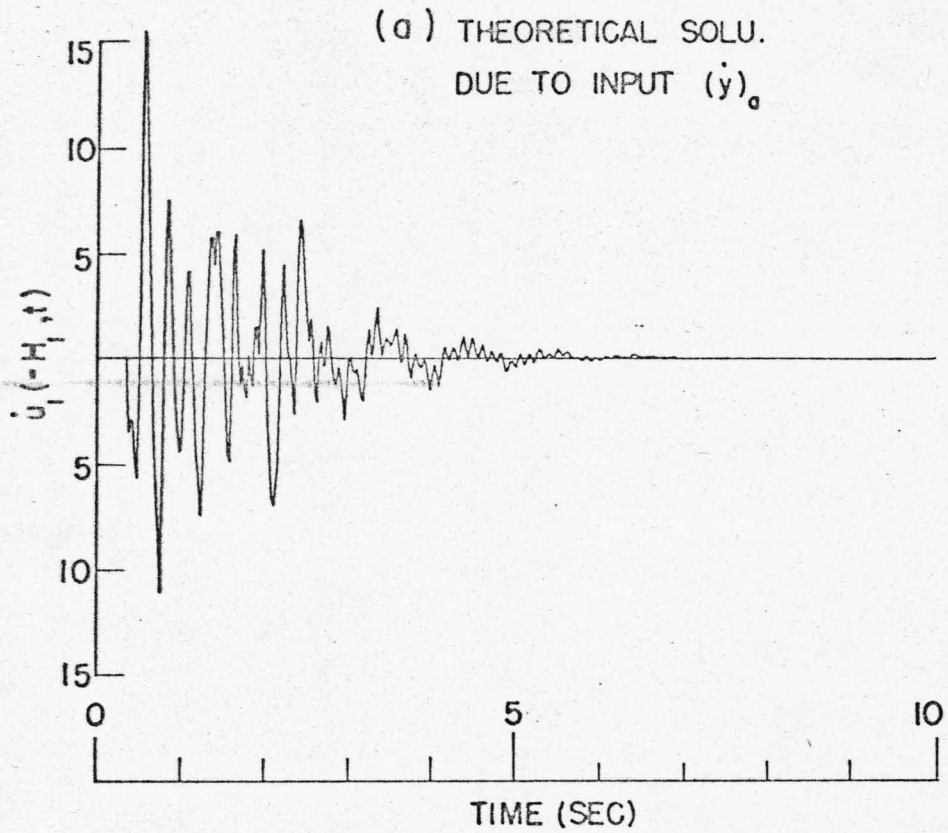


Fig. 4.7 SURFACE RESPONSE OF THE NONVISCIOUS 4-LAYER
SYSTEM

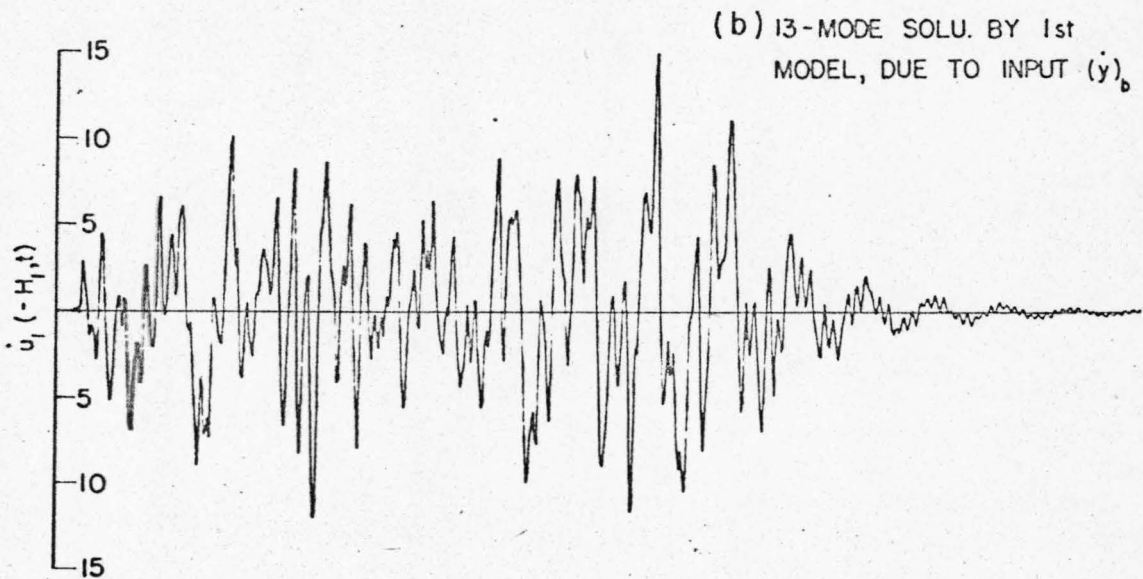
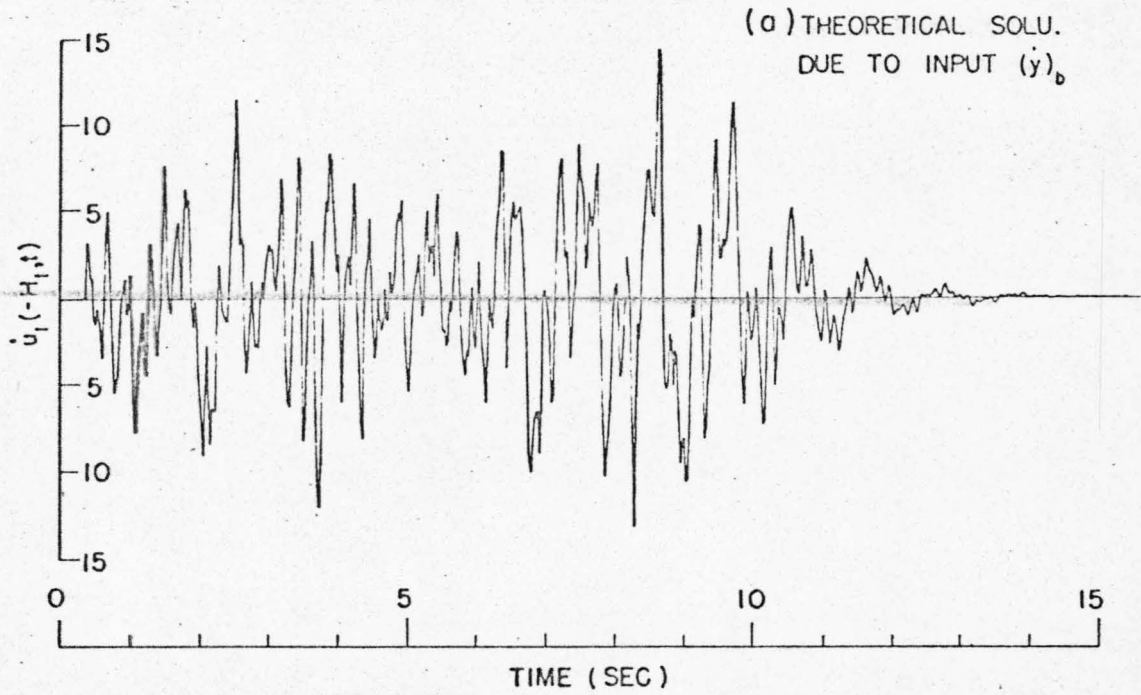


Fig. 4.8 SURFACE RESPONSE OF THE NONVISCIOUS 4-LAYER
SYSTEM

the approximate and the exact solutions is expected because of the good accuracy of the approximate transfer function, $|\bar{H}_1(\omega)|$, achieved previously.

The approximate solution for the base response, $\dot{u}_N(0, t)$, was also computed during the numerical solution of Eq. 4.52. Figures 4.9(a) and 4.9(b) show the computed results with $(\dot{y})_a$ and $(\dot{y})_b$ respectively as the input.

Comparing $\dot{u}_1(-H_1, t)$ with $2\dot{y}(t)$, where $2\dot{y}(t)$ would be the motion at the surface of the foundation if the superficial layers were absent, indicates a general amplification factor of about 2 to 3 for the amplitude of the input motion, with a factor of 3 for the maximum amplitude. The duration of the output is about 50% longer than that of the input. On the other hand, a comparison of $\dot{u}_N(0, t)$ with $2\dot{y}(t)$ indicates a remarkable resemblance between these two motions. As the stiffness of the foundation increases, such resemblance can be expected to be closer and, in the limiting case when the foundation is so stiff that the impedance ratio α_N becomes zero, $\dot{u}_N(0, t)$ will be identical to $2\dot{y}(t)$ according to theory. Since in general the foundation of a given layered system is more or less deformable, the error involved in taking the base motion as $2\dot{y}(t)$ would be proportional to the value of α_N . In actual applications it implies that certain error can be introduced if the motion recorded at the basement level of a building during an earthquake is used as the input for dynamic analysis of some other structures.

In dynamic analysis of ground motion, one of the quantities in which engineers are most interested is the velocity spectrum, S_v , defined as the maximum response of relative velocity of a

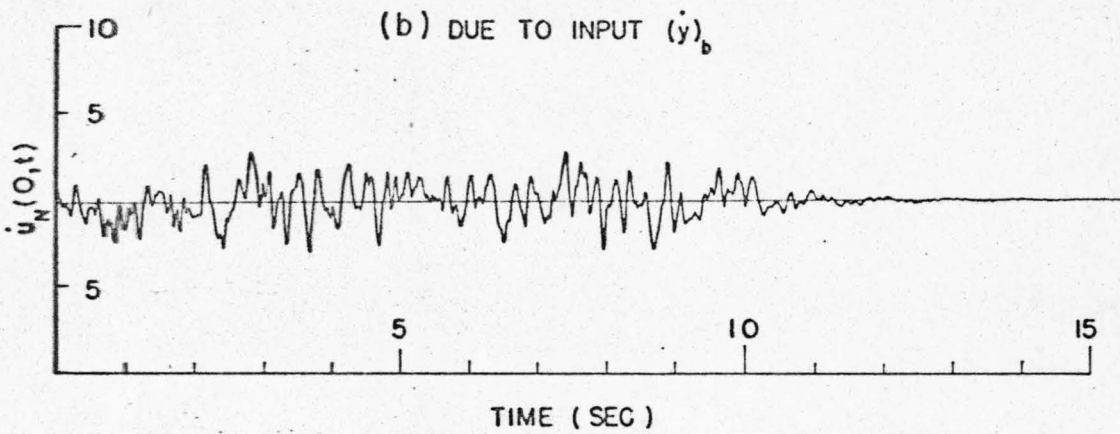
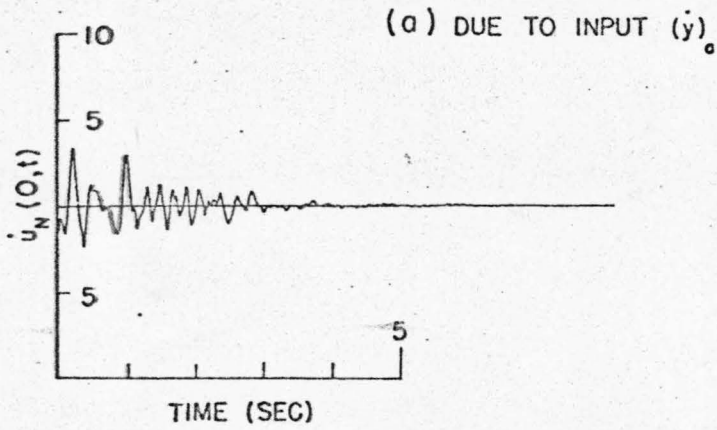


Fig. 4.9 BASE RESPONSE OF THE NONVISCOUS 4-LAYER
SYSTEM

single-degree-freedom oscillator having a certain undamped natural period (or undamped natural frequency) and a certain fraction of critical damping, n . Thus, by considering the input functions as accelerations, the velocity spectra for $(\dot{y})_a$ and $(\dot{y})_b$ were computed and are shown in Figs. 4.10(a) and 4.10(b) respectively. Also in Fig. 4.11 and Fig. 4.12 are shown the velocity spectra computed for both the exact and the approximate solutions of $\dot{u}_1(-H_1, t)$. The natural periods of the layered system, T_r , $r = 1, 2, \dots, 7$, are marked in all the output velocity spectra. Comparing the output spectra with the input spectra leads to the following conclusions.

(a) It is more reliable to examine the damped spectra to see the effect of a layered system on the output spectra because, in general, undamped spectra are highly oscillatory. If a large hump observed in the output spectra is associated with a prominent resonance of the layered system, this hump will be observable in both the undamped and the damped spectra. For instance, a large hump is consistently observed even in the damped output spectra around the fundamental natural period T_1 [see Figs. 4.11(a) and 4.12(a)].

(b) A hump consistently observed in both the undamped and the damped output spectra is not necessarily associated with the resonant effect of a layered system. It can be associated with strong frequency components of the input motion that produce a hump in the input spectra too. For instance, two prominent humps are observed in the output spectra shown in Fig. 4.11. The first hump located around T_1 is doubtlessly associated with the resonance in the fundamental mode of the layered system, but the second

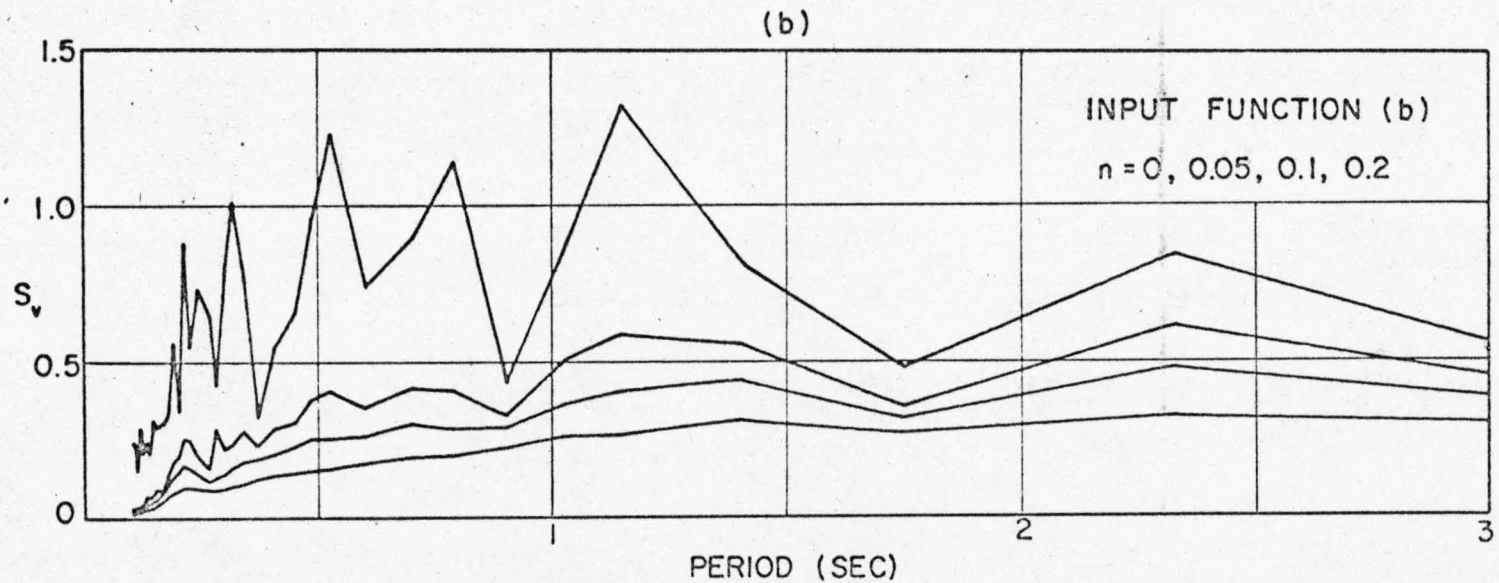
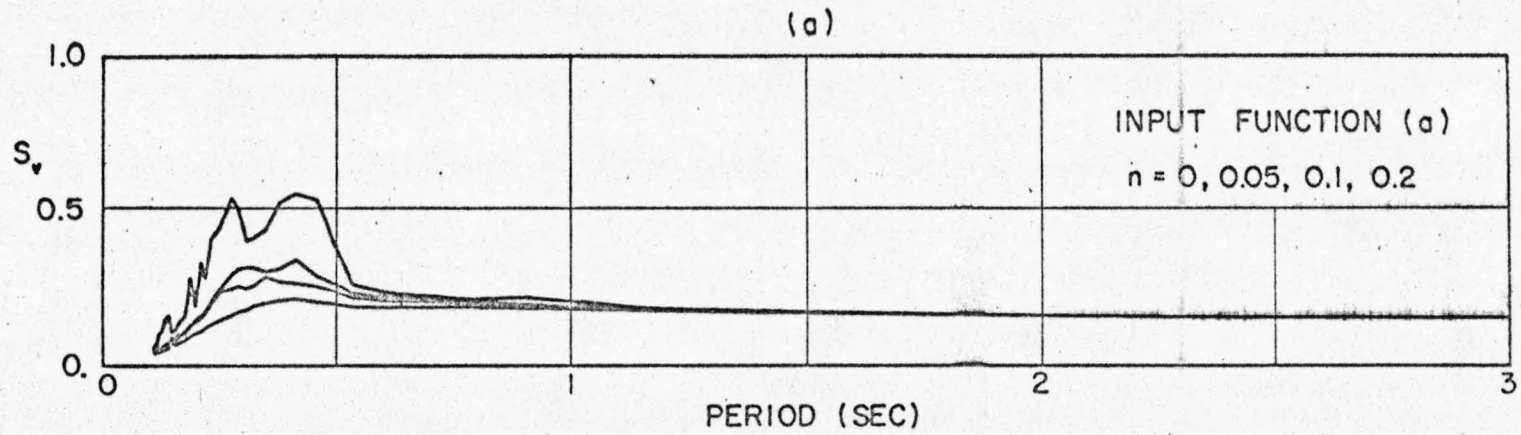


Fig. 4.10 INPUT VELOCITY SPECTRA

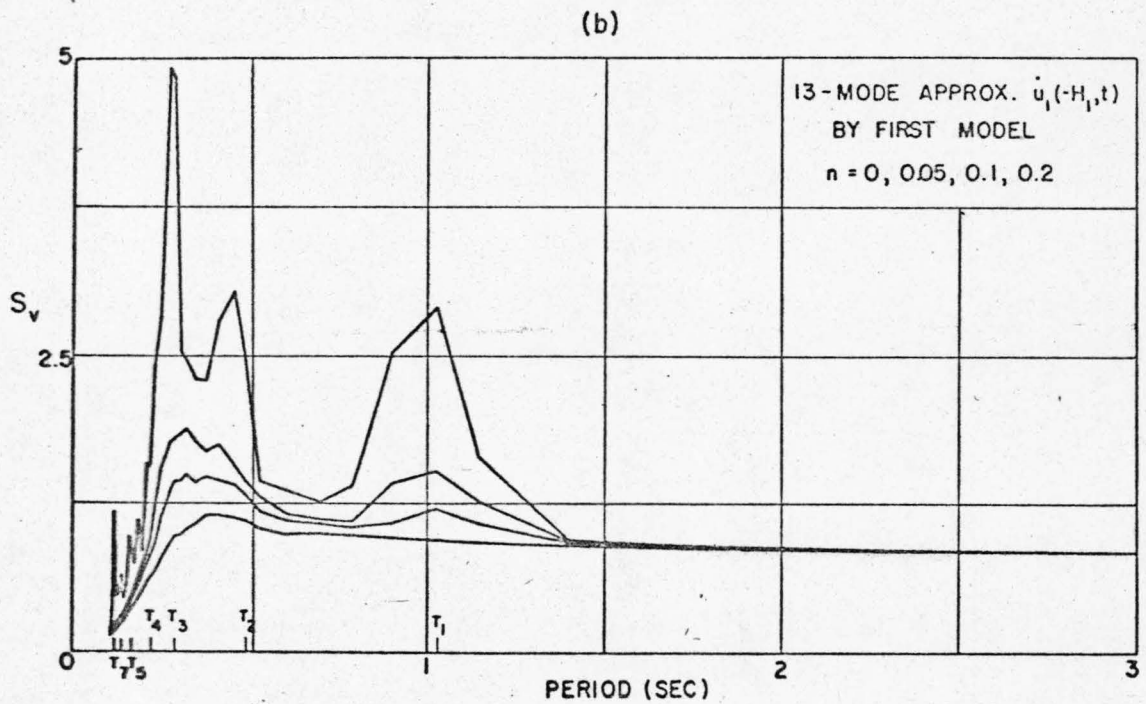
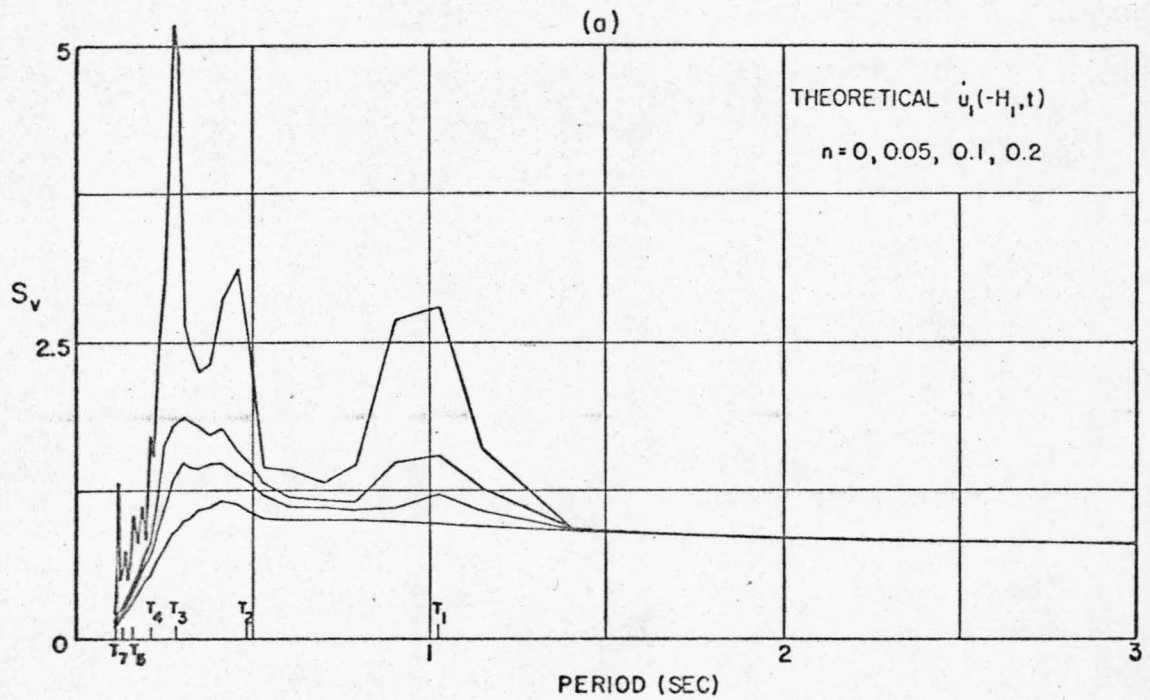
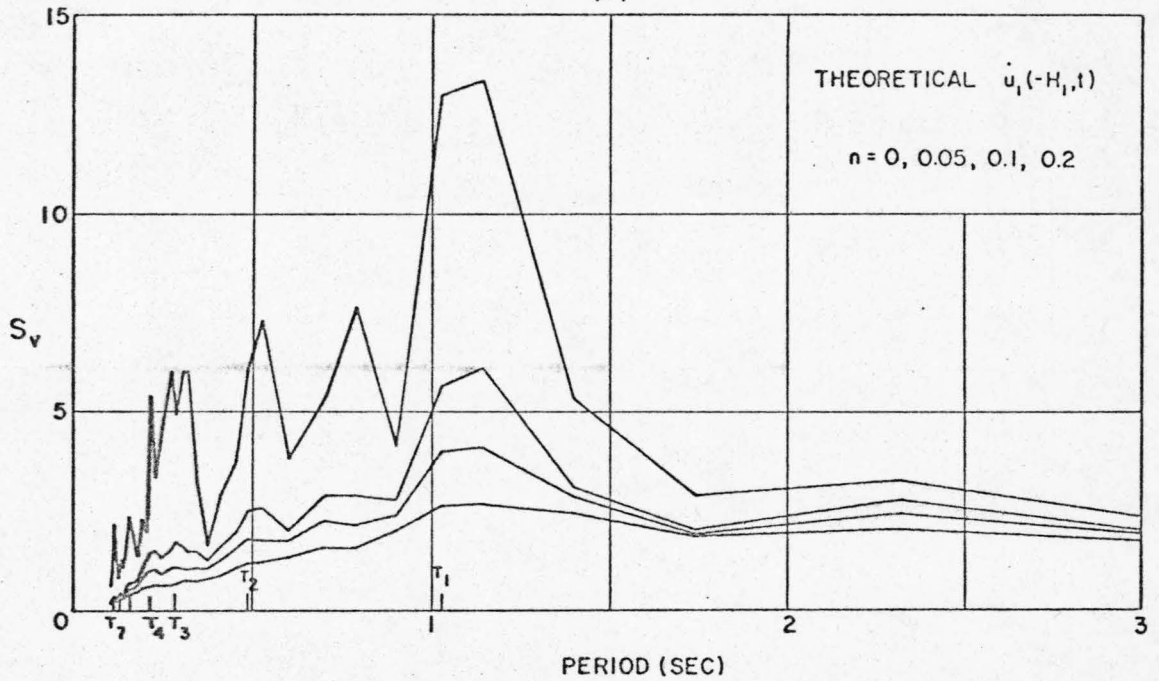


Fig. 4.11 OUTPUT VELOCITY SPECTRA OF THE NONVISCIOUS 4-LAYER SYSTEM [ASSOCIATED WITH INPUT $(y)_a$]

(a)



(b)

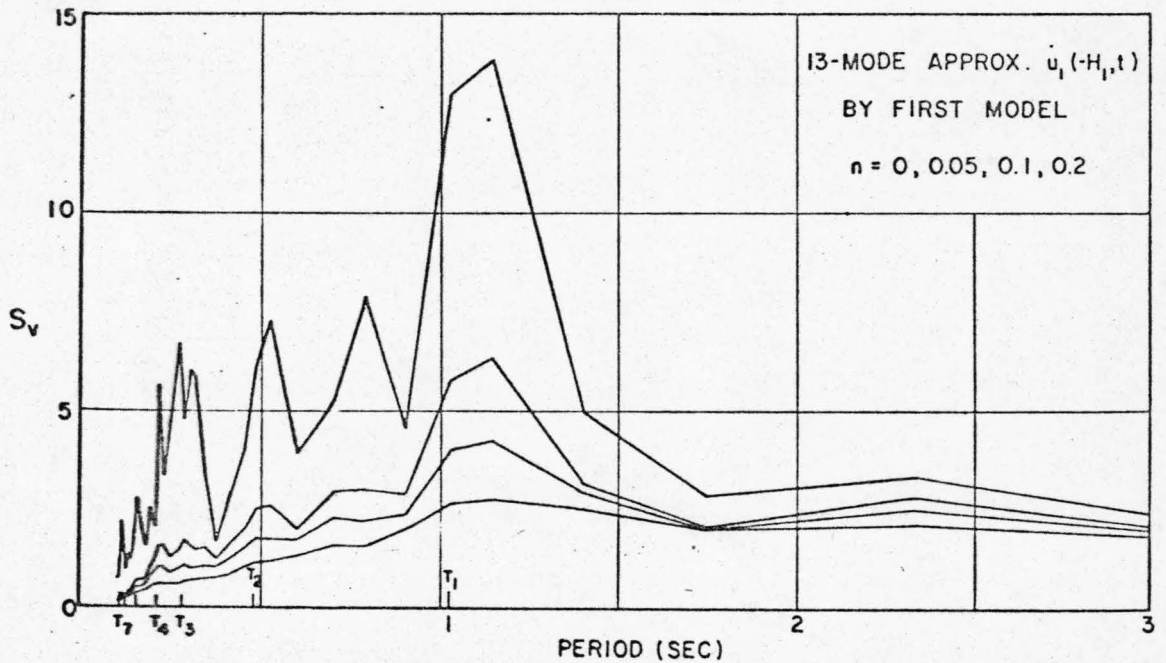


Fig. 4.12 OUTPUT VELOCITY SPECTRA OF THE NONVISCOUS 4-LAYER SYSTEM [ASSOCIATED WITH INPUT $(y)_b$]

hump located between T_2 and T_3 is associated with some strong frequency components of the input $(\dot{y})_a$ that also produce a hump in the input spectra shown in Fig. 4.10(a). Therefore, without knowing the input spectra it is not immediately clear if a hump observed in the output spectra is associated with a layered system.

(c) Except for the fundamental mode, the resonant effects of the higher modes are not clearly reflected by the output spectra. To see more precisely the amplifying effect of the given layered system, we compute the direct spectral ratio, $R(S_v)$, between the output and input spectra associated with the same fractional critical damping.

In Figs. 4.13(a) and 4.13(b) are shown the spectra ratios computed for the velocity spectra of the approximate surface responses to $(\dot{y})_a$ and $(\dot{y})_b$ respectively. The amplification spectrum, $AMP(\omega)$, is also shown accompanying the spectral ratios. Some qualitative observations are made of the spectral ratios as follows:

(a) The undamped spectral ratio indicated by the thick solid lines follows closely the amplification spectrum. In other words, multiplication of the input spectra by $AMP(\omega)$ will give the output spectra approximately. The undamped spectral ratio oscillates about $AMP(\omega)$, being below $AMP(\omega)$ around each of the natural frequencies but above $AMP(\omega)$ elsewhere.

(b) In general, around every natural frequency of the system the spectral ratio associated with larger spectral damping is more depressed, but such tendency is reversed elsewhere. In other words, the oscillatory nature of the spectral ratio decreases with increasing spectral damping. As a consequence, the damped spectral ratio tends to converge to a straight line with increasing spectral damping.

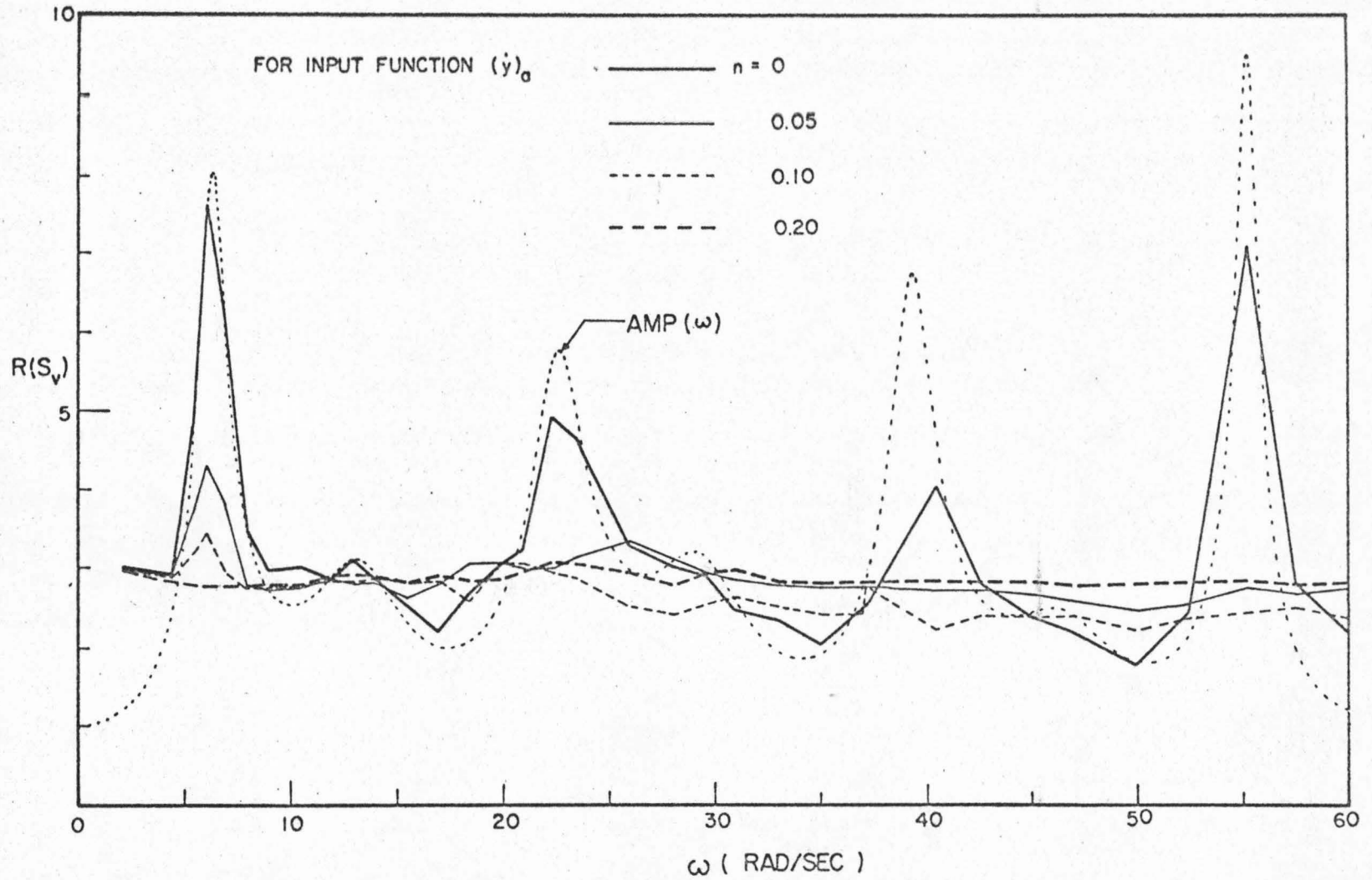


Fig. 4.13(a) SPECTRAL RATIO OF THE NONVISCIOUS 4-LAYER SYSTEM

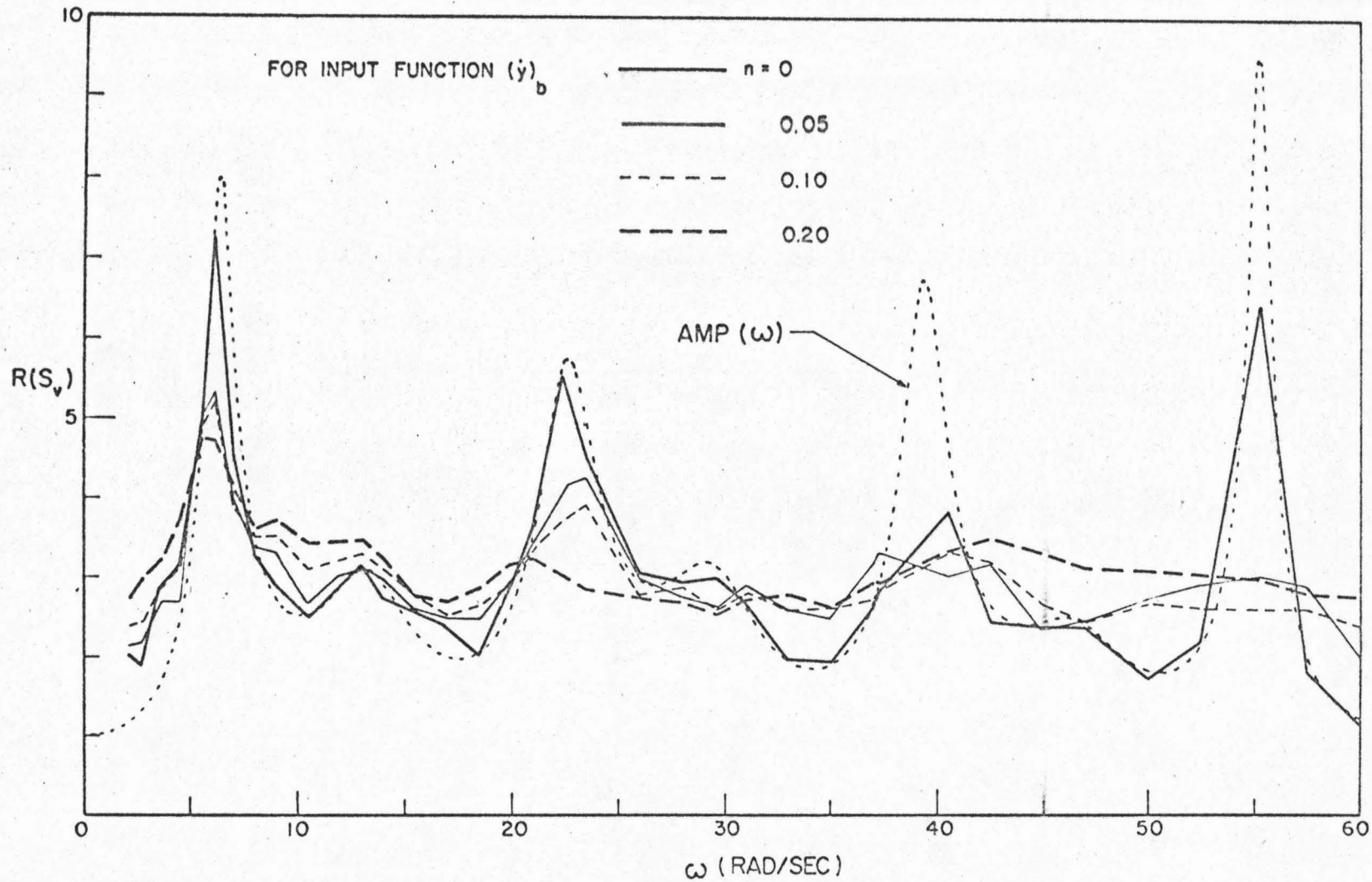


Fig. 4.13(b) SPECTRAL RATIO OF THE NONVISCIOUS 4-LAYER SYSTEM

(c) Damped spectral ratios are more sensitive to the duration of the input motion than are the undamped ones. For a given spectral damping, n , the shorter the duration of the input, the less oscillatory the damped spectral ratios will be. Hence, according to observation (b) the rate at which the damped spectral ratios converge to a straight line will be faster for a shorter duration of the input. In actual applications, it implies that, if the input motion is of an impulse type or has very short duration, a linear amplification of the damped input spectra gives the corresponding output spectra approximately.

C. The First Model for Linearly Viscoelastic Layered Systems

It was proved that the first model is exact for a nonviscous layered system. However, for a linearly viscoelastic layered system this model is no longer exact. The analysis of the model with viscosity present in the layered media will be somewhat more complicated. In the following discussion a lumped representation of the model will again be treated first, and the method of continuous modal analysis is treated later.

(1) The Method of Lumped Masses

To take into account the viscosity of the layered system, a lumped-mass representation of the model similar to the one shown in Fig. 4.2 can be used, except that viscous dashpots must be included. Governing differential equations similar to Eqs. 4.11 and 4.12 can be written as

$$[M]\{\ddot{\tilde{x}}(t)\} + [C]\{\dot{\tilde{x}}(t)\} + [K]\{\tilde{x}(t)\} = -\ddot{\tilde{u}}_N(0,t)\{m\} \quad (4.64)$$

$$\rho_{N+1} c_{N+1} [\dot{\tilde{u}}_N(0,t) - 2\dot{y}(t)] + \tilde{\sigma}_N(0,t) = 0 \quad (4.65)$$

The additional damping matrix, $[C]$, is also an $R \times R$ symmetrical matrix, assumed to be full of nonzero elements for the time being, namely,

$$C_{ij} = C_{ji} \neq 0, \quad i, j = 1, 2, \dots, R \quad (4.66)$$

Physically, Eq. 4.66 means that each mass, m_i , is in general connected to every other mass m_j by a dashpot d_{ij} as well as to the base by d_{ii} . Hence, the off-diagonal elements of $[C]$ are given by

$$C_{ij} = -d_{ij}, \quad i \neq j$$

and the diagonal elements are

$$C_{ii} = \sum_{j=1}^R d_{ij}$$

Consequently, the shear force $\sigma_N(0,t)$ in Eq. 4.65 is given by

$$\tilde{\sigma}_N(0,t) = - \sum_{j=1}^R d_{jR} \dot{\tilde{x}}_j(t) - k_R \tilde{x}_R(t) \quad (4.67)$$

Except for a few simple cases, usually the construction of the damping matrix is complicated. Besides, the damping matrix thus constructed may not, in general, be diagonalized by the orthogonal transformation that diagonalizes both $[M]$ and $[K]$, and the technique of modal analysis will not be applicable to solving Eqs. 4.64 and 4.65. One way to remove such difficulty is to impose

the condition that the system is classically damped such that all three matrices, $[M]$, $[C]$ and $[K]$, can be diagonalized simultaneously under the orthogonal transformation defined by Eq. 4.18. Then the system can be analyzed directly in the transformed domain without having to construct $[C]$, where the damping in each of the normal modes will be determined directly from the exact transfer function of the layered system. From these modal dampings, if desired, the damping matrix can be constructed by a reverse process.

For the lumped system to be classically damped, a necessary and sufficient condition is that the damping matrix can be expressed as a Caughey's series ⁽³⁰⁾,

$$[C] = [M] \sum_{j=1}^R q_j ([M]^{-1} [K])^{j-1} \quad (4.68)$$

where the coefficients q_j are arbitrary constants yet to be determined. The proof of the necessity and sufficiency of the Caughey's series for a passive system to be classically damped was given by O'Kelly ⁽³⁰⁾.

According to Appendix II, the normal mode matrix defined in Eq. 4.18 transforms the damping matrix as follows

$$[A]^T [C] [A] = \sum_{j=1}^R q_j [\tilde{\Lambda}^2]^{j-1} \quad (\text{A.II.2})$$

where it is defined

$$[\tilde{\Lambda}^2]^0 = [I] = \text{identity matrix}$$

is actually not available, $\tilde{\beta}_r$ will be derived directly from the exact transfer function of the layered system, as we have proposed. Then, if the construction of $[C']$ is desired, the reverse process given in Appendix III can be used. Obviously, the matrix $[C']$ constructed this way is not unique, depending on the number S .

By using Eqs. 4.20 and 4.70, Eq. 4.64 is transformed into an uncoupled system as

$$\{\ddot{\tilde{v}}(t)\} + [\tilde{B}]\{\dot{\tilde{v}}(t)\} + [\tilde{\Lambda}^2]\{\tilde{v}(t)\} = -\ddot{u}_N(0,t)[A]^T\{m\}$$

or, in terms of the modal equations,

$$\ddot{\tilde{v}}_r(t) + 2\tilde{\beta}_r \tilde{\omega}_r \dot{\tilde{v}}_r(t) + \tilde{\omega}_r^2 \tilde{v}_r(t) = -\ddot{u}_N(0,t) \sum_{i=1}^R A_{ir} m_r, \quad r = 1, 2, \dots, R$$

Using again the transformed normal coordinate, $\tilde{\xi}_r(t)$, defined in Eq. 4.22, the final system of equations to be solved is, if only the first S modes are considered,

$$\begin{cases} \ddot{\tilde{\xi}}_r(t) + 2\tilde{\beta}_r \tilde{\omega}_r \dot{\tilde{\xi}}_r(t) + \tilde{\omega}_r^2 \tilde{\xi}_r(t) = -\ddot{u}_N(0,t), & r = 1, 2, \dots, S \\ \rho_{N+1} c_{N+1} [\dot{\tilde{u}}_N(0,t) - 2\dot{y}(t)] + \tilde{\sigma}_N(0,t) = 0 \end{cases} \quad (4.72)$$

(2) The Method of Continuous Modal Analysis

Analogous to Eq. 4.72, the system of equations to be solved in this method will be

$$\begin{cases} \ddot{\xi}_r(t) + 2\beta_r \omega_r \dot{\xi}_r(t) + \omega_r^2 \xi_r(t) = -\ddot{u}_N(0,t) & r = 1, 2, \dots, S \\ \rho_{N+1} c_{N+1} [\dot{u}_N(0,t) - 2\dot{y}(t)] + \sigma_N(0,t) = 0 \end{cases} \quad (4.73)$$

where β_r and $\sigma_N(0, t)$ are yet to be determined. In the following, the determination of β_r is discussed first.

Denote by $|H_{1,N}(\omega)|$ the exact amplitude transfer function of the layered system between $u_1(-H_1, t)$ and $u_N(0, t)$. For a linearly viscoelastic layered system of which the media obey the stress-strain law, Eq. 2.3, $|H_{1,N}(\omega)|$ can easily be obtained from Eq. 2.28 as

$$|H_{1,N}(\omega)| = \sqrt{\frac{f_1^2(\omega, -H_1) + g_1^2(\omega, -H_1)}{\text{Re}_{N+1}^2 + \text{Im}_{N+1}^2}} \quad (4.74)$$

Let a representative portion of $|H_{1,N}(\omega)|$ be as that shown in Fig. 4.16. An approximate formula commonly adopted by structural engineers to determine the damping of a particular mode, say, the r^{th} mode, of a building from the response curve of resonance test is⁽³¹⁾

$$\beta_r \approx \frac{\Delta\omega_r}{2\omega_r} \quad (4.75)$$

where $\Delta\omega_r$ is the horizontal distance between the two half-power points A and B, as shown in Fig. 4.14. The use of Eq. 4.75 requires that the damping in the structure be small enough so that, at the resonant frequency ω_r , the contributions to $|H_{1,N}(\omega)|$ from all modes other than the r^{th} mode itself are negligible. However, Eq. 4.75 is invalid for approximate analysis of the model mainly because of the following reasons:

(a) In applying Eq. 4.75 it is assumed that the frequency at which a local maximum of the resonance curve takes place is a natural frequency. But, as shown in Fig. 4.14, it is not uncommon that at a natural frequency, say, ω_{r+1} of the layered system

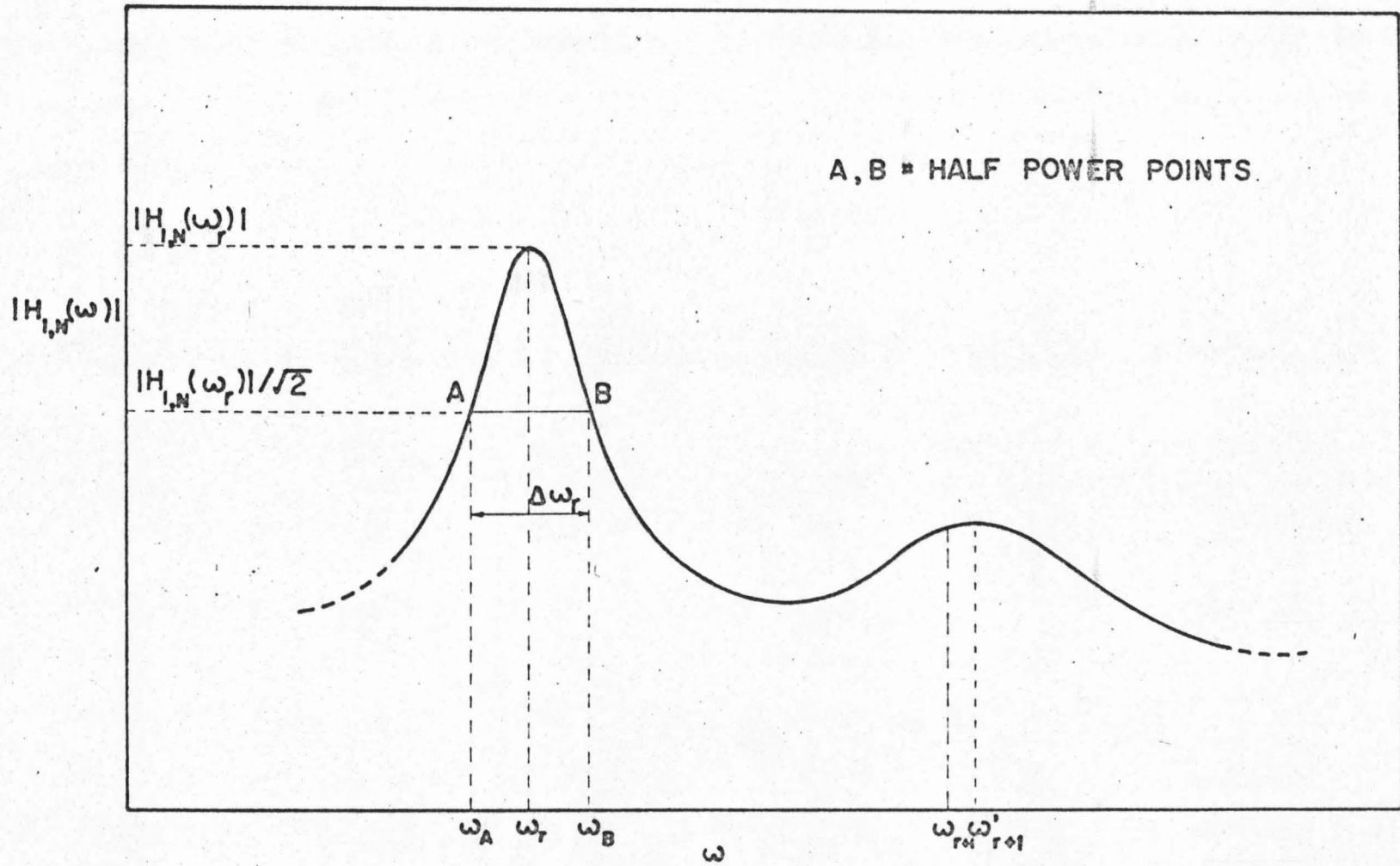


Fig. 4.14 A REPRESENTATIVE SECTION OF $|H_{1,N}(\omega)|$

the transfer function is not a local maximum. The local maximum occurs at a frequency ω'_{r+1} which can be some distance from ω_{r+1} .

(b) For viscous layered systems the transfer function usually is attenuated with increasing frequency. Hence, at a higher natural frequency such as ω_{r+1} the half-power points may not even exist.

(c) The modal dampings in the model need not be small, and hence the assumption that modal interference can be neglected is no longer valid.

Since Eq. 4.75 is not applicable, the following method is developed instead. The basis of this method is to match the approximate amplitude transfer function, $|\bar{H}_{1,N}(\omega)|$, with the exact one, $|H_{1,N}(\omega)|$, at each natural frequency ω_r for $r = 1, 2, \dots, S$, namely,

$$|\bar{H}_{1,N}(\omega_r)| = |H_{1,N}(\omega_r)| \quad (4.76)$$

The exact transfer function has been given in Eq. 4.74. To find the approximate transfer function, let us assume a steady-state input $y(t) = e^{i\omega t}$. The steady-state response at the base can be written after Eq. 4.57 as

$$u_N(0, t) = 2\bar{H}_N(\omega) e^{i\omega t} \quad (4.57)$$

Then, Eq. 4.73 gives the steady-state solution for $\xi_r(t)$ as

$$\xi_r(t) = u_N(0, t) X_r e^{-i\theta_r} \quad (4.77)$$

where, with $\Omega_r = \omega/\omega_r$, it is defined that

$$X_r(\Omega_r, \beta_r) = \frac{\Omega_r^2}{\sqrt{(1-\Omega_r^2)^2 + (2\beta_r \Omega_r)^2}}$$

and

(4.78)

$$\theta_r(\Omega_r, \beta_r) = \tan^{-1} \frac{2\beta_r \Omega_r}{1-\Omega_r^2}$$

Substituting $z_1 = -H_1$ into Eq. 4.56' gives the steady-state surface response

$$u_1(-H_1, t) = \sum_{r=1}^S D_r^{(1)}(-H_1) \xi_r(t) + u_N(0, t) \quad (4.79)$$

Equations 4.77 and 4.79 together give

$$\bar{H}_{1,N}(\omega) = |\bar{H}_{1,N}(\omega)| e^{-i\bar{\Psi}_{1,N}(\omega)} \quad (4.80)$$

with

$$\bar{\Psi}_{1,N}(\omega) = \tan^{-1} \frac{\sum_{r=1}^S D_r^{(1)}(-H_1) X_r \sin \theta_r}{1 + \sum_{r=1}^S D_r^{(1)}(-H_1) \cos \theta_r X_r} \quad (4.81)$$

and

$$|\bar{H}_{1,N}(\omega)| = \left\{ \left[1 + \sum_{r=1}^S D_r^{(1)}(-H_1) X_r \cos \theta_r \right]^2 + \left[\sum_{r=1}^S D_r^{(1)}(-H_1) X_r \sin \theta_r \right]^2 \right\}^{\frac{1}{2}} \quad (4.82)$$

Now, go back to Eq. 4.76 which is to be solved for β_r by iteration. To start the iteration, an initial value for each β_r has to be specified. As a first approximation, we can neglect the contributions to $|\bar{H}_{1,N}(\omega_r)|$ from all modes other than the r^{th} mode, and hence Eq. 4.82 becomes

$$|\bar{H}_{1,N}(\omega_r)| \approx \frac{|D_r^{(1)}(-H_1)|}{2\beta_r^{(1)}}, \quad r = 1, 2, \dots, S$$

which, when substituted into Eq. 4.76, produces the first approximation of β_r

$$\beta_r^{(1)} = \frac{|D_r^{(1)}(-H_1)|}{2|\bar{H}_{1,N}(\omega_r)|}, \quad r = 1, 2, \dots, S \quad (4.83)$$

Using $\beta_r^{(1)}$ as initial values, the iteration can be carried out. The first round of iteration begins from the first mode. Using $\beta_r^{(1)}$ in computing $|\bar{H}_{1,N}(\omega_r)|$, Eq. 4.76 yields

$$\begin{aligned} \frac{D_1^{(1)}(-H_1)}{2\beta_1^{(2)}} &= - \sum_{j=2}^S D_j^{(1)} X_{j,(\omega_1, \beta_j^{(1)})} \sin \theta_{j,(\omega_1, \beta_j^{(1)})} \\ &\pm \left\{ |H_{1,N}(\omega_1)|^2 - \left[1 + \sum_{j=2}^S D_j^{(1)} X_{j,(\omega_1, \beta_j^{(1)})} \cos \theta_{j,(\omega_1, \beta_j^{(1)})} \right]^2 \right\}^{\frac{1}{2}} \\ &= B^+ \text{ or } B^- \end{aligned}$$

where B^+ is obtained by taking the plus sign in front of the radical sign and B^- by the minus sign. If B^+ and B^- have opposite signs, the one with the same sign as that of $D_1^{(1)}(-H_1)$ will be used. How-

ever, if B^+ and B^- are of the same sign the one that has the larger absolute value will be used. The last equation provides $\beta_1^{(2)}$ as the second approximation of β_1 . For $r = 2, 3, \dots, S$, $\beta_r^{(2)}$ can be computed in the same manner, except that the newly computed modal dampings, $\beta_j^{(2)}$, $j = 1, 2, \dots, r-1$, are always used instead of the old values $\beta_j^{(1)}$ in evaluating $|\bar{H}_{1,N}(\omega_r)|$.

The above process is repeated to improve the accuracies of the iterated modal dampings. At the $q-1^{\text{th}}$ iteration the general formula for calculating $\beta_r^{(q)}$ is

$$\begin{aligned}
 & |\bar{H}_{1,N}(\omega_r)| \\
 &= \left\{ \left[1 + \sum_{j=1}^{r-1} D_j^{(1)} X_{j(\omega_r, \beta_j^{(q)})} \cos \theta_j + \sum_{j=r+1}^S D_j^{(1)} X_{j(\omega_r, \beta_j^{(q-1)})} \cos \theta_j \right]^2 \right. \\
 & \left. + \left[\frac{D_r^{(1)}}{2\beta_r^{(q)}} + \sum_{j=1}^{r-1} D_j^{(1)} X_{j(\omega_r, \beta_j^{(q)})} \sin \theta_j + \sum_{j=r+1}^S D_j^{(1)} X_{j(\omega_r, \beta_j^{(q-1)})} \sin \theta_j \right]^2 \right\}^{\frac{1}{2}}
 \end{aligned} \tag{4.84}$$

Defining

$$(\text{ERR})_r^{(q)} = \frac{|\beta_r^{(q)} - \beta_r^{(q-1)}|}{\beta_r^{(q)}} \times 100\% \tag{4.85}$$

as the error of $\beta_r^{(q)}$, the iteration process can be stopped at any desired accuracy whenever the following condition is fulfilled.

$$(\text{ERR})_r^{(q)} \leq \text{prescribed accuracy for } r = 1, 2, \dots, S \tag{4.86}$$

The process converges very rapidly, and usually 3 to 5 iterations are sufficient to obtain modal dampings with a maximum error within 1%.

Having determined β_r , the shearing stress $\sigma_N(0, t)$ in Eq. 4.73 is derived as follows. To derive $\sigma_N(0, t)$ formally by expanding the expression $\mu_N[\partial x_N(z_N, t)/\partial z_N]$ evaluated at $z_N = 0$, as was done in Eq. 4.45 for a nonviscous layered system, is extremely complicated. Instead, a parameter $(C_{\text{eff}})_r$ — effective damping coefficient — is introduced in the same manner as $(m_{\text{eff}})_r$ and $(K_{\text{eff}})_r$ were introduced in Eqs. 4.48 and 4.46 respectively. Hence, we can write

$$(C_{\text{eff}})_r = 2\beta_r \omega_r (m_{\text{eff}})_r \quad r = 1, 2, \dots, S \quad (4.87)$$

and, analogous to Eq. 4.47, $\sigma_N(0, t)$ can be written as

$$\sigma_N(0, t) = - \sum_{r=1}^S [(C_{\text{eff}})_r \dot{\xi}_r(t) + (K_{\text{eff}})_r \xi_r(t)] \quad (4.88)$$

Thus, with $(F)_r$ defined in Eq. 4.50 as $(K_{\text{eff}})_r / \rho_{N+1} c_{N+1}$ and with

$$(Q)_r = (C_{\text{eff}})_r / \rho_{N+1} c_{N+1} \quad (4.89)$$

Eq. 4.73 is rewritten as

$$\left. \begin{aligned} \ddot{\xi}_r + 2\beta_r \omega_r \dot{\xi}_r + \omega_r^2 \xi_r &= -\ddot{u}_N(0, t), \quad r = 1, 2, \dots, S \\ \dot{u}_N(0, t) - 2\dot{y}(t) - \sum_{r=1}^S [(Q)_r \dot{\xi}_r + (F)_r \xi_r] &= 0 \end{aligned} \right\} \quad (4.90)$$

$$[B]_{S \times S} = \begin{bmatrix} & & & & \\ & & & & \\ & & & & \\ & & & 2\beta_r \omega & \\ & & & & \\ & & & & & \end{bmatrix}$$

and

(4.92 cont.)

$$\{\bar{P}(t)\} = \{0, \dots, 0, \overset{S}{2\dot{y}(t)/QQ}, 2\beta_1 \omega \dot{u}_N, \dots, 2\beta_S \omega \dot{u}_N(0, t)\}$$

Equation 4.91 can be solved numerically for $\dot{f}_r(t)$ and $\dot{u}_N(0, t)$ to obtain the desired response, $\dot{u}_j(z_j, t)$, from Eq. 4.56. Observe that Eq. 4.52 can be deduced from Eq. 4.91 by setting $\beta_r = 0$ for $r = 1, 2, \dots, S$.

To check the accuracy of the approximate analysis which takes into account the contributions from the first S modes only, the approximate amplitude transfer function, $|\bar{H}_1(\omega)|$, will be derived to compare with the exact one, $|H_1(\omega)|$. For a steady-state input $y(t) = e^{i\omega t}$, Eqs. 4.77 and 4.57 give the steady-state responses of $\xi_r(t)$ and $u_N(0, t)$ respectively as

$$\xi_r(t) = u_N(0, t) X_r e^{-i\theta_r} \quad r = 1, 2, \dots, S$$

and

$$u_N(0, t) = 2\bar{H}_N(\omega) e^{i\omega t}$$

Substituting $\xi_r(t)$ and $u_N(0, t)$ into the last equation of Eq. 4.90 yields

$$\bar{H}_N(\omega) = |\bar{H}_N(\omega)| e^{-i\bar{\psi}_N(\omega)} = \frac{e^{-i\bar{\psi}_N(\omega)}}{\sqrt{B_R^2(\omega) + B_I^2(\omega)}} \quad (4.93)$$

where

$$B_R(\omega) = 1 + \frac{1}{\omega} \sum_{r=1}^S X_r [(F)_r \sin \theta_r - \omega(Q)_r \cos \theta_r]$$

$$B_I(\omega) = \frac{1}{\omega} \sum_{r=1}^S X_r [(F)_r \cos \theta_r + \omega(Q)_r \sin \theta_r] \quad (4.94)$$

and

$$\bar{\psi}_N(\omega) = \tan^{-1} \frac{B_I(\omega)}{B_R(\omega)}$$

Therefore, the approximate solution for the amplitude transfer function $|H_1(\omega)|$ is

$$|\bar{H}_1(\omega)| = |\bar{H}_{1,N}(\omega)| |\bar{H}_N(\omega)| = \frac{|\bar{H}_{1,N}(\omega)|}{\sqrt{B_R^2(\omega) + B_I^2(\omega)}} \quad (4.95)$$

in which $|\bar{H}_{1,N}(\omega)|$ has been given in Eq. 4.82.

(3) Numerical Examples

The quadruple-layer system that was used to demonstrate the applicability of the first model will be used here with the exception that the layered media are now assumed to be standard linear viscous solids. The parameters τ_j and r_j that describe a standard linear model were given in columns (5) and (6) of Table 2.1. Equation 4.74 then provides the values of $|H_{1,N}(\omega)|$ evaluated at the first 13 natural frequencies, which are listed in Table 4.2. With a maximum error of 1% prescribed, the iteration process defined by Eq. 4.84 yields the modal fractions of critical damping

Table 4.2 MODAL DAMPINGS OF THE 4-LAYER SYSTEM
COMPOSED OF STANDARD LINEAR VISCOUS SOLIDS

MODAL NO.	MODAL FRACTION OF CRITICAL DAMPING	EFFECTIVE DAMPING COEFFICIENT (EQ. 4.92)	
r	$ H_{1,N}(\omega_r) $	β_r (%)	$(Q)_r$
1	136.27	0.604	0.00260
2	42.87	1.109	0.00627
3	12.51	2.333	0.00487
4	8.09	2.664	0.00719
5	3.46	4.273	0.00392
6	2.99	3.916	0.00840
7	1.19	6.270	0.00227
8	0.86	6.088	0.00380
9	0.71	7.314	0.00461
10	0.47	7.416	0.00666
11	0.34	9.926	0.00705
12	0.16	8.940	0.00376
13	0.12	10.275	0.01528

after eight iterations. The results together with $(Q)_r$ computed from Eq. 4.92 are given in Table 4.2. The computing time cost in finding the modal dampings by digital computer is very small.

The 13-mode approximations, $|\bar{H}_1(\omega)|$ and $|\bar{H}_N(\omega)|$, are shown together with their exact counterparts, $|H_1(\omega)|$ and $|H_N(\omega)|$, in Figs. 4.15 and 4.16 respectively, where, by definition $|H_1(\omega)|$ is equal to the amplification spectrum $AMP(\omega)$. A comparison between the approximate and the exact transfer functions indicates

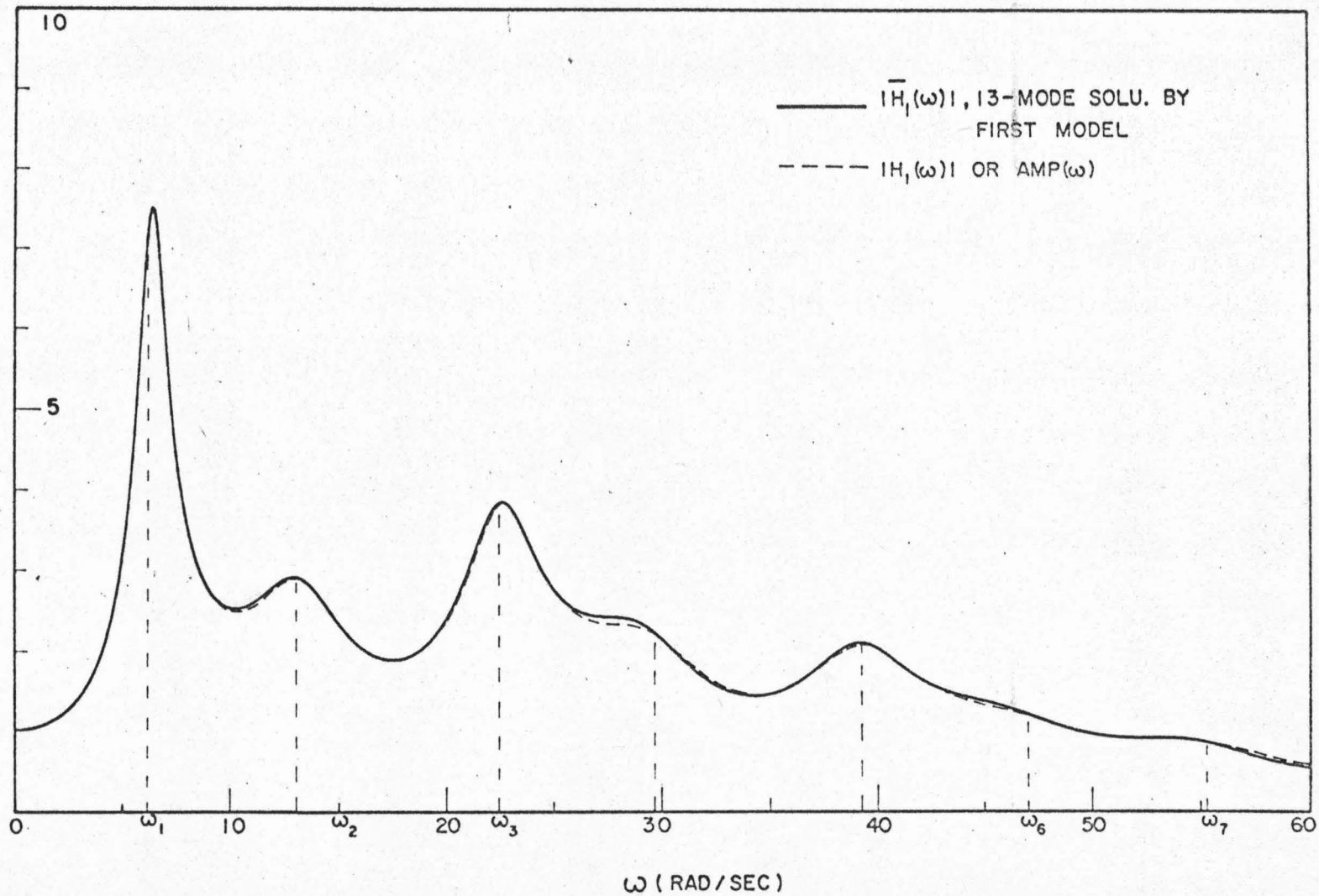


Fig. 4.15 AMPLITUDE TRANSFER FUNCTION OF THE VISCOUS 4-LAYER SYSTEM

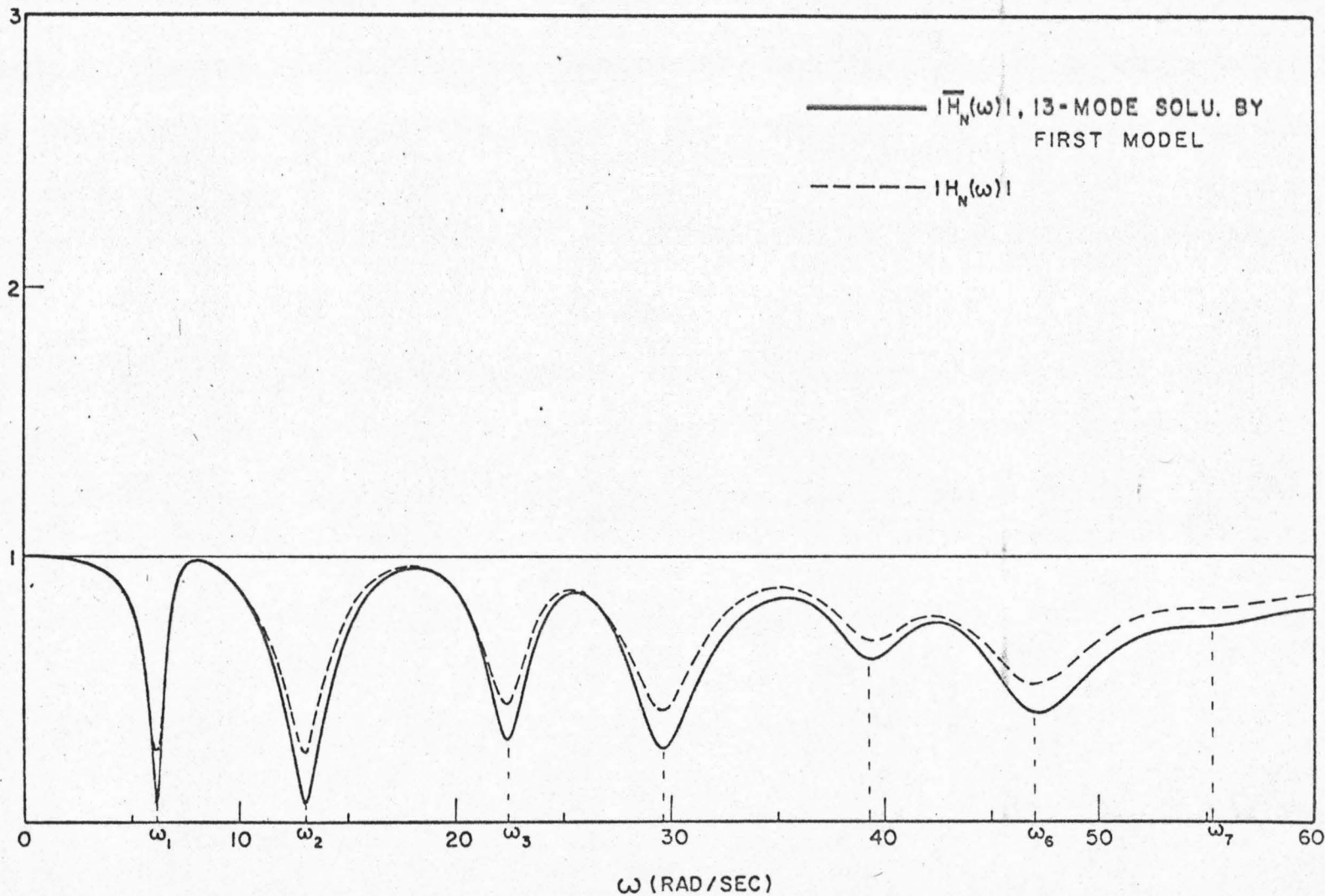


Fig. 4.16 AMPLITUDE TRANSFER FUNCTION OF THE VISCOUS 4-LAYER SYSTEM

that, by considering the contributions from the first 13 modes, the approximate analysis is sufficiently accurate in the prescribed frequency range.

The transient response of the layered system was computed by solving Eq. 4.91 numerically on a digital computer. The inputs used in the calculation are the functions $(\dot{y})_a$ and $(\dot{y})_b$ which are shown in Fig. 4.7. In Figs. 4.17 and 4.18 are shown the results respectively computed for the surface response and the base response. Although exact solutions for the surface response are not available for comparison, the approximate solutions can be expected to possess sufficient accuracy comparable to that achieved for the approximate transfer function. Attenuation of the high frequency components is obvious when the surface response is compared with that obtained for the nonviscous layered system. On the other hand, the base response differs only very little from that computed for the nonviscous layered system, which leads to the conclusion that the base motion is not so sensitive to the presence of viscosity in the system as is the surface motion.

Velocity spectra were computed for the surface responses, and are shown in Fig. 4.19. The effect of viscosity contained in the layered media is clearly exhibited by the rapid decaying of the spectra toward the shorter-period end. For periods longer than 0.5 second the spectra differ only slightly from the corresponding spectra computed for the nonviscous system.

Spectral ratios, $R(S_v)$, were also computed, and the results are shown in Figs. 4.20(a) and 4.20(b). The conclusions drawn previously for the spectral ratios of the nonviscous layered

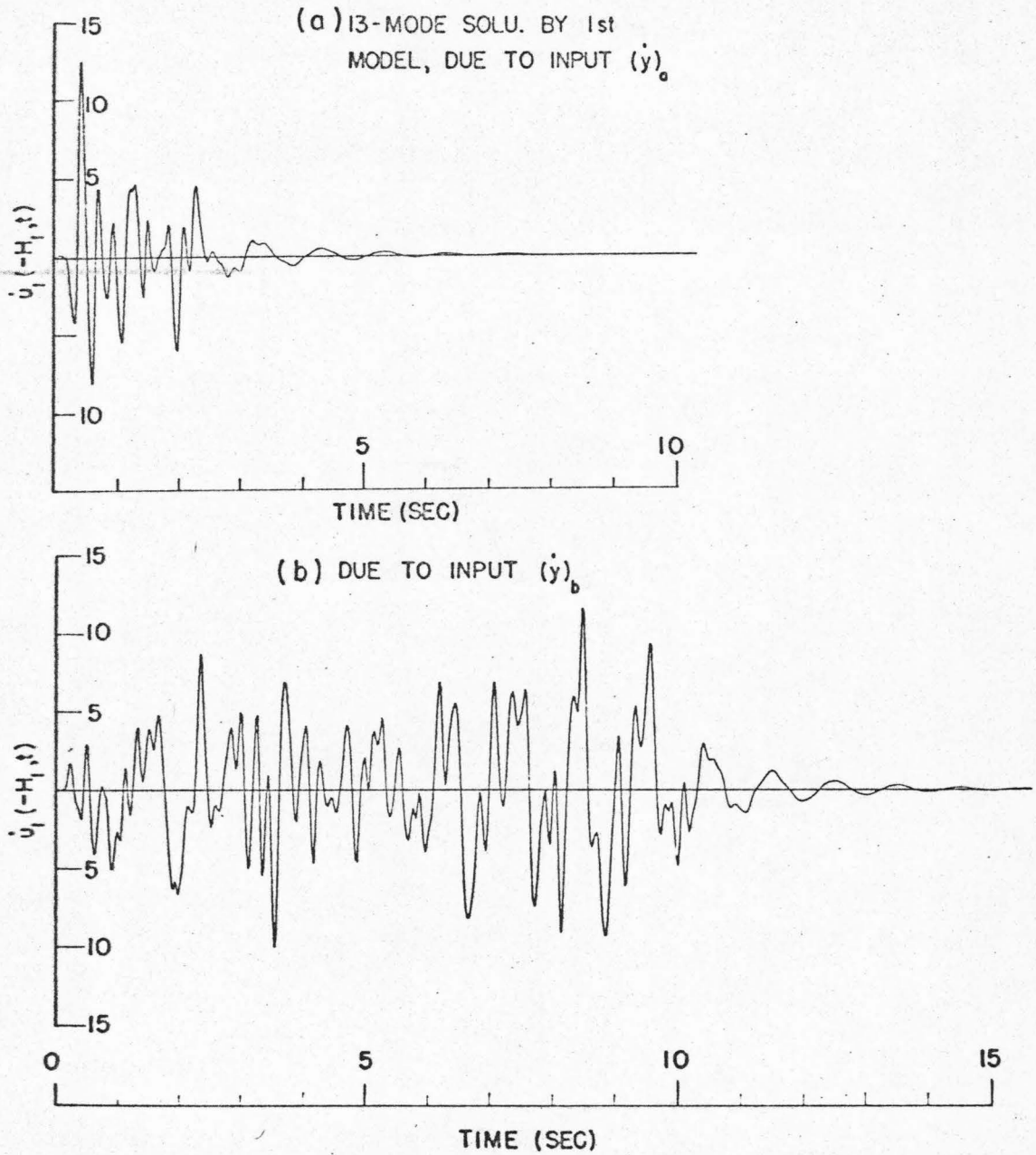


Fig. 4.17 SURFACE RESPONSE OF THE VISCOUS 4-LAYER
SYSTEM

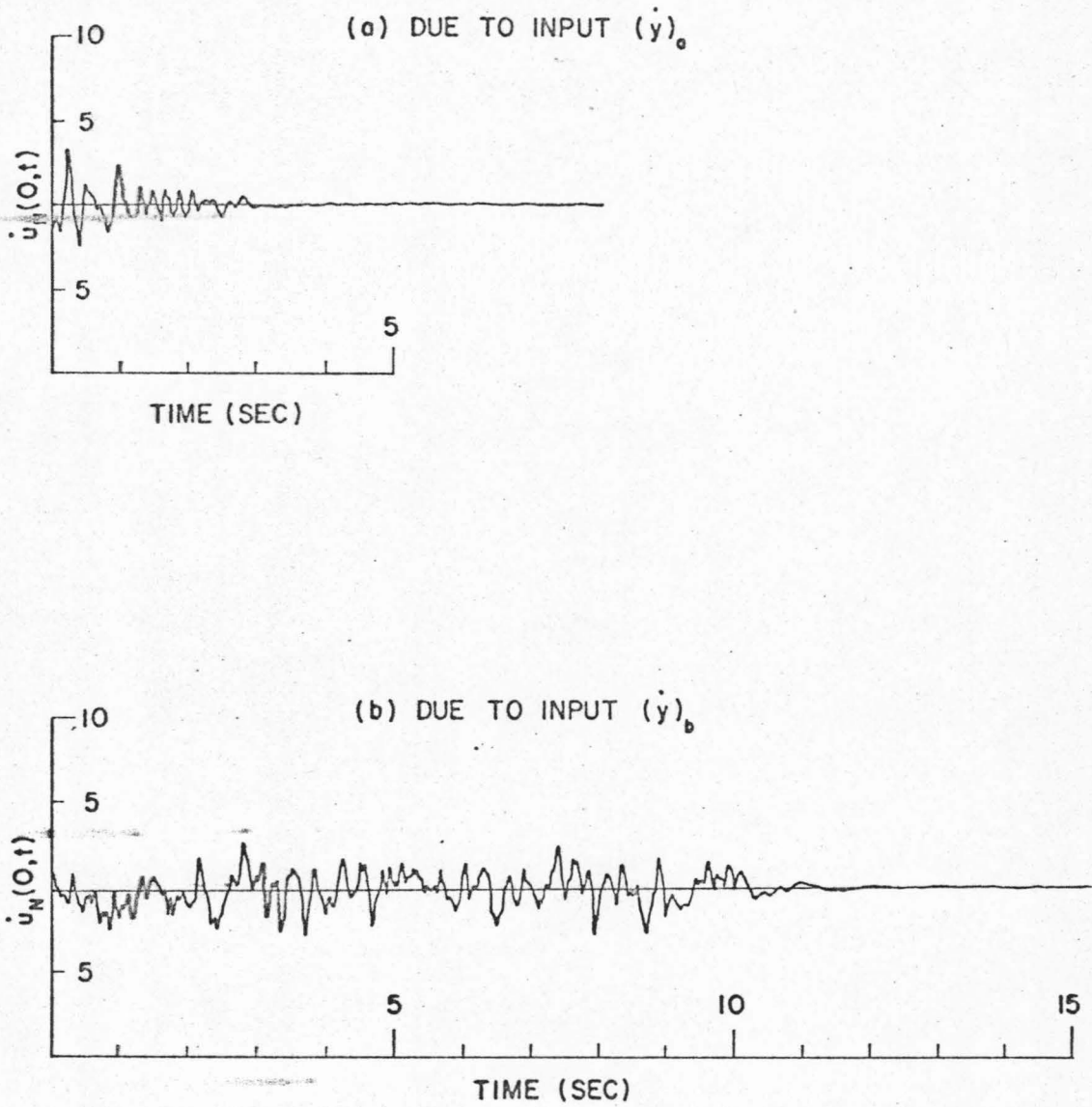


Fig. 4.18 BASE RESPONSE OF THE VISCOUS 4-LAYER SYSTEM

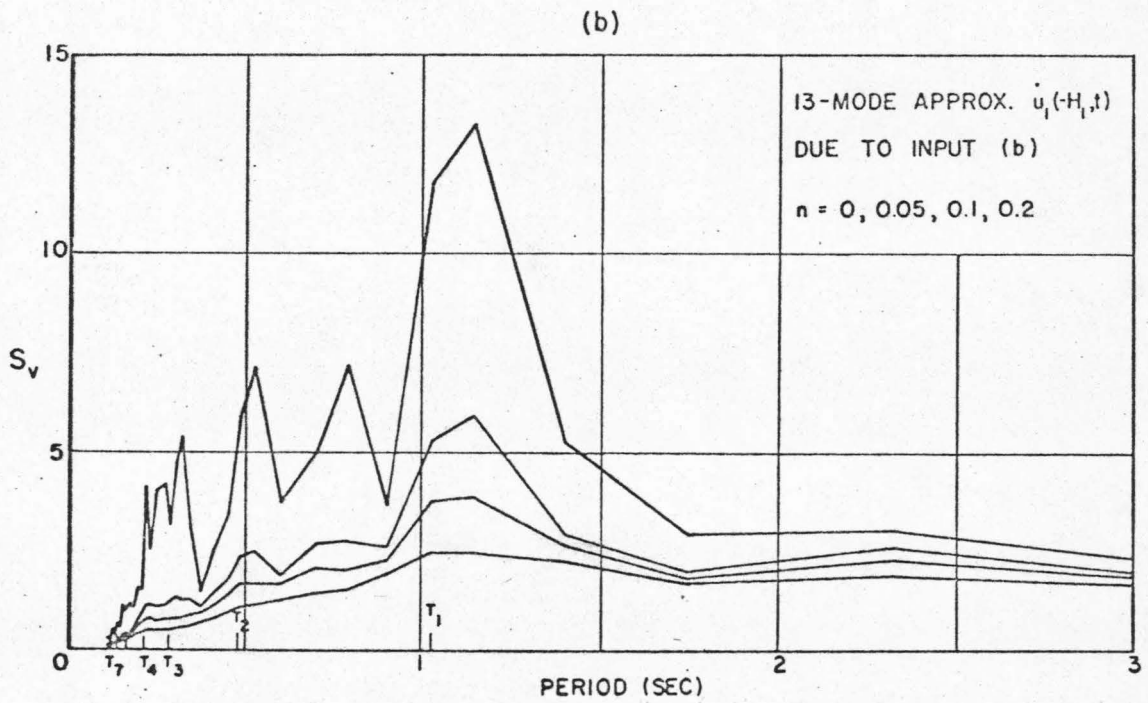
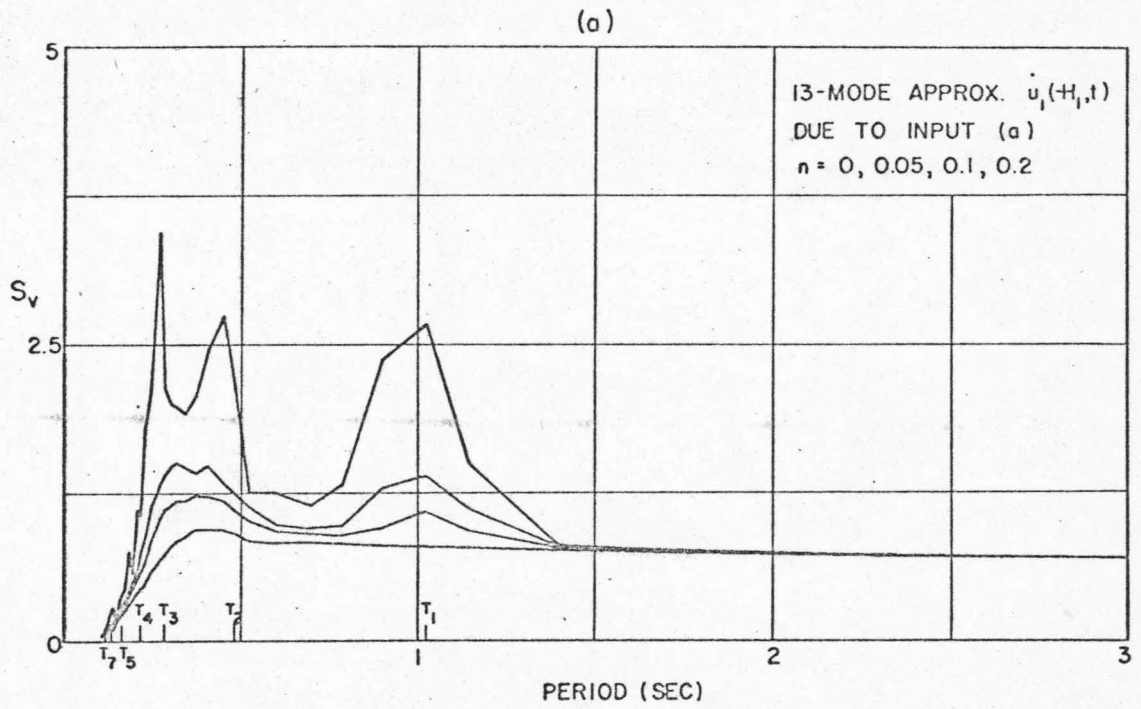


Fig. 4.19 OUTPUT VELOCITY SPECTRA OF THE VISCOUS 4-LAYER SYSTEM

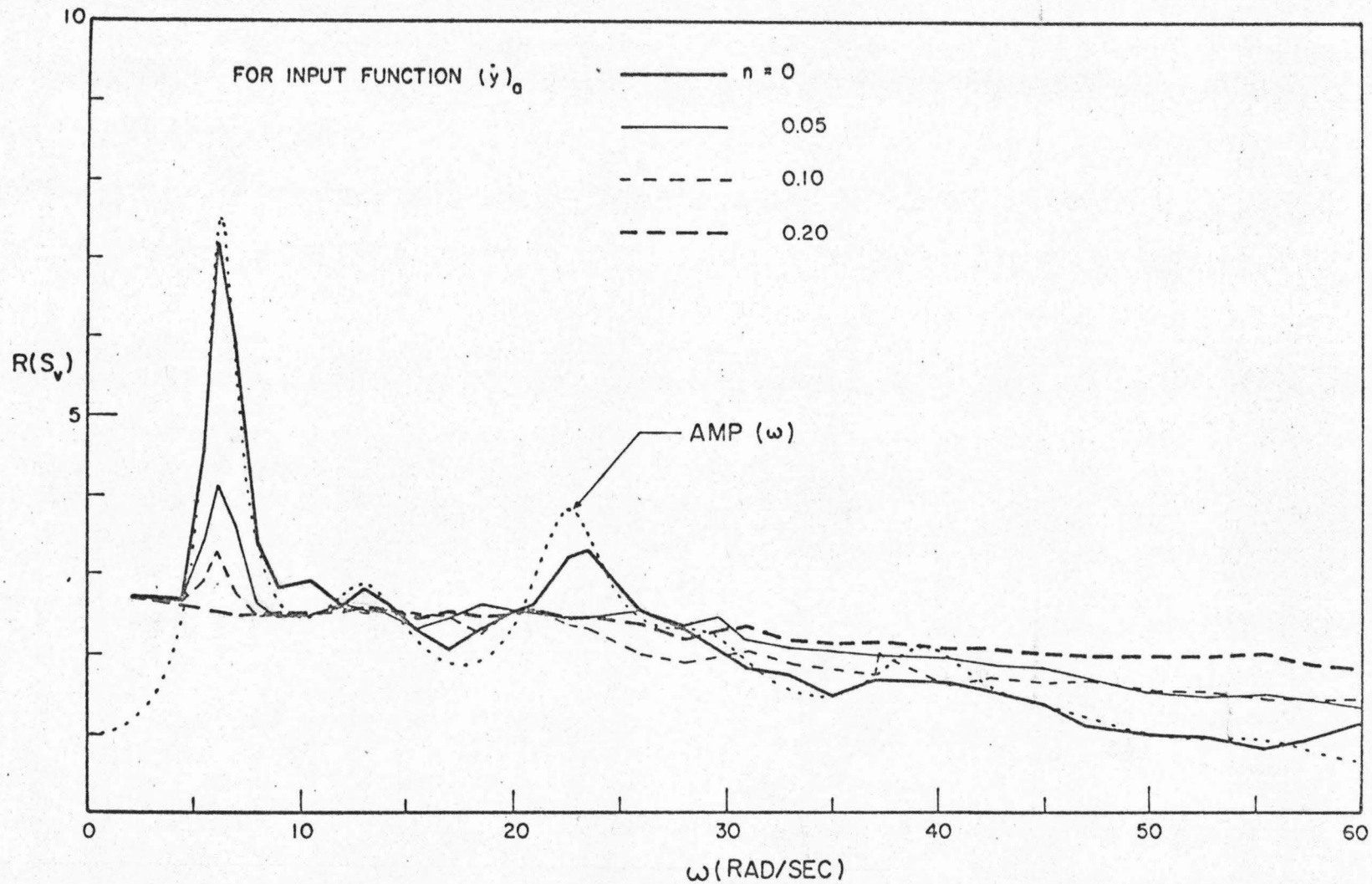


Fig. 4.20(a) SPECTRA RATIO OF THE VISCOUS 4-LAYER SYSTEM

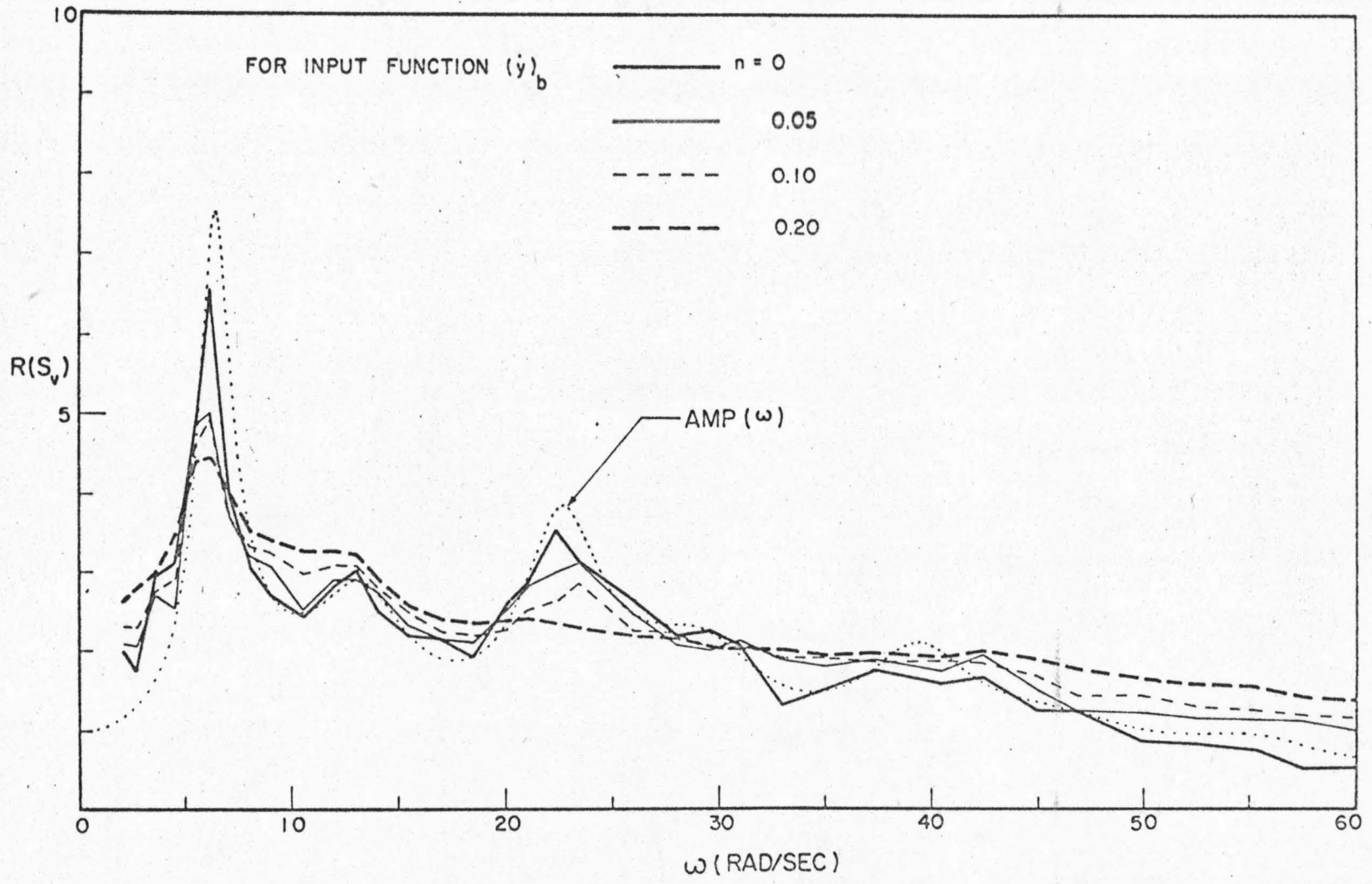


Fig. 4.20(b) SPECTRAL RATIO OF THE VISCOUS 4-LAYER SYSTEM

system remain valid here, except that the spectral ratios in this case have small divergencies toward the high frequency end.

Finally, it should be pointed out that in approximate analysis of the first model for a viscous layered system a smaller number S may be used when compared with that needed for analysis of a nonviscous layered system. For instance, we can use $S = 10$ instead of 13 in the last example while the accuracy of the approximate analysis remains satisfactory. The reason for this is that the higher modes are damped so much that their contributions to the transfer functions in the prescribed range of frequency are practically negligible. The allowance for using a smaller number S implies some savings of the computing time required for the approximate analysis.

D. The Second Model

Numerical examples given for demonstrating the first model showed the resemblance between the base motion $\dot{u}_N(0, t)$ and the input $2\dot{y}(t)$. It was argued that such resemblance is closer with increasing rigidity of the foundation. In terms of transfer function, it means that $|H_N(\omega)|$ is approaching the constant 1 when the impedance ratio α_N is decreasing. When α_N becomes zero, $|H_N(\omega)|$ is simply equal to 1. This observation suggests that, if α_N is small, a second model as a further approximation of a given layered system can be established by assuming that the base motion is identical with the input motion $2y(t)$.

The model is obtained by replacing the dashpot D in the first model by a rigid one to provide the identity between the base motion and the input, while the energy lost into the foundation due

to its deformability is accounted for approximately by incorporating artificially an appropriate amount of viscous damping in the shear beam. An S-mode representation of this model in terms of the transformed normal coordinates, $\xi_r(t)$, is shown in Fig. 4.21 where $\xi_r(t)$ was defined in Eq. 4.40. The method of continuous modal analysis will be used for the approximate analysis of this model.

(1) The Method of Continuous Modal Analysis

Since α_N is assumed zero for the model, we have

$$u_N(0, t) \equiv 2y(t)$$

and

(4.96)

$$(F)_r = (Q)_r \equiv 0 \quad \text{for } r = 1, 2, \dots, S$$

with $(F)_r$ and $(Q)_r$ defined in Eqs. 4.50 and 4.89 respectively. Hence, the equations of motion describing the model can be deduced from Eq. 4.90 as

$$\ddot{\xi}_r(t) + 2\beta_r \omega_r \dot{\xi}_r(t) + \omega_r^2 \xi_r(t) = -2\ddot{y}(t), \quad r = 1, 2, \dots, S \quad (4.97)$$

There are three important points to be noted when Eq. 4.97 is used.

(a) The modal fractions of critical damping in Eq. 4.97 are different from those for the first model because β_r in the second model includes an artificial part accounting approximately for the energy lost into the foundation. Consequently, unless α_N is actually zero in the given system, there is always some damping in the model even if the given system is nonviscous.

$$\ddot{u}_1(-H_1, t) = \sum_{r=1}^S D_r^{(1)}(-H_1) \ddot{\xi}_r(t) + 2\ddot{y}(t)$$

$$(C_{eff})_r = 2\beta_r \omega_r (m_{eff})_r$$

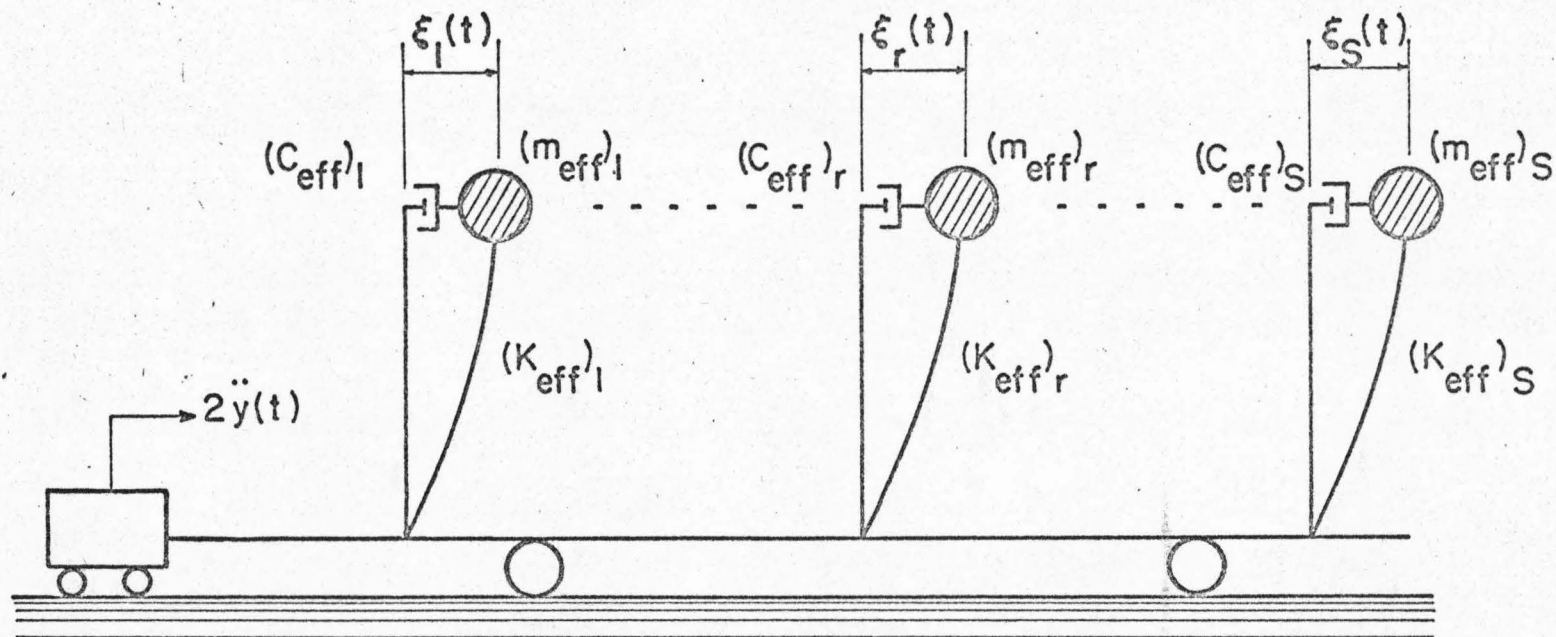


Fig. 4.21 AN S-MODE REPRESENTATION OF THE SECOND SHEAR BEAM MODEL

(b) The input motion is taken to be an acceleration input, $\ddot{y}(t)$, rather than a velocity input as in the first model. Therefore, the corresponding response to be computed is the acceleration response $\ddot{u}_j(z_j, t)$.

(c) The number S is not necessarily the same as that used in the first model. As a matter of fact, numerical examples given later reveal that, if ω_j is the largest natural frequency included in the prescribed frequency range, a rule of thumb for estimating S is

$$S = J + 1 \quad (4.98)$$

which is compared with Eq. 4.62.

It should be pointed out that the second model is expected to give good results only at or near the surface of the layered system. Fortunately, the region of validity of the model will extend further downwards as the rigidity of the foundation increases.

Since $|\bar{H}_N(\omega)|$ is equal to 1 in the second model, we have

$$|\bar{H}_1(\omega)| = |\bar{H}_{1,N}(\omega)| \cdot |\bar{H}_N(\omega)| \equiv |\bar{H}_{1,N}(\omega)|$$

with $|\bar{H}_{1,N}(\omega)|$ given by Eq. 4.82. The basis for determining the modal fraction of critical damping, β_r , which accounts for both the viscosity, if any, in the layered media and the energy lost into the foundation, is to match $|\bar{H}_1(\omega)|$ with the exact solution, $|H_1(\omega)|$, at each of the first S natural frequencies. That is,

$$|\bar{H}_1(\omega_r)| = |H_1(\omega_r)|, \quad r = 1, 2, \dots, S \quad (4.99)$$

The iteration process defined by Eq. 4.84 can then be used to solve Eq. 4.99 for β_r , except that the function $|\bar{H}_{1,N}(\omega_r)|$ at the left-hand side of Eq. 4.84 should be replaced by $|H_1(\omega_r)|$.

With β_r determined, Eq. 4.97 can be solved numerically for $\xi_r(t)$ which, when substituted into Eq. 4.56', give the acceleration response at the surface as

$$\ddot{u}_1(-H_1, t) = \sum_{r=1}^S D_r^{(1)}(-H_1) \ddot{\xi}_r(t) + 2\ddot{y}(t) \quad (4.100)$$

Since Eq. 4.97 is already an uncoupled system, the numerical solution of each of the modal equations in Eq. 4.97 will be extremely simple and time-saving.

(2) Numerical Examples for a Nonviscous Elastic Layered System

The quadruple-layer system with nonviscous media will be analyzed to demonstrate the accuracy of the second model. To estimate the number S to be used, let the prescribed frequency range be from 0 to 60 rad/sec. According to Table 4.1, the number J defined in Eq. 4.98 is equal to 7, which implies S is equal to 8. With a maximum iterative error of 0.5% imposed, the fractions of critical damping for the first 8 modes were computed by the iteration process. The results shown in column (2) of Table 4.3 are those obtained after two iterations.

Shown in Fig. 4.22 are the approximate transfer function, $|\bar{H}_1(\omega)|$, computed from Eq. 4.82 and the exact transfer function, $|H_1(\omega)|$ or $AMP(\omega)$. Some deviations between the two solutions can be seen everywhere except at the natural frequencies where these two solutions were matched. A maximum deviation of 10% to 15% is seen at the valleys of the transfer functions. The value of α_N for the given layered system is equal to 0.506, and the accuracy of the foregoing approximate analysis is considered to be accept-

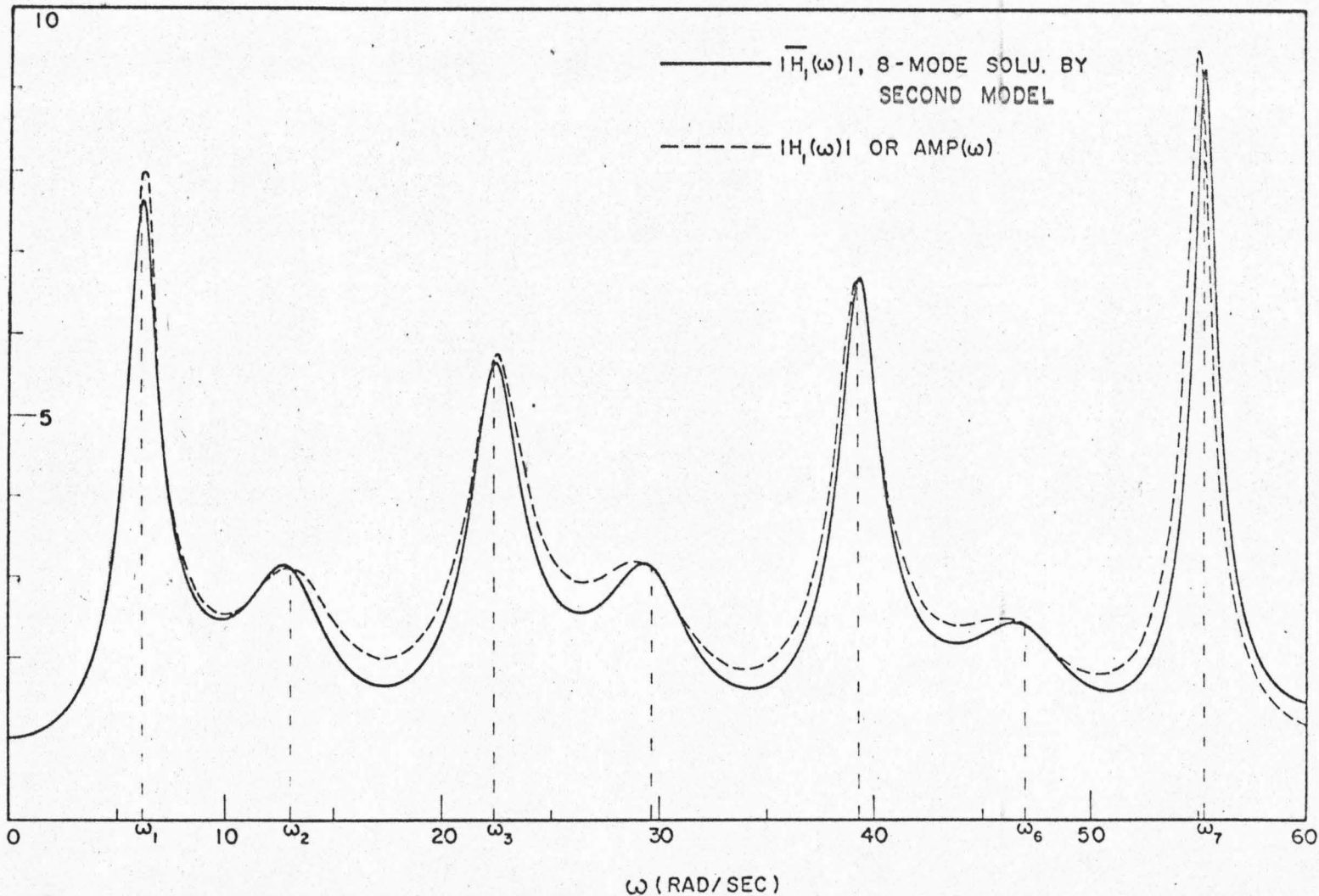


Fig. 4.22 AMPLITUDE TRANSFER FUNCTION OF THE NONVISCIOUS 4-LAYER SYSTEM

Table 4.3 MODAL DAMPINGS IN THE SECOND MODEL FOR THE
4-LAYER SYSTEM

(1) MODAL NO.	(2) NONVISCOUS SYSTEM	(3) VISCOELASTIC SYSTEM
r	β_r (%)	β_r (%)
1	10.753	11.366
2	14.525	15.466
3	4.875	6.956
4	6.811	9.182
5	2.178	5.993
6	5.359	9.154
7	0.876	5.850
8	1.589	14.272

able. For layered systems that have a smaller α_N the accuracy of the approximate analysis will be improved. Note that the accuracy of the approximate analysis would not increase appreciably even if a number S larger than that given by Eq. 4.98 is used. The reason for this is because the modal equations are uncoupled with each other and hence modal interaction is greatly reduced.

To calculate the surface response, the functions $(\dot{y})_a$ and $(\dot{y})_b$ that were used as velocity inputs for the first model are taken as the acceleration inputs $(\ddot{y})_a$ and $(\ddot{y})_b$ respectively. To solve each of the modal equations in Eq. 4.97 numerically, a subroutine developed by Nigam and Jennings⁽³²⁾ was adopted. This scheme is superior to the well known Runge-Kutta method in that it is much faster and more accurate. Besides, this scheme gives an exact solution if the input function varies linearly between consecutive data points. The modal responses obtained from Eq. 4.97

was substituted into Eq. 4.100 to produce the surface response $\ddot{u}_1(-H_1, t)$. The results computed by using $(\ddot{y})_a$ and $(\ddot{y})_b$ respectively as the input function are shown in Fig. 4.23, which are compared with the exact counterparts shown in Figs. 4.7(a) and 4.8(a). As a further comparison, the velocity spectra of the approximate surface responses are shown in Figs. 4.24. The comparison between the 8-mode approximate solutions and the exact counterparts indicates that the accuracy of the approximate analysis is acceptable. Also, it is found that the time required for computing the approximate surface response is about one half that required for computing the exact response by the ray-tracing scheme.

(3) Numerical Examples for a Viscoelastic Layered System

The quadruple-layer system composed of media described by the standard linear model will be analyzed. By imposing a maximum iterative error of 0.5% the iteration process produced the modal fractions of critical damping after four iterations. The modal dampings are listed in column (3) of Table 4.3. The 8-mode approximate solutions, $|\bar{H}_1(\omega)|$ and $\ddot{u}_1(-H_1, t)$, were both calculated by following the same procedures used previously for a nonviscous layered system. In Fig. 4.25 is shown $|\bar{H}_1(\omega)|$ together with the exact solution, $|H_1(\omega)|$. Comparing Fig. 4.25 with Fig. 4.22 shows that the accuracy of the approximate analysis for the viscous system is better than that involved in the analysis of the nonviscous system. The 8-mode surface responses with $(\ddot{y})_a$ and $(\ddot{y})_b$ as input functions are shown in Fig. 4.26. Finally, the velocity spectra of the surface responses were computed, and are shown in Figs. 4.27(a) and 4.27(b) respectively to compare with the corresponding spectra computed by the first model.

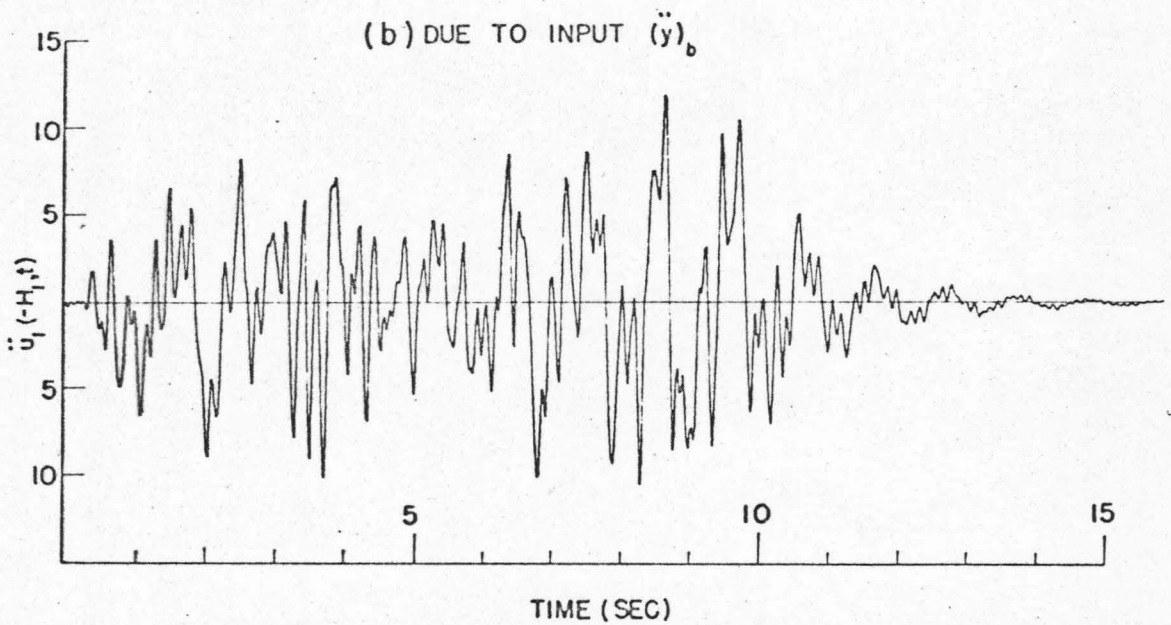
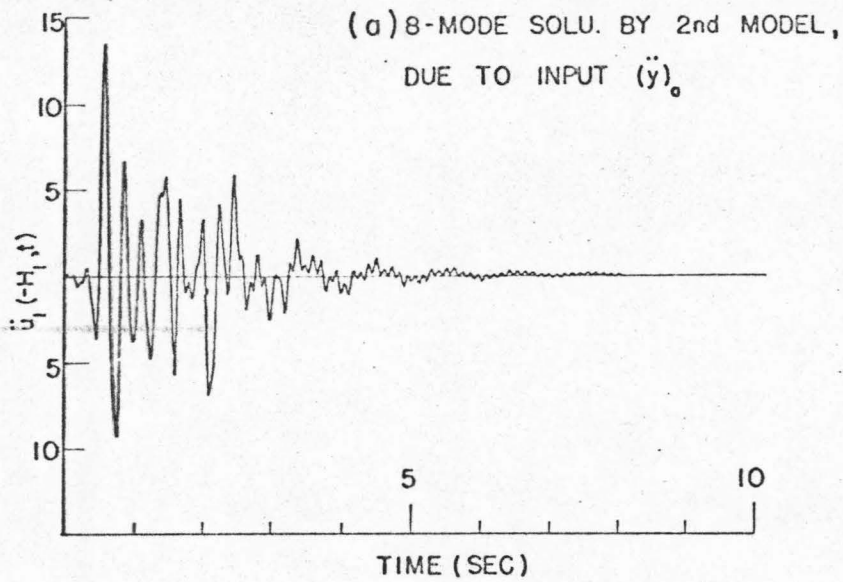


Fig. 4.23 SURFACE RESPONSE OF THE NONVISCIOUS 4-LAYER SYSTEM

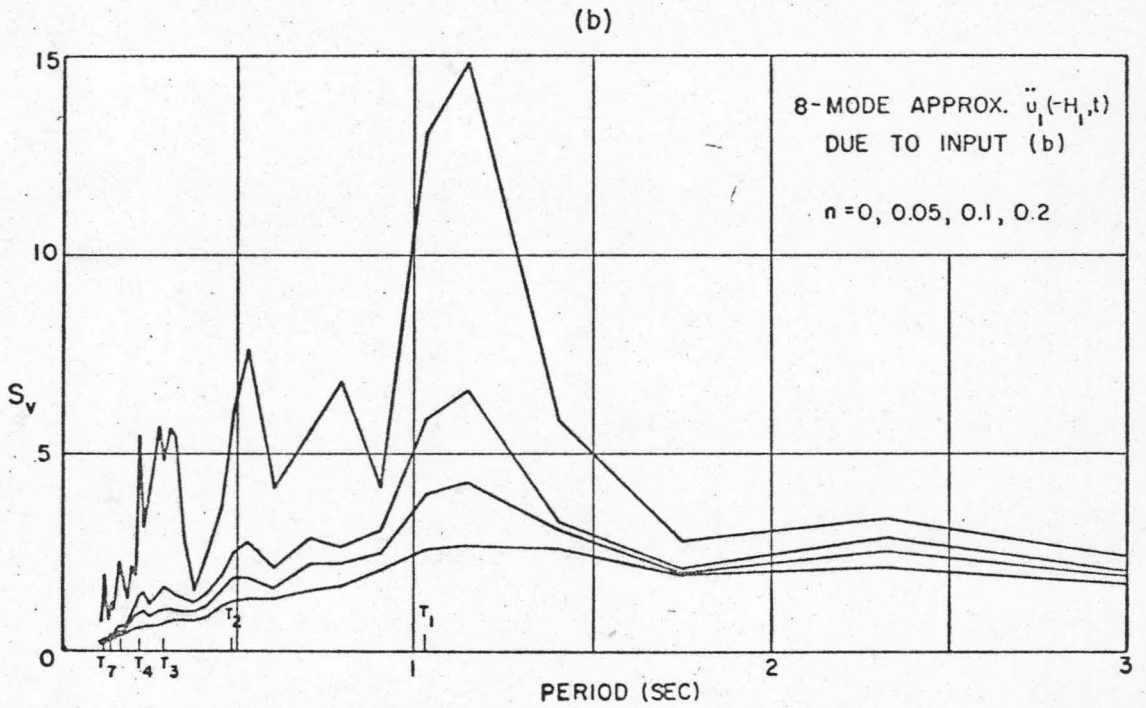
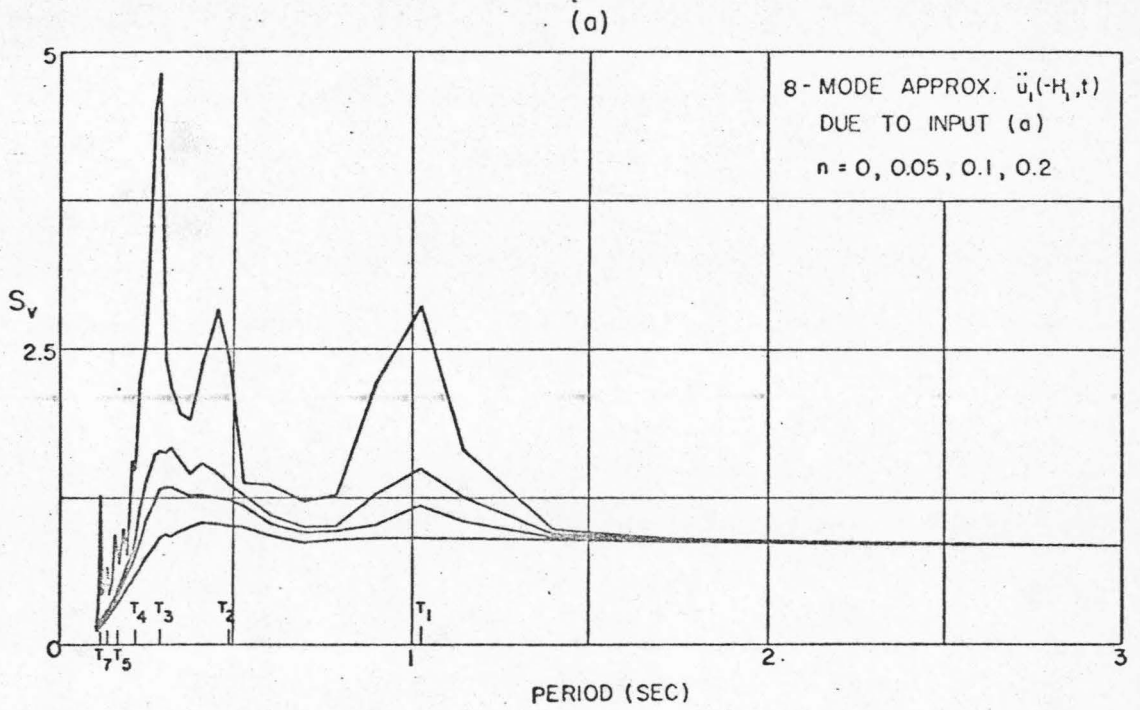


Fig. 4.24 OUTPUT VELOCITY SPECTRA OF THE NONVISCOUS
4-LAYER SYSTEM

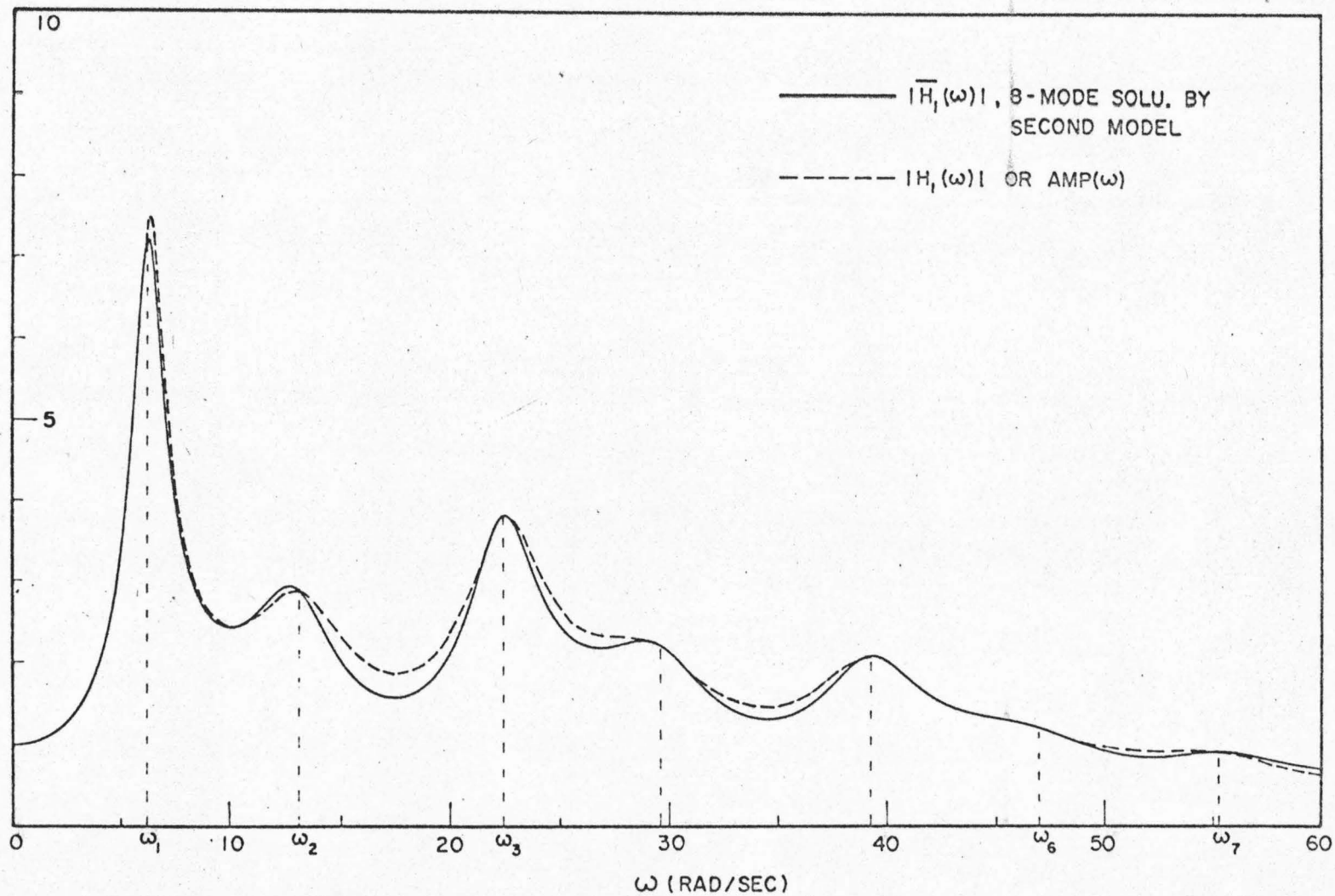


Fig. 4.25 AMPLITUDE TRANSFER FUNCTION OF THE VISCOUS 4-LAYER SYSTEM

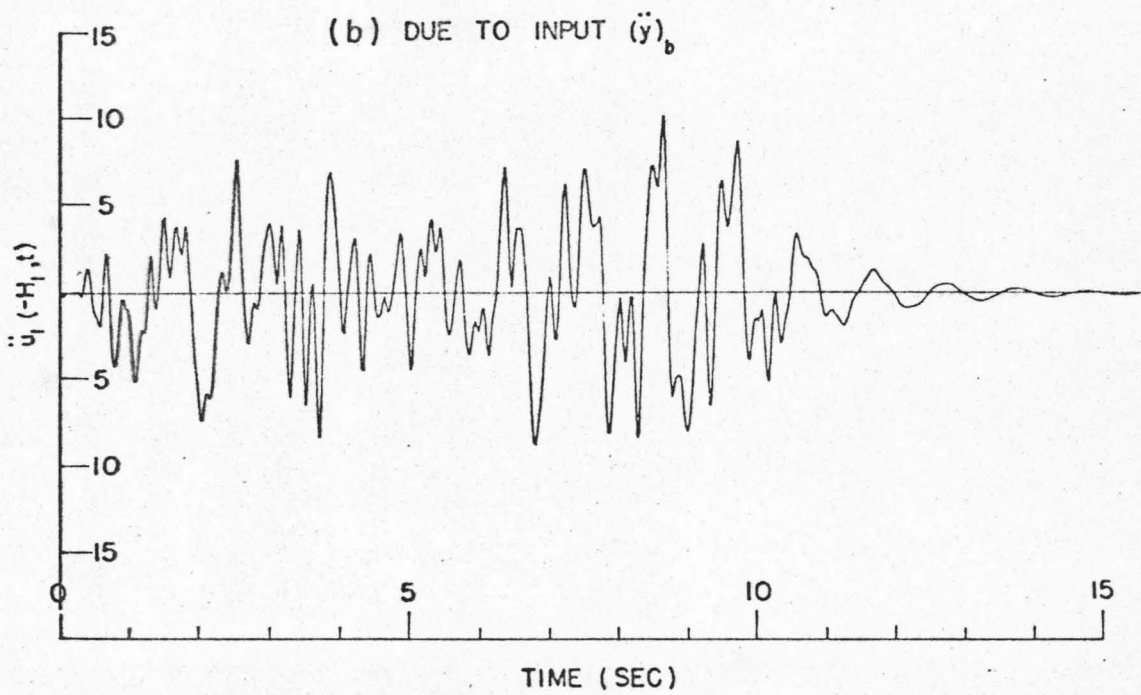
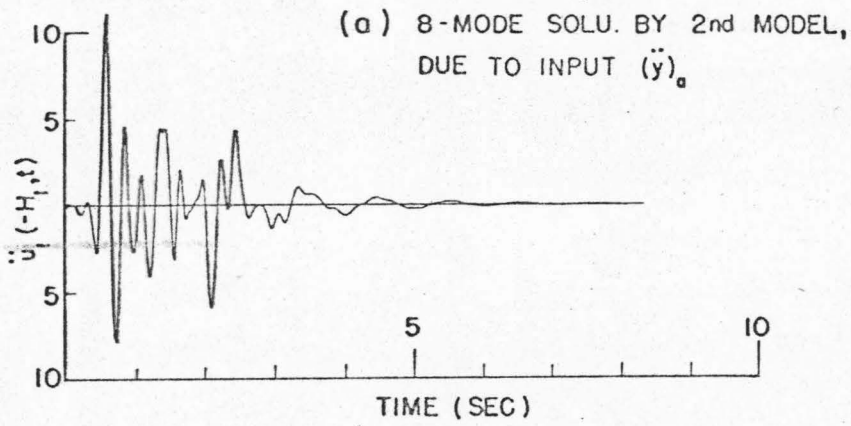
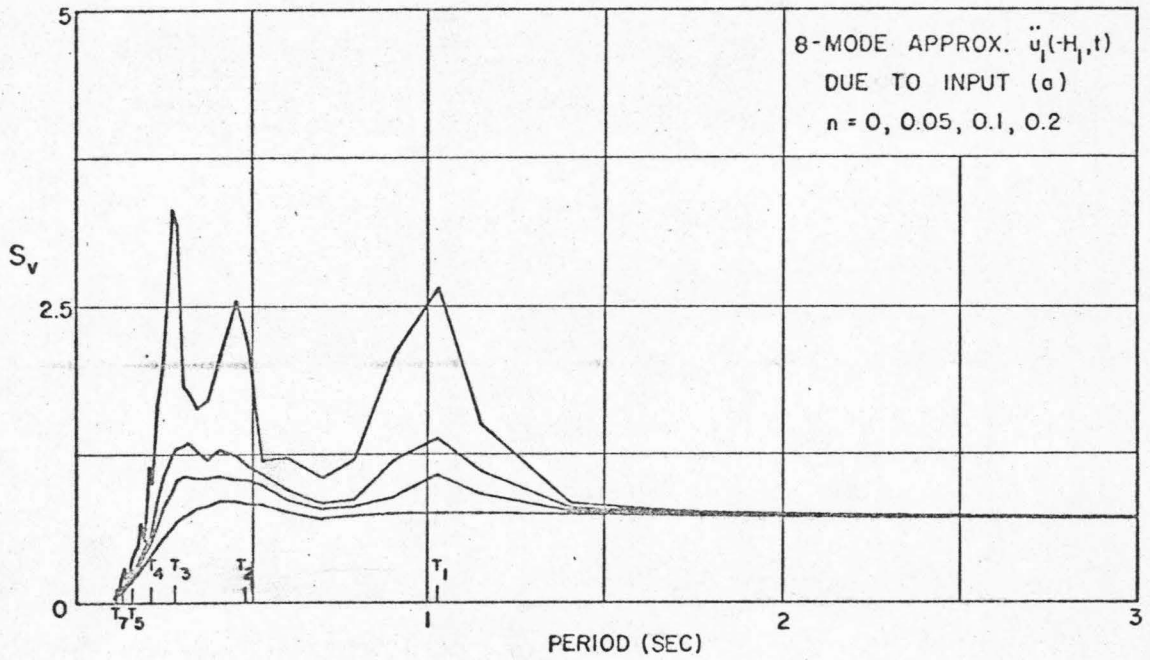


Fig. 4.26 SURFACE RESPONSE OF THE VISCOUS 4-LAYER SYSTEM

(a)



(b)

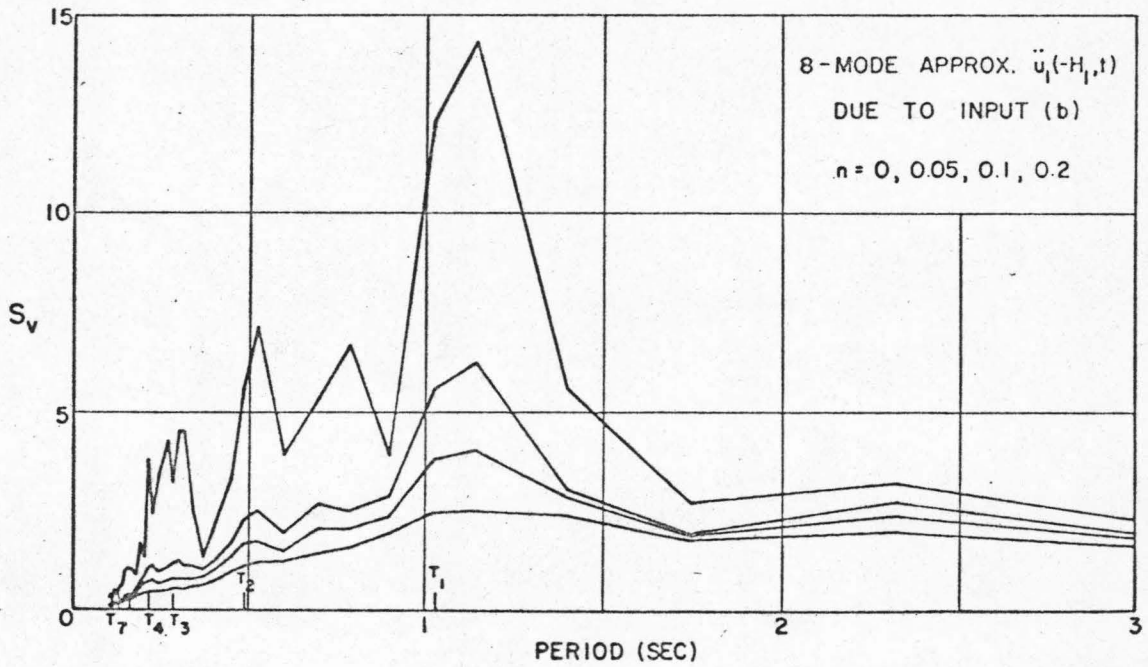


Fig. 4.27 OUTPUT VELOCITY SPECTRA OF THE VISCOUS 4-LAYER SYSTEM

E. Conclusions

Two modified shear beam models were presented for transient analysis of a given layered system. The method of continuous modal analysis was proposed to analyze the models. Numerical examples were given to demonstrate the applicability and the accuracy of both models. Some conclusions are drawn as follows.

(1) The approximate analysis for the first model can achieve any desired degree of accuracy, but considerable computing time is needed. Hence, this model is not recommended for transient analysis of a nonviscous layered system because either the ray-tracing technique or the second model is much more efficient. On the other hand, the numerical examples indicated that in computing the transient response of a nonviscous layered system the approximate analysis for the second model takes only about half the computing time required by the ray-tracing technique. For a viscous layered system the second model is again preferable because the ray-tracing technique is not applicable.

(2) The analysis of the second model is much simpler. But, this model is good only if the impedance ratio α_N is small enough and when only the response near the surface of the system is desired. Numerical computations suggested that, as a rule of thumb, for layered systems that have a value of α_N smaller than 0.5 the second model will be sufficiently accurate for practical interest.

(3) Both models are applicable to any linear viscous layered system of which the media need not be described by any of the linear viscoelastic models mentioned in Chapter II. The iteration process enables one to determine the model dampings

of a given layered system so long as the transfer function is known. Hence, the energy dissipation in the layers can simply be described by certain modal fractions of critical damping while description by any viscoelastic model could be extremely complicated.

(4) Both models can be extended to studying the analogous problem of structure-foundation interaction, with the foundation considered as a uniform half-space. Representation of the foundation by a lumped mass and a spring was used by Fleming et al⁽³³⁾, Lycan and Newmark⁽³⁴⁾, Thomson⁽³⁵⁾, etc., to study this problem. Such a simple representation is obviously insufficient. On the other hand, Kanai⁽²⁰⁾ idealized a building as a uniform shear beam and the foundation as a homogeneous half-space (a single-layer system). He reported good success in matching his theoretical computations with experimental results, which suggests that a correct representation of the foundation by a half-space is necessary for studying the problem of structure-foundation interaction.

(5) There are two sources that can produce a prominent hump in the output velocity spectra of a layered system. The first is associated with the frequency components of the input motion itself, and the second is associated with the large resonance of a certain mode of the layered system. The numerical examples suggested that, if a layered system is to produce a prominent hump in the output spectra, this hump should be observable in both the undamped and damped spectra.

V. APPLICATIONS

A. Introduction

The studies reported in the preceding chapter analyzed an idealized layered system subjected to vertically incident plane body waves. As pointed out in Chapter I, the idealized layered model is only a simplified approach for estimating approximately the influence of actual local geology on arriving seismic waves. Thus, the applicability of the theory depends on the extent that the properties of the local geology and the arriving seismic waves deviate from those of an idealized layered system. Possible deviations between the properties of local subsoils and those of an idealized layered system are given below.

(a) In general, actual subsoils are inhomogeneous and anisotropic. Small-scale or highly localized inhomogeneities can cause significant scattering of the arriving waves in an extremely complicated manner.

(b) During earthquakes of moderate or small intensities, the subsoils may behave linearly with very small damping. However, if the seismic waves produce sufficiently large deformation of the subsoils, the nonlinear, hysteretic behavior may have a significant influence.^(36, 37)

(c) The horizontal dimensions of local subsoils of practical interest are finite whereas an idealized layered model extends infinitely in both horizontal directions. Hence, the theory will be applicable only if the horizontal dimensions of the subsoils are large compared with the depth. Besides, the layer interfaces in actual subsoils are

neither ideally smooth nor necessarily horizontally oriented. Such geometric irregularities constitute another factor that can cause significant wave scattering and produce undesired seismic noise during earthquakes.

Besides the aforementioned deviations in the geological structures of local subsoils, it is also possible that the arriving seismic waves are far from being planar. As illustrated in Fig. 1.1, the ground motion recorded at a station during an earthquake is, in general, due to both body wave and surface wave arrivals, with the latter usually preceded by the former. The relative contribution of either type of waves depends on the epicentral distance and the focal depth of the earthquake considered. For deep-focus earthquakes, especially those with a sufficiently short epicentral distance, the body waves will be incident nearly vertically at the base of the subsoils. Moreover, the body wave arrivals can usually be distinguished clearly from the surface wave arrivals. Hence, the theory can be expected to apply satisfactorily to the body wave arrivals if the subsoils are well defined. For near shallow-focus destructive earthquakes, however, the nature of the seismic waves is much more complicated. In this case, the ground motion may be the result of waves arriving along different paths, and it appears that the response of the subsoils should be treated as a problem of two-dimensional wave propagation. For more distant shallow-focus earthquakes (50 to 100 miles), the seismic waves will approach the local subsoils essentially in the horizontal direction, and the response of the local subsoils can be estimated approximately by the theory only if the following wave length criterion is satisfied.

Let the profile of the subsoils be idealized as a rectangle with a horizontal dimension L and a depth H which is small compared with L , and let the incoming waves be approaching from the left. This is the situation shown in Fig. 5.1, in which λ is the wave length of a certain component of the incoming waves. If the half-wave length, $\lambda/2$, is comparable to or longer than the dimension L , as shown in Fig. 5.1(a), the whole layering will be shaken approximately in phase as if subjected to the excitation of vertically incident plane body waves. On the other hand, if $\lambda/2$ is shorter than L the motions of non-adjacent particles, as illustrated by Fig. 5.1(b), would be correlated so weakly with each other that resonant response of the whole layering as predicted by the theory is very unlikely.

In the case that the body waves are obliquely incident, Haskell's matrix method can be adopted.^(14, 15) Briefly speaking, Haskell's method deals with layering problems subjected to obliquely incident plane body waves, and the response of the layered system is computed in the frequency domain.

Subjected to all the previously mentioned limitations, the theory can reasonably be expected to estimate approximately the influence of well defined local subsoils upon longer-period seismic waves because, with longer wave length, the waves would be less sensitive to the inhomogeneities of the subsoils and the irregularities in the geometric configurations of the layer boundaries. Experimental examples demonstrating the sensitivity of wave length to the structural irregularities of local geology were given by Phinney⁽³⁸⁾ and Ellis and Basham.⁽³⁹⁾ Briefly speaking, the purpose of their experiments is to establish a

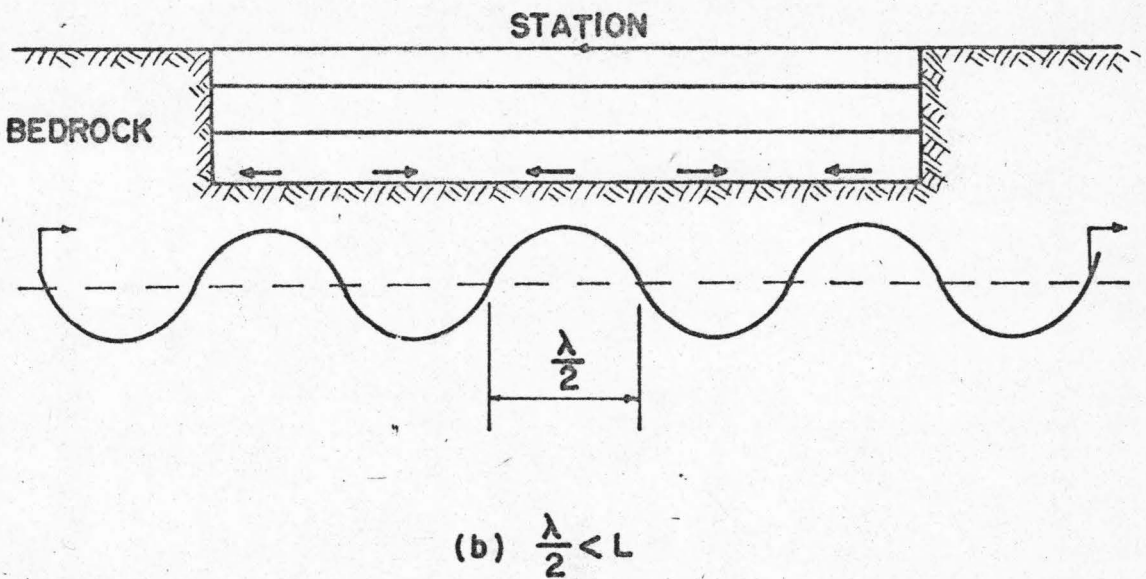
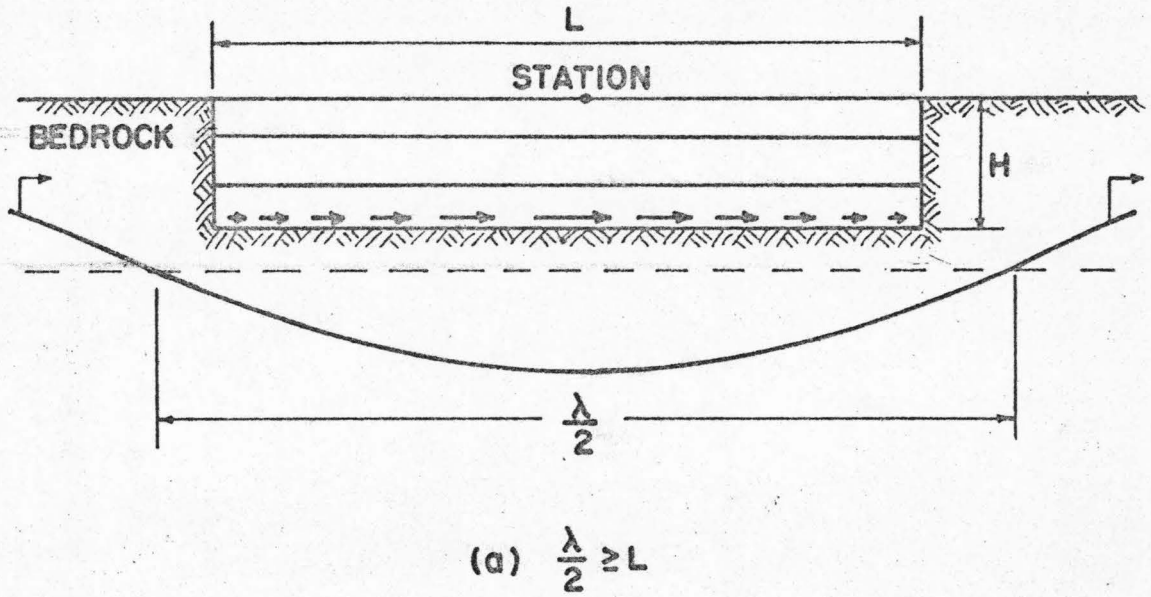


Fig. 5.1 RESPONSE OF IDEALIZED LOCAL GROUND LAYERS TO WAVE COMPONENTS ARRIVING HORIZONTALLY

theoretical layered model for the local earth's crust by analyzing the ground surface motions recorded due to the P-wave arrivals from a number of teleseismic events whose epicentral distances were sufficiently large to avoid the possible interference from surface wave arrivals. Since the authors were considering the crustal layers with a total thickness of approximately 10 kilometers, oblique incidence of the P-waves was assumed and Haskell's method was adopted for a theoretical analysis. The computed layered model was then compared with the local crust actually observed. Phinney carried out his experimental work at Albuquerque and Bermuda. Long-period P-waves within a frequency range of 0.02 to 0.2 cps were recorded at both sites for some distant earthquakes. From the recorded motions, theoretical layered models were computed for the earth's crust at both Albuquerque and Bermuda, and were found in good agreement with the actually observed crustal structures. On the other hand, Ellis and Basham performed their experiments on some deep horizontal sediments, about 5 kilometers thick, at central Alberta. Well-log data showed that these sediments are very well defined. Besides, the topography there is quite featureless. At four sites in central Alberta, short-period P-waves, ranging from 0.1 to 2.5 cps in frequency, were recorded from 34 teleseismic events. The recorded motions were analyzed to obtain the theoretical models. Only moderate success was achieved in matching the theoretical models with the actual geological structures. The difficulty mainly came from the scattering of the short-period waves in the crust and the upper mantle beneath the sediments. Such scattering was believed to be contributed by some apparent

inhomogeneities in the crust. Also, a dipping of the crustal boundary of approximately 15 degrees was required to explain an azimuth deviation observed in the experimental results. Ellis and Basham finally concluded that to interpret the geological structures at central Alberta by using Haskell's method as applied to short-period P-waves is not appropriate.

It should be pointed out that, even if the theory is applicable, the local subsoils need not produce any significant effect during an earthquake. To establish the condition under which significant resonance of the subsoils is likely to take place, let us first examine some examples of actually recorded earthquake events.

B. Examples

(1) The Borrego Mountain Earthquake of 9 April 1968 Recorded at San Onofre

The magnitude 6.5 Borrego Mountain earthquake of 9 April 1968 triggered 114 strong-motion seismographs operated by the Coast and Geodetic Survey in southern California and south - east Nevada.⁽⁴⁰⁾ One of the seismographs was installed at San Onofre. The epicenter was along the San Jacinto Fault Zone in southern California, and San Onofre is along the Pacific coast, approximately 85 miles to the west of the epicenter. Two separate shocks were recorded. The second trailed about 6 seconds behind the first. Both shocks apparently originated from very nearly the same source, and will hereafter be referred to as shock No. 1 and shock No. 2 respectively. For each

shock, horizontal accelerations in the $N33^{\circ}E$ and the $N57^{\circ}W$ directions were recorded. The acceleragrams are shown in Fig. 5.2, from which it is seen that shock No. 2 has larger amplitude and longer duration than shock No. 1.

Velocity spectra were computed for both shocks, and are shown in Figs. 5.3 and 5.4 for the $N57^{\circ}W$ components respectively. A comparison of the velocity spectra for the corresponding components indicates no similarity in the general spectral characteristics nor coincidence in the locations of the spectral peaks. Since both shocks originated from approximately the same epicenter, traveled along the same wave paths, and finally passed through the same local geology, the spectral difference must be associated with the difference in the source mechanism. Hence, we conclude that the local geology at San Onofre did not have appreciable resonance influence on the two shocks recorded. Two possible reasons are given below to explain the apparent suppression of the local geological effect. That is, either because the ground layers are not well defined and the nature of the arriving waves was so complicated that resonance of the ground according to the theory did not occur, or because the amplification spectrum of the ground layers is so flat that no prominent resonance would occur even if the ground layers behaved in accordance with the theory.

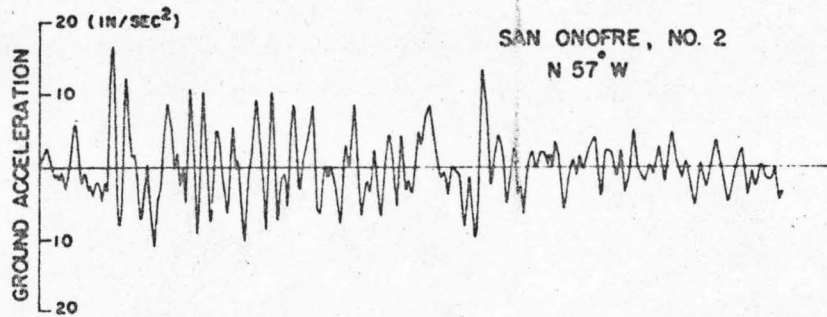
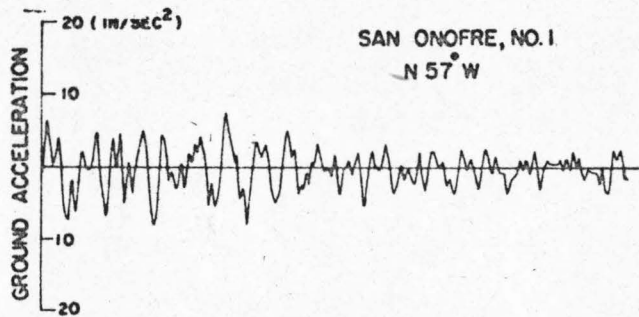
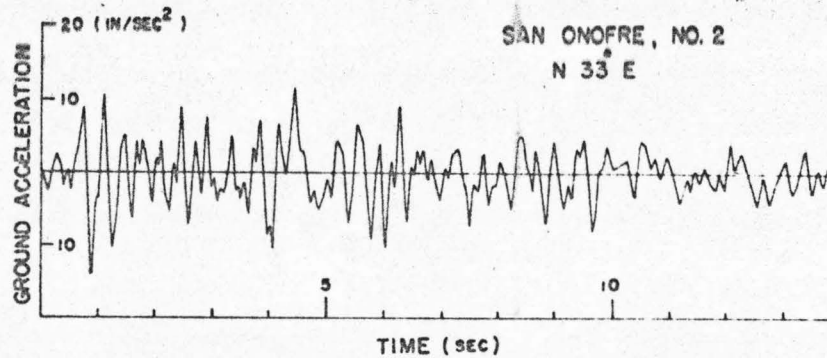
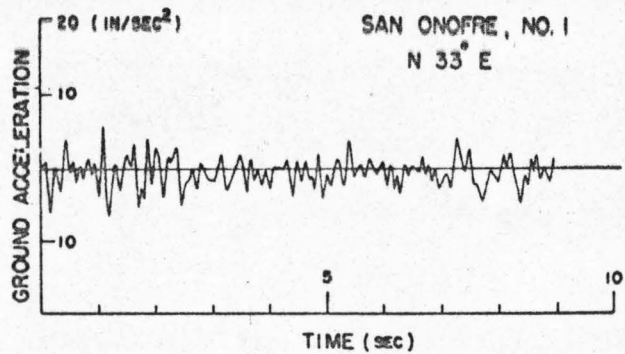


Fig. 5.2 THE TWO SHOCKS OF THE BORREGO MOUNTAIN EARTHQUAKE RECORDED AT SAN ONOFRE, 9 APRIL 1968

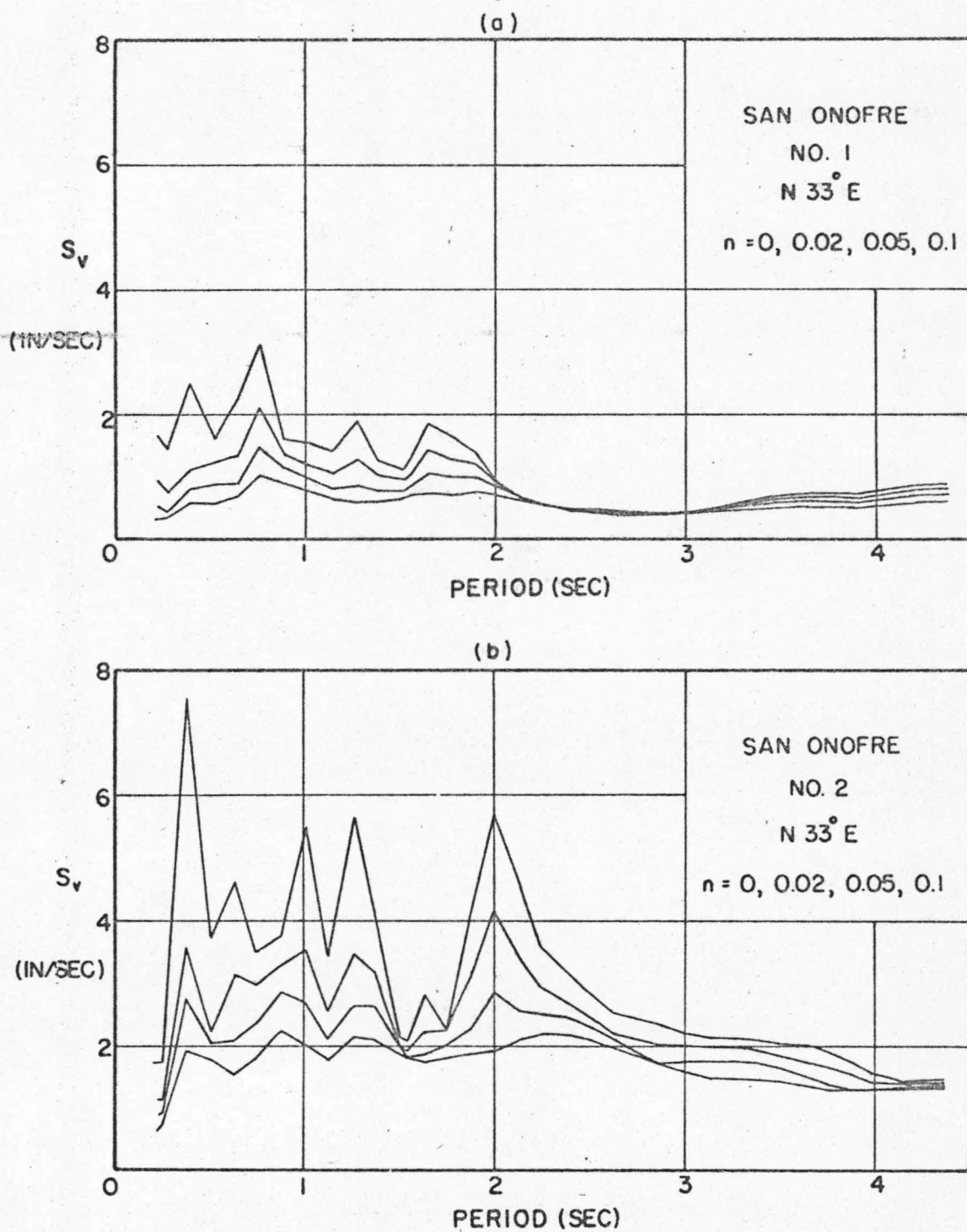


Fig. 5.3 VELOCITY SPECTRA FOR THE SAN ONOFRE SHOCKS
(N33° E)

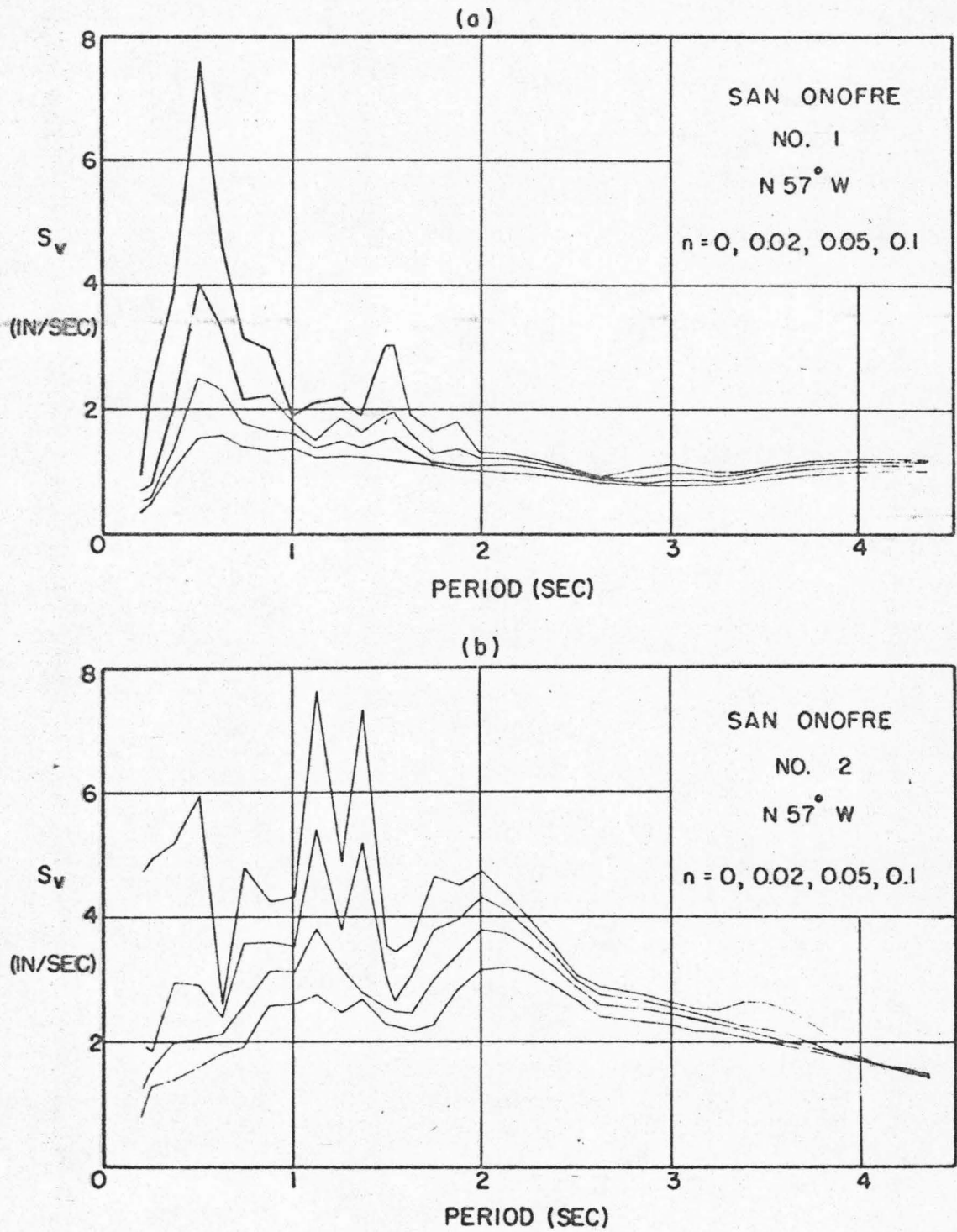


Fig. 5.4 VELOCITY SPECTRA FOR THE SAN ONOFRE SHOCKS
(N 57° W)

The foregoing example reveals that the local geology may not produce any significant effect on arriving seismic waves while the source mechanism, on the other hand, may play an important role in determining the general characteristics of the ground spectra.

(2) The Strong-Motion Earthquakes Recorded in Mexico City on
11 and 19 May 1962

For the strong-motion earthquake recorded at Mexico City, Mexico on 8 July 1957, Zeevaert ⁽⁴⁾ reported an observed dominant period of 2.5 seconds. Later in 1962 two strong-motion earthquakes of magnitude 7 to 7.25 were again recorded at Mexico City on 11 May and 19 May. Both events originated at a distance of approximately 150 miles from the city. For each event, records were obtained from two accelerometers, one installed in the basement of the 43-story Tower Latino Americana (T.L.A.), the other at the ground surface of the Alameda Park (A.P.) which is only two blocks from T.L.A. The accelerometers installed in the basement of T.L.A. was 26 feet below the ground surface.

During each earthquake, two horizontal components of the ground accelerations were recorded. Hence, a total of eight accelerograms were obtained, of which the velocity spectra have been computed by Jennings. ⁽⁴¹⁾ Four of the velocity spectra are shown in Figs. 5.5 and 5.6. A prominent hump located around the period of 2.5 seconds appears in all of the spectra. Such unusual phenomenon could not have been due to any structure-foundation interaction for the ground motions

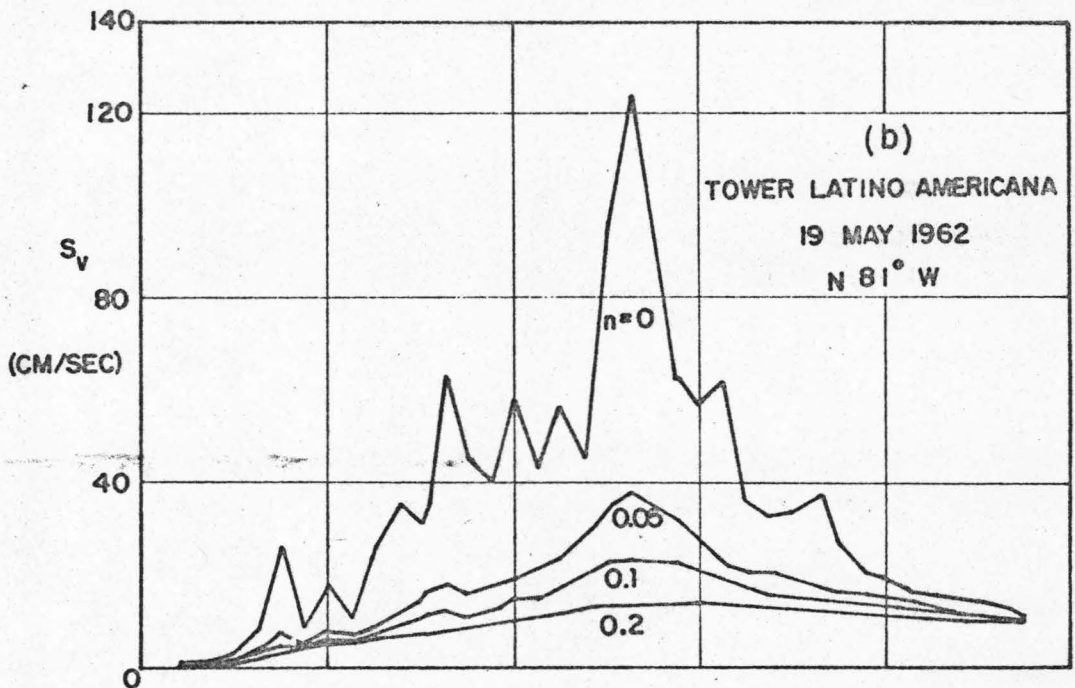
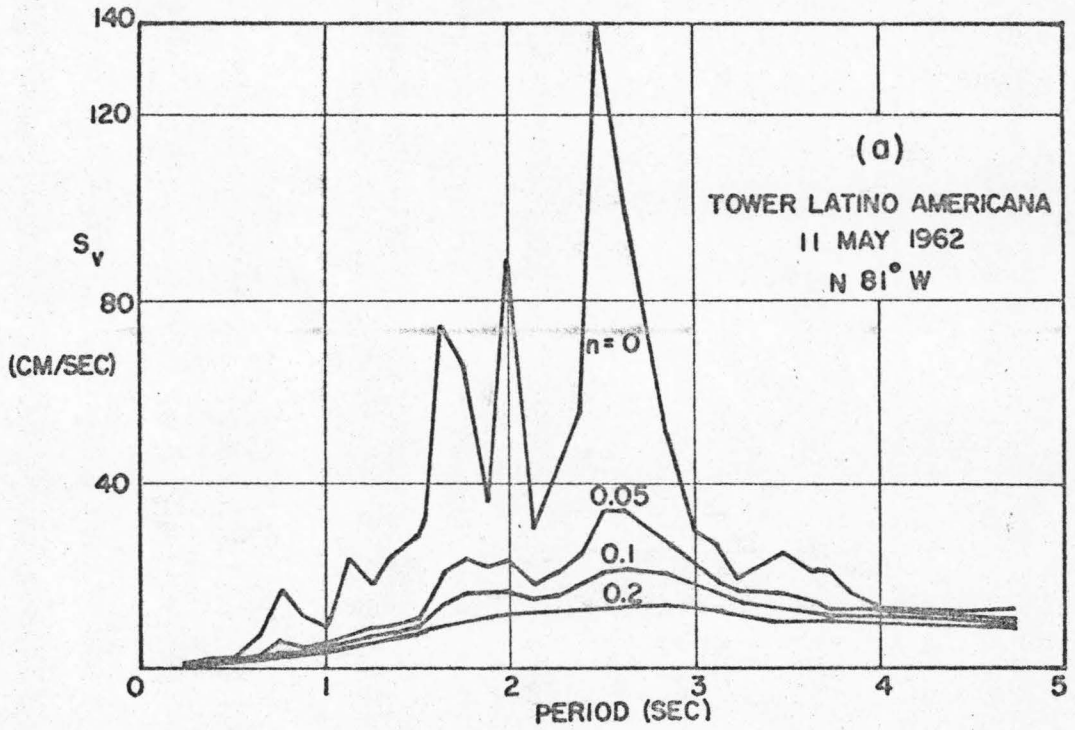


Fig. 5.5 VELOCITY SPECTRA FOR THE TOWER LATINO AMERICANA
N81° W COMPONENT

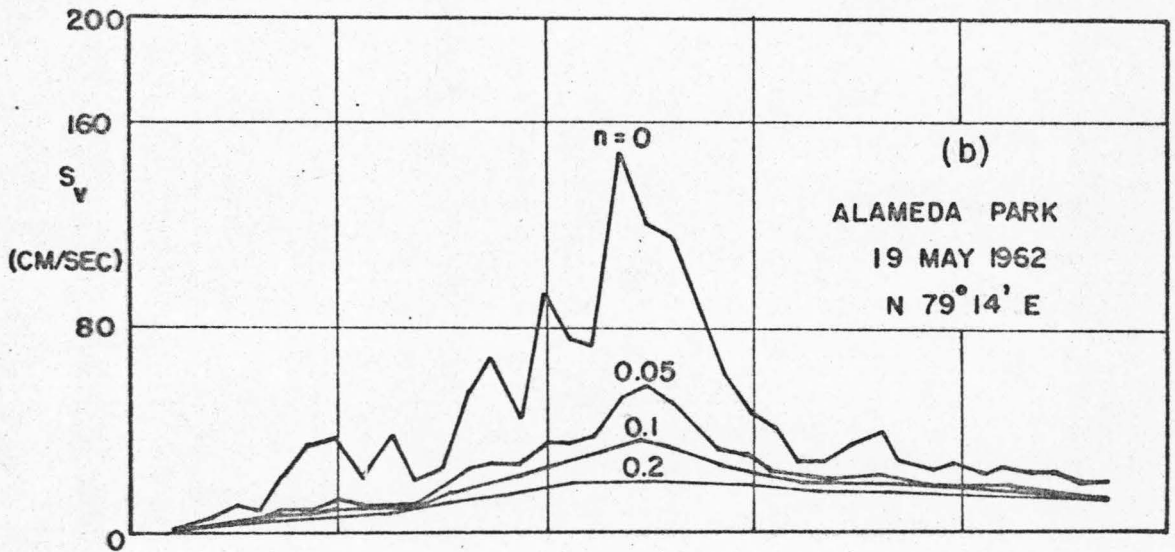
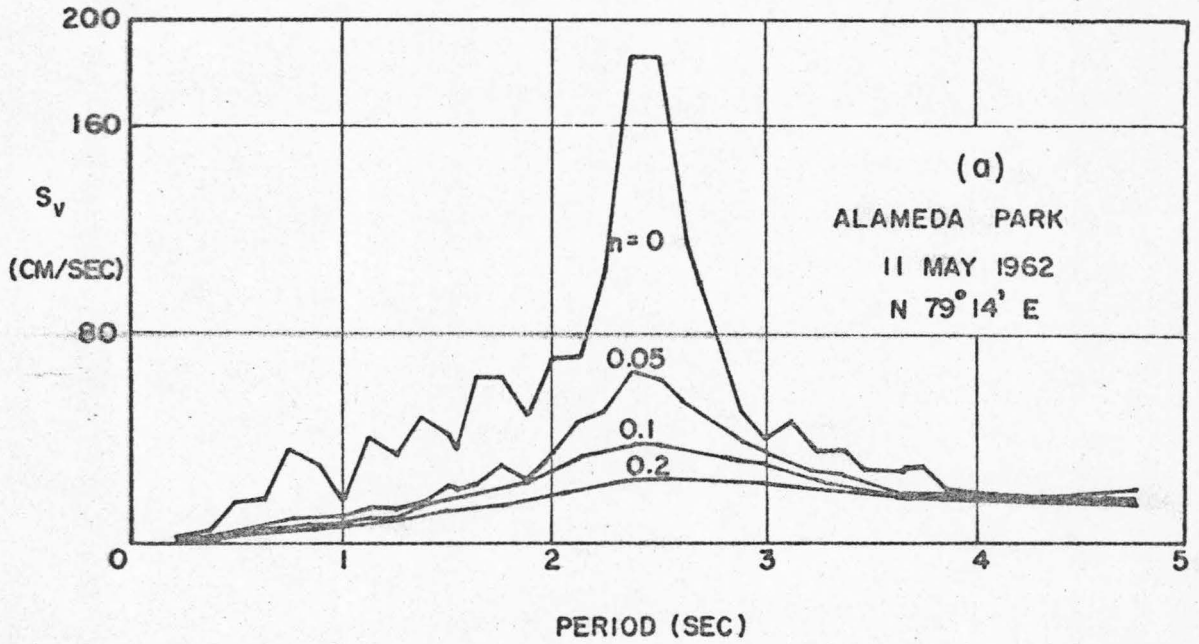


Fig. 5.6 VELOCITY SPECTRA FOR THE ALAMEDA PARK
N79° 14' E COMPONENT

recorded at the T.L.A. site because the A.P. records revealed similar spectral characteristics yet the A.P. site is not adjacent to any building. Doubtlessly, the dominant period observed in the ground motions was associated with the mechanical behavior of some unusual subsoil layers underneath Mexico City.

The central part of Mexico City is located at the west side of the lake bed of the ancient Pleistocene Lake which occupied the basin of the Valley of Mexico. The basin is primarily composed of soft alluvium and lacustrine sediments. At both sites in Mexico City, the first 100 to 150 feet of subsoils are layers of very soft clay with an average water content of 170% up to 300% and a shear wave velocity of 150 to 500 ft/sec. For both earthquakes, the amplitude of the ground motions recorded at the A.P. site was consistently twice as large as that of the motions recorded at the T.L.A. site. By using a shear beam model as an analog for the soft clay deposits, Zeevaert ⁽¹⁾ was able to confirm the foregoing amplitude ratio through mode shape analysis of the shear beam model. In addition, he concluded that the predominant period of 2.5 seconds observed in the ground motions was the fundamental natural period of the clay layers. Zeevaert's analysis suggested that during both earthquake events the clay deposits as a whole were undergoing oscillation essentially in the fundamental mode, which implies that interpretation of the mechanical behavior of the clay deposits at Mexico City by the theory is appropriate. This can be attributed to the following physical observation. Let surface waves be the dominant type of wave arriving at both sites in Mexico City during both earthquakes, as is the situation shown in Fig. 5.1. Suppose that

the waves approach at a velocity of 2 miles/sec. Then, the half-wave length of a component of the incoming waves having a period of 2.5 seconds will be

$$\frac{\lambda}{2} = \frac{1}{2} (2.5 \times 2) = 2.5 \text{ miles}$$

which is very long compared to the depth of the clay layers. Hence, as indicated in Fig. 5.1(a), the response of the first mode can be expected to be relatively large.

A numerical example is given in the following to demonstrate the predominant response of the first mode as indicated by the theory. As a very crude approximation, assume that the mechanical behavior of the clay layers can be represented by those of the first two modes of a single-layer system which has a fundamental natural period of 2.5 seconds. For a single-layer system, the second period is one third of the fundamental one. Therefore,

$$T_1 = 2.5 \text{ sec} \quad \text{and} \quad T_2 = 0.833 \text{ sec}$$

or

$$\omega_1 = 2.51 \text{ rad/sec} \quad \text{and} \quad \omega_2 = 7.53 \text{ rad/sec}$$

Also, it can be shown that the modal participating factors for computing the surface response of the model are

$$D_1^{(1)} = 4/\pi = 1.2732$$

and

$$D_2^{(1)} = -D_1^{(1)}/3 = -0.4244$$

The second shear beam model proposed in Chapter IV was adopted for the theoretical analysis. For simplicity, the following values were

used for the modal fractions of critical damping.

$$\beta_1 = \beta_2 = 5\%$$

The modal responses, $\ddot{\xi}_r(t)$, were computed from Eq. 4.97, in which the artificial earthquake sample No. 2' processed by Jennings ⁽⁴²⁾ has been taken as the input function $\ddot{y}(t)$. Thus, the theoretical ground surface motion is given approximately by Eq. 4.99 as

$$\ddot{u}_1(-H_1, t) = \sum_{r=1}^2 D_r^{(1)} \ddot{\xi}_r(t) + 2\ddot{y}(t) \quad (5.1)$$

Both the input $\ddot{y}(t)$ and the response $\ddot{u}_1(-H_1, t)$ are shown in Fig. 5.7. It can be seen that the high frequency components of the input motion have been suppressed while the low frequency components around the period of 2.5 seconds are predominant. This frequency-selective property is more clearly indicated by the output velocity spectra which, together with the input spectra, are shown in Fig. 5.8. The general characteristics of the output spectra closely resemble those of the spectra shown in Figs. 5.5 and 5.6 although an extremely simplified model has been used in the theoretical analysis.

The last example indicates that, due to the favorable subsoil conditions at Mexico City, during an earthquake the first mode and, probably, the second mode of the subsoils are likely to be excited, provided that the duration of the earthquake is sufficiently long when compared with the fundamental period. In addition, the output velocity spectra have a predictable hump around the period of 2.5 seconds, which depends very little on the detailed characteristics of the input motion. By using statistical techniques, Herrera et al ⁽²¹⁾ have also

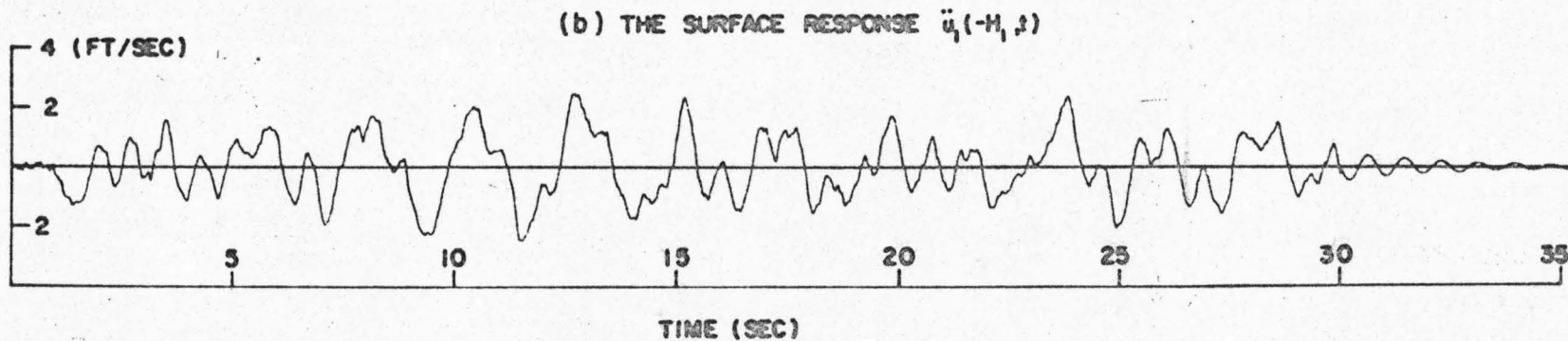
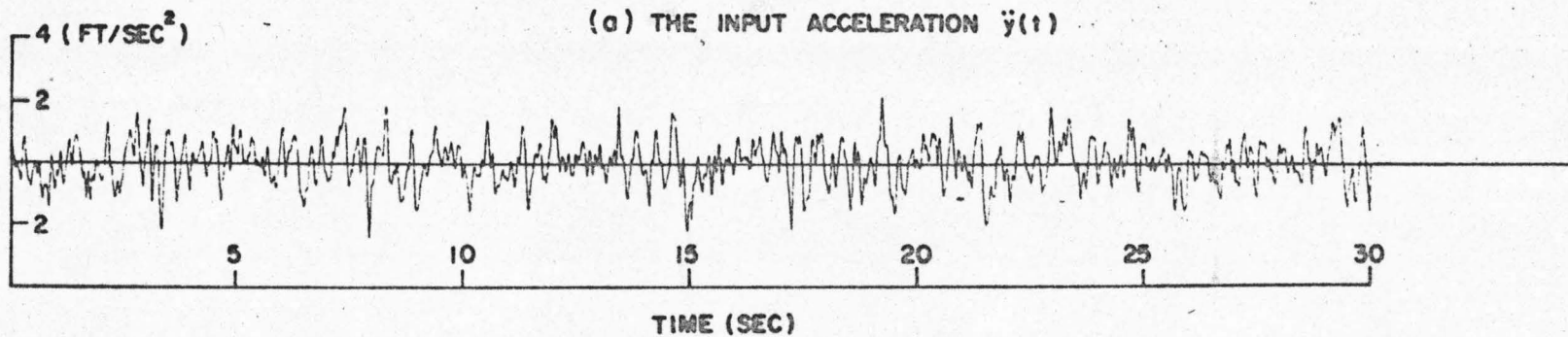


Fig. 5.7 INPUT AND OUTPUT OF THE IDEALIZED MODEL FOR THE SUBSOILS AT MEXICO CITY

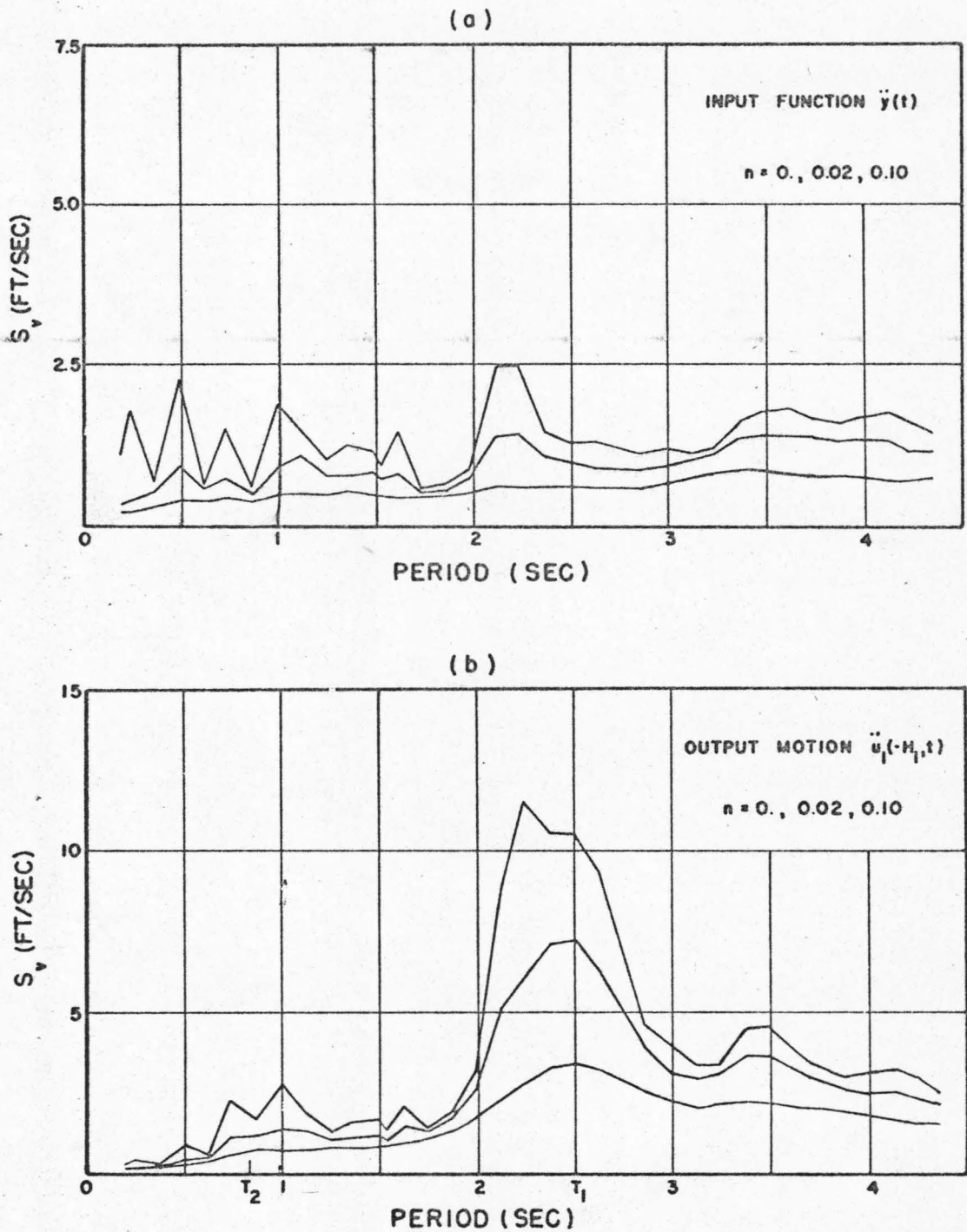


Fig. 5.8 INPUT AND OUTPUT VELOCITY SPECTRA OF THE IDEALIZED LAYERED MODEL FOR THE SUBSOILS AT MEXICO CITY

achieved considerable success in predicting the general characteristics of the velocity spectra for future earthquakes recorded in Mexico City.

(3) The Natural Tremor Recorded at Union Bay, Seattle on 6 March 1967

For the purpose of collecting earthquake data essential to the development of rational seismic design for the planned six-lane R. H. Thomson Expressway Crossing at Union Bay, Seattle, a series of seismograph stations were installed during 1965. The Principal Seismograph System installed at one of these stations consists of three down-hole installations in the bottom of the bay. Details of the layout can be found in Ref. 43 concerning the installation of these instruments. In Fig. 5.9 is a reproduction from Ref. 43 of the geological profile around the Principal Seismograph System in the north-south direction. According to Fig. 5.9, a layer of brown, very soft fibrous peat under the water extends 55 feet into the ground to meet a clay layer about 45 feet thick and containing gray, very soft to soft silty clay. Underneath the clay layer is the till which contains gray, very dense sand and gravel. The three seismometers were installed at different elevations, one in the peat (-8'), one in the clay (-59'), and one in the till (-103'). As far as the total thickness of the peat and clay is concerned, the subsoil conditions are considered well defined because this thickness is small compared with any wave length of practical interest.

Experimental data on the properties of the subsoils at Union Bay were provided by the Shannon & Wilson, Inc., and some of them are listed in Table 5.1. The data for the dynamic modulus of elasticity,

CLAY TILL
O
PEAT

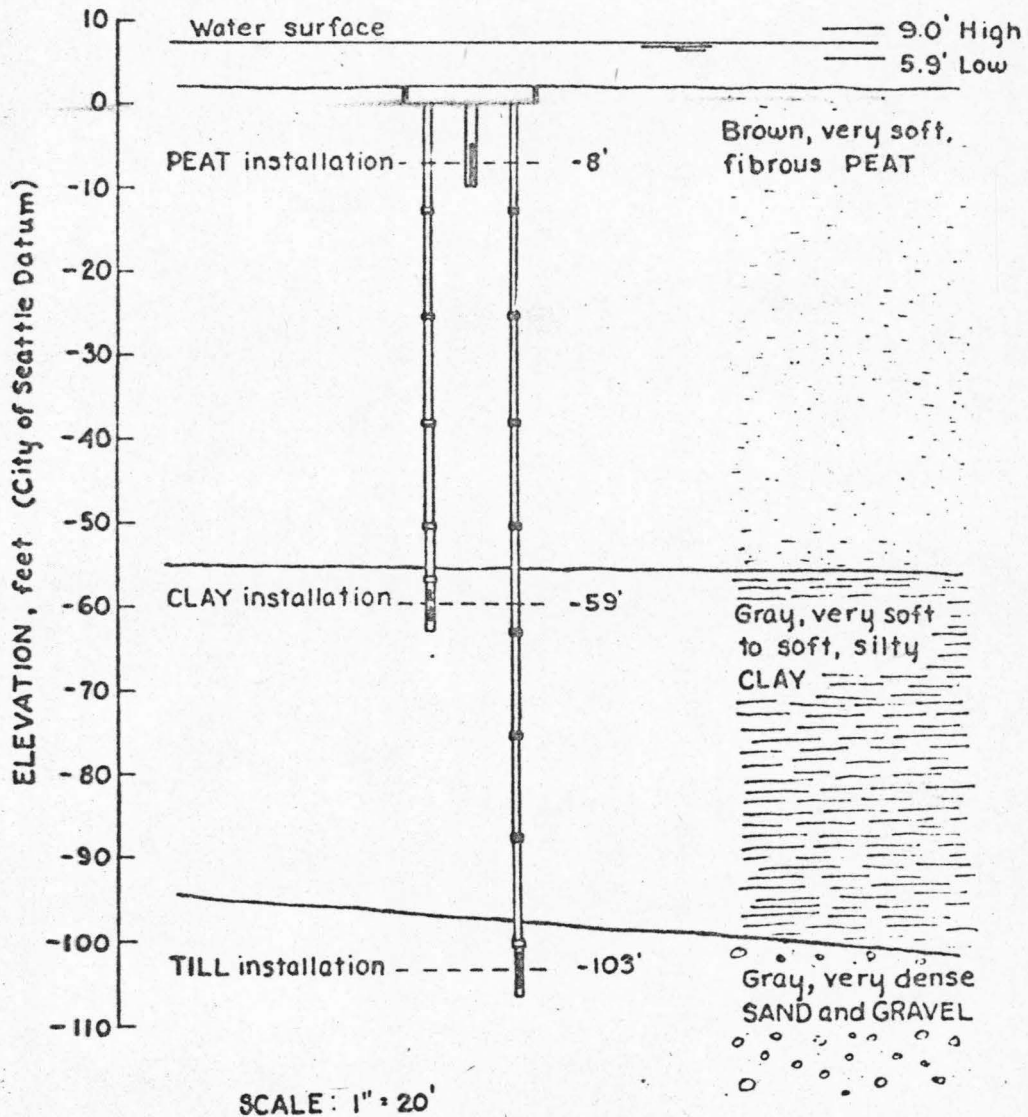
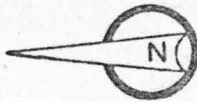


Fig. 5.9 PRINCIPAL SYSTEM PROFILE THROUGH THE SEISMOMETER STATION AT UNION BAY

TABLE 5.1

EXPERIMENTAL DATA FOR SUBSOILS AT THE
PRINCIPAL SEISMOGRAPH STATION, UNION BAY

MEDIUM	AVE. UNIT WT. (pcf)	COMPRESSIONAL WAVE VELOCITY c_p (fps)	DYNAMIC MODULUS OF ELASTICITY E(psi)	MOISTURE CONTENT %
Peat	63.7	500	300 to 800	600 to 1500
Soft Clay	100.			
Med. Clay	110.	3000 to 3600	3000 to 10000	40 to 80
Stiff Clay	128.			
Till	135. up	4600 to 7300	Not Available	10 to 25

E, are those obtained from repetitive loading tests on soil samples under confined pressure to simulate the in situ conditions of the soils.

On March 6, 1967 a natural tremor was recorded at Union Bay by the three downhole seismometers. The tremor lasted for about 16 seconds, with a maximum horizontal acceleration of 0.0075g observed in the clay records. The epicenter was located at 47.6°N and 122.8°W , about 37 kilometers to the west of the station. The focal depth was estimated to be approximately 35 kilometers and was comparable to the epicentral distance. This situation favors the application of the theory because a nearly vertical incidence of the body waves during the tremor can be expected.

Three components of the ground acceleration were recorded by each of the downhole seismometers. They are, respectively, the up-down component, the NS component, and the EW component. We will consider only the horizontal components, of which the traces were provided by the Worthington Christiani Fenco, a Joint Venture, and are reproduced in Figs. 5.10 and 5.11 for the NS and the EW component respectively. The horizontal accelerograms were digitized at the Earthquake Engineering Research Laboratory of the California Institute of Technology at a time interval of 1/80 seconds. A technique of parabolic correction ⁽⁴⁴⁾ was applied to adjust the base line of each of the digitized accelerograms.

A layered model is to be established for theoretical interpretation of the horizontal ground motions recorded. The parameters of the model will be chosen in such a way that the transfer function will match as close as possible the transfer function computed from

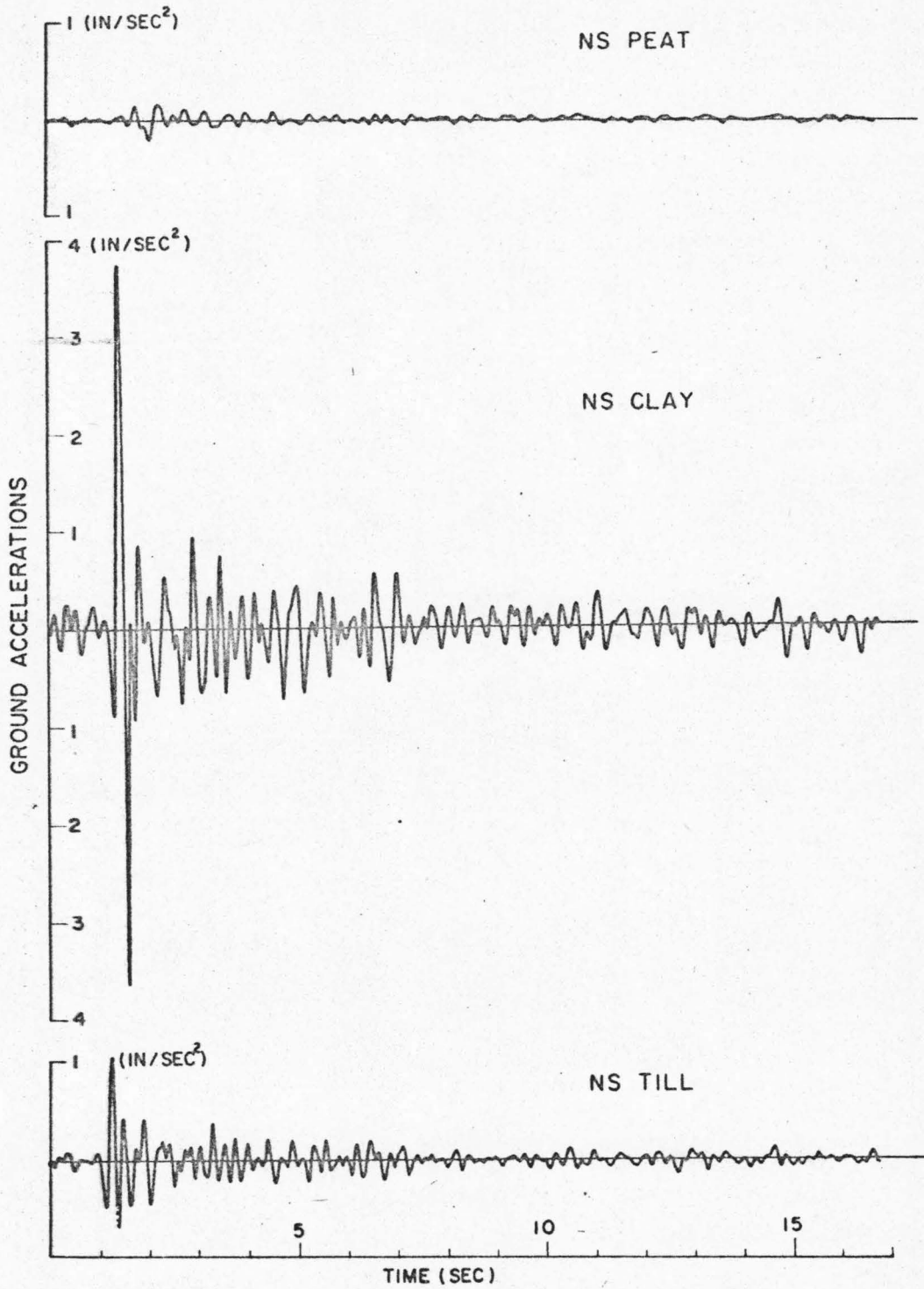


Fig. 5.10 THE NATURAL TREMOR RECORDED AT UNION BAY

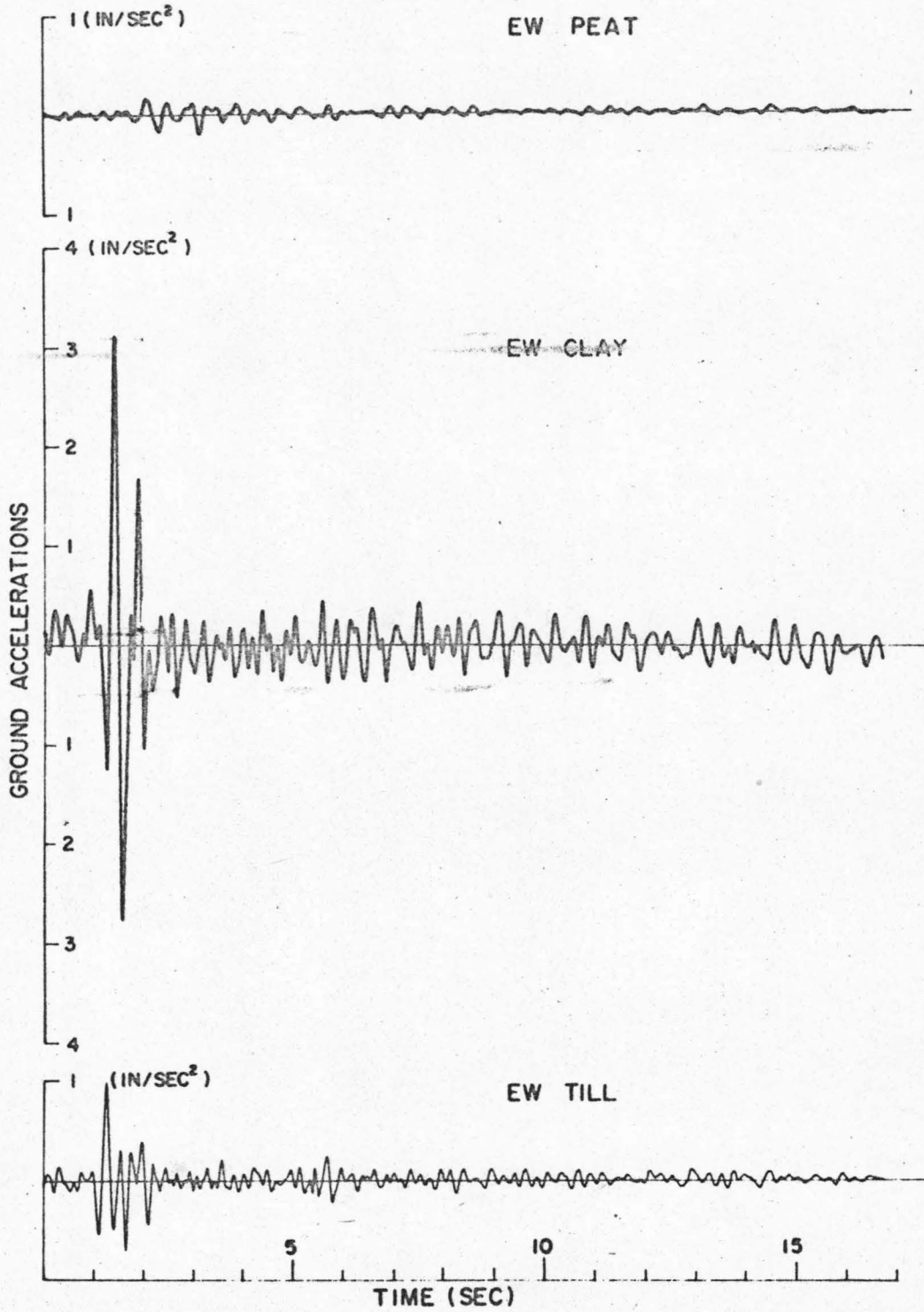


Fig. 5.11 THE NATURAL TREMOR RECORDED AT UNION BAY

the records. For purposes of simplification, the recorded horizontal accelerations were assumed to be contributed purely by SH-waves (horizontally polarized S-waves) although motions of other types of waves may have made some secondary contributions. As a further simplification, the peat layer is neglected in the analysis, and only the clay and the till layers will be taken into consideration. Physically, with the unusually high water content indicated by Table 5.1, the peat media would behave essentially like a viscous fluid and can hardly sustain shear wave motions. This observation is confirmed by the small amplitude of the ground motion recorded in the peat (see Figs. 5.10 and 5.11) and, therefore, justifies the omitting the peat layer in the approximate analysis that follows.

To obtain the transfer function of the actual subsoils, the amplitude spectra of the recorded motions must be calculated. The Fourier amplitude spectra, $|F(\omega)|_0$, were computed for the first 10 seconds of the clay accelerograms (at the elevation of -59 ft.) and the till accelerograms (at the elevation of -103 ft.) at a frequency interval of 0.1 rad/sec, where $|F(\omega)|_0$ is the modulus of the Fourier transform defined in Eq. 3.2. To reduce the highly oscillatory nature of $|F(\omega)|_0$, a smoothing process was applied. The "Hanning" process used by Brady⁽⁴⁵⁾ was adopted. Let the smoothed spectrum be $|F(\omega)|$. Then, the i^{th} interior point of $|F(\omega)|$ is given by

$$|F(\omega_i)| = \frac{1}{4} \left[|F(\omega_{i-1})|_0 + 2|F(\omega_i)|_0 + |F(\omega_{i+1})|_0 \right] \quad (5.2)$$

for $i = 2, 3, \dots, n-1$ if there are totally n data points in $|F(\omega)|_0$. For the exterior points,

$$|F(\omega_1)| = \frac{1}{2} \left[|F(\omega_1)|_0 + |F(\omega_2)|_0 \right]$$

and

(5.3)

$$|F(\omega_n)| = \frac{1}{2} \left[|F(\omega_{n-1})|_0 + |F(\omega_n)|_0 \right]$$

This smoothing process leaves the area under the spectrum curve unaltered, and hence the energy of the ground motion at a particular frequency is simply redistributed among the adjacent frequencies without altering the value of the total energy. In Fig. 5.12(a) to Fig. 5.12(d) are shown the smoothed Fourier amplitude spectra for the NS clay, the NS till, the EW clay, and the EW till accelerogram respectively.

By definition, the transfer function between the motion at the elevation of -59 ft. and that at -103 ft. is given by

$$|H(\omega)|_0 = \frac{|F(\omega)|_{\text{clay}}}{|F(\omega)|_{\text{till}}} \quad (5.4)$$

The results computed for both horizontal components are shown in Fig. 5.13. For purpose of better visualization, the computed transfer functions were further smoothed by hand to give the functions $|H(\omega)|$ shown in Fig. 5.14. In Fig. 5.14, the transfer function for the NS direction is indicated by the solid curve, and that for the EW direction by the dashed curve. Note that the high peaks below the frequency of 5 rad/sec in $|H(\omega)|_0$ have been omitted in the smoothed transfer functions. As will be seen later, any reasonable layered model for the subsoils without the peat layer would not have a transfer function with resonant peaks located below 5 rad/sec. It is possible that these low frequency amplifications might result from mechanical

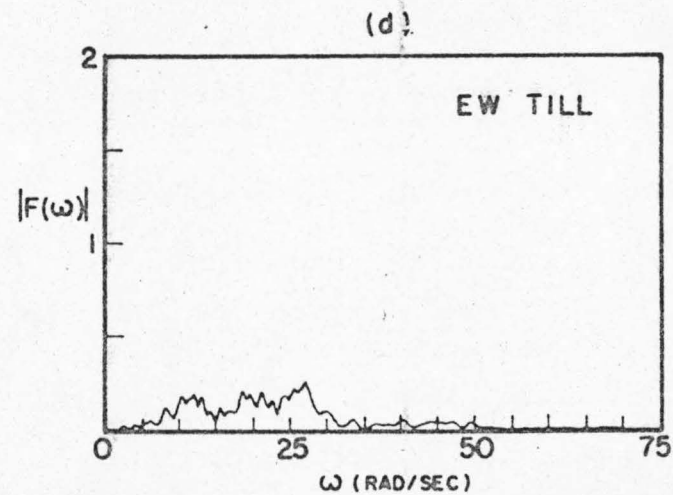
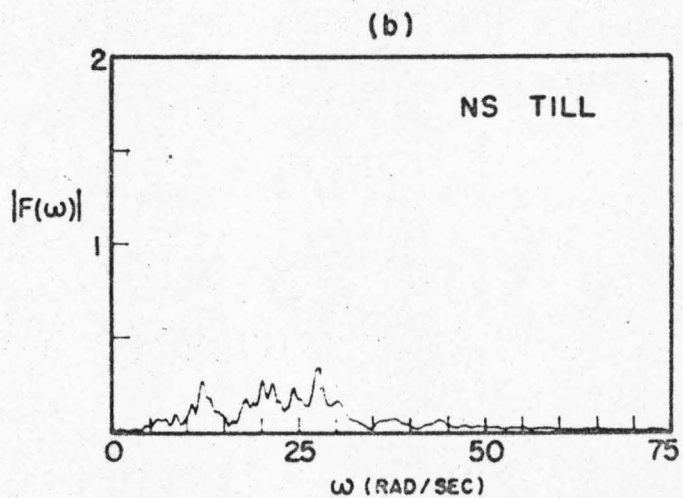
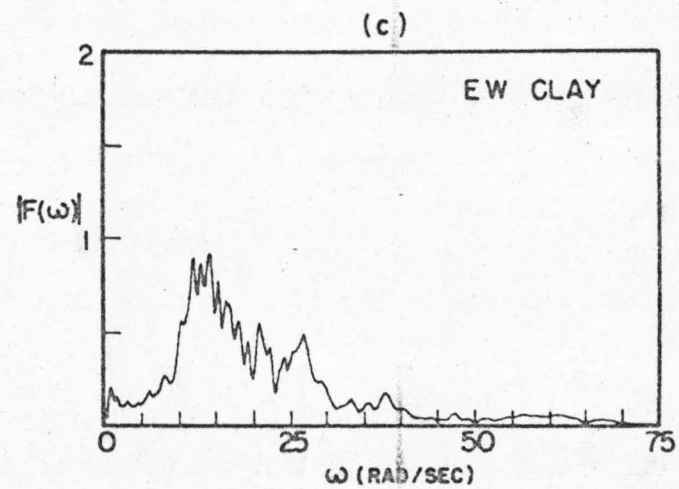
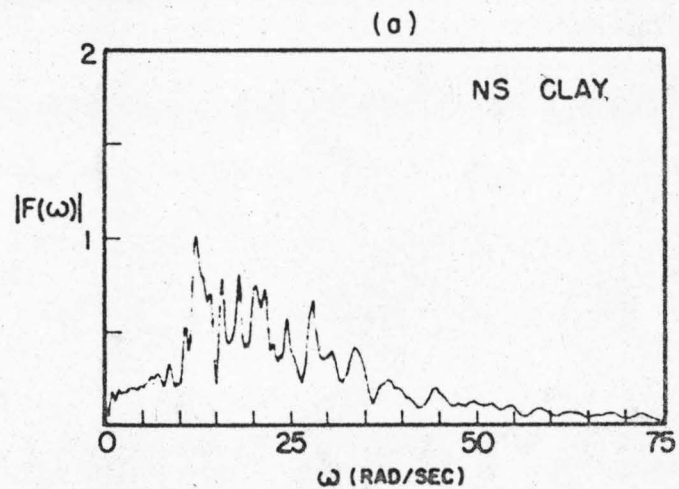


Fig. 5.12 SMOOTHED FOURIER AMPLITUDE SPECTRA OF THE CLAY AND TILL ACCELEROGRAMS RECORDED AT UNION BAY

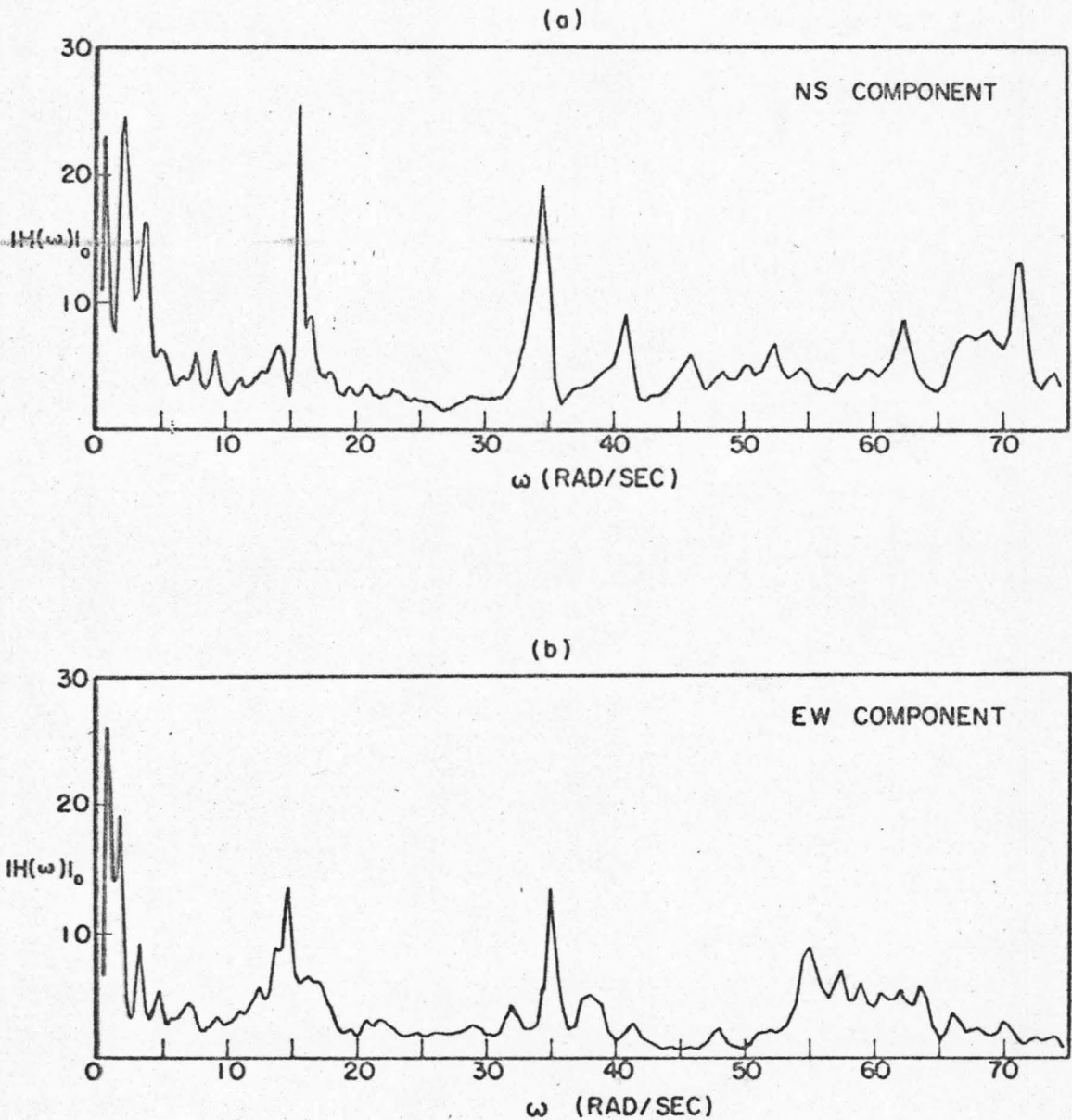


Fig. 5.13 TRANSFER FUNCTIONS FOR UNION BAY SUBSOILS COMPUTED FROM SMOOTHED FOURIER SPECTRA OF THE CLAY AND TILL RECORDS

error of the instruments or from some unknown geological feature.

Fig. 5.14 indicates that the smoothed transfer functions are very well defined in the range of frequencies from 10 to 40 rad/sec, with two prominent peaks located around 15 and 35 rad/sec. The small discrepancy between the NS and the EW transfer functions in the peak locations and the peak heights might be associated with anisotropy of the subsoil. The sloped clay-till interface shown in Fig. 5.9 could also have contributed to this discrepancy. The transfer functions outside the frequency range from 10 to 40 rad/sec are anomalous. Such anomalies could in part be contributed by scattering of the higher frequency components of the incident waves. The fact that the horizontal motions were not purely associated with SH-wave motions is another factor that could cause the anomalies.

In the following, a layered model is to be established in such a way that its transfer function will match the well defined portion of $|H(\omega)|$ as close as possible. Since data on the S-wave velocity, c_s , are not available from Table 5.1, they will be estimated by making use of the measured data for the P-wave velocity, c_p , and the dynamic modulus of elasticity, E . The well known expressions for c_p and c_s are, respectively,

$$c_p = \sqrt{\frac{\lambda + 2\mu}{\rho}} \quad \text{and} \quad c_s = \sqrt{\frac{\mu}{\rho}} \quad (5.5)$$

where ρ is density, and λ and μ are the Lamé's constants of elasticity. Let ν be the Poisson's ratio. Then, by making use of the fact that

$$\mu = \frac{E}{2(1+\nu)} \quad \text{and} \quad \lambda + 2\mu = \frac{E(1-\nu)}{(1+\nu)(1-2\nu)}, \quad (5.6)$$

we can deduce from Eq. 5.5 that

$$c_p = \sqrt{\frac{E}{\rho}} \cdot \sqrt{\frac{1-\nu}{(1+\nu)(1-2\nu)}} \quad (5.7)$$

and

$$\frac{c_p}{c_s} = \sqrt{\frac{2(1-\nu)}{1-2\nu}} \quad (5.8)$$

Define the following ratio

$$Q = \frac{c_p}{\sqrt{E/\rho}} \quad (5.9)$$

From Table 5.1, use the following averaged data for the clay:

$$\begin{aligned} \rho &= 110 \text{ lb/ft}^3, \\ c_p &= 3000 \text{ ft/sec}, \\ E &= 3000 \text{ to } 10000 \text{ psi}, \end{aligned}$$

and the ratio Q can be computed as

$$Q = 8.43 \sim 4.62$$

Substituting Eq. 5.9 into Eq. 5.7 gives the equation for the Poisson's ratio as

$$2\nu^2 + \left(1 - \frac{1}{Q^2}\right)(\nu-1) = 0 \quad (5.10)$$

Hence, ν can be obtained by solving Eq. 5.10, and the result is

$$\nu = 0.492 \sim 0.498,$$

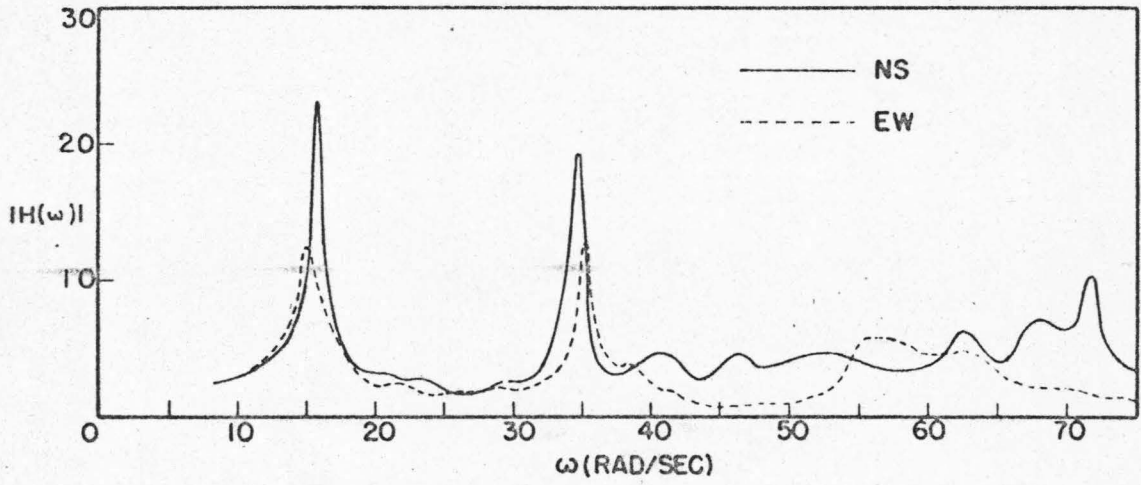


Fig. 5.14 RECORDED TRANSFER FUNCTIONS (SMOOTHED)

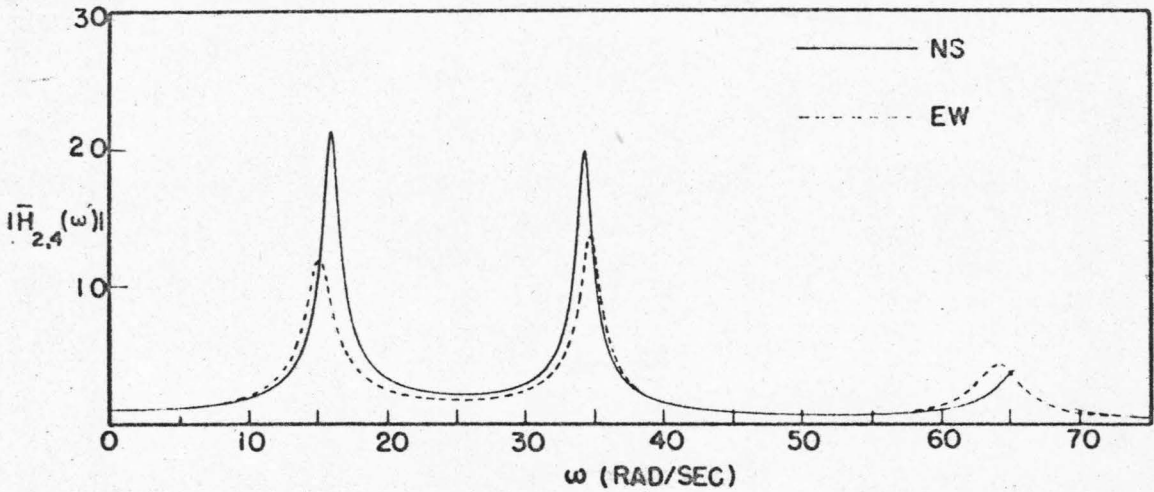


Fig. 5.15 THEORETICAL TRANSFER FUNCTIONS

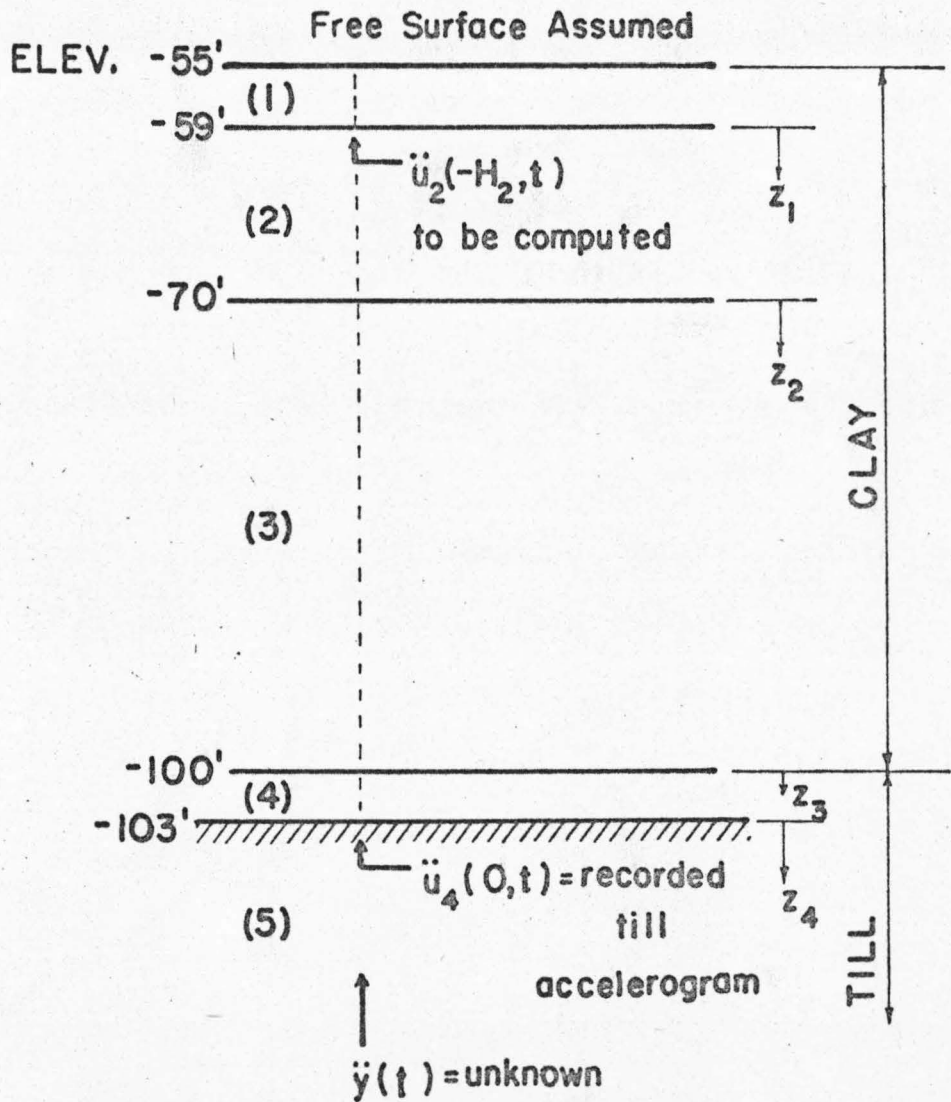
which, from Eq. 5.8, gives

$$\frac{c_p}{c_s} = 8 \sim 16$$

for the clay. This range of velocity ratio is reasonable when compared with the in situ measured ratio of 15 obtained by Rosenblueth et al ⁽²¹⁾ for the clay deposits at Mexico City and the ratio of 5 by Sax and Hartenberger ⁽⁴⁶⁾ for a certain alluvium or weathered zones on earth's surface. Therefore, the estimated value for c_s in the clay at Union Bay is

$$c_s = 200 \sim 450 \text{ ft/sec.}$$

After several trials, the quadruple-layer system shown in Fig. 5.16 was adopted for the theoretical analysis. In order to match both components of the actual transfer function shown in Fig. 5.14, two sets of S-wave velocities, slightly different from each other, were used in the model. In the layered model, the motions $\ddot{u}_2(-H_2, t)$ and $\ddot{u}_4(0, t)$ are, according to Fig. 5.16, the theoretical counterparts of the clay and till accelerograms recorded. Since the input function $\ddot{y}(t)$ is not available, the first 10 seconds of the till accelerogram were taken as the base motion $\ddot{u}_4(0, t)$, from which $\ddot{u}_2(-H_2, t)$ was computed to compare with the clay accelerogram. In Chapter IV, it has already been proved that if the base motion is known the motion anywhere inside the layered system can be computed without knowing the input function $\ddot{y}(t)$ and the parameters of the foundation. In this case, either the first or the second shear beam model established in Chapter IV



PARAMETERS OF THE LAYER MODEL (N=4)

LAYER NO.	THICKNESS H_i (ft)	UNIT WT. ρ_i (pcf)	S-WAVE VELOCITY c_j (ft/sec)	
			NS	EW
(1)	4	100	230	250
(2)	11	105	230	250
(3)	30	115	495	450
(4)	3	130	1500	1500
(5)	∞			

174

Fig. 5.16 THEORETICAL MODEL FOR UNION BAY SUBSOILS

will give the same result for the approximate transfer function, $|\bar{H}_{2,4}(\omega)|$, between the motions $\ddot{u}(-H_2, t)$ and $\ddot{u}_4(0, t)$. Let us adopt the first model.

First of all, the natural frequencies of the layered system were obtained by solving Eq. 2.35 numerically, and the results for the first three modes are listed in Table 5.2. Next, the modal participating factors, $D_r^{(2)}(-H_2)$, were computed from Eq. 4.43. Besides, the limited heights of the resonant peaks in the transfer function $|H(\omega)|$ suggest that some viscous damping should be included in the layers. The method of continuous modal analysis enables us to introduce the viscous damping in terms of certain modal fractions of critical damping, β_r . The values of β_r were so chosen that the 3-mode transfer function, $|\bar{H}_{2,4}(\omega)|$, would match the actual transfer function, $|H(\omega)|$, as close as possible. The formula for computing $|\bar{H}_{2,4}(\omega)|$ can easily be derived from Eq. 4.82 as

$$|\bar{H}_{2,4}(\omega)| = \sqrt{\left(1 + \sum_{r=1}^3 D_r^{(2)} X_r \cos \theta_r\right)^2 + \left(\sum_{r=1}^3 D_r^{(2)} X_r \sin \theta_r\right)^2} \quad (5.11)$$

The values of β_r thus determined for both the NS and EW components are given in Table 5.2, and the 3-mode transfer functions for both components are shown in Fig. 5.15 to compare with $|H(\omega)|$. The comparison indicates good agreement in the frequency range from 10 to 40 rad/sec, especially for the EW component. Hence, the proposed layered model is considered acceptable.

The modal responses, $\ddot{\xi}_r(t)$, were computed from Eq. 4.97, in which the input function $2\ddot{y}(t)$ is simply equal to $\ddot{u}_4(0, t)$. Hence,

TABLE 5.2

NATURAL FREQUENCIES, MODAL PARTICIPATING FACTORS,
AND MODAL DAMPINGS OF THE MODEL FOR UNION BAY

MODAL NO.	(NS)			(EW)		
	ω_r	$D_r^{(2)}(-H_2)$	β_r	ω_r	$D_r^{(2)}(-H_2)$	β_r
	r	(rad/sec)	%	(rad/sec)		%
1	15.813	1.4914	3.5	15.035	1.4333	6.0
2	34.187	-0.6003	1.5	34.698	-0.5513	1.5
3	65.468	0.1608	2.0	64.224	0.1811	2.0

the response $\ddot{u}_2(-H_2, t)$ can be computed by the following formula which was derived from Eq. 4.100

$$\ddot{u}_2(-H_2, t) = \sum_{r=1}^3 D_r^{(2)} \ddot{\xi}_r(t) + \ddot{u}_4(0, t). \quad (5.12)$$

The results for both the NS and the EW component are shown in Figs. 5.17 and 5.18 respectively. In either figure, the corresponding recorded component is also shown for comparison, and the regions in which good agreement is observed are indicated by the arrowheads. Better agreement was achieved in the EW component, which can be expected from the comparison previously made for the transfer functions.

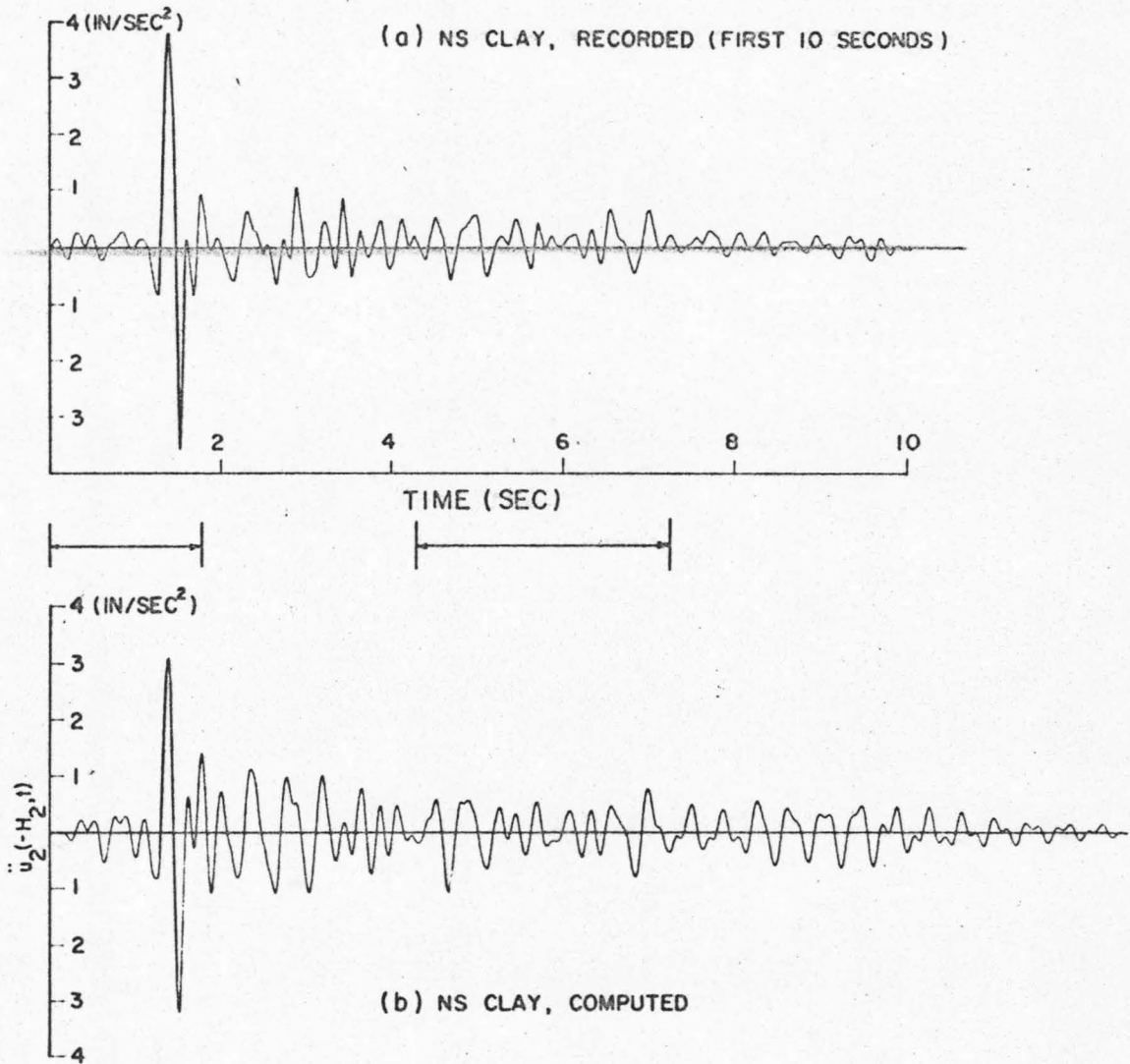


Fig. 5.17 RECORDED AND COMPUTED ACCELEROGRAMS
IN CLAY (NS)

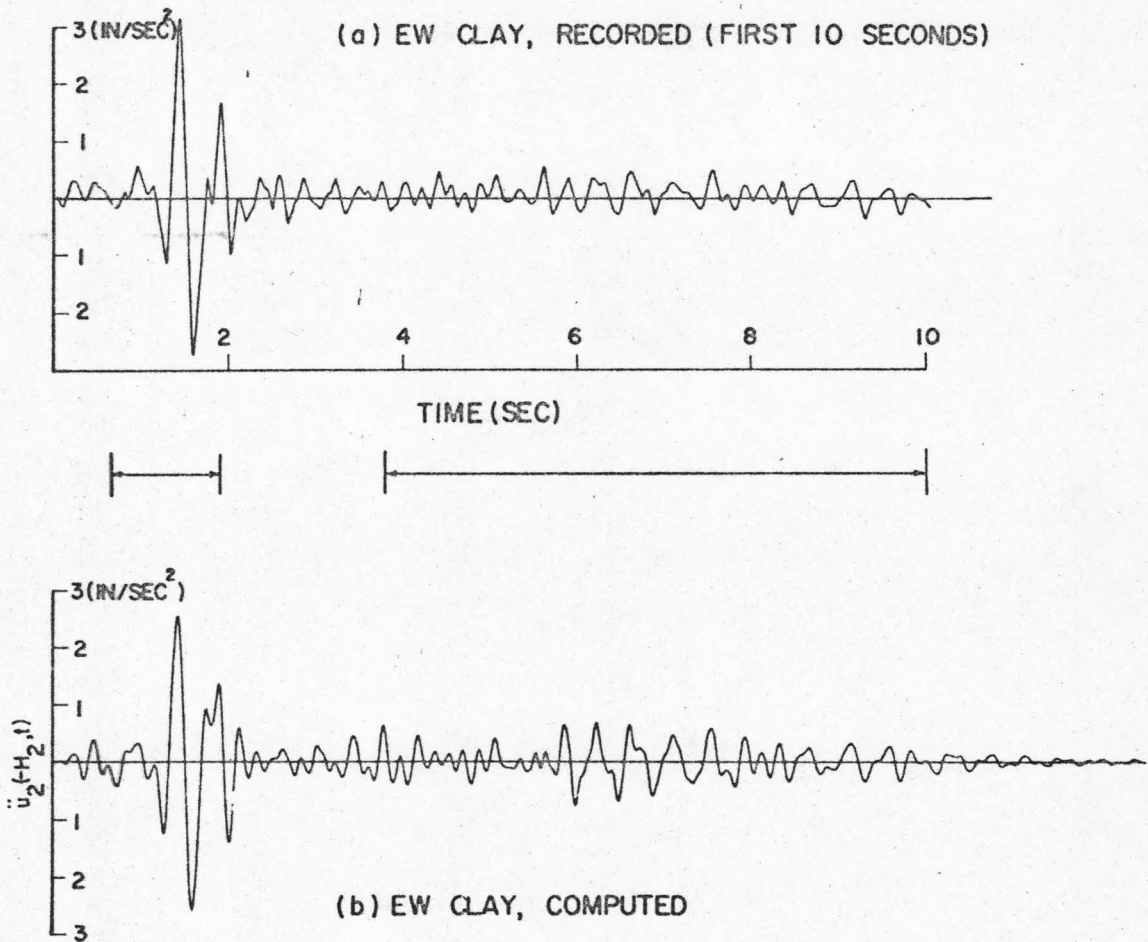


Fig. 5.18 RECORDED AND COMPUTED ACCELEROGRAMS
IN CLAY (EW)

The damped velocity spectra for both the recorded and the computed clay accelerograms were computed. The results for the NS and the EW components are shown in Figs. 5.19 and 5.20 respectively. Again, much better agreement between the spectra is observed in the EW component. In the spectra computed for $\ddot{u}_2(-H_2, t)$, the first three natural periods, T_1 , T_2 , and T_3 , of the layered model are marked. The prominent spectral hump around T_1 is associated with the relatively large response of the first mode during the tremor, as is confirmed by the prominent peak of the transfer function at the fundamental frequency. But, although a peak also appears in the transfer function at the second natural frequency, no prominent spectral hump is observed around T_2 . The reason is, referring to Figs. 5.12(b) and 5.12(d), the input accelerograms contained very weak components around 35 rad/sec which is the second natural frequency of the system. This provides additional evidence that the frequency components of the input can play an important role in determining the general characteristics of the output spectra.

C. Conclusions

For the three examples presented above, the first illustrated how the source mechanism of an earthquake can determine the general characteristics of the velocity spectra of the ground motion while local geology does not have appreciable influence. The second example exhibited the consistent influence of the soft subsoils at Mexico City on the recorded ground motions. The general characteristics of the ground spectra are theoretically predictable, and are

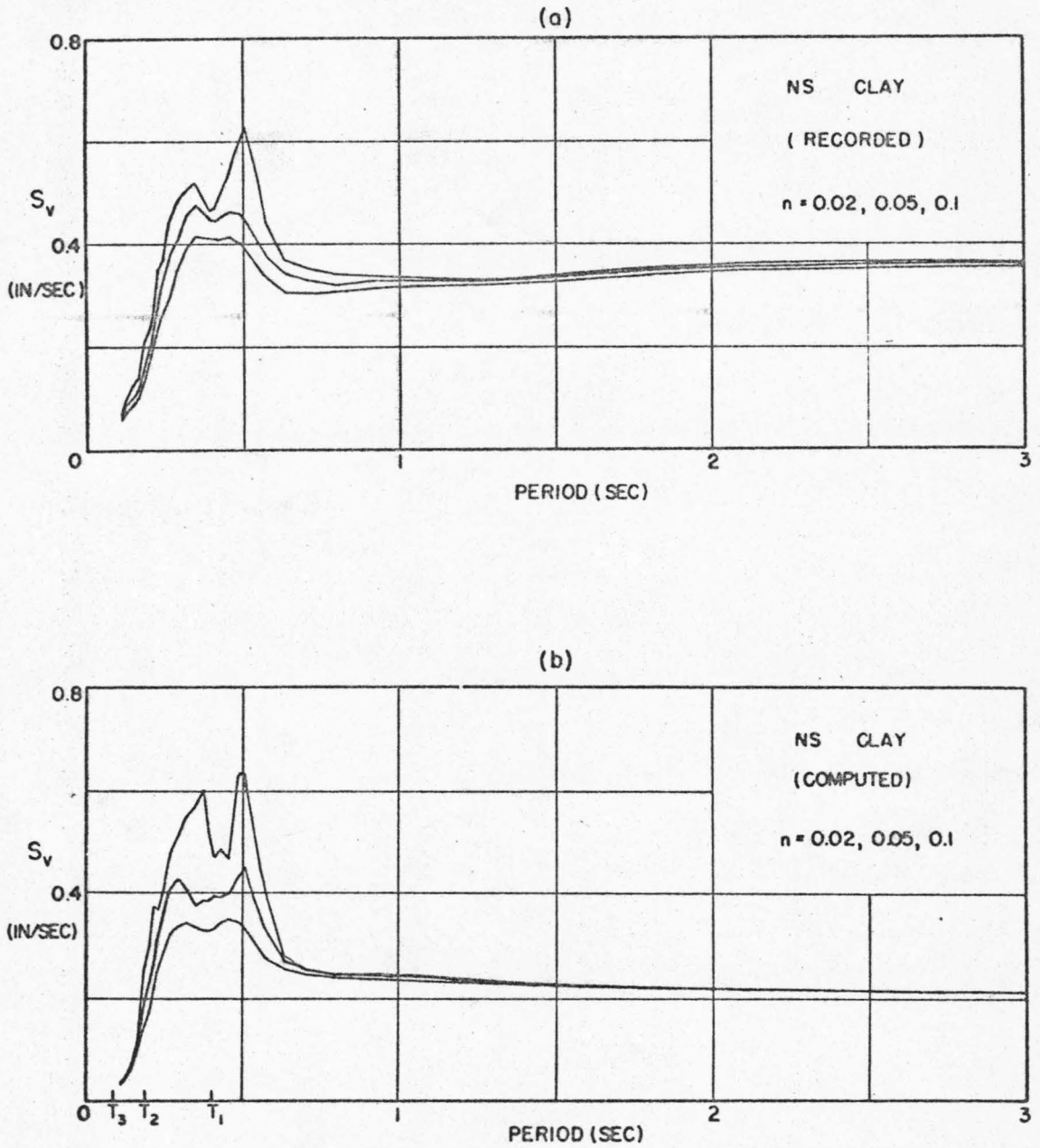


Fig. 5.19 VELOCITY SPECTRA FOR RECORDED AND COMPUTED CLAY ACCELEROGRAMS (NS)

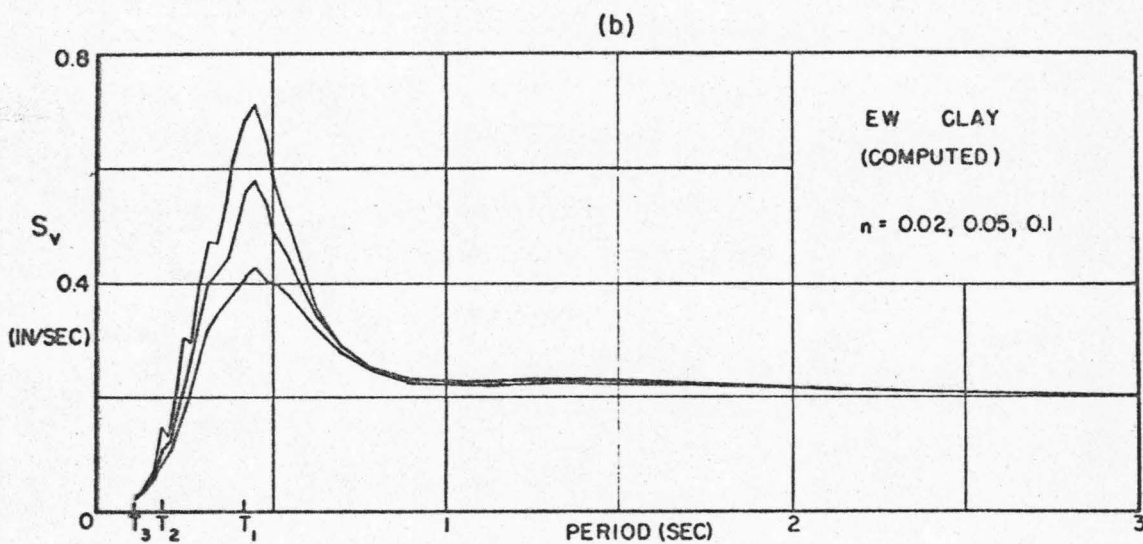
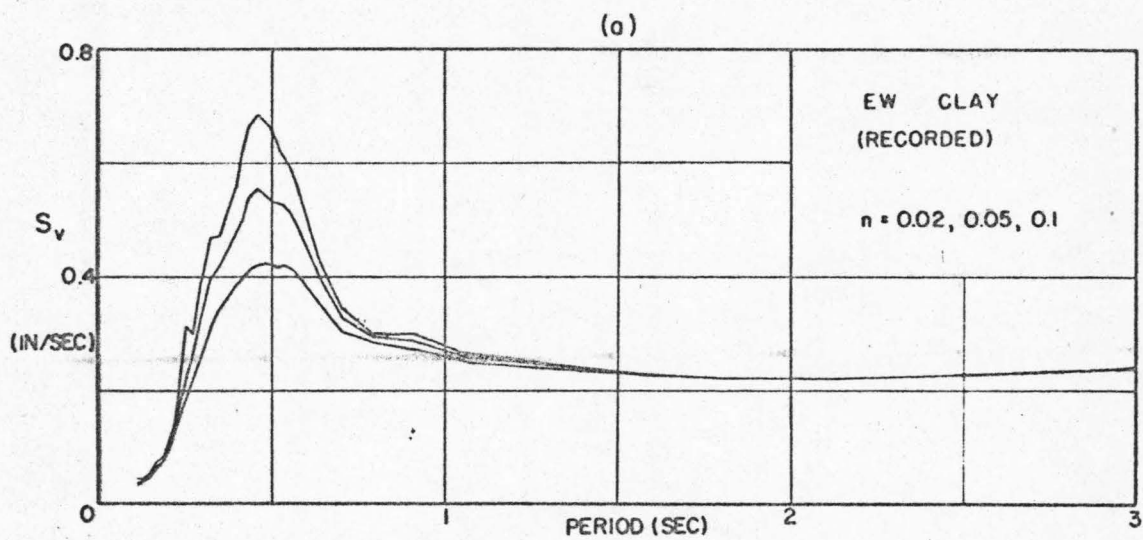


Fig. 5.20 VELOCITY SPECTRA FOR RECORDED AND COMPUTED CLAY ACCELEROGRAMS (EW)

more or less independent of the detailed characteristics of the incident waves. In the third example, the records obtained from a tremor were available at three different elevations in the subsoils of Union Bay. A quadruple-layer system was proposed to interpret the recorded accelerograms. Owing to the well defined subsoil conditions and the favorable location of the focus relative to the site, reasonably satisfactory results were achieved by the proposed model. In addition, this example demonstrated one of the advantages of the technique of continuous modal analysis, that is, the energy dissipation in the layers can be taken into account by certain modal fractions of critical damping and, therefore, the analysis can be started without having to find an appropriate rheological model for the layered media.

Since the velocity spectra of the ground motions are of most practical interest, it will be desirable to know when the spectra would be significantly affected by the local subsoils. From the previous examples we conclude that the following conditions should be satisfied simultaneously if the local subsoils at a given site are to have appreciable effects on the ground spectra.

(i) Geologically the subsoils are well defined. The horizontal dimensions of the subsoils are large compared with the depth. The location of the earthquake source relative to the site favors the approximate fulfillment of the assumption of vertically incident plane body waves. This condition ensures the applicability of the theory.

(ii) The subsoils have an amplification spectrum that includes prominent peaks at certain natural frequencies to ensure large resonance of these modes during an earthquake.

(iii) In terms of the Fourier amplitude spectrum, the incident waves contain sufficiently strong Fourier components around the natural frequencies where the amplification spectrum is prominent.

Thus, in an actual case we expect that a given site with well defined and relatively soft subsoils will produce large resonance of the lower modes of the subsoils during an earthquake that has a sufficiently long duration for the following reasons:

(a) Soft soil deposits, in general, are more likely to be well defined because of the physical processes by which the deposits were formed. On the other hand, with a large difference in stiffness between the subsoil and the bedrock the body waves are more likely to be refracted vertically into the subsoil to give rise to vertically traveling waves inside the layers. Consequently, condition (i) is likely to be satisfied.

(b) The amplification spectrum of soft subsoils usually includes prominent peaks because the soft subsoils have a relatively small value of α_N . However, in actual cases the softer the subsoils are, the larger the viscous damping may be. As a consequence, the higher modes may be damped so much that only the lower modes are still left prominent. Hence, the lower modes of the subsoils will satisfy condition (ii) easily.

(c) It is known that the lower frequency components of the seismic waves are usually subjected to smaller attenuation with

distance. Hence, when arriving at the site, the lower frequency components will usually satisfy condition (iii), especially if the duration of the event is sufficiently long. On the other hand, if horizontally incoming waves are dominant, the lower frequency components are more likely to satisfy the wave-length criterion illustrated by Fig. 5.1(a) to excite the lower modes.

(d) With longer wave length, the lower frequency components are less sensitive to the inhomogeneities and geometric irregularities of the subsoils and hence the response of the lower modes are more likely to predicted by the theory.

The above arguments lead to the conclusion that during an earthquake a site with well defined soft subsoils is likely to produce large resonance in the lower modes if the duration of the earthquake is sufficiently long compared to the fundamental natural period of the subsoils.

VI SUMMARY AND CONCLUSIONS

The studies reported in the previous chapters are summarized in the following, and the important conclusions are presented.

(1) Steady-State Analysis of a Layered System

A recursion formula was derived for finding the response of a linearly viscoelastic N-layer system subjected to vertically incident plane S-waves that are sinusoidally steady-state. Four idealized layered systems were chosen to examine the effect of varying the layer parameters on the general characteristics of the amplification spectrum. General conclusions are:

(a) The deformability of the foundation of a layered system causes the loss of some wave energy into the foundation and, therefore, the amplification spectrum is always finite at the natural frequencies of the system. The impedance ratio α_N can be considered as a measure of this energy loss. This is a well known fact.

(b) For a viscous layered system having stiffnesses gradually increasing with depth, if the properties of the top layer and the foundation are fixed, varying the parameters of the intermediate layers will not significantly change the general characteristics of the amplification spectrum so long as the total thickness of the intermediate layers is fixed also. This conclusion may not be valid for nonviscous systems.

(2) Exact Transient Response of a Nonviscous Layered System

The techniques for digital computation of the exact transient response of a nonviscous layered system were briefly reviewed, among which the ray-tracing technique was given more detailed

treatment. General conclusions are:

(a) The ray-tracing technique has an advantage over the method of frequency-domain in that the former is much faster and any desired accuracy can be achieved. However, to carry out the ray-tracing technique, it may be necessary to adjust slightly the given parameters of a layered system in order to fulfill a required relation between the step size of the numerical scheme and the time interval of a digitized input function.

(b) The ray-tracing technique does not apply to viscous layered systems. Problems involving viscous layered systems must be solved by the method of frequency-domain or, more efficiently, by the approximate methods developed in Chapter IV.

(3) Modified Shear Beam Models for Approximate Transient Analysis of a Layered System

Two modified shear beam models were established for approximate transient analysis of a layered system. The first model, which replaces the uniform half-space with a dashpot, is an exact analog to a nonviscous layered system. It might be approximate if the given system is viscous. The second model is an approximation for layered systems that have a considerable difference in stiffness between the lowest layer and the foundation, and it gives good results only for response near the surface of the system, but it is efficient for digital computation. The method of continuous modal analysis was used to analyze the models approximately. In addition, an iteration process was proposed to account for the viscosity in the layers, if any, by certain modal fractions of critical damping. Numerical examples

were given to demonstrate the accuracy of both models in computing the transient output. Velocity spectra for the output were also computed to examine the effect of a layered system on the input motion.

General conclusions are:

(a) The first model, although accurate, is time-consuming because a coupled equation system has to be solved. Hence, for non-viscous systems, the ray-tracing technique or the second model should be used while, if applicable, the second model is preferable because it costs only about half of the computing time required by the ray-tracing technique. For viscous systems, again the second model is preferable because the ray-tracing technique is not applicable.

Although subjected to some limitations in its applicability, the second model is sufficient for most practical applications.

(b) The method of continuous modal analysis enables one to account for the energy dissipation by modal damping in a very simple way.

(c) Both models can be extended to investigate the analogous problem of shear-wave structure-foundation interaction in which the foundation is the analog of the half-space and the building is the analog of the layered system.

(d) Numerical examples indicate that both the frequency components of the earthquake input function and the mechanical behavior of the layered system can be decisive factors in determining the general characteristics of the output velocity spectra.

(4) Applications

Possible limitations to the applicability of the theory to estimate the influence of local geology upon arriving seismic waves were discussed. Three examples of actual recorded earthquake events were presented, in which the theory was applied to interpret approximately the mechanical behavior of the subsoils and the following conclusions were drawn.

(a) The surface records of at least two earthquakes obtained at the same site are needed in order to see if the local subsoils did have significant influence on the ground motions. With only one earthquake record available there is no way to tell if a prominent peak observed in the velocity spectra is, or is not, due to local geology.

(b) The examples indicated, also, that the source mechanism or, equivalently, the frequency components of the incident waves can play an important role in determining the general characteristics of the ground spectra.

(c) A site with well defined soft subsoils is likely to produce large resonance of the lower modes during a sufficiently long earthquake. In this case, the general characteristics of the ground spectra are predictable from the theory and are more or less independent of the detailed characteristics of the arriving waves.

APPENDIX I

THE ORTHOGONALITY OF THE MODAL-SHAPE FUNCTION $(Z_j)_r$

The modal-shape function $(Z_j)_r$ has been defined in Chapter IV as the r^{th} mode shape within the j^{th} layer of an N-layer system, given by Eq. 4.33 as

$$(Z_j)_r = (G_j)_r \cos \left[(k_j)_r (z_j + H_j) + (\Phi_j)_r \right] \quad (4.33)$$

with

$$(k_j)_r = \omega_r / c_j,$$

$$(G_j)_r = \sqrt{\text{Re}_j^2(\omega_r) + \text{Im}_j^2(\omega_r)},$$

and

$$(\Phi_j)_r = \tan^{-1} \frac{\text{Im}_j(\omega_r)}{\text{Re}_j(\omega_r)}.$$

We want to prove that the modal-shape functions are orthogonal to each other on the interval from $z_1 = -H_1$ to $z_N = 0$ with respect to density, ρ_j , as the weighting function. Observe that the modal-shape functions satisfy the wave equation, Eq. 4.29. Hence, we have

$$(Z_j)_r'' = -(k_j)_r^2 (Z_j)_r \quad \text{A.I.1}$$

and

$$(Z_j)_q'' = -(k_j)_q^2 (Z_j)_q \quad \text{A.I.2}$$

where $(Z_j)_q$ is the q^{th} mode shape.

Multiply Eqs. A.I.1 and A.I.2 by $(Z_j)_q$ and $(Z_j)_r$ respectively, and subtract the latter from the former. Hence,

$$\left[(k_j)_q^2 - (k_j)_r^2 \right] (Z_j)_q (Z_j)_r = (Z_j)_q (Z_j)_r'' - (Z_j)_q'' (Z_j)_r$$

Multiplying both sides of $\rho_j / \left[(k_j)_q^2 - (k_j)_r^2 \right]$ and integrating from $z_j = -H_j$ to $z_j = 0$, we have, upon summing the results from $j = 1$ to N ,

$$\begin{aligned} I &= \sum_{j=1}^N \int_{-H_j}^0 \rho_j (Z_j)_q (Z_j)_r dz_j \\ &= \sum_{j=1}^N \int_{-H_j}^0 \frac{\rho_j}{(k_j)_q^2 - (k_j)_r^2} \left[(Z_j)_q (Z_j)_r'' - (Z_j)_q'' (Z_j)_r \right] dz_j \\ &= \frac{1}{\omega_q^2 - \omega_r^2} \sum_{j=1}^N \mu_j \left[(Z_j)_q (Z_j)_r' - (Z_j)_q' (Z_j)_r \right] \Big|_{-H_j}^0 \quad \begin{array}{l} \text{(by partial} \\ \text{integration)} \end{array} \\ & \qquad \qquad \qquad \text{A.I.3} \end{aligned}$$

Apply the following boundary conditions to Eq. A.I.3.

(i) The stress-free condition at the surface where $z_1 = -H_1$

gives

$$\mu_1 Z_1'(-H_1) = 0 \quad \text{A.I.4}$$

(ii) The continuity of the displacements at the interface where

$z_{j-1} = 0$ and $z_j = -H_j$ gives

$$Z_{j-1}(0) = Z_j(-H_j), \quad j = 2, 3, \dots, N \quad \text{A.I.5}$$

(iii) The continuity of the shearing stresses at the interface where $z_{j-1} = 0$ and $z_j = -H_j$ gives

$$\mu_{j-1} Z'_{j-1}(0) = \mu_j Z'_j(-H_j), \quad j = 2, 3, \dots, N \quad \text{A.I. 6}$$

(iv) The vanishing of the displacement at the base where $z_N = 0$ gives

$$Z_N(0) = 0 \quad \text{A.I. 7}$$

Substituting Eqs. A.I. 4 to A.I. 7 into Eq. A.I. 3 yields

$$I = \sum_{j=1}^N \int_{-H_j}^0 \rho_j (Z_j)_q (Z_j)_r dz_j = 0 \quad \text{if } q \neq r, \quad \text{A.I. 8}$$

provided that $\omega_q \neq \omega_r$.

Next, define $\|Z\|_r^2$ as the norm of $(Z_j)_r$. By definition,

$$\begin{aligned} \|Z\|_r^2 &= \sum_{j=1}^N \int_{-H_j}^0 \rho_j (Z_j)_r^2 dz_j \\ &= \frac{1}{Z} \sum_{j=1}^N \rho_j (G_j)_r^2 \left\{ H_j + \frac{1}{2(k_j)_r} \left[\sin 2 [(k_j)_r H_j + (\Phi_j)_r] - \sin 2 (\Phi_j)_r \right] \right\} \end{aligned}$$

by using Eq. 4.33. Observe that

$$\begin{aligned} &(G_j)_r^2 \sin 2 [(k_j)_r H_j + (\Phi_j)_r] \\ &= 2(G_j)_r^2 \left\{ \cos [(k_j)_r H_j + (\Phi_j)_r] \sin [(k_j)_r H_j + (\Phi_j)_r] \right\} \\ &= -\frac{2}{(k_j)_r} (Z_j(0))'_r (Z_j(0))_r \end{aligned}$$

Similarly,

$$(G_j)_r^2 \sin 2(\Phi_j)_r = -\frac{2}{(k_j)_r} (Z_j(-H_j))'_r (Z_j(-H_j))_r$$

Hence, by applying boundary conditions (i) to (iv)

$$\begin{aligned} \|z\|_r^2 &= \frac{1}{2} \sum_{j=1}^N (G_j)_r^2 \rho_j H_j + \frac{1}{2\omega_r^2} \sum_{j=1}^N \mu_j [(Z_j(-H_j))'_r (Z_j(-H_j))_r - \\ &\quad - (Z_j(0))'_r (Z_j(0))_r] \\ &= \frac{1}{2} \sum_{j=1}^N (G_j)_r^2 \rho_j H_j \end{aligned}$$

A.1.9

APPENDIX II

ORTHOGONAL TRANSFORMATION OF THE DAMPING MATRIX [C]

According to Eq. 4.20, the normal mode matrix, [A], has the following properties

$$[A]^T [M] [A] = [I] \quad \text{and} \quad [A]^T [K] [A] = [\tilde{\Lambda}^2] \quad (4.20)$$

Since, from Eq. 4.68, the damping matrix is given by the Caughey's series as

$$[C] = [M] \sum_{j=1}^R q_j ([M]^{-1} [K])^{j-1}, \quad (4.68)$$

the transformation of [C] is as follows

$$\begin{aligned} & [A]^T [C] [A] \\ &= [A]^T \left[q_1 [M] + q_2 [K] + [M] \sum_{j=3}^R q_j ([M]^{-1} [K])^{j-1} \right] [A] \\ &= q_1 [I] + q_2 [\tilde{\Lambda}^2] + [A]^T [M] \left[\sum_{j=3}^R q_j ([M]^{-1} [K])^{j-1} \right] [A] \quad \text{A.II.1} \end{aligned}$$

Recalling that

$$[A] = [M]^{-\frac{1}{2}} [U], \quad (4.19)$$

where

$$[U]^T [U] = [I], \quad (4.16)$$

we can expand each term under the summation sign of Eq. A.II.1 as

$$[A]^T [M] ([M]^{-1} [K])^{j-1} [A]$$

$$\begin{aligned}
&= [A]^T [M] ([M]^{-1} [K]) \underbrace{(\dots\dots\dots)}_{j-1 \text{ terms}} ([M]^{-1} [K]) [A] \\
&= [A]^T [K] \underbrace{([M]^{-\frac{1}{2}} [M]^{-\frac{1}{2}} [K]) \dots\dots ([M]^{-\frac{1}{2}} [M]^{-\frac{1}{2}} [K])}_{j-2 \text{ terms}} [A] \\
&= [A]^T [K] ([M]^{-\frac{1}{2}} [U] [U]^T [M]^{-\frac{1}{2}} [K]) \\
&\quad \dots\dots ([M]^{-\frac{1}{2}} [U] [U]^T [M]^{-\frac{1}{2}} [K]) [A] \\
&= \underbrace{([A]^T [K] [A]) \dots\dots\dots ([A]^T [K] [A])}_{j-1 \text{ terms}} \\
&= [\tilde{\lambda}^2]^{j-1}
\end{aligned}$$

Hence, Eq. A.II.1 is reduced to

$$[A]^T [C] [A] = \sum_{j=1}^R q_j [\tilde{\lambda}^2]^{j-1} \quad \text{A.II.2}$$

where it is defined that

$$[\tilde{\lambda}^2]^0 = [I] .$$

CONSTRUCTION OF THE DAMPING MATRIX FROM GIVEN MODAL
FRACTIONS OF CRITICAL DAMPING

Consider a classically damped, R-degree-freedom system described by the following system of differential equations

$$[M]\{\ddot{x}(t)\} + [C]\{\dot{x}(t)\} + [K]\{x(t)\} = -\ddot{f}(t)\{m\} \quad \text{A.III.1}$$

in which the damping matrix is unknown. From the assumption that the system is classically damped, the damping matrix can be constructed as a Caughey's series, i. e.,

$$[C] = [M] \sum_{j=1}^S q_j ([M]^{-1} [K])^{j-1} \quad (4.69)$$

where $S \leq R$, and the coefficients q_j are to be determined. The orthogonal transformation defined by Eq. 4.20 then transforms $[C]$ into a diagonal matrix which, from Eq. 4.71, gives

$$2\tilde{\beta}_r \tilde{\omega}_r = \sum_{j=1}^S q_j \tilde{\omega}_r^{2(j-1)} \quad r = 1, 2, \dots, R \quad (4.71)$$

If the natural frequencies and the fractions of critical damping of the first S modes are given, the first S equations of Eq. 4.71 can be rearranged in the following form

$$[\Omega]\{q\} = \{b\} \quad \text{A.III.2}$$

in which

$$\{q\} = \{q_1, q_2, \dots, q_S\},$$

$$\{b\} = \{2\tilde{\beta}_1 \tilde{\omega}_1, 2\tilde{\beta}_2 \tilde{\omega}_2, \dots, 2\tilde{\beta}_S \tilde{\omega}_S\},$$

and

$$[\Omega] = \begin{bmatrix} 1 & \tilde{\omega}_1^2 & \dots & \tilde{\omega}_1^{2(S-1)} \\ \vdots & \vdots & \ddots & \vdots \\ 1 & \tilde{\omega}_r^2 & \dots & \tilde{\omega}_r^{2(S-1)} \\ \vdots & \vdots & \ddots & \vdots \\ 1 & \tilde{\omega}_S^2 & \dots & \tilde{\omega}_S^{2(S-1)} \end{bmatrix}$$

Observe that the determinant of $[\Omega]$ is the well known Vandermonde determinant given by ⁽³⁰⁾

$$\det [\Omega] = \left| \prod_{\substack{i,j=1 \\ i \neq j}}^S (\tilde{\omega}_i^2 - \tilde{\omega}_j^2) \right| \quad \text{A.III.3}$$

Therefore, the inversion of $[\Omega]$ will always exist so long as there are no repeated natural frequencies, and the coefficient vector, $\{q\}$, can be solved.

$$\{q\} = [\Omega]^{-1}\{b\} \quad \text{A.III.4}$$

Substituting q_j , $j = 1, 2, \dots, S$, into Eq. 4.69 will give the desired damping matrix.

REFERENCES

1. Zeevaert, L., "Strong Ground Motions Recorded During Earthquakes of May the 11th and 19th, 1962 in Mexico City", Bull. Seis. Soc. Am., Vol. 54, No. 1, Feb. 1964, pp. 209-231.
2. Gutenberg, B., "Effects of Ground on Earthquake Motion", Tran. Am. Geoph. Union, Vol. 37, 1956, pp. 757-760.
3. Gutenberg, B., "Effects of Ground on Earthquake Motion", Bull. Seis. Soc. Am., Vol. 47, 1957, pp. 221-250.
4. Zeevaert, L., "Base Shear in Tall Building During Earthquake of July 8, 1957 in Mexico City", Proc. 2nd World Conf. Earthq. Eng., Japan, 1960, pp. 983.
5. Kanai, K., "Relation between the Nature of Surface Layer and the Amplitudes of Earthquake Motions, Part I to IV", Bull. Earthq. Res. Inst., (I) Vol. 30, 1952, pp. 31-37; (II) Vol. 31, 1953, pp. 219-226; (III) Vol. 31, 1953, pp. 276-279; (IV) Vol. 34, 1956, pp. 167-183.
6. Kanai, K., "The Requisite Conditions for the Predominant Vibration of Ground", Bull. Earthq. Res. Inst., Vol. 35, 1957, pp. 475-471.
7. Kanai, K., Osada, K., and Yoshizawa, S., "Observational Study of Earthquake Motion in the Depth of the Ground, Part V", Bull. Earthq. Res. Inst., Vol. 32, 1954, pp. 363.
8. Suzuki, T., "On the Angle of Incidence of the Initial Motion Observed at Hongo and Mitaki", Bull. Earthq. Res. Inst., Vol. 10, 1932, pp. 517.
9. Sezawa, K., and Kanai, K., "Possibility of Free Oscillations of Strata Excited by Seismic Waves", Bull. Earthq. Res. Inst., Vol. 8, 1930, pp. 1-11; Vol. 10, 1932, pp. 1-18 and pp. 273-298.
10. Sezawa, K., and Kanai, K., "Decay Constant of Seismic Vibrations of a Surface Layer", Bull. Earthq. Res. Inst., Vol. 13, 1935, pp. 251-265.

11. Sezawa, K., and Kanai, K., "The Rate of Damping in Seismic Vibrations of a Surface Layer of Varying Density or Elasticity", Bull. Earthq. Res. Inst., Vol. 13, 1935, pp. 484.
12. Matthiesen, R.B., Duke, C.M., Leeds, D.J., and Frasen, J.C., Site Characteristics of Southern California Strong-Motion Earthquake Stations, Part I and II, Dept. of Eng., Univ. of Calif., Los Angeles, Calif., Rept. No. 62-65, 64-15, Feb. 1964.
13. Herrera, I., and Rosenblueth, E., "Response Spectra on Stratified Soil", Proc. 3rd. World Conf. Earthq. Eng., Vol. I, 1965, New Zealand, pp. I-41.
14. Haskell, N.A., "Crustal Reflection of Plane P and SV Waves", Jour. Geoph. Res., Vol. 67, 1962, pp. 4751-4767.
15. Haskell, N.A., "The Dispersion of Surface Waves in Multi-Layered Media", Bull. Seis. Soc. Am., Vol. 43, 1953, pp. 17-34.
16. Takahasi, R., "A Short Note on a Graphical Solution of the Spectral Response of the Ground", Bull. Earthq. Res. Inst., Vol. 33, 1955, pp. 259-264.
17. Onda, I., "1. Plane Pulse Propagation Through a Heterogeneous Medium with a Periodic Structure", Bull. Earthq. Res. Inst., Vol. 44, 1966, pp. 1-12.
18. Gupta, R.N., "Reflection of Plane Elastic Waves from Transition Layers with Arbitrary Variation of Velocity and Density", Bull. Seis. Soc. Am., Vol. 56, No. 3, June 1966, pp. 633-642.
19. Gupta, R.N., "Reflection of Elastic Waves from a Linear Transition Layer", Bull. Seis. Soc. Am., Vol. 56, No. 2 April 1966, pp. 511-526.
20. Kanai, K., "Some New Problems of Seismic Vibrations of a Structure", Bull. Earthq. Res. Inst., Part I, Vol. 53, 1963; Part II, Vol. 54, 1964.
21. Rosenblueth, E., Herrera, I., and Rascon, O.A., "Earthquake Spectrum Prediction for the Valley of Mexico", Proc. 3rd. World Conf. Earthq. Eng., Vol. I, 1965, New Zealand, pp. I-61.

22. Baranov, V., and Kunetz, G., "Film Synthetique avec Reflexions Multiples Theorie et Calcul Pratique", Geophysical Prospecting Vol. 8, 1960, pp. 315-325.
23. Whitman, R.V., Effect of Local Soil Conditions upon Seismic Threat to Nuclear Power Plant, Report Prepared for Stone and Webster Eng. Corp., Sept. 1968.
24. Idriss, I.M., and Seed, H.B., Response of Horizontal Soil Layers During Earthquakes, Soil Mechanics and Bituminous Material Research Laboratory, Univ. of Calif., Berkeley, Calif., Aug. 1967.
25. Idriss, I.M., and Seed, H. B., "An Analysis of Ground Motions During the 1957 San Francisco Earthquake", Bull. Seis. Soc. Am., Vol. 58, No. 6, Dec. 1968, pp. 2013.
26. Zener, C.M., Elasticity and Anelasticity of Metals, Univ. of Chicago Press, Chicago, 1948.
27. Hillier, K.W., "A Method of Measuring some Dynamic Elastic Constants and its Application to the Study of High Polymers", Proc. Phys. Soc. London, Vol. 62, 1949, pp. 701.
28. Trorey, A.W., "Theoretical Seismograms with Frequency and Depth Dependent Absorption", Geophysics, Vol. 27, 1962, pp. 766.
29. Bulirsch, R., and Stoer, J., "Numerical Treatment of Ordinary Differential Equations by Extrapolation Methods", Numerische Matematik, No. 8, 1966, pp. 1-13.
30. O'Kelly, M.E.J., Vibration of Viscously Damped Linear Dynamic Systems, Ph.D. Thesis, California Institute of Technology, Pasadena, Calif., May 1964.
31. Nielsen, N.N., Dynamic Response of Multistory Buildings, Ph.D. Thesis, California Institute of Technology, Pasadena, Calif., June 1964.
32. Nigam, N.C., and Jennings, P.C., Digital Calculation of Response Spectra from Strong-Motion Earthquake Records, Report of the Earthquake Engineering Laboratory of the California Institute of Technology, June 1968.

33. Fleming, J.F., Screwvala, F.N., and Kondner, R.L., "Foundation Superstructure Interaction under Earthquake Motion", Proc. 3rd. World Conf. Earthq. Eng., 1965 New Zealand, pp. 1-22.
34. Lycan, D.L., and Newmark, N.N., "Effects of Structure and Foundation Interaction", Proc. ASCE, Jour. Eng. Mech. Div., No. EM5, Vol. 87, 1961.
35. Thomson, W.T., "A Survey of the Coupled Ground-Building Vibrations", Proc. 2nd. World Conf. Earthq. Eng., Vol. 2, Japan, 1965, pp. 833.
36. Theirs, G.R., and Seed, H.B., "Cyclic Stress-Strain Characteristics of Clay", Proc. ASCE, Jour. Soil Mech. Found. Div., Vol. 94, No. SM2, Mar. 1968, pp. 555.
37. Humphries, W.K., and Wahls, H.E., "Stress History Effects on Dynamic Modulus of Clay", Proc. ASCE, Jour. Soil Mech. Found. Div., Vol. 94, No. SM2, Mar. 1968, pp. 371.
38. Phinney, R.A., "Structure of Earth's Crust from Spectra of Long-Period Body Waves", Jour. Geoph. Res., Vol. 69, No. 14, July 1964, pp. 2997.
39. Ellis, R.M., and Basham, P.W., "Crustal Characteristics from Short-Period P Waves", Bull. Seis. Soc. Am., Vol. 58, No. 5, Oct. 1968, pp. 1681-1700.
40. Strong-Motion Instrumental Data on the Borrego Mountain Earthquake of 9 April 1968, A Report by the Joint Efforts of the Seismological Field Survey and the Earthquake Engineering Research Laboratory of the California Institute of Technology, Aug. 1968.
41. Jennings, P.C., Velocity Spectra of the Mexican Earthquake of 11 May and 19 May 1962, Report of the Earthquake Engineering Research Laboratory of the California Institute of Technology, Aug. 1962.
42. Jennings, P.C., Response of Simple Yielding Structures to Earthquake Excitation, Ph.D. Thesis, California Institute of Technology, June 1963.

43. R. H. Thomson, Expressway Crossing of Union Bay, Seattle, Washington, Worthington Christiani Fenco, A Joint Venture, Dec. 1965.
44. Berg, G.V., and Housner, G.W., "Integrated Velocity and Displacement of Strong Earthquake Ground Motion", Bull. Seis. Soc. Am., Vol. 51, No. 2, April 1961, pp. 175-189.
45. Brady, A.G., Studies of Response to Earthquake Ground Motion, Ph.D. Thesis, California Institute of Technology, June 1966.
46. Sax, R.L., and Hartenberger, R.A., "Seismic Noise Attenuation in Unconsolidated Material", Geophysics, Vol. 30, No. 4, Aug. 1965, pp. 609.